Department of Chemical Engineering and Chemical Technology
Imperial College London

Cell cycle heterogeneity study by an integrated modelling and experimental approach

A thesis submitted for the degree of Doctor of Philosophy of Imperial College London

David García Münzer

Abstract

Mammalian cell cultures are intrinsically heterogeneous at different scales (from the molecular to bioreactor level). The cell cycle is at the centre of capturing heterogeneity since it plays a critical role in the growth, death, productivity and product quality of mammalian cell cultures. Attempts to model the cell cycle heterogeneity are not new and have proved to be challenging both experimentally and computationally. Most current cell cycle models rely on biological variables (mass/volume/age) that are non-mechanistic and difficult to experimentally quantify to describe cell cycle transition and to capture the culture heterogeneity.

In this thesis, the development of integrated modelling and experimental approaches that facilitates the study of cell cycle subpopulations in cell cultures is presented. The recently proposed closing the loop framework (Kiparissides et al., 2011) is employed to facilitate the development of cell cycle models with biological relevance and applicable to real life problems (industrial and clinical). The work herein presents a novel experimental-modelling platform whereby experimental quantification of key cell cycle metrics (cell cycle timings, cell cycle fractions, and cyclin expression determined by flow cytometry) is used to develop a cyclin and DNA distributed model for the industrially relevant GS-NS0 cell line. The cell cycle model captured the population heterogeneity, which further enables *in silico* studies of the complex system. It is envisaged that this modelling approach will pave the way for model-based developments of industrial cell lines and clinical studies. A second cell cycle model was developed to assist the industrially relevant selection of temperature profiles in mammalian cell cultures. The combined experimental-mathematical approach avoided unnecessary experimentation and guided the model development for the temperature selection. The model was successfully validated by predicting different temperature profile scenarios. The presented contributions assist the development of meaningful mathematical models with predictive capabilities accounting for the cell cycle heterogeneity in bioprocesses.

Declaration

Originality

The work described in this thesis was carried out by the author (or in collaboration) in the Department of Chemical Engineering, Imperial College London, United Kingdom between October 2010 and August 2014. To the best of my knowledge, it does not contain work by any other person, unless otherwise acknowledged.

Copyright

The copyright of this thesis rests with the author and is made available under a Creative Commons Attribution Non-Commercial No Derivatives licence. Researchers are free to copy, distribute or transmit the thesis on the condition that they attribute it, that they do not use it for commercial purposes and that they do not alter, transform or build upon it. For any reuse or redistribution, researchers must make clear to others the licence terms of this work.

.

Acknowledgements

First of all to both supervisors, Sakis and Stratos, I would like to express my sincere gratitude for the last 4 years. You gave me the opportunity to pursue this personal goal, as well as your support, guidance, advices, lots of your patience and time (although I could not afford it!). Your guidance went beyond the scientific level, for which I'm deeply thankful.

The financial support from the European Commission under the MULTIMOD Training Network, FP7/2007-2013, grant agreement No 238013 is gratefully acknowledged for making this possible.

A special thank you to all the MULTIMODers, BSEL and CPSE group members. The many meetings, discussions, courses and more are great memories of all these years. Particularly, I would like to thank Chon aka "lab soul-mate, apoptotic guru" for his invaluable help in the lab, the many discussions and new perspectives (on London's weather). Of course, many thanks to the rest of the Greek crew, Dr. Michael Georgiadis and Dr. Margaritis Kostoglou, whose contributions were essential for this thesis. Similarly, a big and sincere thank you to "the Swiss" (Marija and Miro) for the fruitful and enjoyable collaboration.

To my family, I can't ever be thankful enough. My beloved parents and sisters, you have all supported me on every decision and on every day. Thank you for listening and helping me to cope with the ups and downs. Thanks to my friends, unlucky readers, and French in-laws, who always asked for progress, shared your perspectives and kept me laughing. At last, a heartfelt thanks to Lu. You joined me early in this journey and never left me alone. I feel lucky to have shared with you every day. You have witnessed from the very first successful flow cytometer test until today. Thank you for being here and all your support.

Thank you all.

Table of Contents

Abstract		1
Declaration		2
Acknowledgements		3
Table of Contents		4
Nomenclature		6
List of Figures		8
List of Tables		14
List of Publications		15
CHAPTER 1	**Introduction**	17
	1.1. Aims and Objectives	18
CHAPTER 2	**Literature Review**	21
	2.1. Fundamentals of Mammalian Cell Biology	21
	2.2. The Cell Cycle	27
	2.3. Cell Culture Systems	32
	2.4. Cell Culture Modelling	32
	2.5. Mathematical Framework	42
CHAPTER 3	**Materials and Methods**	46
	3.1. GS-NS0 cultures	46
	3.2. HFN 7.1 cultures	47
	3.3. Assays	49
CHAPTER 4	**Cyclin Blueprint of the GS-NS0 Cell Line**	61
	4.1. Introduction	61
	4.2. Objectives	62
	4.3. Methodology	62
	4.4. Results & Discussion	65
	4.5. Conclusions	89
CHAPTER 5	**Effect of Culture Conditions on the Cell Cycle**	91
	5.1. Introduction	91
	5.2. Objectives	92
	5.3. Methodology	92
	5.4. Results & Discussion	94

	5.5. Conclusions	112
CHAPTER 6	**Development of a Cyclin Distributed Cell Cycle Model of GS-NS0 Cell Line**	113
	6.1. Introduction	113
	6.2. Objectives	114
	6.3. Methodology	114
	6.4. Model Development & Experimental Validation	115
	6.5. Model Analysis & Re-estimation of Significant Model Parameters	120
	6.6. Results & Discussion	123
	6.7. Conclusions	137
CHAPTER 7	**Development of an Unstructured Metabolic and Temperature Dependent Cell Cycle Model in Hybridoma Cell Cultures**	139
	7.1. Introduction	139
	7.2. Objectives	140
	7.3. Methodology	141
	7.4. Model Development & Experimental Validation	141
	7.5. Model Analysis & Re-estimation of Significant Model Parameters	146
	7.6. Results & Discussion	151
	7.7. Conclusions	170
CHAPTER 8	**Conclusions & Future Directions**	172
	8.1. How to Capture the Heterogeneity	173
	8.2. Linking Cell Cycle & Apoptosis	175
	8.3. Metabolism & Segregation	176
Bibliography		178
Appendices	Appendix I.	192
	Appendix II.	193
	Appendix III.	195

Nomenclature

Amm	extracellular ammonia concentration (mM)
critB threshold	Cyclin B1 critical threshold for transition G_2/M-G_1 phase (%cyclin)
critE threshold	Cyclin E1 critical threshold for transition G_1-S phase (%cyclin)
cycB	Cyclin B1 distributed content (% cyclin)
CycBgrow	Cyclin B1 growth rate (%cycB/h)
cycE	Cyclin E1 distributed content (% cyclin)
CycEgrow	Cyclin E1 growth rate (%cycE/h)
DNA	DNA distributed content (DNA relative content)
DNAgrow	DNA synthesis rate (DNA/h)
$f_{i=G1,S,G2M,G0}$	Cell fraction in phase i (dimensionless)
f_{lim}	Monod kinetics functions (dimensionless)
f_{inh}	Monod kinetics functions (dimensionless)
f_{res}	Resistance factor to metabolic stresses (dimensionless)
f_{upt}	Monod kinetics functions (dimensionless)
$F_{i=Glc,Gln}$	Substrate feeding flowrate (mL/h)
F_{OUT}	Sampling flowrate (mL/h)
Glc	extracellular glucose concentration (mM)
Glc_{feed}	Glucose concentration in the feed (mM)
Gln	extracellular glutamine concentration (mM)
Gln_{feed}	Glutamine concentration in the feed (mM)
Glu	extracellular glutamate concentration (mM)
k_{dGlu}	Glutamate affinity death parameter (mM)
k_{dmax}	Cell maximum death rate (h^{-1})
k_{i-j}	Transition rate from cell cycle phase i to cell cycle phase j (h^{-1})
k_{lys}	Specific cell lysis rate (h^{-1})
k_T	Temperature factor (dimensionless)
K_{dAmm}	Monod constant parameters for death (mM)
K_{deg}	Glutamine degradation rate (h^{-1})
$K_{i=Glu,Glc,Lac,Gln,Amm,upt}$	Monod constant parameters (mM)

Lac	extracellular lactate concentration (mM)
mAb	Antibody concentration (mg/L)
$m_{i=Glc,Gln}$	Maintenance substrate coefficient (mmol/cell/h)
m, n, p, q	exponential factors to capture sensitivity towards the respective substrate/metabolite (dimensionless)
$N_{i=G1,S,G2}$	number of cells distributed on a variable for each phase (cells)
$Q_{i=G1,S,G2}$	Cell cycle specific antibody production (mg/cell/h)
$q_{i=G1G0,S,G2M}$	Cell cycle specific antibody production (mg/cell)
$Q_{i=Glu,Glc,Gln}$	Substrate consumption rate (mM/cells/h)
Q_{Lac}	Lactate consumption rate (mM/cells/h)
r_i	growth functions of the distributed variable (h^{-1})
r_T	Constant rate (h^{-1})
$t_{initial=G1,S,G2M}$	Initial estimate time to transit phase i (h)
$t_{i=G1,S,G2M}$	Time to transit phase i (h)
$total$	Total number of viable cells (cells)
$phase_{i=G1,S,G2}$	Number of cells in phase i (cells)
$prob_{G1}$	G_1 transition probability (dimensionless)
$prob_{G2}$	G_2 transition probability (dimensionless)
(S)	Substrate dependence (dimensionless)
V	Volume (mL)
$X_{i=G1,S,G2M,G0}$	Cell density in phase i (cell/mL)
X_V	Viable cell density (cell/mL)
X_D	Death cell density (cells/mL)
Y_{Amm}	Yield ammonia on substrate (mmol/mmol)
$Y_{i=Glu,Glc,Gln}$	Yield biomass on substrate (cells/mM)
$Y_{Lac/Lacinitial}$	Yield lactate on substrate (mmol/mmol)
$\alpha 1$	Constant of glutamine maintenance coefficient (mM*L/cell/h)
$\alpha 2$	Constant of glutamine maintenance coefficient (mM)
$\Gamma_{i=G1,G2}$	cyclin transition functions (dimensionless)
Γ_S	DNA transition function (dimensionless)
μ	Cell growth rate (h^{-1})

List of Figures

Figure 2.1	Eukaryotic cell structure. Organelles: 1)nucleolus, 2) nucleus, 3) ribosome, 4) vesicle, 5) rough ER, 6) Golgi apparatus, 7) cytoskeleton,8) smooth ER, 9) mitochondria, 10) vacuole, 11) cytoplasm, 12) lysosome, 13) centriole, 14) chromatin. [Adapted from: http://commons.wikimedia.org/wiki/File:Biological_cell.svg].	22
Figure 2.2	Antibody structure. Notation: C = constant regions, V = varaible regions, S-S = disulphide bonds, pupple circles = glycosylation.	26
Figure 2.3	Glutamine synthetase reaction. [Adapted from: (Barnes et al., 2000)].	27
Figure 2.4	The cell cycle.	29
Figure 2.5	Cyclin expression pattern. [Adapted from: http://en.wikipedia.org/wiki/File:Cyclin_Expression.svg].	30
Figure 2.6	Classification of biological models according to Fredrickson et al. (1970).	33
Figure 2.7	Model development framework for biological systems. [Adapted from:(Kiparissides et al., 2011)].	42
Figure 3.1	General flow cytometry data analysis for cyclin quantification. 1) Forward vs Side scatter, 2) DNA fluorescence area vs height, 3) DNA gating, 4) DNA deconvolution, 5) Bivariate cyclin vs DNA plot. Colour: Red - cyclin stained sample, blue – isotype stained sample.	57
Figure 4.1	Comparison thymidine arrest versus DMSO arrest. A) Thymidine arrest and control cell cycle distributions; B) DMSO arrest and control cell cycle distributions; C) DNA histograms following the thymidine cell cycle arrest release; D) DNA histograms following the DMSO cell cycle arrest release; E) Cell cycle distribution after arrest release. *Statistically significant ($p<0.05$).	66
Figure 4.2	Bivariate cyclin fluorescence plots with respect to DNA at time=0h after thymidine arrest: Top adjunct histogram shows DNA distribution; right side adjunct histogram shows cyclin fluorescence distribution; and embedded bar chart presents cyclin fluorescence quantification for each cell cycle phase (n=3, error bars = standard deviation) . A) Cyclin D1; B) Cyclin E1; C) Cyclin B1. Colour notation: purple for Cyclin D1,	68

green for Cyclin E1, blue for Cyclin B1, black for control groups. Gates reflect the isotype region versus the positive defined region for each cyclin. *Statistically significant (p<0.05).

Figure 4.3 Bivariate cyclin fluorescence plots with respect to DNA at time=0h after DMSO arrest: Top adjunct histogram shows DNA distribution; right side adjunct histogram shows cyclin fluorescence distribution; and embedded bar chart presents cyclin fluorescence quantification for each cell cycle phase (n=3, error bars = standard deviation). A) Cyclin D1; B) Cyclin E1; C) Cyclin B1. Colour notation: purple for Cyclin D1, green for Cyclin E1, blue for Cyclin B1, black for control groups. Gates reflect the isotype region versus the positive defined region for each cyclin. *Statistically significant (p<0.05). 69

Figure 4.4 Cell cycle distribution proliferation assay. A) EdU versus DNA time bivariate plots; B) EdU Positive Population; C) EdU Negative Population; (n=3, error bars=standard deviation). 71

Figure 4.5 Average cyclin expression levels for the control experiments for the first 24h. Notation: vertical dashed pattern bars represent the thymidine control group, solid bars represent the DMSO control group, diagonal pattern bars represent EdU control. Cyclin E1 (green), Cyclin D1 (purple), and Cyclin B1 (blue). *Statistically significant (p<0.05). 73

Figure 4.6 Average cyclin expression levels for the arrest control experiments over 4 days of batch culture. A) Cyclin E1 expression; B) Cyclin B1 expression. Notation: vertical dashed bars represent the thymidine control group, solid bars represent the DMSO control group, diagonal patterned bars represent the EdU control group, (n=3, error bars=standard deviation). *Statistically significant (p<0.05). 74

Figure 4.7 Cyclin E1 expression profiles. A) after thymidine arrest release; B) after DMSO arrest release; C) EdU positive cells; D) EdU negative cells. Notation: bars represent % cyclin relative expression normalised to cell cycle phase (left axis) and the solid line represents % cells expressing cyclin above isotype control (right axis). 76

Figure 4.8 Cyclin B1 expression profiles. A) after thymidine arrest release; B) after DMSO arrest release; C) EdU positive cells; D) EdU negative cells. Notation: bars represent % cyclin relative expression normalised to cell cycle phase (left axis) and the solid line represents % cells expressing cyclin above isotype control (right axis). 78

Figure 4.9 Cyclin D1 expression profiles. A) after thymidine arrest release; B) after DMSO arrest release. Notation: bars represent % cyclin relative expression normalised to cell cycle phase (left axis) and the solid line represents % cells expressing cyclin above isotype control (right axis). 81

Figure 4.10 Average cyclin expression before and after glutamate exhaustion. A) after thymidine arrest release; B) after DMSO arrest release; C) Proliferation assay; (error bars=standard deviation). *Statistically significant ($p<0.05$). 82

Figure 4.11 Batch cell culture profiles. A) Cell growth and viability; B) mAb titre; C) Glutamate concentration; D) Proliferation assay - proliferation marker Ki-67 and viability; E) Glucose and lactate concentration after thymidine arrest; (n=3, error bars=standard deviation). 84

Figure 4.12 Batch cell culture profiles. A) Glucose and lactate concentration after thymidine arrest; B) Glucose and lactate concentration after DMSO arrest; C) Glucose and lactate concentration proliferation assay; (n=3, error bars=standard deviation). 87

Figure 4.13 Batch cell culture profiles. A) G0/G1 phase distribution; B) S phase distribution; C) G2//M phase distribution; (n=3, error bars=standard deviation). 88

Figure 5.1 Batch temperature cell growth and apoptosis. A) Cell growth and viability; B) % Early Stage Apoptotic cells; C) % Late Stage Apoptotic cells versus % Death cells. Notation: vertical dotted line indicates time of the temperature shift, (n=3, error bars=standard deviation). 95

Figure 5.2 Batch temperature shift metabolic and antibody profiles. A) Glutamate concentration and mAb titre; B) Glucose specific consumption rate; C) Lactate specific production rate; D) Antibody specific production rate. Notation: vertical dotted line indicates time of the temperature shift, (n=3, error bars=standard deviation). 97

Figure 5.3 Batch temperature cell cycle and cyclin D1 profiles. A) %G1/G0 phase; B) %G2/M phase; C) Cyclin D1 profile for G1/G0 phase. Notation: vertical dotted line indicates time of the temperature shift, (n=3, error bars=standard deviation). 99

Figure 5.4 Medium shift experiment cell growth and apoptosis. A) Cell growth and viability; B) % Ki-67 positive cells and % Early Stage Apoptotic cells. Notation: Fresh medium (FM), % viability and % Ki-67 positive without connecting lines, viable cells (Xv) and % Early apoptotic with 102

connecting lines, (n=3, error bars=standard deviation).

Figure 5.5 Medium shift experiment metabolic and antibody profiles. A) Glucose and lactate concentration; B) Glutamate concentration and mAb titre. Notation: Fresh medium (FM), substrate (glucose, glutamate) without connecting lines, lactate and mAb with connecting lines, (n=3, error bars=standard deviation). 103

Figure 5.6 Medium shift experiment cyclin profiles. A) Cyclin profiles in the 100% fresh medium; B) Cyclin profiles in the 50% fresh medium; C) Cyclin profiles in the 0% fresh medium; D) %G1/G0 phase; E) %S phase; F) %G2/M phase. Notation: Fresh medium (FM), (n=3, error bars=standard deviation). 106

Figure 5.7 Schematic representation of the cell cycle and apoptosis. 108

Figure 5.8 Medium shift experiment cyclin versus gene expression. A) Cyclin D1 vs p21 expression; B) Cyclin E1 vs p21 expression; C) Cyclin B1 vs p21 expression; D) Cyclin D1 vs trp53bp2 expression; E) Cyclin E1 vs trp53bp2 expression; F) Cyclin B1 vs trp53bp2 expression. Notation: Fresh medium (FM), (n=3, error bars=standard deviation). 110

Figure 6.1 Model results for the control experiments. A) Cell growth and viability; B) Glucose and lactate concentration profiles; C) Glutamate and mAb concentration profiles; D) Cell cycle distribution. Notation: dots represent experimental data (n=3, error bars=standard deviation), lines represent the simulation results. 124

Figure 6.2 Model results for the thymidine arrest release experiment. A) Cell growth and viability; B) Glucose and lactate concentration profiles; C) Glutamate and mAb concentration profiles; D) Cell cycle distribution. Notation: dots represent experimental data (n=3, error bars=standard deviation), lines represent the simulation results. 129

Figure 6.3 Model results for the DMSO arrest release experiment. A) Cell growth and viability; B) Glucose and lactate concentration profiles; C) Glutamate and mAb concentration profiles; D) Cell cycle distribution; E) Cell cycle distribution delay growth. Notation: dots represent experimental data (n=3, error bars=standard deviation), lines represent the simulation results. Grey lines: simulation with estimated parameters (Table 6.1). Black lines: simulation with DMSO delay parameters (Table 6.1). 131

Figure 6.4 Model results for undisturbed higher cell density experiment. A) Cell 135

growth and viability; B) Glucose and lactate concentration profiles; C) Glutamate and mAb concentration profiles; D) Cell cycle distribution. Notation: dots represent experimental data (n=3, error bars=standard deviation), lines represent the simulation results.

Figure 7.1 Cell cycle model schematic representation. 146

Figure 7.2 Batch shake flask cultures at 37 °C. A) Cell growth, viability and mAb profiles; B) Cell cycle distribution; C) Glucose and lactate profiles; D) Glutamine and Ammonia profiles. Notation: dots represent experimental data (n=3, error bars=standard deviation), lines represent the simulation results. 153

Figure 7.3 Batch shake flask cultures shifted to 33 °C at the start of cultivation. A) Cell growth, viability and mAb profiles; B) Cell cycle distribution; C) Glucose and lactate profiles; D) Glutamine and Ammonia profiles. Notation: dots represent experimental data (n=3, error bars=standard deviation), lines represent the simulation results. 155

Figure 7.4 Fed-batch bioreactor cultures at 37 °C. A) Cell growth, viability and mAb profiles; B) Glucose and lactate profiles; C) Glutamine and Ammonia profiles; D) G1/G0 phase; E) S phase; F) G2/M phase. Notation: dots represent experimental data (n=2, error bars=standard deviation), lines represent the simulation results. 158

Figure 7.5 Fed-batch bioreactor culture shifted to 33 °C at the start of cultivation. A) Cell growth, viability and mAb profiles; B) Glucose and lactate profiles; C) Glutamine and Ammonia profiles; D) G1/G0 phase; E) S phase; F) G2/M phase. Notation: dots represent experimental data (n=1), lines represent the simulation results. 161

Figure 7.6 Temperature shifted fed-batch cultures to 33 °C at 30h. A) Cell growth, viability and mAb profiles; B) Glucose and lactate profiles; C) Glutamine and Ammonia profiles; D) G1/G0 phase; E) S phase; F) G2/M phase. Notation: vertical grey dotted line indicates time of the temperature shift, dots represent experimental data (n=2, error bars=standard deviation), black lines represent the simulation results. 165

Figure 7.7 Temperature shifted fed-batch culture to 33 °C at 76h. A) Cell growth, viability and mAb profiles; B) Glucose and lactate profiles; C) Glutamine and Ammonia profiles; D) G1/G0 phase; E) S phase; F) G2/M phase. Notation: vertical grey dotted line indicates time of the temperature shift, dots represent experimental data (n=1), black lines 167

represent the simulation results.
Figure 8.1 Cell cycle model development. 174
Figure AI.1 Batch temperature shift glucose and lactate profiles. 192
Figure AI.2 Batch temperature shift productivity profiles divided in culture phases. 192
Figure AIII.1 Cell cycle model schematic representation. 195
Figure AIII.2 Conservation test study 196

List of Tables

Table 3.1	Flow cytometers configurations.	55
Table 6.1	GSA Indexes and parameters values for the cyclin distributed cell cycle model. Outputs: XV=viable cell density, fG1=G1/G0 cell fraction, fS=S cell fraction, fG2=G2/M cell fraction, and mAb=antibody titre.	122
Table 7.1	GSA Indexes and parameters values for the temperature dependent cell cycle model. Outputs: XV=viable cell density, [mAb]=antibody titre, fG1=G1 cell fraction, fS=S cell fraction, fG2M=G2/M cell fraction, and fG0=G0 cell fraction.	149
Table AIII.1	Conservation test.	196

List of Publications

Journal Publications

[1] **García Münzer D.G.**, Kostoglou M., Georgiadis M.C., Pistikopoulos E.N., Mantalaris A. (2014). "Cyclin and DNA distributed cell cycle model for an industrial cell-line". *Submitted to PLoS Computational Biology*.

[2] **García Münzer D.G.**, Ivarsson M., Usaku C., T. Habicher, Soos M., Morbidelli M., Pistikopoulos E.N., Mantalaris A. (2014). "An unstructured model of metabolic and temperature dependent cell cycle arrest in hybridoma batch and fed-batch cultures". *Accepted in Biochemical Engineering Journal.*

[3] Usaku C., **García Münzer D.G.**, Pistikopoulos E.N., Mantalaris A. (2014). "Linking the cell cycle and apoptosis with metabolic profiles in the batch culture of GS-NS0". In-preparation.

[4] Fuentes-Garí M., Misener R., **García Münzer D.G.**, Velliou E., Kostoglou M., Georgiadis M.C., Panoskaltsis N., Pistikopoulos E.N., Mantalaris A. (2014). "Decoding leukemia heterogeneity: a combined experimental/modeling approach". In-preparation.

[5] **García Münzer D.G.**, Kostoglou M., Georgiadis M.C., Pistikopoulos E.N., Mantalaris A. (2013). "Developing a cyclin blueprint as a tool for mapping the cell cycle in GS-NS0". Biochemical Engineering Journal, Volume 81, 15 December 2013, Pages 97-107.

Note. The contents of the above mentioned publications set the foundation of some the chapters within this thesis. Specifically, the following chapters and publications are linked:

- Chapter 4 is based on: Journal Publication [1] and [5]
- Chapter 6 is based on: Journal Publication [1]
- Chapter 7 is based on: Journal Publication [2]

Peer-Reviewed Conference Publications

[6] **García Münzer D.G.**, Kostoglou M., Georgiadis M.C., Pistikopoulos E.N., Mantalaris A. (2014). "A cyclin distributed cell cycle model in GS-NS0". Computer Aided Chemical Engineering, v.33, 19-24.

[7] **García Münzer D.G.**, Kostoglou M., Georgiadis M.C., Pistikopoulos E.N., Mantalaris A. (2013). “Dynamic cyclin profiling as a tool to segregate the cell cycle”. Proceedings of the 23rd Meeting of the European Society of Animal Cell Technology (ESACT).

[8] Usaku C., **García Münzer D.G.**, Pistikopoulos E.N., Mantalaris A. Proceedings (2013). “Cell cycle and apoptosis: a map for the GS-NS0 cell line at the genetic level and the link to environmental stresses”. Proceedings of the 23rd Meeting of the European Society of Animal Cell Technology (ESACT).

Conference Presentations & Posters

[9] Fuentes-Garí M., Misener R., **García Münzer D.G.**, Velliou E., Panoskaltsis N., Kostoglou M., Georgiadis M.C., Pistikopoulos E.N., Mantalaris A. (2014). “Towards personalized treatments for leukemia based on cell cycle heterogeneity: an experimental/modeling approach”. AIChE Annual Meeting, Atlanta – USA.

[10] Fuentes-Garí M., Misener R., **García Münzer D.G.**, Velliou E., Panoskaltsis N., Pistikopoulos E.N., Mantalaris A. (2014). “Development and experimental validation of a cyclin-based population balance model of the cell cycle in leukaemia cell lines”. TERMIS-EU, Genova – Italy.

[11] **García Münzer D.G.**, Pistikopoulos E.N., Mantalaris A. Oral Presentation: “Mapping the Cell Cycle in GS-NS0: (2012). “Developing a cyclin blueprint as a tool for optimizing productivity”. AIChE Annual Meeting, Pittsburgh – USA.

[12] **García Münzer D.G.**, Pistikopoulos E.N., Mantalaris A. (2011). “Population balance modelling in cell culture systems”. Marie Curie Research Symposium, Warsaw – Poland.

CHAPTER 1

Introduction

Over the last years, the biotechnology industry has reported a continuous and rapid growth (18% in 2012, US market) led by the introduction of several monoclonal antibodies (mAbs) and diabetes products (Aggarwal, 2014). In 2011 and 2012, the mAbs market perceived a double digit growth rate, maintaining their ranking as the highest selling class of biologics. Therefore, the mAbs production, which represents a fraction of the biotech sector, is facing the challenge to meet the growing demand of these products. These biologics are commonly produced by mammalian cell culture systems due to their ability to perform human compatible post-translation modifications (glycosylation) of proteins. However, batch to batch variability, low product yields, and poor product quality are common problems associated with the bio-processing of these products. The intrinsic difficulties of the mammalian cell factories are reflected in their complex production systems, where productivity and product quality are controlled by a large number of coordinated metabolic reactions influenced by culture parameters. Most importantly, mammalian cell culture systems are intrinsically heterogeneous at all scales from the genetic to bioreactor level (Davies et al., 2013; Du et al., 2013; Pichler et al., 2011). The key underlying source of heterogeneity is the cell cycle segregation (Karra et al., 2010; Pilbrough et al., 2009) being at the centre of cellular growth, death, and productivity, which varies during the different cell cycle phases. Therefore, a better understanding and knowledge of the cell cycle timings, transitions, and associated production profiles can aid the development (modelling, control, and optimisation) of these industrially relevant systems (Dutton et al., 2006).

Mathematical models and computational tools can avoid unnecessary experimentation and facilitate our understanding of the biological systems (Bailey, 1998). However, as Bailey (1998) argued, “even the simplest living cell is a system of such forbidding complexity that any mathematical description of it is an extremely modest approximation”. Thus, the formulation of mathematical models for biological systems requires a balance between the model description (both in structure and

computational solution times) and the required experimental measurements for quantification/validation. Furthermore, careful consideration needs to be taken since the employed experimental tools and errors play an important role in the model validation (Sidoli et al., 2005). However, the bio-industry needs to adopt more accurate and biologically significant quantification techniques (Kuystermans et al., 2012), which will inherently require efficient computational tools to analyse the data. Therefore, the task of representing the biological systems adequately using relevant mathematical models and experimental quantification techniques is rather challenging. Towards this direction, the biological model development framework (Kiparissides et al., 2010a) facilitates the formulation of high fidelity models that capture the biological functions, while remaining tractable in order to be further used in model-based control and optimisation. Hence, the development of mathematical models that capture the heterogeneity of the cell population, both at the biophase and at the cellular level, can aid the study of these complex systems.

1.1. Aims and Objectives

The aim of this thesis is the development of integrated modelling and experimental approaches that facilitates the study of cell cycle subpopulations in cell cultures with individual growth/metabolic and productivity characteristics. The model development combines cell models that account for growth, death, metabolism, and productivity of segregated cell cultures; whereas the experimental approaches focus on the determination of key cell cycle features for the mathematical model development, such as population distribution, cyclin expression, and transition profiles. The proposed approach captures the heterogeneity of the system, relies on experimentally measurable/quantifiable process variables, and employs model analysis tools for model refinement and approximation. Overall, the goal is to systematically develop accurate mathematical cell cycle models for biological systems with predictive power.

The thesis is structured in three sections: Introduction, Literature Review and Materials/Methods (chapter 1-3), Experimental approaches (chapter 4 & 5), Mathematical modelling (chapter 6 & 7), and Conclusions/Future directions (chapter 8). The following scientific objectives have been set in order to study the cell cycle heterogeneity.

- ***Introduction (chapter 1)***

  The central subject addressed in this thesis is introduced, as well as the key aims and objectives for the following chapters.

- ***Review of key scientific contributions (chapter 2)***

  First, an overview of the biological principles underlying the studied system is presented with an emphasis on the cell cycle. Secondly, a critical review of relevant modelling approaches in the field is performed. Finally, the biological model development framework is introduced.

- ***The materials and methods used are described (chapter 3)***

  The materials and experimental assays are described, as well as the modelling analysis method is presented.

- ***Identification of the cell cycle blueprint for the GS-NS0 cell line (chapter 4)***

  The proposed experimental approach which aims to elucidate the cell cycle blueprint for the GS-NS0 cell line is presented. The cell cycle blueprint encompasses the characteristic cyclin profiles, timings, and thresholds.

  The expression of three cyclins (D1, E1, and B1), is studied under both disturbed and undisturbed growth, by flow cytometry in batch cultures of GS-NS0. The disturbed growth cases involved two different DNA synthesis inhibitors, thymidine and dimethyl sulfoxide (DMSO). Both control runs (established in parallel to the disturbed cases) and a proliferation assay (tracking a specific cell population that was active at DNA synthesis) were used as undisturbed growth cases.

- ***Study of the effect of culture conditions on the GS-NS0 cell cycle (chapter 5)***

  The effect of temperature and medium shifts is presented both for the cell cycle and cell programmed death (apoptosis). The studies aimed to provide insight on the cell cycle regulation and its link with apoptosis (for future model development), while varying key culture conditions (i.e. temperature and nutrient variations).

- ***Development of a first principles cyclin distributed and DNA model for GS-NS0 cultures (chapter 6)***

  A biologically-relevant cell cycle model for the GS-NS0 cell line based on the experimentally derived cell cycle blueprint is presented in this chapter. The model is developed employing the mathematical modelling framework based on the experimental observations. A first principles mathematical model to describe the cell cycle using cyclin E1 for G_1/G_0 phase, DNA for the S phase, and cyclin B1 for the G_2/M phase is proposed. The model description includes the cell growth, basic metabolism, and cell cycle specific mAb production. The model structure is studied by global sensitivity analysis (GSA) identifying parameters with a significant effect on the model output. After, the significant parameters are re-estimated using the data from a set of control batch experiments. Finally, the model predictions are compared to experimental data of disturbed (after cell arrest release) and undisturbed cell growth.

- ***Development of an unstructured temperature and metabolic dependant model for a hybridoma cell culture (chapter 7)***

  In this chapter, the model development framework is used to formulate a (fed)-batch temperature dependent cell cycle model for a mAb producing murine hybridoma cell line. An unstructured cell cycle model accounting for the distribution of proliferating (G_1, S, G_2/M) and arrested cells (G_0) in (fed)-batch culture is developed and applied to predict temperature shifts from 37 °C to 33 °C. The model describes viable cell concentration, basic metabolism and antibody concentration. The model is validated experimentally at different temperature conditions, both for batch and fed-batch cultures.

- ***Identification of future directions & improvements (chapter 8)***

  Finally, in chapter 8 the main findings and conclusions are reviewed. In addition, suggestions for future research directions in this field are proposed.

CHAPTER 2

Literature Review

The most relevant contributions and state-of-the-art for the topics addressed in this thesis are presented in this chapter. Initially, the fundamentals of cell biology are introduced, followed by an overview of the cell cycle. Then, the cell cycle regulatory machinery is reviewed. Subsequently, key scientific contributions in the field of mammalian cell modelling are discussed. Finally, the biological modelling development framework is outlined.

2.1. Fundamentals of Mammalian Cell Biology

Mammalian cell culture systems are commonly used for the production of mAbs due to their ability to perform human compatible post-translation modifications (glycosylation) of proteins. The cell structure is elaborate and complex, highly compartmentalised, containing a variety of organelles with different functions. Since the focus is on mammalian cell culture systems, the fundamentals of their biology are presented herein.

2.1.1. Cell structure

The cell is a complex entity able to carry out elaborate synthesis processes. These complex systems resemble to chemical plants, where different units known as organelles perform specific functions to convert and transport biochemical components. Mammalian cells are eukaryotic (Figure 2.1), which are differentiated by the presence of a membrane-bound structure known as the nucleus. The nucleus or nuclear envelop occupies 10% of the total volume (Alberts et al., 2008) and contains the DNA organised in chromosomes. Its main function is to maintain the integrity of the genes in the chromosomes and control the activity of the cell by means of regulating the gene expression. The nucleus is connected to the endoplasmatic reticulum (ER). The ER is a membrane network that is found throughout the cell. The ER can occur as rough or smooth. The rough ER is named after its appearance due to bound ribosomes, which are responsible for protein

manufacturing. The smooth ER is responsible for synthesis of lipids and steroids, among others.

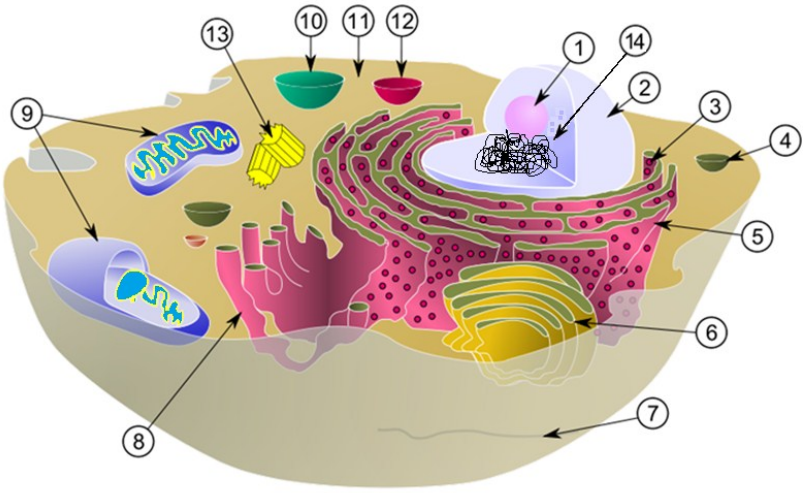


Figure 2.1. Eukaryotic cell structure. Organelles: 1)nucleolus, 2) nucleus, 3) ribosome, 4) vesicle, 5) rough ER, 6) Golgi apparatus, 7) cytoskeleton,8) smooth ER, 9) mitochondria, 10) vacuole, 11) cytoplasm, 12) lysosome, 13) centriole, 14) chromatin. [Adapted from: http://commons.wikimedia.org/wiki/File:Biological_cell.svg].

Nearby to the ER is found the Golgi apparatus. The Golgi apparatus is a membrane-bound structure that is integral in modifying, sorting, and packaging the different macromolecules previously synthesised in the ER. Another important unit is the mitochondria, responsible for the chemical energy production (adenosine triphosphate – ATP). The cell contains several other organelles, e.g. lysosomes, vacuoles, which are not included here as they are not relevant for the discussion.

2.1.2. Cell metabolism

The cell is not only physically structured but also chemically structured, and is constituted of different biochemical components. In order to maintain itself (growth, reproduction, structure maintenance, and adaptation to the environment), the cell undergoes a large number of chemical reactions and processes, known as metabolism.

Two major classes of processes are encountered: anabolic processes – where energy is used to build components (e.g. proteins) and catabolic processes – where compounds are broken down in order to produce and collect energy. The cell goes through different anabolic and catabolic processes in series, parallel or cyclic, which are known as metabolic pathways.

Catabolism

During catabolism molecules are broken down in order to produce usable energy by the cell (ATP). The main process where energy is produced mammalian cells is divided in 4 steps: glycolysis, oxidative decarboxylation of pyruvate, tricarboxylic acid cycle (TCA), and oxidative phosphorylation.

Glycolysis is the catabolic process where glucose is converted into two molecules of pyruvate in order to release free energy in the form of ATP and reduced nicotinamide adenine dinucleotide (NADH). The net yield of the process is 2 ATP and 2 NADH molecules. Subsequently, in the absence of oxygen, the pyruvate is fermented into lactic acid or ethanol. However, in the presence of oxygen, a more efficient path is followed to completely oxidise the pyruvate into carbon dioxide.

First, the pyruvate is decarboxylated and coenzyme A is coupled to the acetyl molecule to produce Acetyl-CoA and carbon dioxide, while producing 1 NADH (which will produce 3 ATP by oxidative phosphorylation) per pyruvate. The resulting Acetyl-CoA (per pyruvate) enters (coupling with oxaloacetate) the TCA inside the mitochondria and is converted in a series of steps back into oxaloacetate. During the cycle a total of 3 molecules of carbon dioxide, 3 NADH, 1 flavin-adenine dinucleotide (FADH), and 1 guanosine triphosphate (GTP) per pyruvate molecule are produced. Further the NADH and FADH undergo oxidative phosphorylation, where 3 ATP are formed per molecule of NADH, 2 ATP are formed per molecule of FADH, and 1 ATP is formed per molecule of GTP.

The anaerobic route (only glycolysis and fermentation) results in the production of only 8 ATP molecules per glucose, whereas the aerobic route gives a total of 38 ATP molecules from the same glucose molecule. The produced ATP is to be used as chemical energy for anabolism.

The amino acid metabolism is closely linked to the above described catabolic processes. Several of the carbon skeletons of the amino acids come from the intermediates of glycolysis and TCA. Similarly, some of the amino acids can pass from the cytosol into the mitochondria to be converted into intermediates of the aforementioned catabolic processes. The amino acids not used in biosynthesis can be oxidized to generate metabolic energy, whereas their nitrogen atoms are carried through various forms (e.g. ammonia, urea).

Anabolism

During anabolism key components are biosynthesised in several energy requiring reactions. Among the most important components are pentoses, nucleic acids, nucleotides, amino acids, proteins, fatty acids, and lipids.

- Pentoses, Nucleotides, ,Nucleic Acids, and Nucleotide Sugar Donors: The monomeric units of 5 carbon sugars, called pentoses, are common in the cell. These are present in the backbone of the cell (RNA and DNA) as ribose and deoxyribose. Pentoses are formed by oxidizing and decarboxilating glucose. This process generates nicotinamide adenine dinucleotide phosphate (NADPH) and a key intermediate, ribulose-5-phosphate. From the latter, ribose and deoxyribose are formed to be used for the synthesis of nucleic acids. The pentose phosphate pathway is not only an important anabolic pathway for the production of pentoses but also a catabolic pathway. Nucleic acids are made of nucleotides, which are monomeric units. These are synthesised by a complex number of steps and are literally constructed atom by atom. Another important biosynthetic process involves the activation of monosaccharide (e.g. glucose) to nucleotide sugars donors (NSDs), which play a key role as substrates in the post-translational modifications to proteins. The metabolic synthesis of NSDs is closely related to the central carbon metabolism and glutamine as a nitrogen source.
- Fatty Acids and Lipids: The fatty acids are key molecules used for energy storage and cell structure. Fatty acids are synthesised by two carbons at a time and comprise the successive addition of an acetyl unit. Fatty acids are added to a glycerol molecule for the final assembly of lipids. Usually, the third carbon in the glycerol backbone contains a polar group. This particular constitution allows the lipids to form cell structure compounds (membranes).
- Proteins and Amino Acids: Amino acids are either obtained from the environment or synthesised. There is a total of 20 amino acids commonly found in cells and can be can be grouped into families according to their carbon skeleton. The amino acids that cannot be synthesised by the cells are known as essential amino acids, which are cell line dependent and need to be supplied in the culture medium. The amino acids that can be synthesised usually are derived from intermediates of either glycolysis or TCA, whereas the amino group present in the amino acids is derived from inorganic sources in the environment (e.g. ammonia).

The proteins are constituted of amino acids and protein synthesis is achieved in a series of steps. First the DNA is transcribed in the nucleus into a chain of messenger RNA (mRNA). The single strand of mRNA leaves the nucleus and migrates to the cytoplasm. In the cytoplasm, particularly in the rough RE, where the ribosomes are present, the translation step takes place. Each triplet of consecutives nucleic acids (known as codon) corresponds to a specific amino acid. The translation of mRNA is done by an anticodon (known as tRNA). The tRNA is the corresponding pairing triplet of the codon, which carries the corresponding amino acid. The sequence of anticodons will give rise to the sequence or chain of amino acids forming the protein. Subsequently, the protein folds to assume its structure. Many proteins undergo an additional step referred as post-translational modifications. This step is initiated at the ER and finalised in the Golgi apparatus. The protein is modified by the attachment of functional groups (mainly sugars), which induce the formation of new links within the structure. This is a key step for the production of mAbs.

2.1.3. Antibodies

Antibodies are proteins used by the immune system to identify and neutralise foreign objects (or antigens) such as bacteria and viruses. The antibody recognises and binds specifically to (deactivating) the antigen. Antibodies are made of four polypeptide chains: two identical heavy chains and two identical light chains. Each chain is composed of structural domains. The chain contain domains are constant or variable, the latter being the one which gives the specificity to the antibody. The domains have a three dimensional structure defined by the intermolecular forces and disulphide bonds, which are formed in the rough ER (where the oxidizing environment is key for this process). The four chains come together to give a Y-shaped structure (Figure 2.2).

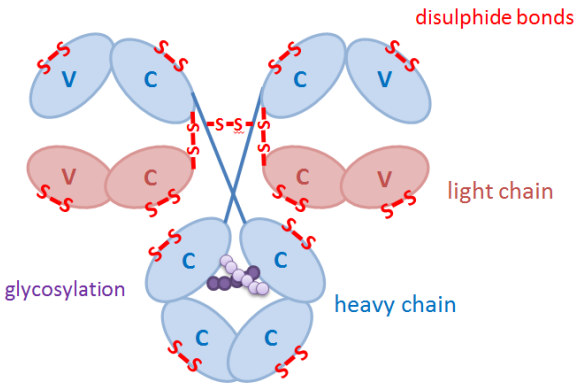


Figure 2.2. Antibody structure. Notation: C = constant regions, V = varaible regions, S-S = disulphide bonds, pupple circles = glycosylation.

The antibody production is exactly as for a protein; however, these compounds do required the post-translation modification in order to be functional. Glycosylation is the principal post-translational modification, which consists of the covalent addition of oligosaccharides on the protein. There are two possible structures for the addition: N – linked glycosylation or O – linked glycosylation. The N – linked refers to the covalent binding of the N-acetylglucosamine to the amide groups (asparagine) in the protein; while the O – linked refers to binding of N-acetylgalactosamine to the hydroxyl groups (serine, threonine, or hydroxylysine) of the protein (Alberts et al., 2008).

Antibodies are produced by B lymphocytes cells, which have a limited life-span. Due to the importance of antibodies, their production is of great interest. Therefore, ways to immortalise the producing cells have been envisaged and applied. Usually, the B lymphocyte cell (producing the antibody of interest) is fused with an immortalised B lymphocyte tumour cell, creating a hybridoma cell. These hybrid cells are a permanent and stable production platform for the industrial production of antibodies (known as monoclonal antibodies since they are all derived from the same parent cell).

2.1.4. Glutamine, glutamate and glutamine synthetase

Glutamine and glutamate are non-essential amino acids, as they can be synthesised by a large variety of cells (Barnes et al., 2000). Specifically, the glutamine synthetase (GS) enzyme catalyses the formation of glutamine (Figure 2.3), however the endogenous levels of the GS enzyme can be very low in some cell

lines. Even so, the role of glutamine is crucially important for mammalian cells. Among the most important roles is its metabolism, which provides a source for nitrogen, protein synthesis, biosynthesis of amino acids, and more (Meister, 1985). Similarly, glutamine serves as an energy source for cells (Reitzer et al., 1979).

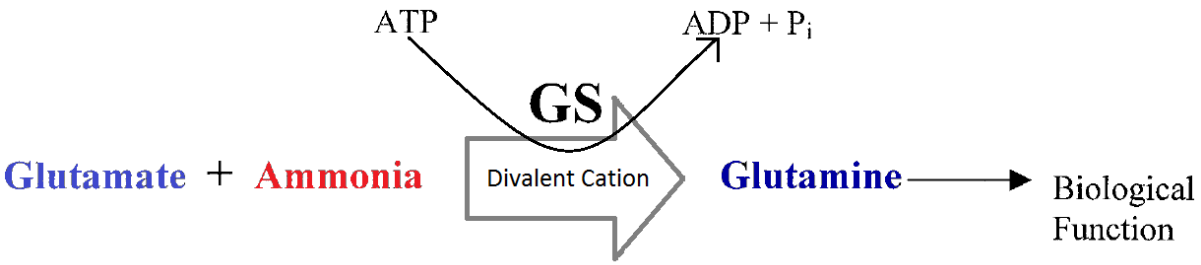


Figure 2.3. Glutamine synthetase reaction. [Adapted from: (Barnes et al., 2000)].

Using recombinant DNA technology is possible to create a plasmid vector containing the GS gene and a heterologous protein. A biochemical selection marker was built given the key role of glutamine for the cells survival (Butler and Jenkins, 1989) and the low levels of the GS enzyme in some cells (Bebbington et al., 1992). Thus, cells with low levels of endogenous GS that are transfected with the plasmid vector and exposed to glutamine-free media, which allow selecting the cells with expression of the gene of interest. The survival of transfected cells in a glutamine-free media plus increasingly concentrations of methionine sulfoxamine (MSX, which binds to the GS enzyme and prevents the production of glutamine), ensures the cells are stably expressing at high levels the GS gene and hence the heterologous protein (working as a biochemical selection marker). This system is commercially used for the production of antibodies.

2.2. The Cell Cycle

The structure and the metabolism of the cell have been reviewed in the previous sections. However, a key process in the cell is the sequence of events taking place between the time a cell is born until it divides to give birth to two daughter cells, repeating the process all over again. This series of events are defined as the cell cycle. The cell cycle comprises four main phases, which follow a time sequence (Figure 2.4). The main events taking place on each phase are described.

- First gap (G_1): this phase is characterised by an increased physiological activity comprising growth and synthesis. The cell synthesises different organelles, functional proteins, and enzymes that will be required for the DNA replication. The cell has a control mechanism to ensure that is ready for DNA synthesis (known as the restriction point) and progress to the synthesis (S) phase. The G_1 phase has a variable length, which have been reported to be as short as 4h in CHO cells (Sitton and Srienc, 2008) but also approximately 9h in a typical human cell proliferating (Alberts et al., 2008). However, when conditions (internally or externally) are not favourable for DNA synthesis the cells enter a resting quiescent state known as G_0 (Pardee, 1989). The cell can remain in this state for a variable period of time (between days to years) before it resumes proliferation or undergoes programmed death (apoptosis).

  Cell death is triggered extracellularly or intracellularly (Alberts et al., 2008). Known extracellular factors that trigger the process are the exhaustion of nutrients (particularly survival factors – e.g. certain amino acids) or the accumulation of toxic metabolites (e.g. ammonia and lactate). The internal factors that could lead to cell death usually are linked to quality control (e.g. abnormal, non-functional cells) or when the cells are stressed.
- Synthesis (S): DNA replication occurs during this phase while cell growth continues. The chromosome duplication process has been reported to last approximately 6 hours (Sitton and Srienc, 2008). Once the cell has completed the DNA replication enters a second gap (G_2).
- Second gap (G_2): throughout this phase the cell continues growing and control (Murray, 1994) that everything is ready for the next phase Mitosis (M) in order to divide. Typically this is a short gap of about 3h including division (Sitton and Srienc 2008).
- Mitosis (M): the cell cycle is completed by giving birth to two daughters cells. In this phase, cellular energy is focused on the division and cell growth has stopped. The first part of this process consists on the division of the nuclear envelop in two parts, each of which contains one genome. In mammalian cells the division is completed in less than an hour.

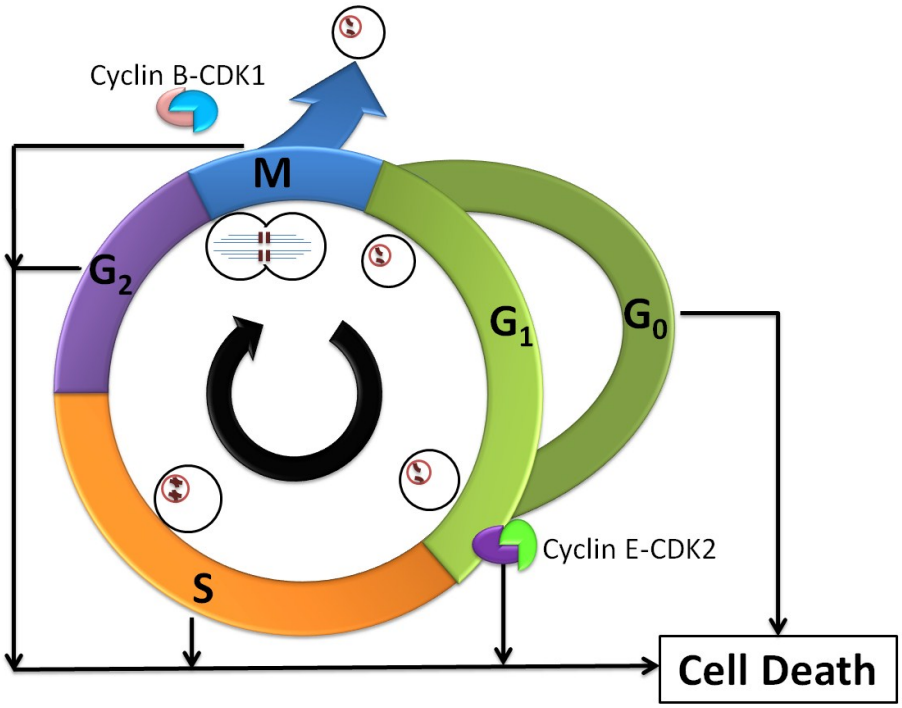


Figure 2.4. The cell cycle.

Although the length depends on the cell type and its environment, mammalian cells complete the cycle in about 24h (Alberts et al., 2008).

2.2.1. Cyclins

The transition from one phase to another of the cell cycle is a highly regulated process. There are two key classes of regulatory molecules, cyclins and cyclin-dependent kinases (CDKs) (Darzynkiewicz et al., 1996). The cyclins act as regulatory units and have no catalytic activity. The CDKs are catalytic subunits and are inactive in the absence of their partner cyclin (with which they form a heterodimer). The heterodimer coordinates the entry into the next phase. This is achieved by activating or inactivating target proteins, e.g. proteins and enzymes required for DNA replication in the S phase. The presence of CDKs remains constant through the cycle (Morgan, 1995), while the cyclins amount varies in a cyclical fashion (in response to molecular signals or checkpoints).

Progression between the G_1-S checkpoint has been reported to be regulated by two cyclins, cyclins D and E (Turchi et al., 2000). Cyclin D1 is expressed early in G_1, associates with CDK4 and CDK6, and is responsible for the phosphorylation of the retinoblastoma protein (pRb), which is essential for progression to the S phase.

However, cyclin D expression is reported to remain invariable or at low level in normal proliferating cells (Gong et al., 1994; Gong et al., 1995). In addition, cyclin D is reported to be regulated by extracellular signals (Sherr, 1993), accumulating as a response to extracellular growth factors and declining rapidly in their absence. Cyclin E1 is expressed in mid-G_1 and associates to CDK2 (Figure 2.4). The cyclinE1-CDK2 complex is bounded with other promoters, such as p33, phosphorylates histone H1 and other proteins in late G_1 and early S phase. Cyclin E1 expression is reported to peak at the G_1-S transition and to degrade through the S phase progression (Gong et al., 1994). Cyclins D and E together are responsible for carrying the cell through the restriction point between the G_1-S phases.

Similarly, cyclin B1 is reported to regulate the cell's entrance into mitosis (Gong et al., 1993). Cyclin B1 expression initiates in late S phase, accumulates to a maximum between the G_2-M transition and rapidly degrades in late M phase. Cyclin B1 forms a heterodimeric complex with CDK1 (Figure 2.4) forming the Maturation Promoting Factor (MPF), which activity is essential to trigger the entrance to mitosis (Darzynkiewicz et al., 1996). Cyclin expression patterns are, in general, reproducible in normal cells of different lineages; alas, tumour cell lines display different expression patterns (Gong et al., 1994). The expression of cyclins is cyclic and specific to cell cycle points (Figure 2.5).

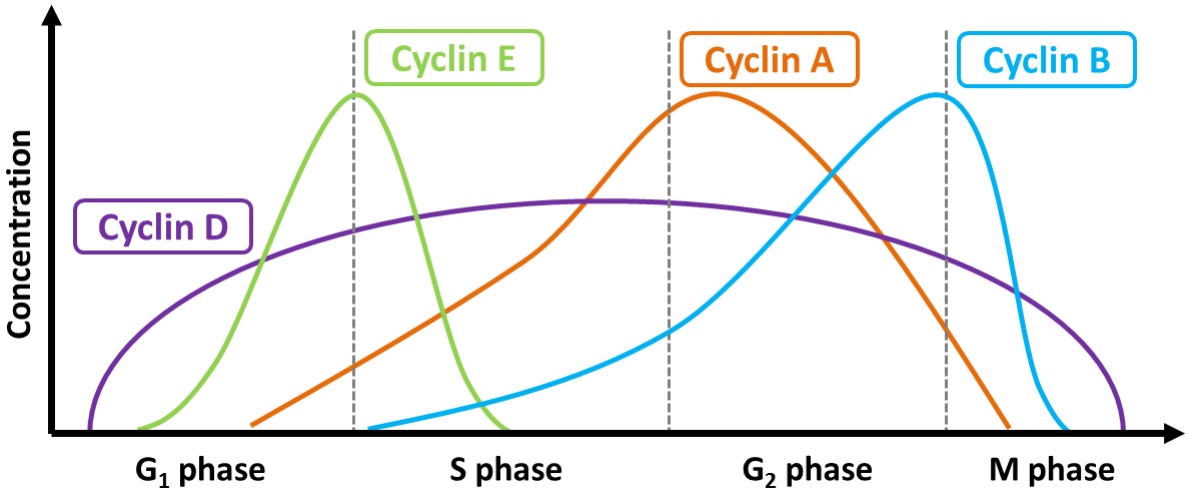


Figure 2.5. Cyclin expression pattern. [Adapted from: http://en.wikipedia.org/wiki/File:Cyclin_Expression.svg].

The cell cycle events are positively regulated by the cyclin-CDK complexes, whereas negative control is regulated by cyclin-dependent inhibitors (CDI) on the

cyclin-CDK complexes. For instance the cyclinE-CDK2 complex is targeted by two CDIs (i.e. p27 and p21), as well as other G_1 complexes, in order to inactivate them. The inactivation of the complexes can induce cell arrest in the corresponding cell cycle phase, or trigger other cell events such as apoptosis. Evidence supports that apoptosis and the cell cycle are intimately linked, or even cell-cycle specific (Meikrantz and Schlegel, 1995). The two processes, cell cycle progression and apoptosis, depend on the balance of cyclins, CDKs, and CDIs. A key regulator is p53, which is a transcription factor that induces apoptosis or cell cycle arrest genes in response to various stress signals, such as DNA damage, heat shock, or hypoxia (Seth et al., 2006). Therefore, it can be considered as a switch between the cell cycle progression and the onset of apoptosis (Fussenegger and Bailey, 1998).

2.2.2. Cell Death

The cells can undergo programmed cell death (apoptosis) or necrosis. Apoptosis is irreversible and is activated in response to the accumulation of non-lethal stresses (e.g. nutrient depletion, growth factor deprivation, toxic metabolite accumulation) (Seth et al., 2006). Apoptosis is characterized both by morphological changes (e.g. cell shrinkage, membrane blebbing, disruption of membrane structure) and intracellular events that lead to cell destruction. There are two main pathways that result in apoptosis: the death receptor and the mitochondrial pathway. The death receptor pathway is dependent on the binding or lack of binding of ligands. This will trigger the expression of Caspase 8 and Caspase 3, which are proteins considered as initiators and final executors of cell death. The mitochondrial pathway is triggered by the controlled release of pro-apoptotic factors that are sequestered in the mitochondria intermembrane space. Both pathways involved a series of pro-apoptotic and anti-apoptotic factors that control the event; whereas necrosis is the premature cell death due to violent changes in the environment (e.g. mechanical stresses). After cell death, the cell lyses resulting in the disintegration of the cell due to membrane breakage.

2.3. Cell Culture Systems

Cell culture processes for the production of antibodies can be classified as batch or continuous. The most relevant culture systems are described below.

Batch cultures are characterized by the consumption of nutrients in time with the concurrent toxic metabolite accumulation. The batch process is largely hindered either by the exhaustion of a nutrient or high levels of toxic metabolites, hence resulting in low cell densities. An advantage of this cultivation system is the low control requirements. The nutrient limitation is usually overcome by operating on a fed-batch mode. Therefore, the addition of a concentrated fed at specific time intervals avoids the nutrient deprivation, although the fed regime is constrained by the reactor working volume. In addition, since the medium is not withdrawn from the culture, the accumulation of toxic metabolites is inevitable. Fed-batch culture systems are characterized by longer cultivation times as well as higher cell densities, though require a higher level of control and monitoring.

Continuous cultures are usually chemostat or perfusion systems. Chemostat cultures are continuously fed with fresh medium at a given flowrate, which is simultaneous and equal to the removal rate of the cell containing medium maintaining constant volume. Thus, a steady state operation can be achieved, with a constant cell density in the bioreactor by controlling the flowrate. The constant medium addition and toxic metabolite removal prolong the culture time, but the removal of proliferating cells limits the achieved cell densities and product titre. Perfusion cultures are also characterized by a constant feed of fresh medium and removal at the same rate of cell-free medium. This operation mode overcomes the cell density issues of the chemostat. The disadvantages of this system are the complex control and operation.

2.4. Cell Culture Modelling

The use of mathematical models can provide a systematic means to study complex systems (Bailey, 1998), such as cell cultures. The complexity arises from several aspects such as the structure of the cells (compartmentalization, chemical structure), the heterogeneity at different scales (bioreactor, cell cycle, genetic), and their metabolism (adaptability to changing environments). The previous mentioned aspects have made of the cell culture modelling to be grouped on two major areas.

The first area is related to the segregation of the cell population and the second area is the structure of the cell description. A final aspect that has been taken into account in the modelling is the probabilistic nature of events (i.e. deterministic versus stochastic). Despite the plethora of models and advancement in modelling techniques, cell culture models can be still classified using the systematic framework introduced by Fredrickson et al. (1970).

In Figure 2.6, segregation refers to taking into account the heterogeneity of the cell population. Cell cultures are rarely synchronised and therefore, each cell possesses individual characteristics (either from a structural or functional point stand). Alternatively, an unsegregated model considers the cell population as a lumped biophase and deals with it as an average cell (homogeneous). Structure can arise from a physical space distribution (e.g. compartments) or from a biochemical point stand. The latter provides a detailed description of the cell components (e.g. metabolites, proteins, among others) and their interaction (in an attempt to capture the complex biological system). The unstructured model treats the cell as a single component "biomass", and minimal structure is provided (more of a black-box approach). Whereas the most common approach for the event description is the deterministic approach (the progression of events is known), the stochastic approach allows introducing randomness and uncertainty into the processes.

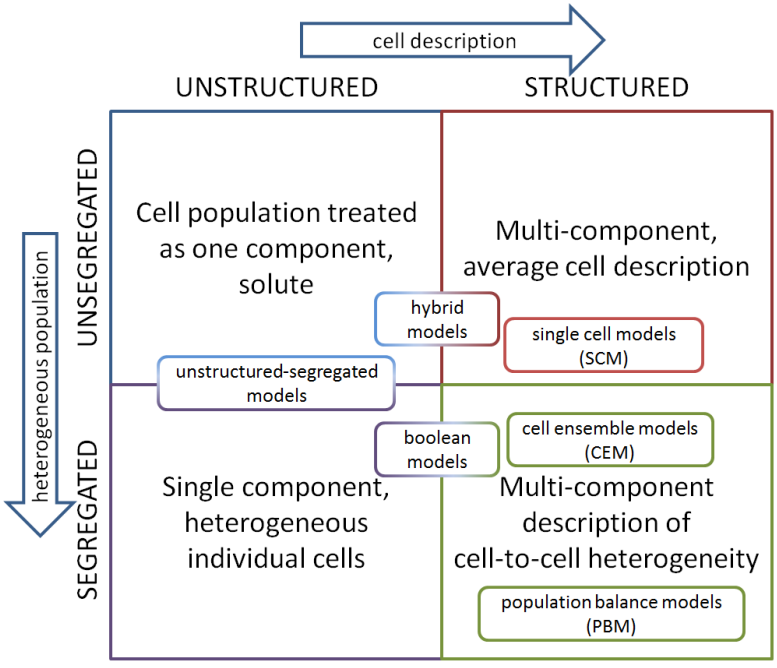


Figure 2.6. Classification of biological models according to Fredrickson et al. (1970).

The unsegregated/unstructured/deterministic models can be seen as simple representations, while the segregated/structured/stochastic models are complex and computationally intensive representations of the system. Each model has advantages and drawbacks (e.g. formulation time, parameter estimation/availability and computational time) and the end use should drive the selection criteria. The biological modelling literature is vast, thus an attempt to summarise the most significant contributions – emphasising in the cell cycle modelling – is presented.

2.4.1. Structured Models

The evolution from unstructured to structured models has been (and will be) tightly linked to the development of analytical techniques. The development of detailed analytical techniques has enabled the elucidation of the structure and function of biological systems. Hill (1910) and Michaelis and Menten (1913) described different systems with a similar mathematical expression. The Hill function was reported describing the binding of oxygen to haemoglobin (Hill, 1910), whereas Michaelis-Menten showed that the rate of an enzyme catalysed reaction (*v*) is proportional to the concentration of the enzyme-substrate complex ([S]), Equation (2.1).

$$v = V_{max} \frac{[S]}{K_m + [S]} \tag{2.1}$$

Similarly, Monod (1949) applied an identical function as Michaelis and Menten to describe microbial growth. These contributions shaped the foundations of biological modelling and are still used widely in unstructured models. The underlying concept is that cell growth and metabolic pathways are ultimately limited by enzyme catalysed reactions. Further attempts to describe and predict cell cultures made use of Monod's model to describe growth based on multiple substrates. One of the first attempts to include structure in the modelling of mammalian cells was reported by Batt and Kompala (1989), where metabolic detail (mechanisms) was introduced. In order to keep the model tractable, the intracellular constituents were lumped into a number of metabolic pools. The formulated dynamic model consisted of a set of differential equations, which described main substrate consumption, byproduct formation, cell growth, and antibody production. Further contributions in the field of antibody synthesis and secretion were presented in the work of Bibila and Flickinger

(1991). The authors included in their model the structure of the antibodies (heavy and light chain assembly) and also metabolic pathways (Bibila and Flickinger, 1992a, 1992b). An important feature of their work was the use of factorial design analysis to identify the most significant parameters in the antibody secretion rate. The increasing structural detail in the models leads to complex formulations to capture the cell biology. Models of high metabolic and compartmentalisation detail are referred as Single Cell Models (SCM). One of the most comprehensive structured models for animal cells is the one proposed by Sanderson et al. (1999). The model includes 50 components, over three regions of the cell culture (i.e. medium, cytoplasm, and mitochondria). The metabolic description featured glycolysis, TCA, production and use of fatty acids/amino acids, membrane transport, product formation, and cell growth/death. It is an extraordinary attempt to capture the cell's complex functioning and in principle it can be extended and applied to a variety of animal cell cultures. Further, the model is used for the optimisation of the medium initial conditions and feeding strategies. The incorporation of high biological detail supported the better understanding and design of processes, though at a clear expense (i.e. validation issues, parameter estimation, and computational cost).

In order to overcome the difficulties associated with SCM, a new type of models called "hybrid models" were proposed. Hybrid models consisting of both unstructured and structured elements brought a trade-off between detail and computational cost. A hybrid model consisting of an unstructured (i.e. nutrient uptake, metabolite production, cell growth, and death) and structured (antibody production) elements (Ho et al., 2006) was compared to a SCM (Sanderson et al., 1999) adapted for the study of GS-NS0 cell line. Ho et al. (2006) highlighted the difficulties in extending the SCM due to the over parameterised nature of it (with over 350 parameters), while the hybrid model successfully predicted the experimental data with less than 30 parameters. Similarly, a hybrid model considering an unstructured growth and death, but accounting for glucose and 19 amino acids metabolism has been proposed (Kontoravdi et al., 2007b). The model requires 68 parameters, which can be modified to account for different cell lines. More recently, the attention in the inclusion of structure in mammalian cell modelling has been directed towards product quality (i.e. glycosylation). In this area, the dynamic model of the Golgi apparatus compared to a

plug flow reactor (Jimenez del Val et al., 2011), can potentially be coupled to a NSDs metabolic model in order to predict and optimise glycosylation patterns in mAbs.

2.4.2. Structured-Segregation

In order to account for the cell culture heterogeneity, it is required to segregate the population. This represents a major challenge due to the difficulties to experimentally measure and validate such heterogeneity. Particularly, mammalian cell culture heterogeneity ranges from the genetic to the bioreactor level. Therefore, published mammalian cell segregated models are less common than unsegregated models (Bailey, 1998; Sidoli et al., 2004). Two main trends capture the heterogeneity in the cell population: Cell Ensemble Models (CEMs) and Population Balance Models (PBMs), both will be discussed. CEMs capture the heterogeneity or segregation by including a large number (cluster) of SCMs that differ according to key cellular properties. The approach is based on the assumption that a sufficiently large number of individual cells will represent the behaviour of the population. Domach and Shuler (1984) used this approach to predict steady state and transient distributions of *E. coli* cultures with 250 modelled cells. Similarly, Henson (2005) investigated the synchronisation and cell cycle oscillations of continuous cultures of yeast *S. cerevisiae* with a CEM of 10,000 modelled cells. A total of six intracellular species (defining the heterogeneity) were included in the model. The reported computational time of an ensemble model for one hour of dynamic modelling involving 1,000 cells required about 200s on a Pentium IV 1.4GHz processor with 64MBs of memory. An important advantage of the CEM approach is the ability to incorporate SCMs with computational feasibility. On the other hand, the number of cells included in the model will limit the resolution of the obtained distributions, as well as the possibility to perform computational demanding *in silico* experiments (model-based control and optimisation).

2.4.3. Population Balance Models (PBMs)

An alternative to model segregation in cell culture systems is based on the population balance equation (PBE). PBE describes the number distribution of internal cell states (e.g. age, mass, DNA) as a function of time. Such equations are a number balance on a population with respect to certain number of properties of

interest. This type of formulation allows incorporation of information about stage-to-stage transition (e.g. cell cycle) and partition of cell material upon cell division. Therefore, PBMs are the most accurate way of describing the cell culture heterogeneity. PBMs can be classified as follows (Mantzaris et al., 2001a):

- Single or Multi-variable: depends on the number of cell properties used to describe the state of a single cell at a given time. Multi-variable models are more detailed and can describe the cell state with more accuracy.
- Single or Multi-staged: depends on the number of cell cycle stages that are included in the formulation. Each stage will require and additional PBE to describe the number balance within that stage (and transitions from it).
- Mass or Aged structured: if the cell state is described by properties obeying mass conservation – the model is considered mass structured, while if age is used to differentiate cells – the model is considered age-structured.

PBMs were introduced in biological systems by Fredrickson et al. (1967). However, their application to bioprocesses has been limited by two main challenges: 1) the difficulties of solving a partial-integro-differential equation and 2) experimentally determining distribution data (Villadsen, 1999). The first challenge is further amplified since PBMs are coupled with the ordinary integro-differential equations accounting for the cell metabolism, substrate uptake and/or product formation, which add further complexity. The second challenge relies on the need to determine the intrinsic physiological state functions (e.g. growth rates, stage transition, division, death rates), which is rather experimentally challenging.

The generic structure of a cell PBE is presented in Equation (2.2). Cells are considered heterogeneous on a basis of a state variable "*x*" (either single or multi-variable). Therefore, the number of cells with a particular state at a particular time is tracked. This is referred as the number distribution on the stage "i" (if the model is multi-staged) and is denoted as $N_i(x,t)$. This quantity will vary in time and reflects the accumulation of cells in stage i with state x (first term on the LHS Equation (2.2)). Changes on the number of cells are given due to different events related either to the metabolism or cell cycle transition. The second term on the LHS Equation (2.2) accounts for the loss of cells due to their transition to other states with rate $r_i(x,S)$

where S reflects the substrate dependence. This term is mainly related to metabolism, e.g. single cell growth.

$$\frac{\partial \mathrm{N_i(x,t)}}{\partial \mathrm{t}} + \frac{\partial}{\partial \mathrm{x}}[r_i(x,S)N_i(x,t)] = -\Gamma_{\mathrm{i}}(x,S)N_i(x,t) + \Gamma_{\mathrm{j}}(x,S)N_j(x,t) - DN_i(x,t) - k_d(S)N_i(x,t) + 2\int_{x_{min}}^{x_{max}} \Gamma_{\mathrm{j}}(y,S)p(x,y,S)N_j(y,t)\,dy \quad (2.2)$$

The other events varying the cell number are related to stage changes (terms on the RHS Equation (2.2). The first term on RHS stands for the cells leaving stage i (e.g. cell division or cell cycle transitions) with a rate Γi(x,S). The second term on RHS is associated with the number of cells that might enter stage i coming from stage j, such as cell cycling (but different from cell birth). The third term on the RHS accounts for the dilution depending on the reactor operation mode. The fourth term on the RHS accounts for the death of cells in stage i with rate kd. Cell birth is represented by the last term on the RHS as a parent cell of state y dividing to give birth to two daughter cells of state x. The partition function p(y,x,S) expresses the probability of a mother cell with state y will give birth to a cell of state x (if assumed to be independent on the substrate p(y,x)). Cells in stage i are being born through the division of cells in stage j. Since cells can be at different states of the state continuum, in order to include all parent cell divisions, integration is required for all possible parent cells ranging from a minimum, x_{min}, to a maximum, x_{max}. The formulation is completed by specifying the physiological state functions r, Γ, k_d, and p indicated in Equation (2.2). The growth r and death k_d rates are usually coupled with a cell (un)-structured model. The transitions between stages Γ, is either modelled deterministically (if well understood) or allowed to include randomness when this fits best knowledge. The partition function usually accounts either for equal partition or for symmetric distribution (e.g. Beta) centred at equal partition allowing for the less probable unequal partition. Further, it should be noted that there are several points of coupling between the population balance, the cell model and overall mass balances. The presented formulation gives rise to the aforementioned challenges. Therefore, most of the available PBMs in cell cultures are coupled to unstructured models in order to reduce the computational burden. The computationally intensive nature of the formulation is demonstrated in several studies (Fadda et al., 2012b; Mantzaris et al., 2001a; Mantzaris et al., 2002; Pinto et al., 2007; Sidoli et al., 2006; Stamatakis,

2013) with increasing complexity (i.e. number of stages, number of variables or level of structure). Although the development and improvements in computer power is also perceived in these studies (Karra et al., 2010; Pinto et al., 2007).

Two main features characterise the existing model formulations: age or mass/volume based PBMs. Early reports used age as the sole distribution variable. Cazzador and Mariani (1993) modelled the growth and productivity of mAbs in hybridoma cells. The model is multi-staged (3 cell cycle phases) and age structured. It considered a stochastic transition to the G_0 phase and different productivities throughout the cell cycle stages. Hatzis et al. (1995) formulated a multi-stage (3 stages not correlated with the cell cycle) and multi-variable (mass and age structured depending on the stage) PBM for ciliate growth. The transition rates were assumed to be random and dependent either on age or mass. Martens et al. (1995) proposed a three stages PBM for the hybridoma cell cycle and unstructured metabolism including energy considerations. Cells were considered to die after a fixed time in the apoptotic stage. More complex formulations were reported (Cain and Chau, 1998; Rounseville and Chau, 2005) using age and an additional intracellular property (e.g. product, RNA). However, the age-based PBM formulations have the disadvantage that age as a distributed variable is difficult to experimentally quantifiable.

Consequently, mass/volume based PBMs attempted to overcome the difficulties of using age as the distributed variable. Mantzaris et al. (2002) presented a mass structured PBM with 2 stages (with product produced in the 2^{nd} stage). The model assumed no cell death and cells were cultured in a chemostat (with a linear growth rate w.r.t. mass and substrate inhibition). The PBM model was used to design a controller to operate the bioreactor showing its potential industrial relevance (although it was not experimentally validated). The authors aimed to control productivity by manipulating the feed substrate concentration, which affects the population growth and productivity. The unique coupling of a PBM with a SCM was reported by Sidoli et al. (2006). The multistaged (2 lumped cell cycle phases: G_0/G_1 and $S/G_2/M$) mass based PBM was coupled to a SCM (Sanderson et al., 1999). The transitions between stages were assumed to occur randomly after a critical mass checkpoint. However, the detailed formulation demonstrated the computational intensive nature of the PBM-SCM description (with over 700 parameters). Liu et al.

(2007) formulated a multistaged (3 stages: G_1, S, and G_2/M) and multi-variable (DNA content and cell volume) PBM. The transition from G_1 to S and division from G_2/M was considered to be dependent on the cell's volume, while the transition from S to G_2/M was determined by the DNA content. Cell death could occur at any of the stages and the cell metabolism was unstructured. The authors suggest that some of the model prediction discrepancies were due to the unstructured model used for single cell growth. Recently, Karra et al. (2010) formulated a multistage (3 stages: G_0/G_1, S, G_2/M) mass structured PBM with unstructured metabolism for mammalian cell culture processes. The authors were able to perform parameter estimation using simulated annealing due to the low computational requirements. The obtained results showed a reasonable fit with a minimum computational requirement (single run ~9s). Recently, Fadda et al. (2012a) proposed a PBM based on cell size and DNA content to describe the proliferation of adherent cells inside a Petri dish. The authors showed the advancement of the computational power by using the model for fitting parameters, although reference was made (Fadda et al., 2012b) to the prohibitively increasing computational solution time when increasing the number of grid points to increase the accuracy of the solution. Similarly, the theoretical study of a volume-based PBM to investigate the dynamics of a single gene with feedback suggested that to solve the full model compared to proposed reduced-model for the same number of cells it would take 100 times more computation time (Stamatakis, 2013).

PBMs present an accurate description of cell culture heterogeneity, although with clear experimental challenges. Mass/volume-based PBMs aimed to resolve the experimental disadvantages of the age formulation; however it still misses the biological and mechanistic relevance to truthfully capture the mammalian cell cycle. Consequently, the utilization of biomarkers can address the experimental challenges and to rigorously capture the cell cycle heterogeneity (Munzer et al., 2013).

2.4.4. Unstructured-Segregation

Both, the computational and experimental challenges of CEMs and PBMs have been avoided by models using ordinary differential equations. This type of models avoids the computational burden of CEMs and PBMs as its solution is fast. Moreover, it avoids some of the validation issues of over parameterised models (as it

tends to be rather unstructured). Similarly, the cell cycle transitions are based on the assumption of a steady state observed during exponential of growth (also referred as balanced exponential growth). Thus, Watanabe and Okada (1967) expressed the expected cell cycle fractions as a function of the cell cycle times. Such expressions were used by Suzuki and Ollis (1989) to explicitly formulate a cell cycle model for antibody production in chemostat cultures. Linardos et al. (1992) used Suzuki's model to study cell death, linking it to the fraction of cells in G_1. Further Uchiyama and Shioya (1999) adapted the cell cycle model for the industrial amylase fed-batch production. The authors fully exploited the cell cycle segregation and included cell cycle specific productivities. Similarly, an unstructured model comprising different macromolecules was presented by Jang and Barford (2000). Specifically, the model accounted for the production of macromolecules (e.g. lipids, DNA, RNA), monoclonal antibodies, and basic metabolism (glucose/glutamine consumption, producing lactate/ammonia) both in batch and fed-batch. The model features the division of the cell population in two groups: viable and arrested cells, including segregation into the model. Recently, Lam et al. (2008) proposed a model for (fed)-batch hybridoma culture accounting for the cell cycle segregation (3 phases) and specific cell cycle productivity. The authors used the model for model-based optimisation proving the computational advantages of the modelling approach. The unstructured segregation of the cell cycle presents clear computational advantages over more complex formulations. The unstructured segregation provides fast computational times and enables it to be used for model-based applications. However, the model formulation based on characteristic times to complete every cell cycle phase limits once again its biological relevance.

2.4.5. Boolean models

The computational advantages of the ordinary differential equation models using kinetic rates are evident, while its validation is limited by experimental challenges of determining the kinetic constants. This limitation applies to any cell cycle model using a reaction network. Therefore, another modelling strategy is the use of Boolean switching networks. Boolean functions provide the state of a variable (e.g. active, inactive), neglecting the notion of rates. This type of modelling is useful to study concepts of the cell cycle, but has limited applicability as it is not quantitative

and cannot be used for prediction purposes. However, recent contributions (Singhania et al., 2011) aimed to combine Boolean networks with quantifiable continuous variables.

The presented cell cycle model contributions provide an overview of the state of the art. The key (dis)advantages of each modelling approach were discussed. Overall a balance between the model detail in terms of structure and segregation regulates the computational intensive nature of the system. Similarly, the inclusion of detail introduces experimental challenges for the model validation. Ultimately, the selection of the cell cycle modelling approach is subjected to all these conditions, as well as the final intended model application.

2.5. *Mathematical Framework*

The mathematical models presented in this thesis were developed using the recently proposed biological model development framework (Kiparissides et al., 2011; Kontoravdi et al., 2010). The framework aims at the systematic development of biological models based on first principles and further refinement of the models by using model-based tools in order to avoid unnecessary experimentation.

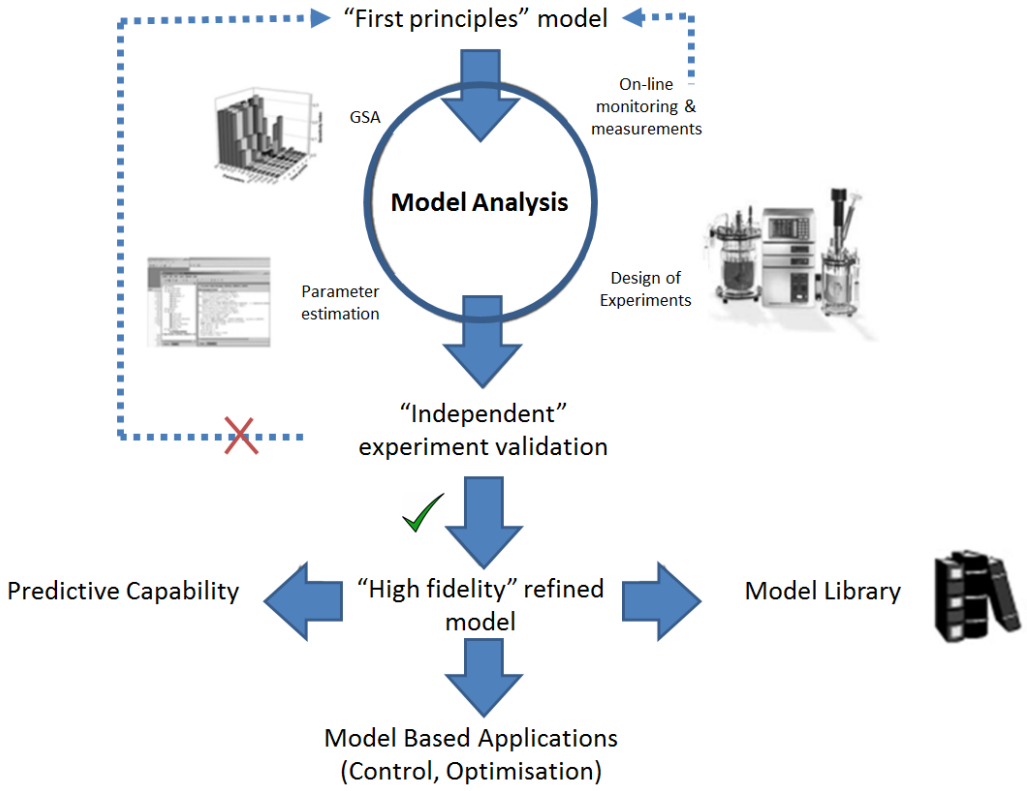


Figure 2.7. Model development framework for biological systems. [Adapted from:(Kiparissides et al., 2011)].

The framework follows a closed-loop approach that can be recursively applied for model development. Briefly the framework consists of 4 main steps:

1. Model development. During this step the model type (i.e. structure, segregation) and the model equations are define through first principles.
2. Model analysis. The uncertainty introduced by the model parameters is evaluated against the outputs in order to identify the most significant or sensitive parameters.
3. Model validation. The significant parameters are estimated from tailor-made experiments or available existing experiments, whereas the insignificant parameters are set to their nominal values. The model validity is tested against a set of independent experiments of varying conditions. This procedure can be recursively repeated until satisfactory prediction.
4. Model-based optimisation and control. Optimise or control the model inputs towards a desired goal.

2.5.1. Sensitivity Analysis

Model analysis techniques aim to study the model structure as well as the parameter-output relations. Particularly, parameter sensitivity analysis studies the variation of the model outputs by using the parameters as sources of uncertainty. This type of quantitative analysis allows selecting the most significant parameters (or with greater effect on the outputs), thus reducing the number of parameters to be (re)-estimated experimentally. There are three categories of sensitivity analysis methods: screening, local, and global (Saltelli et al., 2000).

Screening methods evaluate one factor at a time, which makes them computationally efficient and attractive to be used when there are a substantial number of input factors. However, the results are rather qualitative as the method ranks the results in order of importance. Further, the analysis is limited to only first order interactions, due to the-one-factor-at-a-time variation, lacking precision when used in non-linear models (Saltelli et al., 2000). Local methods evaluate the impact of a factor on the model output by computing the derivatives of variation of the output with respect to the input factors. Local methods are limited by the different order of magnitudes of the uncertainties and therefore are not suitable for non-linear models (Saltelli et al., 2000). Global sensitivity analysis (GSA) methods provide quantitative

results varying all parameters simultaneously, while the sensitivity is measured over the entire range of each input factor. Therefore, this is the preferred method when dealing with non-linear models and with input factors of varying order of magnitudes (Saltelli et al., 2000).

Biological models usually contain parameters of different orders of magnitude and are non-linear. These characteristics make GSA the most appropriate tool for studying biological models. The simultaneous variation of parameters allows accounting for the different orders of magnitude as well as for higher order interactions. GSA can aid the model development process by identifying the most significant parameters on the variability of model outputs. Thus, the output uncertainty is efficiently reduced and the model predictability improved, if the uncertainty on the identified significant model inputs (parameters) is reduced. A number of GSA techniques are available such as the Sobol's method (Saltelli et al., 2000; Sobol, 2001), the derivative-based global sensitivity measures (Kucherenko et al., 2009), and high dimensional model representation (Rabitz and Alis, 1999; Ziehn and Tomlin, 2009), among others. A key aspect to consider when selecting the GSA method is the computational effort of the models and methods (Kiparissides et al., 2009; Ziehn and Tomlin, 2009).

2.5.2. Parameter Estimation and Model Validation

Parameter estimation is carried out either using already existing data or from tailor-made experiments. Existing data can be a good source for parameter estimation, particularly if the experiments cover a range of conditions. However, the optimal experimental design is meant to be used as a tool to maximize the information content of experimental data (Kontoravdi et al., 2010). Specifically, the optimal experiment is tailored for the re-estimation of the parameters identified as most significant in the sensitivity analysis. The experiment design aims to determine the optimal settings (conditions) and measurements times to minimize the confidence of the estimated parameters.

After parameter estimation, the model can be validated against a set of independent data or experiments with varying conditions. The model development sequence of designing experiments, performing it, and use of the generated data

can be done iteratively until satisfactory agreement between the model prediction and the experimental data is achieved (Kiparissides, 2012; Kiparissides et al., 2011; Kontoravdi et al., 2010). Once the model is validated it can be used for model-based applications (optimisation, control). The biological model development framework presents an approach to develop high fidelity models from initial conception through its experimental validation and application.

CHAPTER 3

Materials and Methods

The materials and methods used at the experimental and modelling level are reported in this section. A series of batch and fed-batch cell culture experiments covering different cell lines and culture conditions were carried out. The key experimental conditions are outlined in this chapter, while further details are reported within each experimental chapter (4 & 5). Similarly, the general features of the different data and model analysis methods are introduced herein, whereas further detail is presented in the corresponding chapters.

3.1. GS-NS0 cultures

3.1.1. Cell Culture

GS-NS0 cells (kindly provided by Lonza; passage 5) with expression of a chimaeric B72.3 IgG4 antibody were cultured. Cells were cultured in suspension in a NU-5500E (Triple Red) humidified incubator set at 37 °C and 5% CO_2. Mixing was accomplished using a Stuart SSL1 orbital shaker (Bibby Scientific) at 125rpm. The culture medium consisted of glutamine free advanced-DMEM (Invitrogen), 2X MEM-Vitamins (Gibco), 1X Non-Essential Amino Acids (Sigma-Aldrich), 2X MEM-Amino Acids (Gibco), 2X GS-Supplement (SAFC), 1X Penicillin/Streptomycin (Gibco), 4.5 g/L MSX (Sigma-Aldrich) and 10% (v/v) fetal bovine serum (Gibco) or 10% (v/v) dialyzed fetal bovine serum (Gibco).

3.1.2. Cell bank

A cell bank for the cell line was previously created (Kiparissides, 2012). Briefly, cells from the master cell bank were expanded in 250mL Erlenmeyer flasks (Corning) prior to long term storage in a liquid nitrogen tank. Cells from cultures in mid-exponential growth – with over 85% viability – were centrifuged at 800rpm for 5min and the supernatant was aspirated. Cells were re-suspended in a medium mix containing fresh medium and 7.5% (v/v) DMSO (Sigma-Aldrich) to reach an end

concentration of $1*10^7$ cells/mL. Subsequently 1mL aliquots were transferred to cryovials (Corning) and stored in a 5100 Cryo 1 °C Freezing Container (Nalgene) at -86 °C overnight, and finally the cryovials were transferred to long term storage to the liquid nitrogen tank.

Cryovials removed from the liquid nitrogen storage were thawed in a 37 °C water batch for 2-4min. The contents of the cryovial were transferred to 10mL of fresh warm medium (37 °C) and centrifuged at 800rpm for 5min. The supernatant was aspirated and the cell pellet re-suspended in 10mL of fresh warm medium before being inoculated at $2*10^6$ cells/mL in a 125mL Erlenmeyer (Corning) with 25mL working volume. Cells were passaged 3-4 times before starting an experiment.

3.1.3. Batch experiments

GS-NS0 cells were cultured in triplicate in 1L Erlenmeyer flasks (Corning) with 200mL working volume at a seeding cell concentration of $2.5*10^5$ cells/mL or $6.5*10^5$ cells/mL in a humidified incubator containing 5% CO_2. At the start of the batch experiments the temperature was set to 37 °C, and in some cases shifted to 35 °C or 39 °C after 30h. Mixing was accomplished using a Stuart SSL1 orbital shaker (Bibby Scientific) at 125rpm.

The medium shift experiments of the GS-NS0 cells were cultured in triplicate in 250mL Erlenmeyer flasks (Corning) with 50mL working volume at a seeding cell concentration of $5*10^5$ cells/mL in a humidified incubator containing 5% CO_2. The temperature was set to 37 °C and mixing was accomplished using a Stuart SSL1 orbital shaker (Bibby Scientific) at 125rpm.

3.2. HFN 7.1 cultures

HFN 7.1 murine hybridoma cell cultures were conducted as part of a collaborative effort between the Biological Systems Engineering Laboratory (BSEL) at Imperial College and The Morbidelli Group at ETH Zurich. Specifically, Marija Ivarsson (PhD candidate) and Dr. Miroslav Soos (Senior Scientist) from ETH were involved in the fed-batch experiments. Similarly, Chonlatep Usaku (PhD candidate) from BSEL was involved in the batch experiments.

3.2.1. Cell Culture

HFN 7.1 murine hybridoma cells (ATCC CRL-1606) (Schoen et al., 1982) adapted to the chemically defined, protein- and peptide-free culture medium TurboDoma TP6 (Cell Culture Technologies) were used. The medium was prepared following the vendor's instruction and supplemented with 4.5g/L D-glucose, 4mM L-glutamine, and 0.1% (w/v) pluronic F-68. Cells were sub-cultured in suspension for 14 days at 37 °C in a humidified incubator containing 5% CO_2 and subsequently used for batch and fed-batch cultivations.

3.2.2. Cell bank

A common/joint working cell bank between ETH and Imperial College was built for the HFN 7.1 culture studies. Cells from the master cell bank were expanded in Erlenmeyer flasks (Corning) prior to long term storage in a liquid nitrogen tank. Cells from cultures in mid-exponential growth – with over 95% viability – were centrifuged at 660rpm for 3min and the supernatant (conditioned medium) was aspirated. Cells were re-suspended in a medium mix containing: 70% (v/v) fresh medium (TurboDoma TP6), 20% (v/v) conditioned medium, 10% (v/v) dimethyl sulfoxide (DMSO, Sigma-Aldrich) to reach an end concentration of $2*10^7$ cells/mL. Subsequently 1mL aliquots were transferred to cryovials (Corning) and stored in a 5100 Cryo 1 °C Freezing Container (Nalgene) at -20 °C for 2h, then at -80 °C for 2h, and finally the cryovials were transferred to long term storage to the liquid nitrogen tank.

Cryovials removed from the liquid nitrogen storage were thawed in a 37 °C water batch for 2-4min. The contents of the cryovial were transferred to 10mL of fresh warm medium (37 °C) and centrifuged at 660rpm for 3min. The supernatant was aspirated and the cell pellet re-suspended in 10mL of fresh warm medium before being inoculated at $3*10^6$ cells/mL in a 125mL Erlenmeyer (Corning) with 25mL working volume. Cells were passaged 14 days before starting an experiment.

3.2.3. Batch experiments

HFN 7.1 cells were cultured in triplicate in 1L Erlenmeyer flasks (Corning) with 240mL working volume at a seeding cell concentration of 6e5 cells/mL in a

humidified incubator containing 5% CO_2. At the start of the batch experiments the temperature was set to either 37 °C, 35 °C or 33 °C. Mixing was accomplished using a Stuart SSL1 orbital shaker (Bibby Scientific) at 125rpm.

3.2.4. Fed-batch experiments

HFN 7.1 fed-batch cultures were performed in a parallel bioreactor system (DasGip) equipped with online temperature, pH and dissolved oxygen measurement probes (Mettler-Toledo), a pitched-blade impeller, and a porous sparger (10 µm). Cells were seeded into the bioreactor at a cell concentration of $6*10^5$ cells/mL in a working volume of 1L. Dissolved oxygen was controlled at 50% air saturation with a constant airflow of 3L/h and an oxygen on demand strategy. pH setpoint 7.2 over the whole culture and controlled initially by CO_2 sparging and in some cases by base addition (2mol/L NaOH) depending on the lactate production of the growing cells. Temperature was either set to 37 °C and kept constant throughout the culture or shifted to mild hypothermia 33 °C at three different time points (t = 0, 30, 76h) by changing the controller setpoint. The time required for the reactor to reach the new temperature setpoint was negligible short (<10min). A continuous feed of amino acids (RPMI-1640 50x, Sigma), vitamins (RPMI-1640 100x, Sigma), trace elements (trace element mix 1000x, Bioconcept), and L-glutamine (64mmol/L) was initiated 30 hours after inoculation with a constant pump rate of 2.33mL/h. D-glucose feeding solution (1mol/L) was fed from the beginning of the culture to keep glucose at a setpoint of 20mM. The pump rate of the glucose solution was adjusted every 12 hours according to the measured viable cell concentration and specific glucose consumption resulting in a semi-continuous feeding mode.

3.3. Assays

Specific assays were conducted to measure and infer information from the experiments.

3.3.1. Cell cycle arrest

The use of different chemical agents was aimed to arrest and synchronise a fraction of the cell population. Herein, synchronisation refers to the cell alignment to a particular property, which in this case is the DNA content. After releasing the cells

from the arrest, the synchronised moving population was tracked using the DNA content as a criterion until it was not possible any longer to distinguish the population. Two chemical agents were used to synchronise the cultures, thymidine and DMSO. The above mentioned arresting agents were used with simultaneous control cultures.

Thymidine. GS-NS0 cell cycle arrest using thymidine (final concentration of 2mM; Sigma Aldrich) consisted of a double block. Thymidine was added to the desired concentration to the culture medium of cells in mid-exponential growth for 12h, then the cells were washed twice with phosphate buffered saline (PBS; Gibco) and re-suspended in the culture medium and incubated for another 12h at which time thymidine was added to the medium for a second time (second block) for 12h. The cells were then washed twice and re-suspended in culture medium at $2.5*10^5$ cells/mL and cultured for 6 days. A control group, which included all the centrifugation and washing steps without exposure to thymidine, was established. Sampling was performed at the beginning and end of each blocking. After the arrest release the culture was sampled every 2h for the first 10h, and every 24h afterwards.

DMSO. GS-NS0 cell cycle arrest using DMSO (final concentration 0.45% v/v) consisted of a single block. DMSO was added to the desired concentration to the culture medium of cells in mid-exponential growth for 36h, and then the cells were washed twice with PBS and re-suspended in the culture medium at $2.5*10^5$ cells/mL and cultured for 6 days. A control group, which included all the centrifugation and washing steps without exposure to DMSO, was established. Sampling was performed at 0, 24 and 36h during the arrest phase and after the arrest release every 2h between 12 and 24h, and every 24h afterwards.

3.3.2. Cell proliferation assay

Cells were exposed to a DNA nucleoside analogue to thymidine (5-ethynyl-2-deoxyuridine, EdU) that contains an alkyne, which could be later detected by a copper catalysed reaction between the alkyne and an azide-coupled flourochrome. Cells in mid-exponential growth were exposed to 30μM of 5-ethynyl-2´-deoxyuridine (EdU, Invitrogen C10419) for a period of 3 hours. After the exposure, the cells were washed twice with PBS and re-suspended in the standard growth medium (in the

absence of EdU) and cultured in batch mode for 6 days. A control group, which included all the centrifugation and washing steps without exposure to EdU, was established. Samples were taken every 2h for the first 20h and every 24h afterwards.

3.3.3. Sampling, cell counts and viability

All batch samples were counted manually using a haemocytometer under a Leica DM-IL inverted phase microscope (Leica). Viable cell concentration and viability were calculated by a dye-exclusion method using Erythrosin-B stain solution (ATCC).

All fed-batch samples were counted using a CedeX cell counter (Innovatis) by the trypan blue exclusion method.

HFN 7.1 samples (1.5-2mL) were taken twice a day and centrifuged at 660rpm for 3min. The cell-free supernatant was stored at -20 °C for metabolic profiling and antibody (IgG1) titre determination. $1*10^6$ cells were fixed by drop wise addition of 1 mL of 75% v/v ice-cold ethanol (VWR) for flow cytometry analysis. The fixed cells were stored at -20 °C prior to cell cycle analysis.

GS-NS0 samples (1.5-2mL) were taken and centrifuged at 800rpm for 5min. The cell-free supernatant was stored at -20 °C for metabolic profiling and antibody (IgG4) titre determination. Flow cytometry samples were prepared by fixing $1*10^6$ cells by drop wise addition of 1 mL of 75% v/v ice-cold ethanol (VWR) or 100% v/v ice-cold methanol (Sigma) depending on the cyclin to be analysed. If no cyclin analysis was performed, 1 mL of 75% v/v ice-cold ethanol (VWR) was used. The fixed cells were stored at -20 °C prior to cell cycle analysis.

3.3.4. Metabolic profiling

All the batch culture extracellular concentrations of ammonium, lactate, glutamine, glutamate, and glucose were measured from the stored supernatant samples with the Nova BioProfile 400 Analyzer (Nova Biomedical).

HFN 7.1 fed-batch glucose and lactate concentrations were measured immediately after sampling using a Super GL compact instrument (Hitado). The glutamine concentration of fed-batch cultures was measured from the supernatant by

HPLC (ZORBAX Eclipse Plus C18 4.6 mm x 150 mm, Agilent Technologies) according to Agilent's application note (5990-3283EN). Prior to the HPLC measurement, supernatant samples were filtered at 4000 rcf, 4 °C for 25 min using a Vivaspin500 (5 kDa) centrifugation filter (Satorius Stedim). Ammonium concentrations were determined using the L-Glutamine/Ammonia (Rapid) Assay Kit (K-GLNAM, Megazyme) following the vendor's protocol.

3.3.5. Extracellular antibody quantification

HFN 7.1 cultures monoclonal antibody (IgG1) concentrations were determined from the supernatant by standard affinity chromatography using a PA ImmunoDetection® Sensor Cartridge (Applied Biosystems) containing immobilized protein G.

GS-NS0 cultures monoclonal antibody (IgG4) quantification was performed using a high pressure liquid chromatography (HPLC) Agilent 1260 Infinity system (Agilent Technologies). The supernatant was filtered through a 13mm syringe filter with 0.22µm PTFE membrane (VWR, 28145-491) prior to injection. The affinity column, Bio-Monolith Protein A (Agilent Technologies, 5069-3639) was used to quantify IgG4 antibody in the samples by comparison to a calibration curve. The sample (50uL) was injected and loaded into the column at a flowrate of 1mL/min with a 100% PBS pH 7.4 mobile phase for 2 minutes. After, a change in gradient was performed to a 100% acetic acid 0.5M pH 2.6 mobile phase to elute, which was maintained for 5 minutes. Finally the column was again conditioned with 100% PBS pH 7.4 mobile phase for 2 minutes. The elution was monitored with a UV detector at 280 nm. The calibration curve was built from triplicate injections of a dilution series of cB72.3 antibody standard, kindly provided by Lonza biologics.

3.3.6. Cell cycle analysis

The cell cycle analysis was performed by flow cytometry. The workflow of the sample preparation depended on the assays performed.

Cell fixation and permeabilisation

GS-NS0 cells (aprox. $1*10^6$ cells/sample) were harvested, fixed, and permeabilised. The fixation agent was a choice depending on the cyclin to be

analysed on the sample. Specifically, cells were fixed and permeabilised by drop wise addition of 1mL of 75% v/v ice-cold ethanol (VWR) for cyclin E1 analysis or 100% v/v ice-cold methanol (Sigma) for cyclin B1 or D1 analysis. The fixed cells were stored at -20 °C for up to 2 days prior to cyclin analysis or up to 2 weeks otherwise.

HFN 7.1 cells (aprox. $1*10^6$ cells/sample) were fixed and permeabilised by drop wise addition of 1 mL of 75% v/v ice-cold ethanol (VWR). The fixed cells were stored at -20 °C for up to 2 weeks prior to analysis.

Prior to flow cytometry analysis, fixed cell samples from the batch culture were washed with a rinsing solution with 1% w/v bovine serum albumin (Sigma) and 0.01% w/v sodium azide (Sigma Aldrich) in PBS. Similarly, fixed fed-batch cell samples were washed twice with 1% w/v fetal bovine serum (PAN Biotech GmbH) in PBS. The sample preparation continued either with the EdU detection, Ki-67 proliferation marker, cyclin staining, or DNA staining.

EdU detection

The cells were centrifuged, the rinsing solution removed and cell membrane permeabilisation was aided with 50µL of a saponin based wash reagent (component E, C10419, Invitrogen) following the vendor instructions for 15min at room temperature. The EdU was detected by adding 0.5mL of the click-IT reaction cocktail (prepared as per the vendor instructions). Incubation was performed for 30min at room temperature in the dark, followed by washing with the rinsing solution. The workflow continued with the Ki-67 proliferation marker or cyclin staining.

Ki-67 proliferation marker

The GS-NS0 cells were centrifuged, the rinsing solution removed and 50µL of a saponin based wash reagent was added. Then 20µL of a PE Mouse Anti-Human Ki-67 or the isotype (BD, 556087) were added to stain for the proliferation marker. Incubation was performed for 30min at room temperature in the dark, followed by washing with the rinsing solution. The protocol continued with the DNA staining.

The HFN 7.1 fed-batch cell pellet was re-suspended to a concentration of $1*10^7$ cells/100µL and 5µL FITC conjugated Mouse Anti-Human Ki-67 antibody was added

(556026, BD Pharmingen) for 30 minutes in the dark at room temperature. The protocol continued with the DNA staining.

Cyclins

The GS-NS0 cells were centrifuged, the rinsing solution removed and 50µL of a saponin based wash reagent was added. Antibodies used for cyclin staining were: mouse IgG1 anti-human cyclin B1 FITC-labelled (BD, 554108); mouse IgG1 FITC-labelled isotype control (BD, 554108); rabbit polyclonal IgG FITC-labelled anti-cyclin E1 (Bioss USA, bs-0573R-FITC); rabbit polyclonal IgG FITC-labelled anti-mouse isotype control (Bioss USA, bs-0296R-FITC); mouse IgG2a anti-human cyclin D1 FITC-labelled (Invitrogen, AHF0088); mouse IgG2a FITC-labelled isotype control (Invitrogen, MG2a01). The antibodies were used according to the supplier instructions. Briefly, incubation was performed at room temperature for 30min in the dark followed by washing with the rinsing solution. The protocol continued with the DNA staining.

DNA

The GS-NS0 cells were centrifuged, the rinsing solution removed and 1mL of rinsing solution was added. The DNA was stained by adding 1µL of FxCycle violet stain (Invitrogen, F10347). Alternately, after centrifugation and removing the rinsing solution, 1mL of 50µg/mL propidium iodide (PI; Sigma, P4170), 100µg/mL of ribonuclease A (Sigma, R4875) in PBS was added. Incubation was performed at room temperature for 30min in the dark.

The HFN 7.1 batch cell pellet was stained for DNA by adding 1mL of 50 µg/mL propidium iodide (PI; Sigma, P4170) and 100 µg/mL of ribonuclease A (Sigma, R4875) in PBS at room temperature for 30min in the dark. The HFN 7.1 fed-batch cell pellet was washed with 1% w/v fetal bovine serum (PAN Biotech GmbH) in PBS. DNA was stained by the addition of 0.5 mL 1 µg/ml propidium iodide (P4864, Sigma) and 100 µg/ml ribonuclease A (EN053, Thermo Scientific) in PBS and incubated for 30 minutes in the dark at room temperature.

Flow cytometry set-up

Flow cytometry was performed on a LSRFortessa (BD) at Imperial College. Two types of configuration were used depending on the staining. For samples stained for

cyclin and PI-stained DNA, or solely PI-stained DNA an excitation wavelength of 488 nm with a emission 530/30 filter was used for FITC and an excitation wavelength of 561nm with a emission 582/15 filter for PI. For all other samples using FxCycle-DNA stain an excitation wavelength of 405 nm with a emission 450/50 filter was used for the violet stain; 488 nm with a emission 530/30 filter was used for FITC; 561 nm with a emission 582/15 filter was used for PE; and an excitation wavelength of 640nm with a emission 670/14 filter was used for Alexa647. Apart from the isotype controls, unstained cell samples were used as negative controls, and single colour controls to compensate. 10,000 events/sample were collected.

At ETH a Calibur flow cytometer (BD) with an excitation wavelength of 488 nm was used. The PI was collected on a 585/42 filter and FITC on a 530/30 filter. Single colour controls were used for compensation and between 10,000-20,000 events/sample were collected.

Table 3.1. Flow cytometers configurations.

Flow Cytometer	Stains	Excitation Laser (nm)	Emission filter
LSRFortessa	PI-stained DNA	561	582/15
	FITC-stained cyclins	488	530/30
	FxCycle-DNA stain	405	450/50
	FITC-stained cyclins	488	530/30
	PE-stained Ki-67	561	582/15
	Alexa647-EdU stain	640	670/14
Calibur	PI-stained DNA	488	585/42
	FITC-stained Ki-67	488	530/30

3.3.7. Cyclin Quantification

The flow cytometry data was analysed using FlowJo software (Tree Star Inc). In order to analyse the data, a sequence of steps were followed:

1. First, the cell population was selected from the forward versus side scatter plot.
2. Then, a doublet discrimination analysis was performed based on the peak versus area plots of the DNA staining (i.e. PI or FxCycle).

3. In addition, the cell cycle (PI or FxCycle) histogram was gated to remove the apoptotic cells, debris, and aggregates.
4. The DNA histogram was de-convoluted using the software platform tool into G_1/G_0, S, and G_2/M.
5. Cyclin expression profiles were extracted from the bivariate plots (cyclin vs DNA) by:
    i. First a gate around the isotype-stained sample was applied to exclude any non-specific binding.
    ii. Above the non-specific binding region, a cyclin positive expression region was defined and gated (Figure 3.1).
    iii. The non-specific binding and cyclin positive region gates previously defined i-ii) were applied to each cell cycle phase (subpopulations of the DNA deconvolution).
    iv. The cyclin measured fluorescence and the corresponding isotype control (fluorescence) was compared for each of the deconvoluted cell cycle phases. This treatment standardizes the data to a common expression level using the isotype control as a reference.
    v. Finally, the data from step iv) were normalised assuming minimal cyclin expression at a corresponding cell cycle phase, which enables the cyclin quantification by comparison.
    vi. Overall, the selection of the normalisation is based on the collected data as it shows the results coherently. Specifically, cyclin D1 expression was assumed to be minimal in the S phase, cyclin E1 expression in G_2/M and cyclin B1 in G_1/G_0.

The dynamic cyclin expression profile can be re-constructed from the normalised cyclin expression vi) and the frequent experimental sampling points. This is done by plotting the cyclin content of the cell cycle phase that the partially synchronised moving population (after an arrest release) is traversing. Similarly, by plotting the cyclin content of the cell cycle phase that the positive or negative EdU population (after the copper catalysed reaction for EdU) is traversing, the dynamic cyclin profile is elucidated.

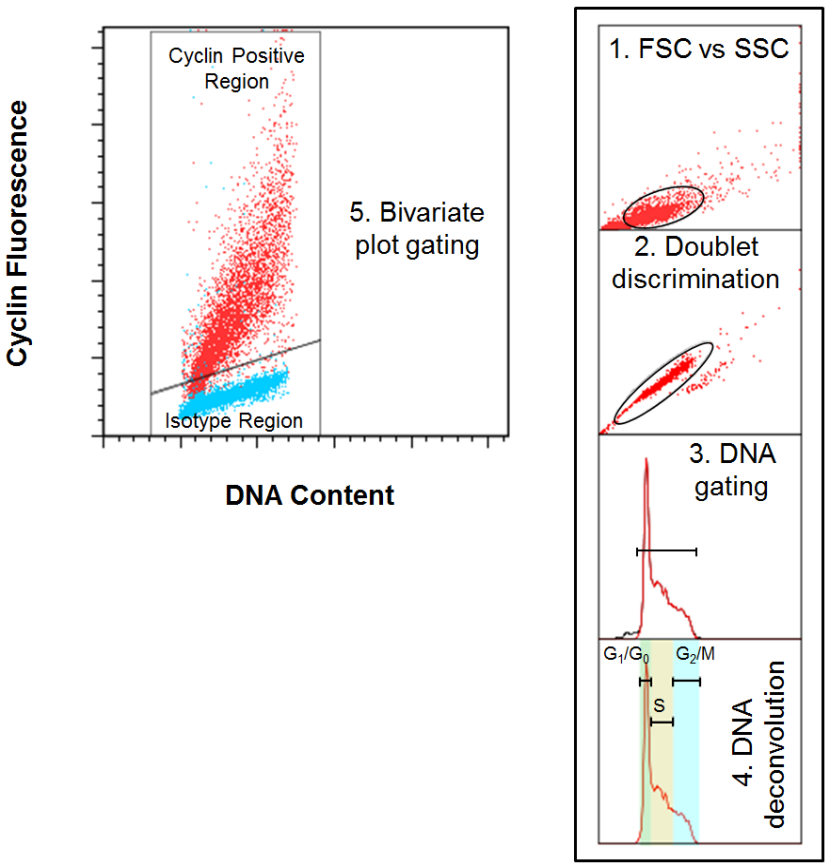


Figure 3.1. General flow cytometry data analysis for cyclin quantification. 1) Forward vs Side scatter, 2) DNA fluorescence area vs height, 3) DNA gating, 4) DNA deconvolution, 5) Bivariate cyclin vs DNA plot. Colour: Red - cyclin stained sample, blue – isotype stained sample.

3.3.8. Apoptosis analysis

The apoptosis analysis was carried by Chonlatep Usaku (PhD candidate). The fraction of early stage apoptotic (ESA) cells, late stage apoptotic (LSA) cells, and viable cells were determined by the Annexin-V-FITC (Biolegend, 640906) and Propidium Iodine (PI, Sigma-Aldrich, P4170) dual staining assay. The cell pellet (approx. $3*10^5$ cells) directly after harvesting (without fixation by alcohol) was re-suspended in Annexin binding buffer (Biolegend, 422201). Cells were initially stained with the Annexin-V-FITC according to the manufacturer instructions and then stained with 20 µg/mL of PI. The stained samples were incubated for 20 minutes in the dark at room temperature. The data collection was done using an LSRFortessa cell analyser (BD Biosciences) using an excitation wavelength of 488nm for Annexin-V-FITC and an excitation wavelength of 561nm for PI, and collected with a 530/30nm and a 610/20nm filter, respectively. At least 30,000 events were recorded for each sample and were then analysed using FlowJo software (Tree Star Inc).

3.3.9. Gene expression

Gene expression was carried out exclusively by Chonlatep Usaku (PhD candidate). The materials and method is shown herein for reference purposes, as some of the data is shown and used in the discussion in chapter 5.

RNeasy® Mini kit (Qiagen, 74104) was used to extract total RNA from the cell pellets as per the manufacturer instruction. The purity of the extracted RNA was assessed using Biophotometer (Eppendorf AG, Germany). The criterion of the ratio of the 260nm absorbance to the 280nm absorbance value being greater than 1.9 was used to determine the RNA purity. Total RNA was immediately used as a template to synthesise complementary DNA (cDNA) using Reverse Transcription System (Promega Ltd, A3500) as per the manufacturer instruction. The cDNA was synthesised using random primers as building blocks and the synthesis reaction was performed on the GS1 thermo cycle (G-Storm, UK) with a temperature profile starting at room temperature for 10 minutes, then at 42 °C for 40 minutes and finally storing at 4 °C. cDNA was then used as a template for the real-time PCR using StepOnePlus™ Real-Time PCR machine (Applied Biosystems, USA) with SensiFAST™ Hi-ROX SYBR (Bioline, BIO-92005). Dissociation curves were also conducted to check if any non-specific amplification occurred during the PCR reaction. By using $\Delta\Delta$Ct approach, the gene expressions of interest were shown in the form of the relative fold changes which were normalised to *gapdh* (housekeeping gene) and with respect to the sample at the beginning of the culture (day 0). Key transcriptional markers involved in both apoptosis and the cell cycle, were selected (Browne and Al-Rubeai, 2011).

3.3.10. Statistical analysis

Values represent the mean ± standard deviation (SD) and were based on triplicate experiments (unless otherwise stated). Statistical analysis of the results was performed with SigmaStat (Systat Software Inc.) using an analysis of variance (ANOVA) test to study the effect of treatments with a level of significance of $p<0.05$ with data drawn from a normally distributed population. If the data were drawn from a non-normally distributed population or with unequal variances, the Kruskal-Wallis

ANOVA on ranks was performed using the Student-Newman-Keuls method in order to make multiple comparison with a significance of $p<0.05$.

3.3.11. Model analysis and parameter estimation

Global sensitivity analysis

All models were implemented in gPROMS® modelling software and all computational tasks were performed using a desktop computer with an Intel® Core™ i7 CPU. As mentioned, biological models are usually non-linear and include several parameters of varying orders of magnitude. Therefore, GSA was applied as it is the preferred sensitivity analysis method for this type of systems. Output variables of interest were evaluated such as viable cell concentration, mAb titre, and the cell cycle fractions. The GUI-HDMR software tool was used for the GSA. The software combines the RS-HDMR method in a graphical user interface in MATLAB (Ziehn and Tomlin, 2009). The selection was based on the software availability, the low computational efforts of the method, and the computational burden of the PBMs.

The sampling points were generated using the sobolset function in MATLAB. The uncertainty associated to the model parameters was ±50% from the nominal values, which are taken from literature or experimental data when available and when are not available an approximated order-of-magnitude value is assigned (Sidoli et al., 2006). Each scenario was evaluated using the go:MATLAB tool of the gPROMS® modelling software. The gO:MATLAB allows an entire gPROMS model to be called as a single function from inside MATLAB. The sensitivity indexes (SIs) were calculated at characteristic time points (e.g. early exponential, exponential, decline phases) using the GUI-HDMR software by supplying the rescaled (between 0-1) input values (parameters) and the corresponding output values. The SIs are the result of the GSA and varies between 0 and 1, with 0 being not significant.

Parameter estimation and model validation

To evaluate the results SIs a threshold of 0.1 was selected, representing an experimental error of 10% (Sidoli et al., 2005). The SIs above the defined threshold, were identified as significant parameters and were re-estimated based on the experimental available data (as indicated on chapter 6 & 7). The non-significant parameters were fixed at their nominal value. All model and parameter estimation

calculations were implemented in gPROMS® (Process Systems Enterprise, 1997-2012). Parameter estimation in gPROMS is based on the Maximum Likelihood formulation, which provides simultaneous estimation of parameters in both the physical model of the process and the variance model of the measuring instruments.

The model predictions were compared to the experimental data after re-estimating the significant parameters. Similarly, the models were validated against independent experimental data not used in the previous model development steps.

CHAPTER 4

Cyclin Blueprint of the GS-NS0 Cell Line

In chapters 4 & 5, the cell cycle blueprint for the GS-NS0 cell line is presented. In particular in chapter 4, a set of experimental assays - chemical arrests and proliferation assays - are used to elucidate the cyclin profiles, timings, and thresholds. The expression of three cyclins (D1, E1, and B1) was studied by flow cytometry in batch cultures of GS-NS0. The different experimental assays consistently confirmed the observed cyclin blueprint. These results constitute the pillar for the cyclin distributed model presented in chapter 6, as well as lead to the experimental study carried in chapter 5.

4.1. Introduction

The cell cycle is at the centre of cellular growth and death as well as productivity, which vary during the different cell cycle phases. As presented it is divided in sequentially distinctive phases: G_1 (first gap), S (synthesis), G_2 (second gap) and M (mitosis). Moreover, when the conditions, either internally or externally, are not favourable for DNA synthesis, the cells enter a quiescent state "G_0" (Pardee, 1989). The transition between the cell cycle phases is highly regulated and it is closely linked with the cell programmed death (Fussenegger and Bailey, 1998). Two key classes of regulatory molecules, cyclins and cyclin-dependent kinases (CDKs), have been identified to regulate the transition process between cell cycle phases (Darzynkiewicz et al., 1996). Cyclins are regulatory units and have no catalytic activity, while CDKs are catalytic subunits and inactive in the absence of their cyclin partner with which they form a heterodimer.

The development of biologically relevant and mechanistically accurate mathematical models has been hindered by experimental and computational challenges. However, single cell analysis techniques such as flow cytometry provide quantitative cellular information (Darzynkiewicz et al., 2001) that can help to build biologically relevant models. In particular, bivariate analysis of cyclin expression alongside DNA content can prove to be a suitable biomarker for the cell cycle

transitions. As reported, progression between the G_1-S checkpoint is regulated by two cyclins, cyclins D and E (Turchi et al., 2000). Similarly, cyclin B1 is reported to regulate the cell's entrance into mitosis (Gong et al., 1993). Although a number of studies have dealt with cyclin regulation in various human cell lines (Darzynkiewicz et al., 1996; Frisa and Jacobberger, 2009; Gong et al., 1993), few have addressed this for industrially-relevant cell lines. Studies on industrially-relevant cell lines have mainly focused on the underlying mechanisms of the regulatory pathways (Ponzio et al., 1998; Turchi et al., 2000). Therefore, the cyclin phase-dependent expression profiles and thresholds for industrially-relevant cell lines are currently lacking, which can aid the development of biologically relevant cell cycle models.

4.2. Objectives

The aim of this chapter is to develop the cell cycle blueprint for the GS-NS0 cell line. The following scientific objectives were set:

- Design and perform GS-NS0 culture experiments that would allow elucidating the cell cycle blueprint.
- Identify the cyclin expression profiles, timings, and thresholds for cell cycle phase transition.
- Quantify the cyclin profiles to make them suitable for a mathematical model development.
- Estimate the cell cycle timings for the GS-NS0 cell line.

4.3. Methodology

A series of batch culture experiments covering both disturbed and undisturbed growth of the GS-NS0 cell line were carried out to study the cyclin expression by flow cytometry. The first set of experiments involved the disturbed growth by arresting the cells using two different DNA synthesis inhibitors (thymidine and DMSO). Simultaneous control runs, which were not treated with the chemical agents, were established. The undisturbed study consisted of a proliferation assay tracking a specific cell population that was active at DNA synthesis. All the specifics of the materials and methods were reported in chapter 3.

4.3.1. Studied cyclins

Three cyclins were investigated: two G_1 class cyclins (D1 and E1), and one G_2 cyclin (B1). The reason for studying two G_1 class cyclin is that Cyclin D expression is reported to remain invariable or at low level in normal proliferating cells (Gong et al., 1994; Gong et al., 1995), therefore a second G_1 class cyclin that regulates the G_1-S transition was also studied. Cyclin D1 was not studied in the proliferation assay.

4.3.2. Thymidine arrest

The use of different chemical agents DNA synthesis inhibitors (i.e. thymidine and DMSO) is aimed to arrest and synchronise a cohort or fraction of the cell population. After the cell arrest, the cells are re-suspended in fresh medium and "released from the arrest". The synchronised cohort was tracked following the criteria of aligned DNA content (Section 3.3.1.). The selection of the two inhibitors was based on their relevance (commonly used in previous studies) and the differences in the arrest mechanism (Kumar et al., 2007; Sunley and Butler, 2010).

Thymidine arrest mechanism involves the nonselective inhibition of potassium ion channels proteins (Ouadid-Ahidouch and Ahidouch, 2008) and indirectly arrests the cells in two phases G_1 and S. The cell cycle arrest using thymidine involved a double block (Harper, 2005). A control group including all the centrifugation and washing steps without exposure to thymidine was established. After the thymidine exposure, the cells were washed and re-suspended in fresh culture medium and batch cultured.

4.3.3. DMSO arrest

DMSO is a frequently used chemical agent in bioprocessing given its efficient and reversible arrest in the G_1 phase (Allen et al., 2008; Fiore and Degrassi, 1999). The arrest is attributed to an imbalance in the cell cycle regulation machinery caused by the DMSO (Fiore et al., 2002; Ponzio et al., 1998). Thus, DMSO provides a different arrest mechanism when compared to thymidine. A single block using DMSO was added to mid-exponential growing cells. A control group, including all the centrifugation and washing steps without exposure to DMSO was established. After

the exposure, the cells were washed and re-suspended in fresh culture medium and batch cultured.

4.3.4. Proliferation assay

Cell proliferation assays provide a direct way to study cell proliferation by tracking a specific initial population that was active at DNA synthesis. Moreover, the short duration and low concentration of the EdU proliferation assay pose a minor disturbance to the cell culture (Cappella et al., 2008). After the EdU exposure, the cells were washed and re-suspended in fresh medium and batch cultured. A control group was established, including all the centrifugation and washing steps without exposure to EdU.

4.3.5. Cyclin quantification

The flow cytometry data was analysed as described in the materials and methods (Section 3.3.7.). Briefly, the cell population is gated for doublet discrimination, apoptotic cells, debris, and aggregates. The DNA was deconvoluted using the software platform to identify three cell cycle phases (G_1/G_0, S, G_2/M). The cyclin expression is extracted from the bivariate plots (cyclin fluorescence vs DNA). Both a non-specific binding region (isotype-stained samples) and a positive expression region (above isotype expression) are defined. These regions are applied to each deconvoluted cell cycle phases. The cyclin measured fluorescence is compared to the corresponding isotype control (fluorescence) for each cell cycle phase. Finally, the data from the previous step were normalised assuming minimal cyclin expression at a corresponding cell cycle phase, which enables the cyclin quantification by comparison. Cyclin D1 expression was assumed to be minimal in the S phase, cyclin E1 expression in G_2/M (Gong et al., 1994) and cyclin B1 in G_1/G_0 (Gong et al., 1993). Then, the dynamic cyclin expression can be re-constructed from the normalised cyclin expression and the frequent experimental sampling points.

4.4. Results & Discussion

4.4.1. Cell arrest

The differences between the thymidine double block and DMSO single block arrest were evident at different levels. First, differences in the cell cycle distributions (Figure 4.1A) were observed when compared to the control runs. The thymidine arrested the cells both in the G_1 (50% of the population, $p<0.05$) and early S phase (Figure 4.1C, t=0h). The DMSO exposure resulted in a significant fraction (approx. 75%, $p<0.05$) of cells arrested in G_1 (Figure 4.1B) when compared to the control cultures (and thymidine). DMSO proved to be more efficient as a higher fraction of cells was arrested in the G_1 phase. However, the arrest fraction is dependent on the DMSO concentration, as well as exposure time (Fiore et al., 2002; Ling et al., 2003; Liu et al., 2001; Wang et al., 2004). Moreover, the effectiveness to group the cells in the G_1 phase using thymidine depends on the timings of the double block (Harper, 2005).

Secondly, the time taken for the cells to resume proliferation (after removing the chemical agents) was different. Thymidine arrest appeared to be less severe and easily reversed, as a cohort of cells resumed proliferation after 2h (Figure 4.1C, E). The partially synchronised population was investigated for 10h until it was no longer possible to distinguish it, as the culture re-established an asynchronous growth. After the DMSO arrest release, the cells resumed proliferation after 12h (Figure 4.1D, E). The synchronised population was studied between 12 and 24 h following the release until it was no longer possible to distinguish it. Initial estimates of the cell cycle timings are inferred from the synchronised moving populations. Specifically, the thymidine synchronised population readily exits G_1 towards the S phase (in the first 2h), and then leaves completely the S phase after 4-6h. Similarly, the G_2/M phases is traversed in 4h (Figure 4.1E). The DMSO synchronised population resumed proliferation after 12h and completes the G_1 phase in approximately 4-6h, accompanied with an increase in the S phase population. However, these initial timing estimates need further validation due to the disruptive nature of the arrest experiments. The differences in the time to resume proliferation can be attributed to the different arrest mechanisms (Figure 4.1E).

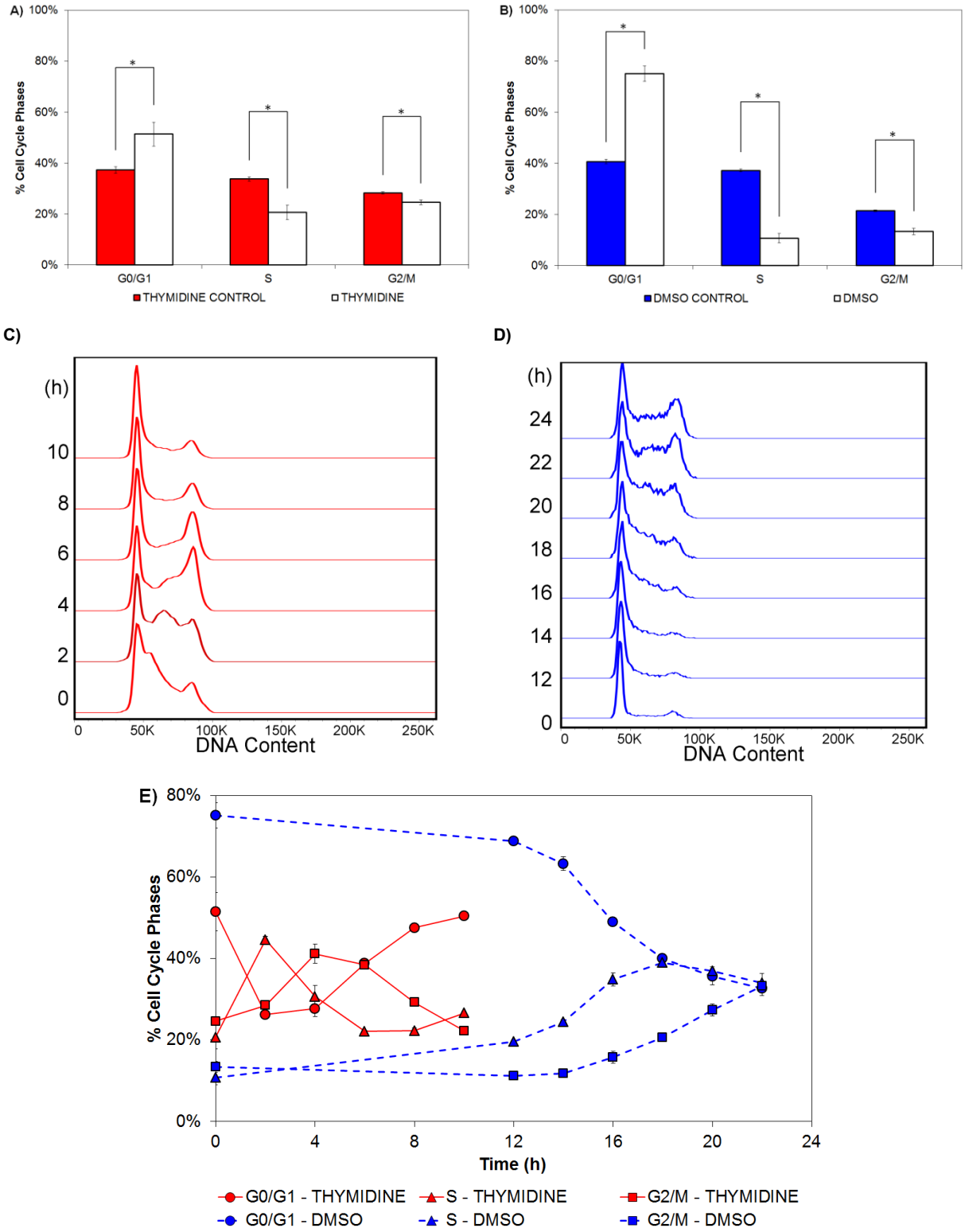


Figure 4.1. Comparison thymidine arrest versus DMSO arrest. A) Thymidine arrest and control cell cycle distributions; B) DMSO arrest and control cell cycle distributions; C) DNA histograms following the thymidine cell cycle arrest release; D) DNA histograms following the DMSO cell cycle arrest release; E) Cell cycle distribution after arrest release. *Statistically significant ($p<0.05$).

The thymidine arrest mechanism has been reported (Harper, 2005; Ouadid-Ahidouch and Ahidouch, 2008; Sunley and Butler, 2010) to be associated with an amino acid imbalance due to the excess of thymidine, as well as the non-selective inhibition of the potassium ion channel proteins (stimulating Ca^{2+} influx, as well as CDK and cyclin oscillation). Thus, after thymidine removal, the imbalance and blockage seemed to be promptly reversed and proliferation is resumed soon after. In contrast, the DMSO arrest seemed to have a more pronounced effects on the cell cycle machinery, which is supported by previous reports (Ponzio et al., 1998; Wang et al., 2004). Particularly, DMSO inhibits the synthesis of cyclin D2, introducing an imbalance in the levels of p27[KIP1] and p21[CIP1]. Both CDIs (p27 and p21) act in concert to inhibit the cyclin E1/CDK2 complex, selectively arresting in the G_1 phase. This was supported both qualitatively and quantitatively by comparing the cyclin bivariate fluorescence plots with respect to the DNA content of the arrest and control groups. In the thymidine case, no major alterations are observed in the cyclin fluorescence side histograms (Figure 4.2A-C). Some differences are observed in the cyclin B1 side histogram, although it can be attributed to the variation of the cell cycle distributions (Figure 4.2C). In contrast, the DMSO cyclin fluorescence side histograms showed noticeable qualitative alterations (Figure 4.3A-C). Such differences were quantitatively confirmed to be statistically significant for the lower cyclin E1 and D1 expression following DMSO release (Figure 4.3A-B). These variations support the longer time to restart proliferation for the arrested population in G_1. Nonetheless, once proliferation was resumed the time to establish an asynchronous growth was comparable (10-12h) for both arrest protocols.

Despite the observed differences, single cell attributes can be inferred by monitoring the partially synchronised moving populations after the arrest release. Particularly, initial estimates of the cell cycle can be inferred, as well as the dynamic evolution of the cyclin profiles (Section 4.4.3.).

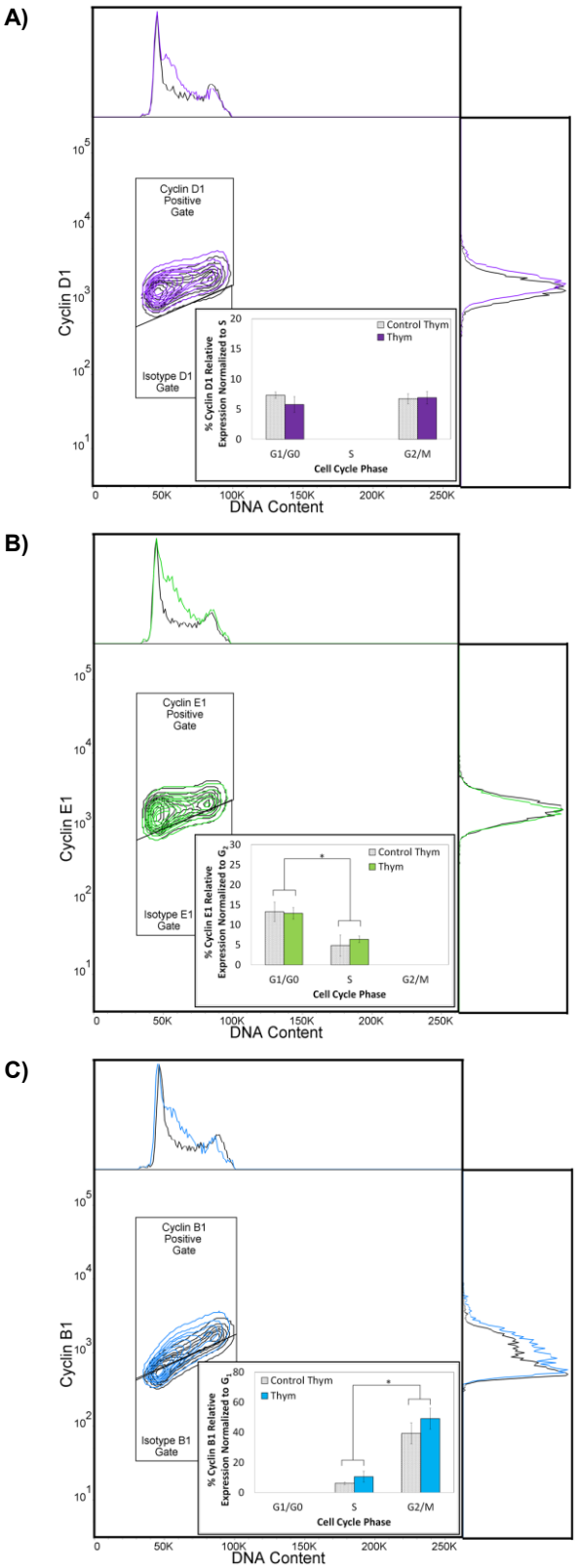


Figure 4.2. Bivariate cyclin fluorescence plots with respect to DNA at time=0h after thymidine arrest: Top adjunct histogram shows DNA distribution; right side adjunct histogram shows cyclin fluorescence distribution; and embedded bar chart presents cyclin fluorescence quantification for each cell cycle phase (n=3, error bars = standard deviation) . A) Cyclin D1; B) Cyclin E1; C) Cyclin B1. Colour notation: purple for Cyclin D1, green for Cyclin E1, blue for Cyclin B1, black for control groups. Gates reflect the isotype region versus the positive defined region for each cyclin. *Statistically significant ($p<0.05$).

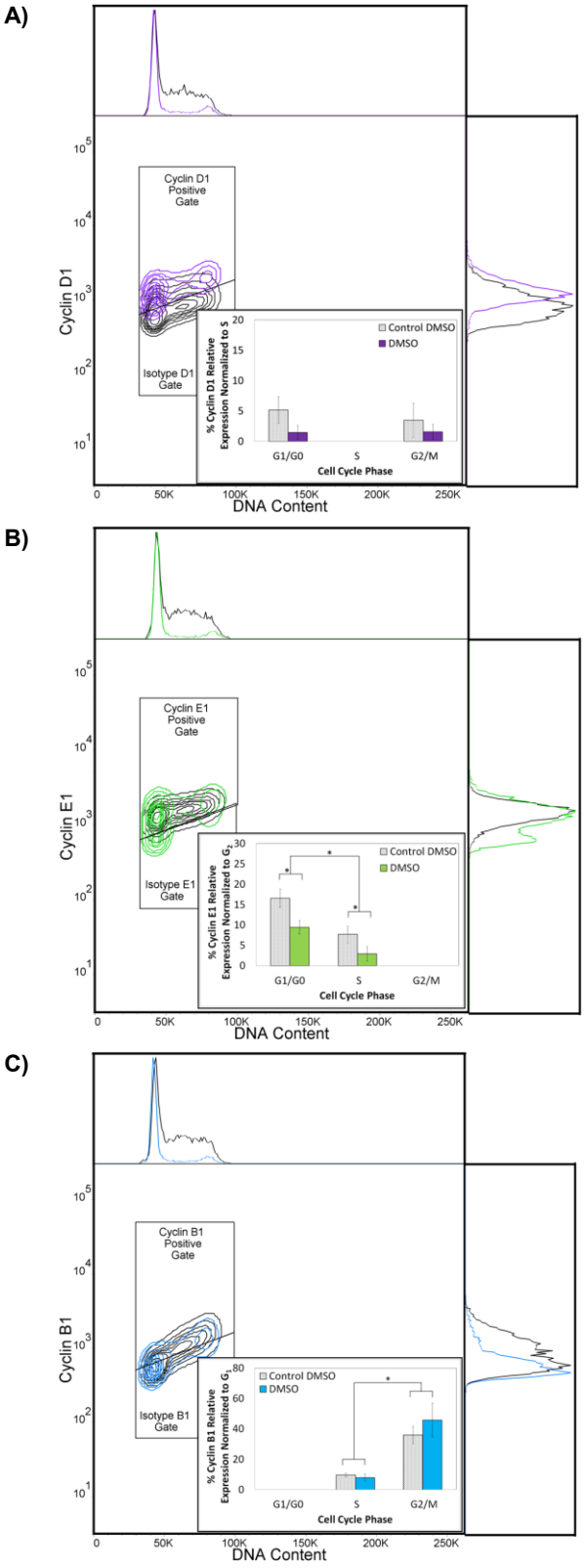


Figure 4.3. Bivariate cyclin fluorescence plots with respect to DNA at time=0h after DMSO arrest: Top adjunct histogram shows DNA distribution; right side adjunct histogram shows cyclin fluorescence distribution; and embedded bar chart presents cyclin fluorescence quantification for each cell cycle phase (n=3, error bars = standard deviation). A) Cyclin D1; B) Cyclin E1; C) Cyclin B1. Colour notation: purple for Cyclin D1, green for Cyclin E1, blue for Cyclin B1, black for control groups. Gates reflect the isotype region versus the positive defined region for each cyclin. *Statistically significant ($p<0.05$).

4.4.2. Proliferation assay

A specific population active at DNA synthesis was identified by labelling the DNA base analogue (i.e. EdU) introduced into its DNA. Further, two populations can be distinguished based on the EdU reaction: a positive population that was active at DNA synthesis, and a negative population that did not incorporate the EdU into its DNA (Figure 4.4A). The average transit times based on the DNA content (i.e. G_0/G_1, S and G_2/M phases) are estimated by tracking the EdU positive and negative cells (Figure 4.4B-C).

From the EdU positive population (Figure 4.4B) the G_2/M time is estimated. The population entered between 0-2h of culture the G_2/M phase (as indicated by the increase in the fraction). Likewise, a significant increase in the G_1/G_0 phase is observed at 4h, indicating that the initial EdU positive population transit through the G_2/M phase in approximately 4h. Further, an increase in the S phase fraction (which was minimal between 8-10h) was observed at 12h. Thus, it can be inferred that the population that entered G_1/G_0 at 4h, completed the transition at 12h, for an average 8h traverse of the G_1/G_0 phase. The S phase estimate is based on the EdU negative population (Figure 4.4C). The negative G_1/G_0 population exit the phase at approximately 2h, with the simultaneous increase in the S phase. The S phase cell fraction peaks at 8h, with the concurrent increase in the G_2/M phase. Thus, a traversing time for the S phase of approximately 6h can be estimated. A total average cycle or doubling time of 18h is calculated under the given experimental conditions for the GS-NS0 cell line. This value is in agreement with the previous reported maximum growth rate of $0.04h^{-1}$ that corresponds to a doubling time of 17.3h (Kiparissides, 2012). The estimated duration of cell cycle phases from the proliferation assay confirmed the previously observed timings after the arrest release. As in the arrest experiments, single cell attributes (i.e. dynamic cyclin profiles) can be estimated on the identified specific moving populations.

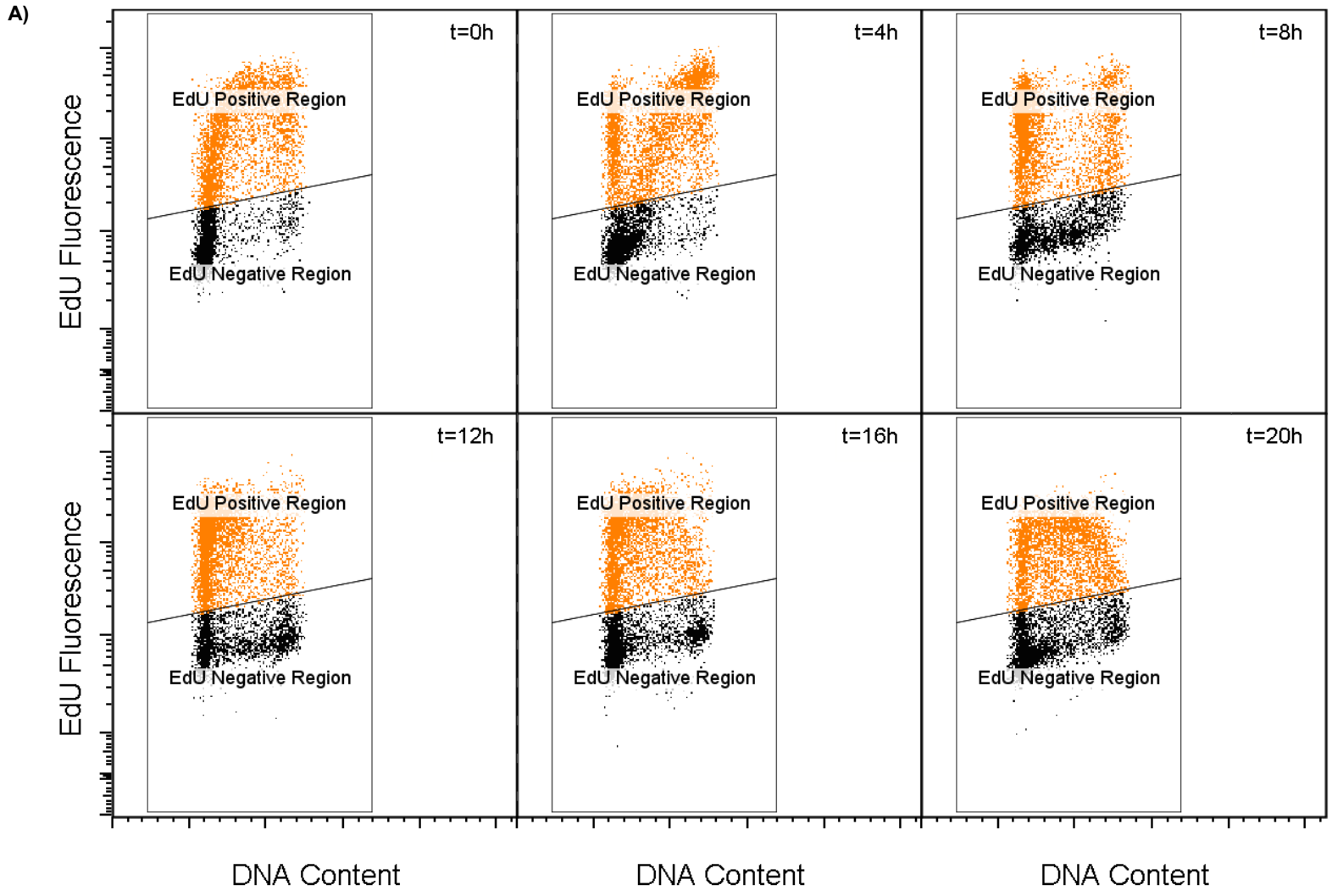


Figure 4.4. Cell cycle distribution proliferation assay. A) EdU versus DNA time bivariate plots; B) EdU Positive Population; C) EdU Negative Population; (n=3, error bars=standard deviation).

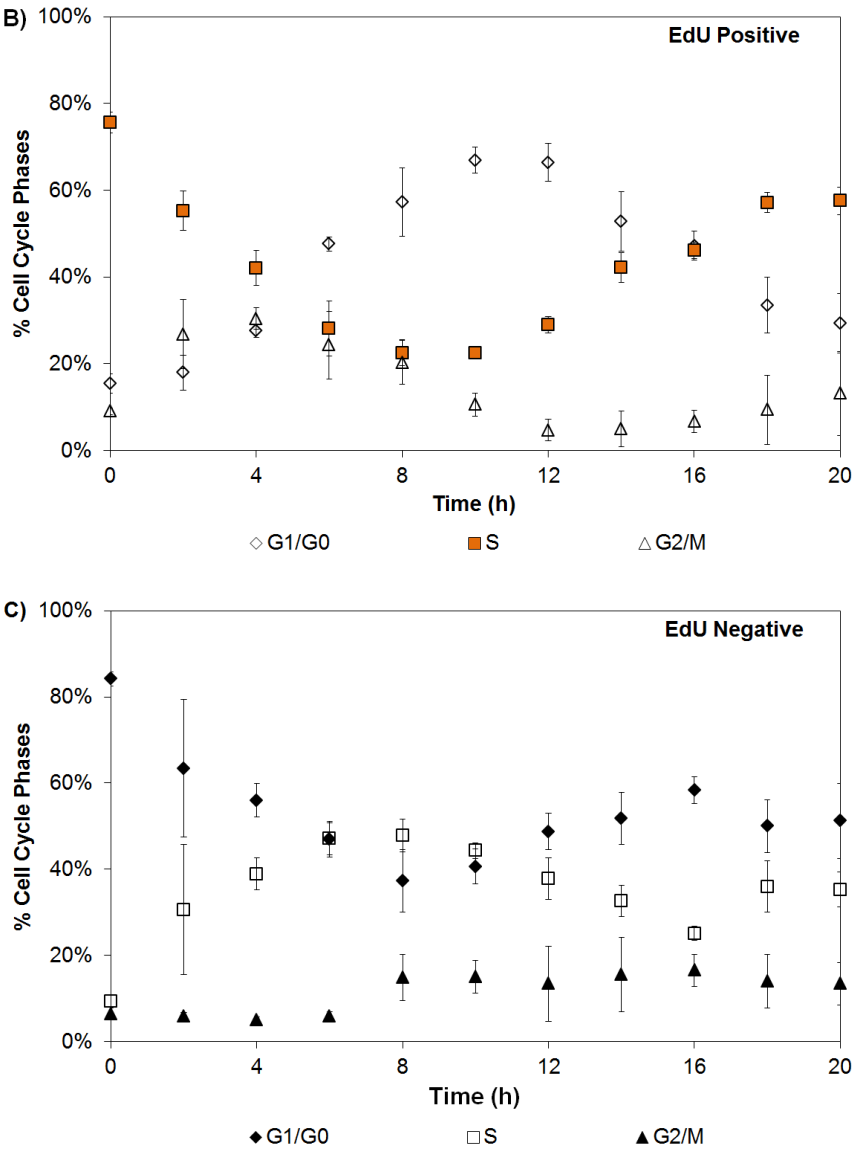


Figure 4.4. (Continued). Cell cycle distribution proliferation assay. A) EdU versus DNA time bivariate plots; B) EdU Positive Population; C) EdU Negative Population; (n=3, error bars=standard deviation).

4.4.3. Dynamic cyclin profiles

The control experiments established the baseline of the cell's behaviour. Therefore, average cyclin expression levels of the normal cell behaviour (representative of the control runs) are shown in Figure 4.5. Overall a good agreement among the different control experiments was observed. In particular, cyclin E1 and cyclin B1 showed a statistically significant difference in the cyclin expression between the phases. Contrary, cyclin D1 did not show statistical variation.

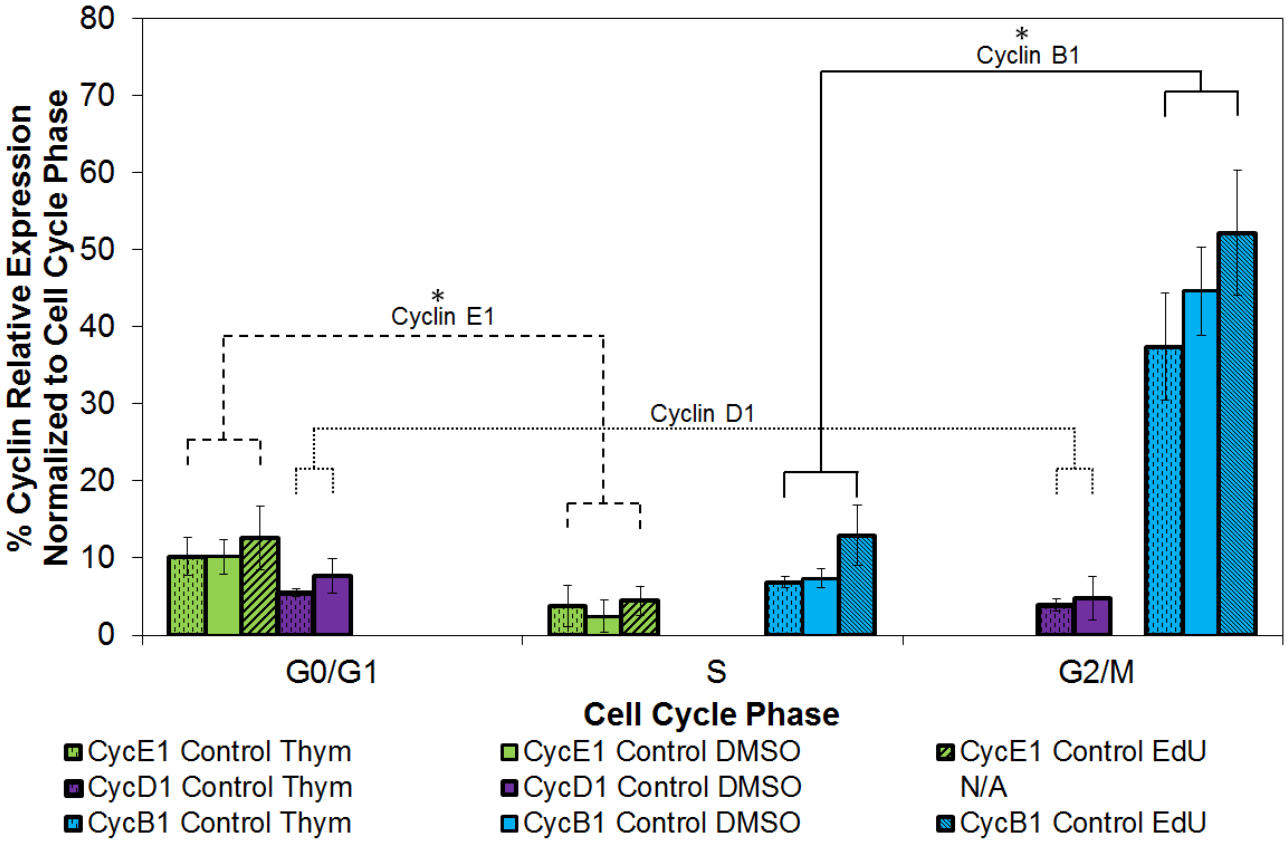


Figure 4.5. Average cyclin expression levels for the control experiments for the first 24h. Notation: vertical dashed pattern bars represent the thymidine control group, solid bars represent the DMSO control group, diagonal pattern bars represent EdU control. Cyclin E1 (green), Cyclin D1 (purple), and Cyclin B1 (blue). *Statistically significant ($p<0.05$).

The identified statistical difference of cyclin E1 and cyclin B1 was further investigated in the control runs of the arrest experiments over the first 4 days. The cyclin profiles were split through the S phase (in four regions, S1 to S4) using the DNA content as criteria (Figure 4.6). Cyclin E1 expression (Figure 4.6A) showed a significant difference ($p<0.05$) between G_1/G_0 and the S phase starting from the S2 region onwards (S3-S4). This subdivision and statistical analysis aid the establishment of the cyclin E1 threshold, which can be narrowed to the transition from G_1/G_0 to the S1 phase subdivision at the presented levels. Cyclin B1 expression (Figure 4.6B) was found significantly different ($p<0.05$) from the S phase regions (S2 to S4) to the G_2/M expression. The cyclin B1 profile increased along the S phase and peaked at G_2/M, which suggests the fast build-up and threshold of the cyclin.

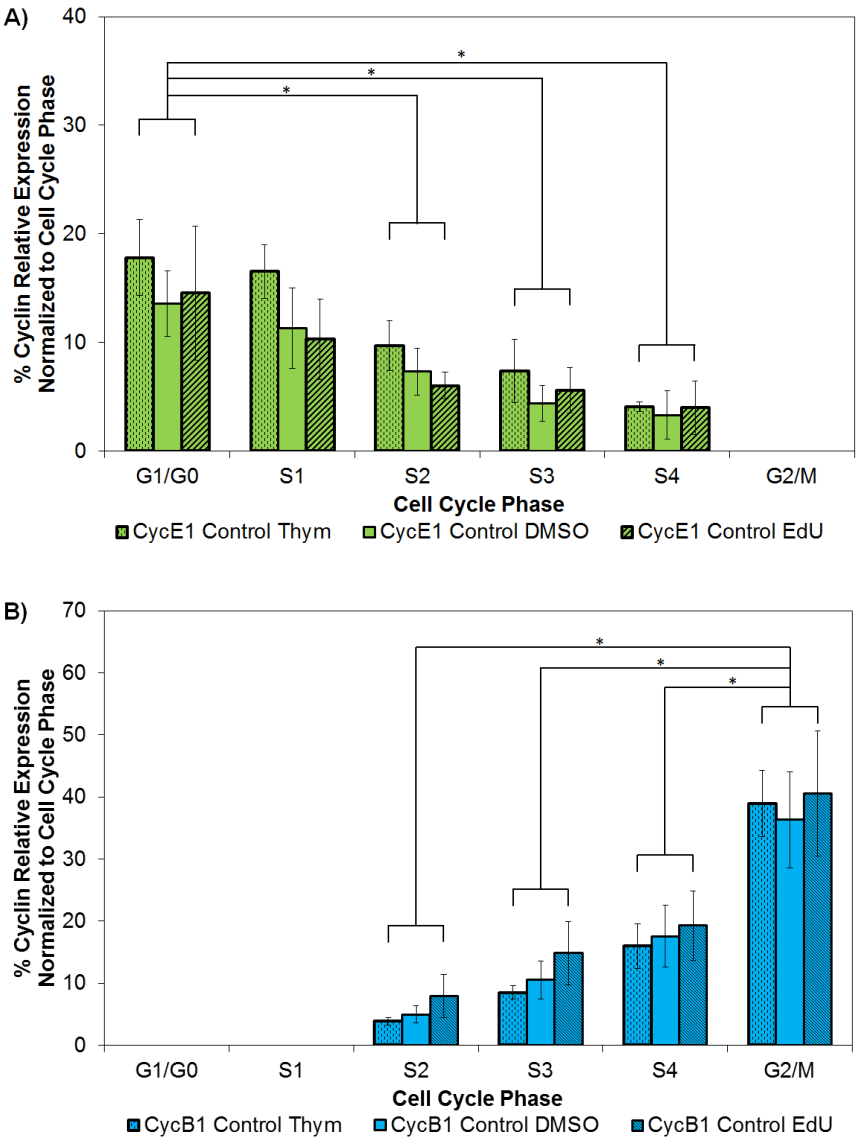


Figure 4.6. Average cyclin expression levels for the arrest control experiments over 4 days of batch culture. A) Cyclin E1 expression; B) Cyclin B1 expression. Notation: vertical dashed bars represent the thymidine control group, solid bars represent the DMSO control group, diagonal patterned bars represent the EdU control group, (n=3, error bars=standard deviation). *Statistically significant ($p<0.05$).

The presented profiles do not account for the dynamics of the system. However, the study of the partially synchronised populations (after the arrest release) and the EdU populations (from the proliferation assay) can aid to elucidate the dynamics of the cyclin blueprint. Thus, the normalised cyclin expression for each time point of the different identified moving population traversing a particular cell cycle phase (as observed in the cell cycle distribution) was plotted.

Cyclin E1

The cyclin E1 profiles are shown both for the synchronised moving population after the arrest experiments (Figure 4.7A-B) and for the identified populations of the proliferation assay (Figure 4.7C-D). The profiles showed a consistent pattern of expression. Briefly, cyclin E1 was normalised to be minimum in G_2/M phase (Gong et al., 1994). Cells that would transit the G_1 phase would show a positive cyclin expression usually of at least 8% (Figure 4.7A). Cyclin E1 build-up (taking approximately 6h) was observed in populations that were clearly identified as entering and progressing through the G_1 phase (Figure 4.7B-D).The previously suggested threshold was confirmed to be consistently at least 15%. Similarly, the cyclin E1 degradation after the G_1-S transition was observed to be fast, taking less than 2h to levels below 6%. An increasing number of cyclin E1 positive cells (cells expressing cyclin E1 above the isotype control) is associated with the build-up of the cyclin levels. Consistently, the percentage of cyclin E1 positive cells were maximum (above 90%) near the G_1-S transition.

Cyclin B1

Cyclin B1 showed a consistent pattern of expression among the different experiments (Figure 4.8). The cyclin B1 expression was normalised to the G_1 phase based on the assumption that its expression is minimum at this phase (Pozarowski and Darzynkiewicz, 2004). Cyclin B1 increased from minimal at G_1, to between 10-20% while traversing the S phase, towards a maximum in the G_2/M phase. Once the populations entered G_2/M phase the expression grew rapidly, in approximately 2h to a maximum and threshold of 40-50%. Finally, after the G_2/M to G_1 transition the cyclin is rapidly degraded. Cyclin B1's expression is associated with an increase in the percentage of cyclin B1 positive cells (cells expressing cyclin B1 above the isotype control). Consistently, the lowest percentage (below 50%) of positive cyclin B1 cells was observed in G_1/G_0 phase. In the S phase the percentage rapidly increased towards the transition S to G_2/M, up to 80-90%.

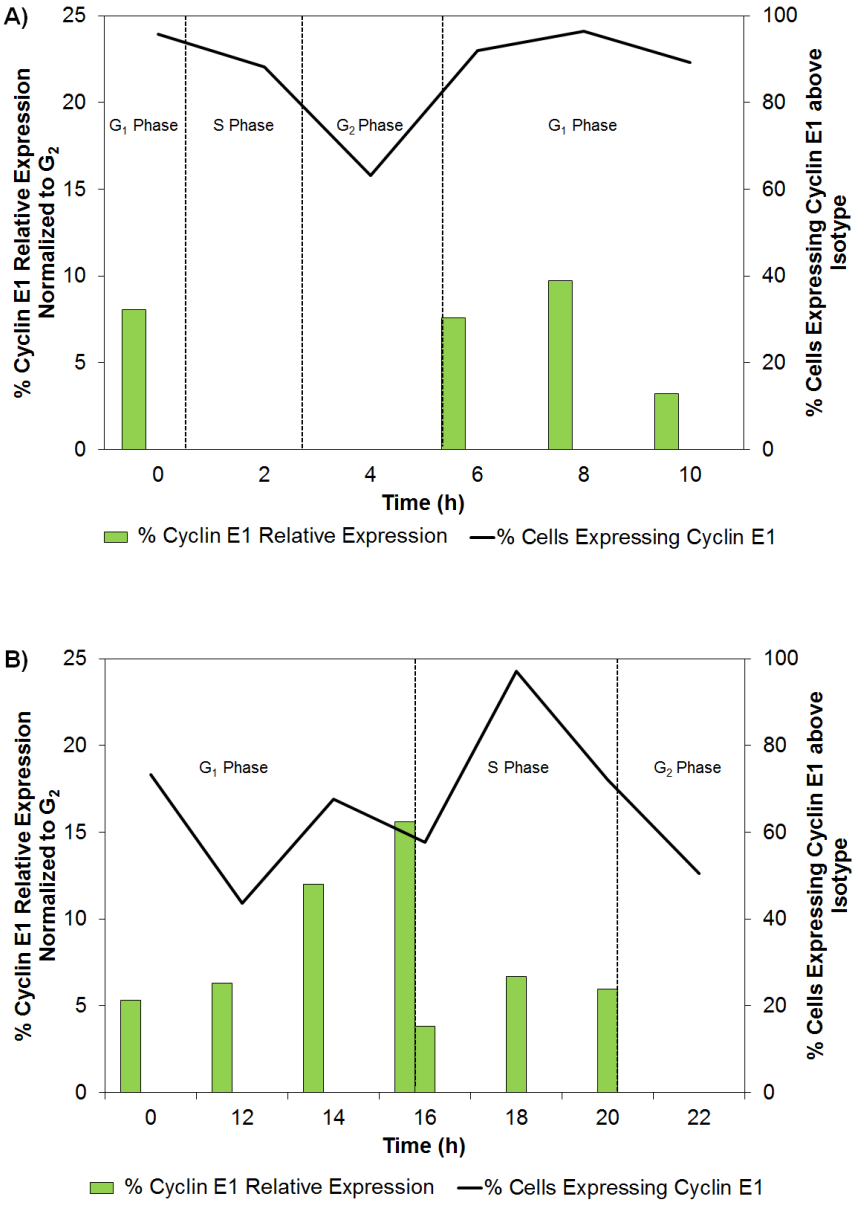


Figure 4.7. Cyclin E1 expression profiles. A) after thymidine arrest release; B) after DMSO arrest release; C) EdU positive cells; D) EdU negative cells. Notation: bars represent % cyclin relative expression normalised to cell cycle phase (left axis) and the solid line represents % cells expressing cyclin above isotype control (right axis).

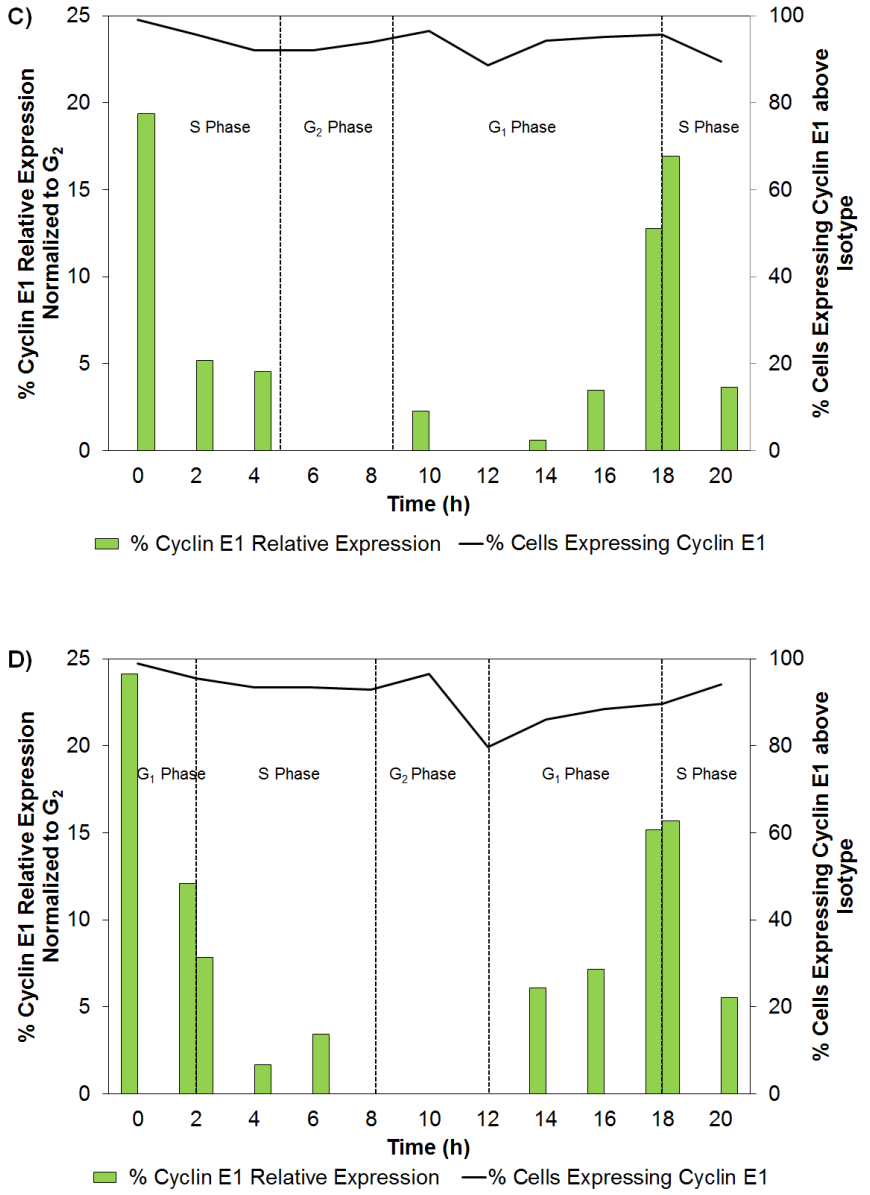


Figure 4.7. (Continued). Cyclin E1 expression profiles. A) after thymidine arrest release; B) after DMSO arrest release; C) EdU positive cells; D) EdU negative cells. Notation: bars represent % cyclin relative expression normalised to cell cycle phase (left axis) and the solid line represents % cells expressing cyclin above isotype control (right axis).

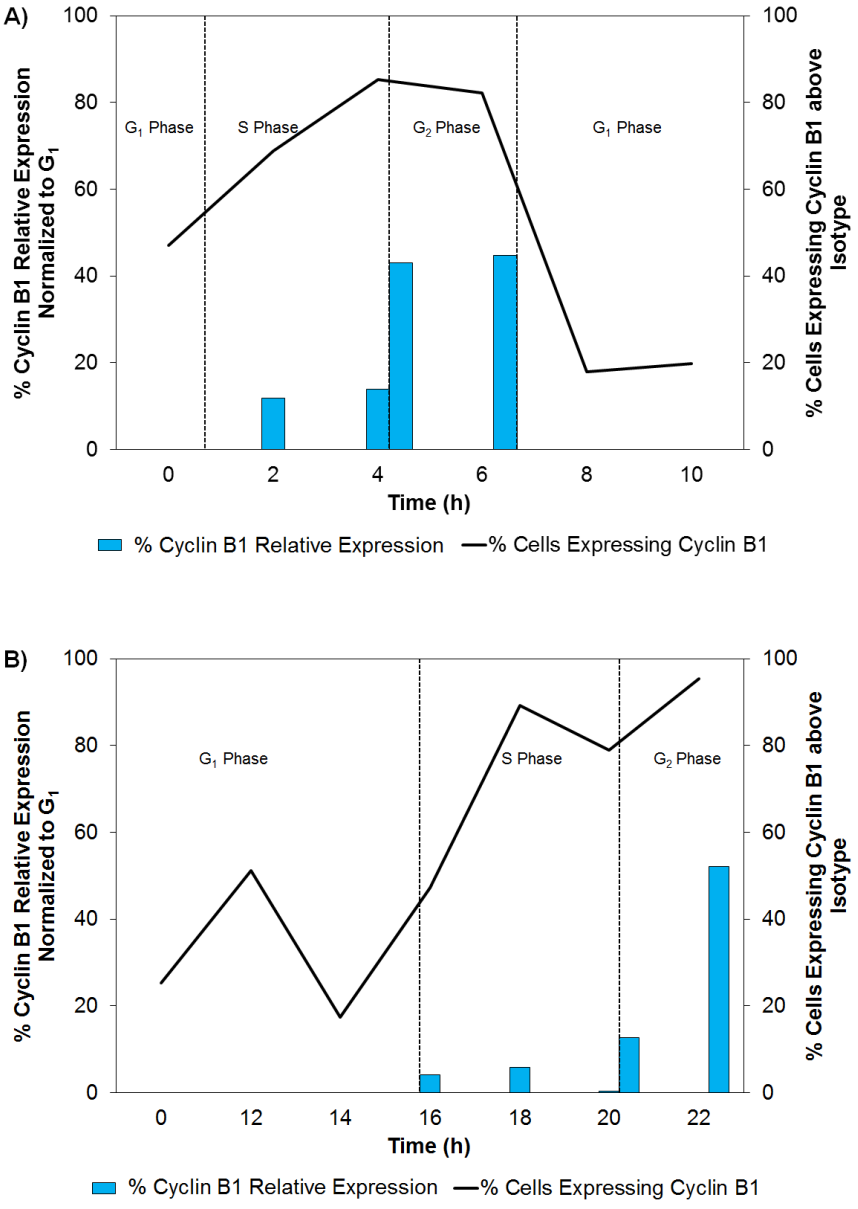
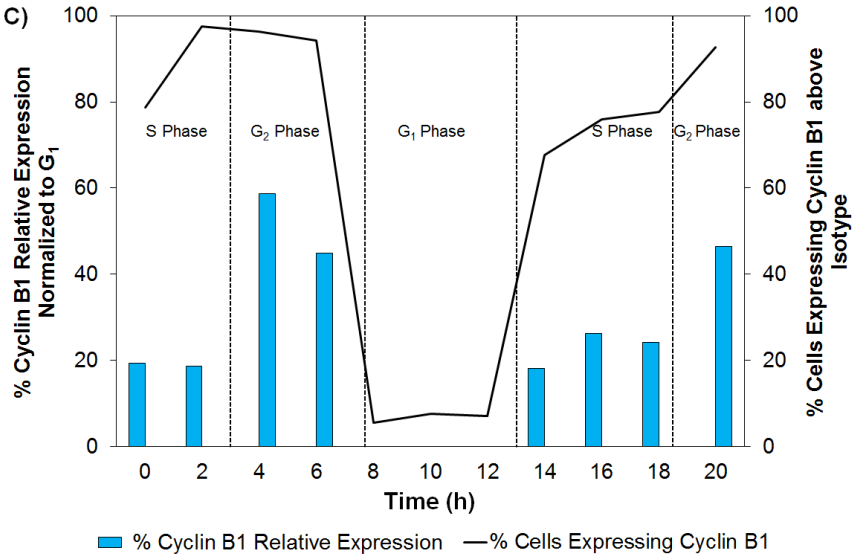


Figure 4.8. Cyclin B1 expression profiles. A) after thymidine arrest release; B) after DMSO arrest release; C) EdU positive cells; D) EdU negative cells. Notation: bars represent % cyclin relative expression normalised to cell cycle phase (left axis) and the solid line represents % cells expressing cyclin above isotype control (right axis).



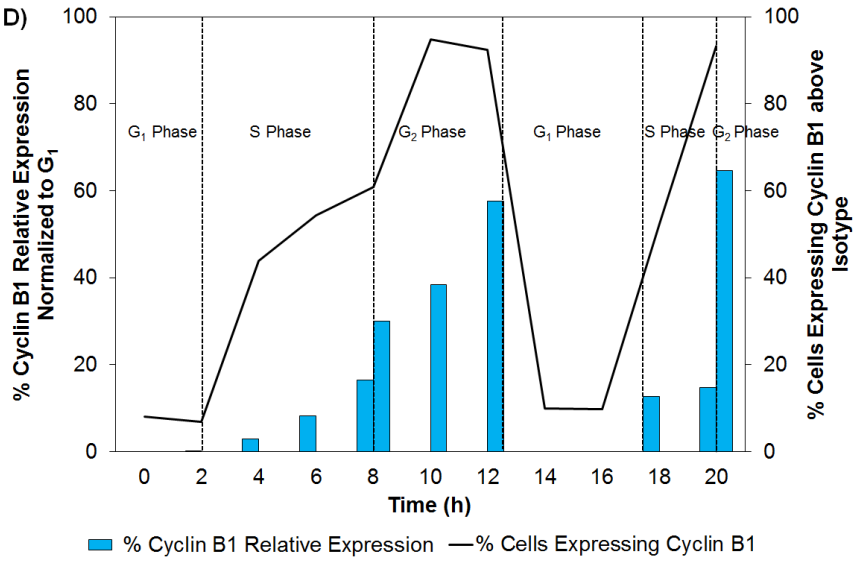


Figure 4.8. (Continued). Cyclin B1 expression profiles. A) after thymidine arrest release; B) after DMSO arrest release; C) EdU positive cells; D) EdU negative cells. Notation: bars represent % cyclin relative expression normalised to cell cycle phase (left axis) and the solid line represents % cells expressing cyclin above isotype control (right axis).

Cyclin D1

Cyclin D1 showed a less conserved profile (Figure 4.9), which did not vary significantly between the cell cycle phases. The cyclin D1 expression was analysed by normalising to the S phase. Despite considering other normalisation alternatives (i.e. G_1 or G_2 phase), no clear profile was observed. Overall, cyclin D1's expression profile varied between 4-8% when the moving population traversed either G_1 or G_2/M phases. Following the thymidine release, a high percentage of cyclin D1 positive cells (above 90%) was observed (Figure 4.9A). However, after the DMSO release when cyclin D1 expression is low, a high percentage of cyclin D1 positive cells was observed and vice versa. Due to observed differences, the cyclin D1 profile cannot be fully established. The observed fairly invariable cyclin D1 profile is in agreement with previous studies (Gong et al., 1995; Stacey and Hitomi, 2008). In addition, cyclin D have been reported to provide a link between the external environment and the actual cell cycle machinery (Sherr, 1993). The observed patterns reported herein seemed to indicate the proliferative state of the population (either with the percentage of cyclin D1 expressed or a high percentage of cells expressing cyclin D1).

Further analysis of the cyclin expression was carried considering the availability of glutamate, which is key for the GS cell line and it was usually exhausted between day 2 and 3 under the culture conditions (Section 4.4.4.). The analysis revealed that all the cyclins (D1, E1, and B1) showed a significantly lower expression ($p<0.05$) after glutamate was exhausted from the medium (Figure 4.10). These results suggest the existing link between the culture conditions and cell cycle machinery.

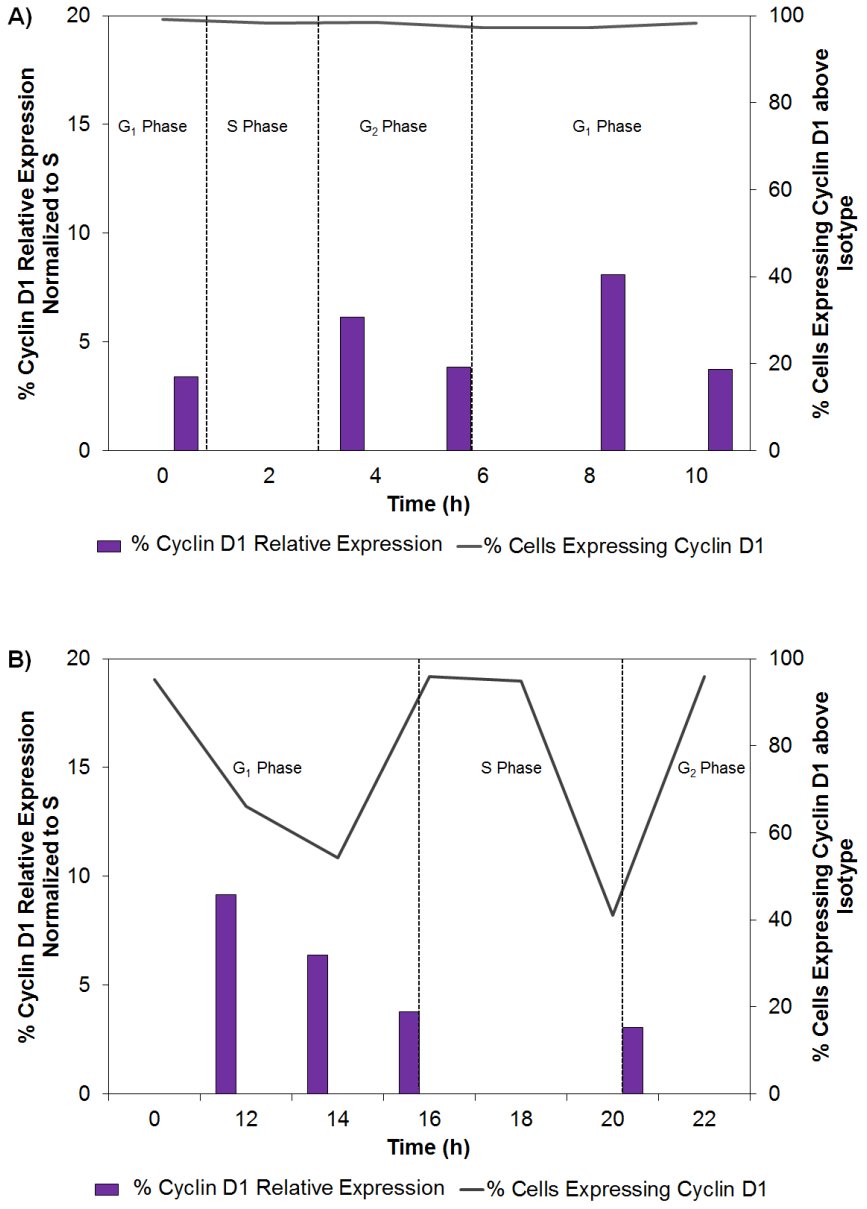


Figure 4.9. Cyclin D1 expression profiles. A) after thymidine arrest release; B) after DMSO arrest release. Notation: bars represent % cyclin relative expression normalised to cell cycle phase (left axis) and the solid line represents % cells expressing cyclin above isotype control (right axis).

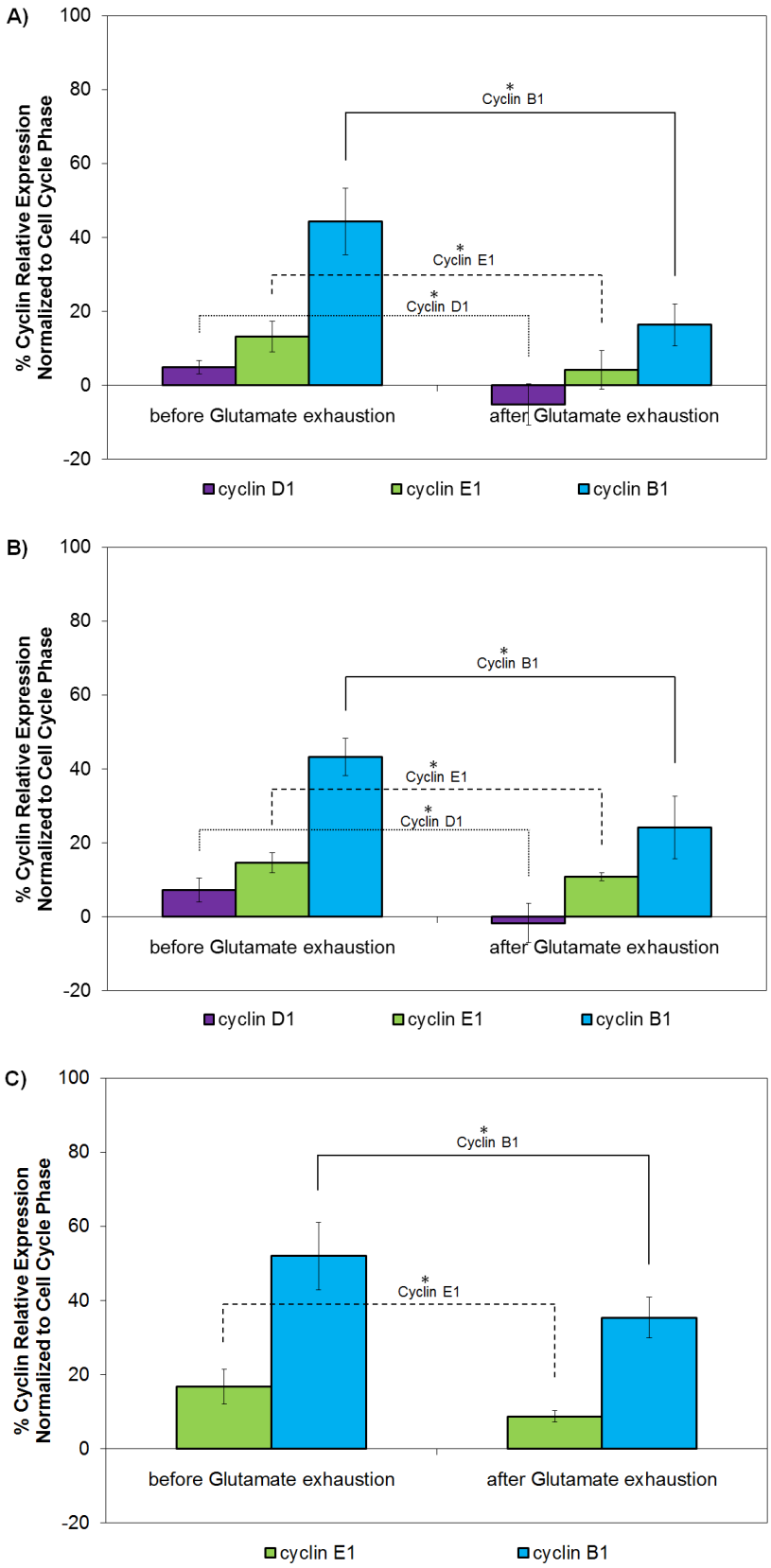


Figure 4.10. Average cyclin expression before and after glutamate exhaustion. A) after thymidine arrest release; B) after DMSO arrest release; C) Proliferation assay; (error bars=standard deviation). *Statistically significant ($p<0.05$).

4.4.4. Batch cell culture profiles

The batch culture profiles are presented in this section. Cell growth was similar across all batch cultures (Figure 4.13A). No statistical differences were identified in the cell density between the corresponding control and proliferation assay or after arrest release culture. The thymidine control and after arrest culture showed a significant higher ($p<0.05$) cell density at 96h. This could be attributed to the handling of the cells prior to start the batch cultures, as the thymidine experiment required a double block. Therefore, the cells treated with thymidine (and control) were centrifuged two times more than any of the other cultures. However, this did not have an effect on the mAb titre between all the control groups (Figure 4.13B). The DMSO treated culture did show a significantly ($p<0.05$) lower mAb titre after 72h of culture. Although DMSO has been used to increase productivity in hybridoma cells (Wang et al., 2004), there are no reports on the DMSO effects after arrest release.

The viability was consistently around 90% in all experiments for the first 96h of culture (Figure 4.13A). After 96h the viability rapidly decreased. The decrease in viability is associated with the exhaustion of glutamate (key amino acid for the cell line), which gets exhausted between 48-72h of culture (Figure 4.13C). After 72h, the glutamate concentration is below the detection limit (i.e. 0.2mM) and remains below detection in most cases. In few experiments, glutamate presence is detected at 144h. The late detection of glutamate could be plausibly associated with cell lysis, although the possibility that it is synthesised from other sources cannot be discarded.

The cell marker Ki-67 was used to determine the proliferative state of the cell population and discriminate between the G_0 and G_1 fractions in the proliferation assay. A high proliferative state was observed and it is highly correlated with the cell viability (Figure 4.13D). The decline of the cell viability was accompanied by a drop in the positive percentage of Ki-67 cells, indicating that some of the cells are entering the non-proliferative state (G_0). The commitment to apoptosis in the G_0 phase cannot be confirmed, as it was not quantified in these experiments.

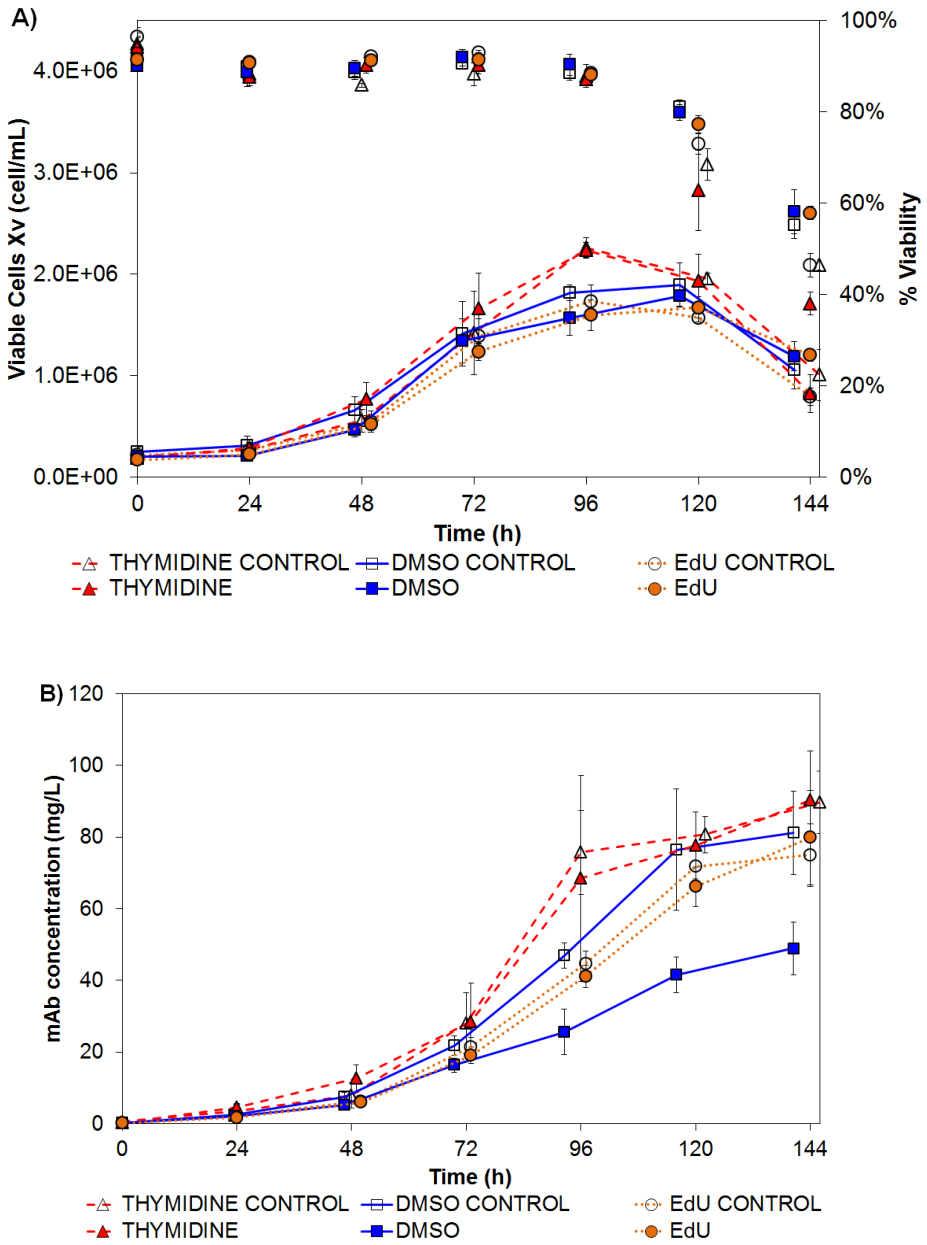


Figure 4.11. Batch cell culture profiles. A) Cell growth and viability; B) mAb titre; C) Glutamate concentration; D) Proliferation assay - proliferation marker Ki-67 and viability; E) Glucose and lactate concentration after thymidine arrest; (n=3, error bars=standard deviation).

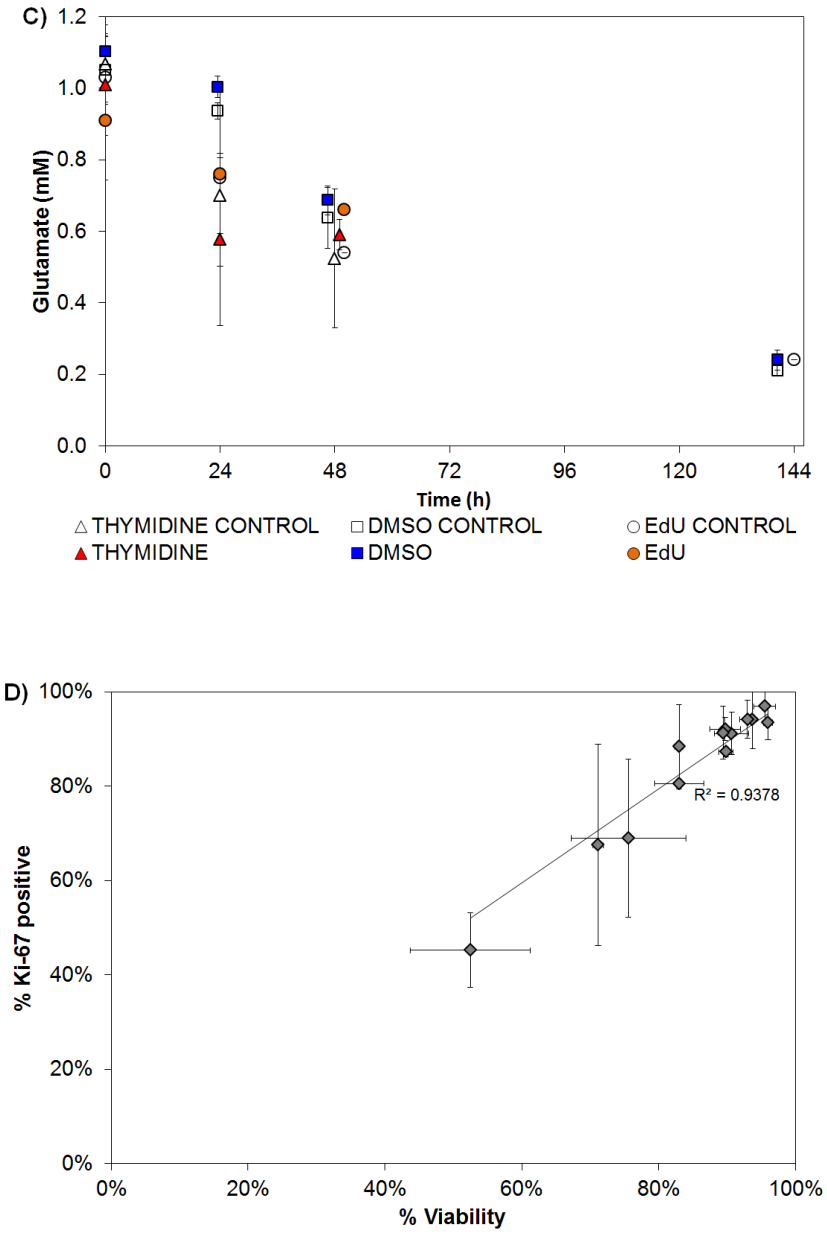


Figure 4.11. (Continued). Batch cell culture profiles. A) Cell growth and viability; B) mAb titre; C) Glutamate concentration; D) Proliferation assay - proliferation marker Ki-67 and viability; E) Glucose and lactate concentration after thymidine arrest; (n=3, error bars=standard deviation).

The glucose and lactate profiles are shown for the arrest experiments in Figure 4.12A-B and for the proliferation assay in Figure 4.12C. The glucose consumption did not show major differences between the control and arrest release groups. Exposure to thymidine appeared to result in the cells being metabolically more active during the first 24h, as a significant lactate production (24h after release) was observed (Figure 4.12A). After this point, the lactate profile is comparable to the control. The metabolic activity seems to be a short-term effect of the arrest mechanism. The blockage of ion potassium channels can lead to the accumulation of cyclin dependent inhibitors p27 and p21 (Ghiani et al., 1999). A plausible overexpression of p27, which inhibits growth (Carvalhal et al., 2003) is accompanied by an increase in the glucose consumption and lactate production rates. Similarly, Bi et al. (2004) reported more metabolically active cells when arresting CHO cells at G_1 phase using p21. Although DMSO exposure has also been reported to imbalance p21 and p27 (Ponzio et al., 1998), this did not result on an increased lactate production at 24h. On the contrary, DMSO treated cells did not show lactate production (below detection limit of 0.2g/L) the first 24 hours (Figure 4.12B). Plausibly the reason for not observing an increased lactate is that: 1) the p21/p27 imbalances were reported after exposing the cells at 3 times higher DMSO concentration than that used herein; and 2) the released cells did show an approximately 14h lag phase to resume proliferation. After 48h, the DMSO culture showed comparable lactate production levels to the control. The glucose and lactate profiles of the proliferation assay did not show statistical differences (Figure 4.12C) compared to the control group. This is in agreement with the less disruptive nature of the proliferation assay.

Finally, the cell cycle distributions are shown (Figure 4.13A-C). The trends are comparable between the corresponding control and proliferation assay or after arrest culture. In particular, an asynchronous growth was re-established between 24-48h of culture in the after arrest release cases.

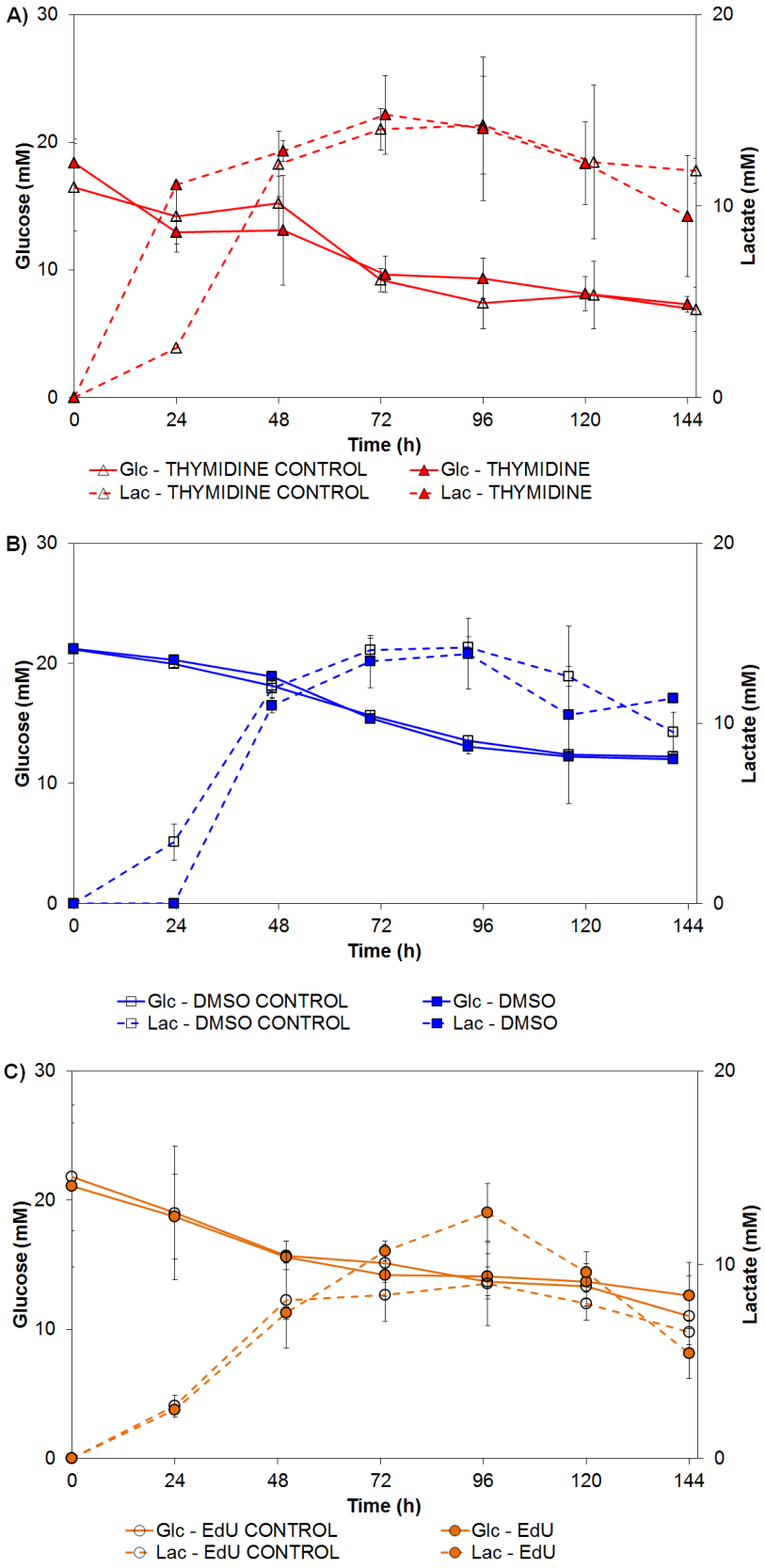


Figure 4.12. Batch cell culture profiles. A) Glucose and lactate concentration after thymidine arrest; B) Glucose and lactate concentration after DMSO arrest; C) Glucose and lactate concentration proliferation assay; (n=3, error bars=standard deviation).

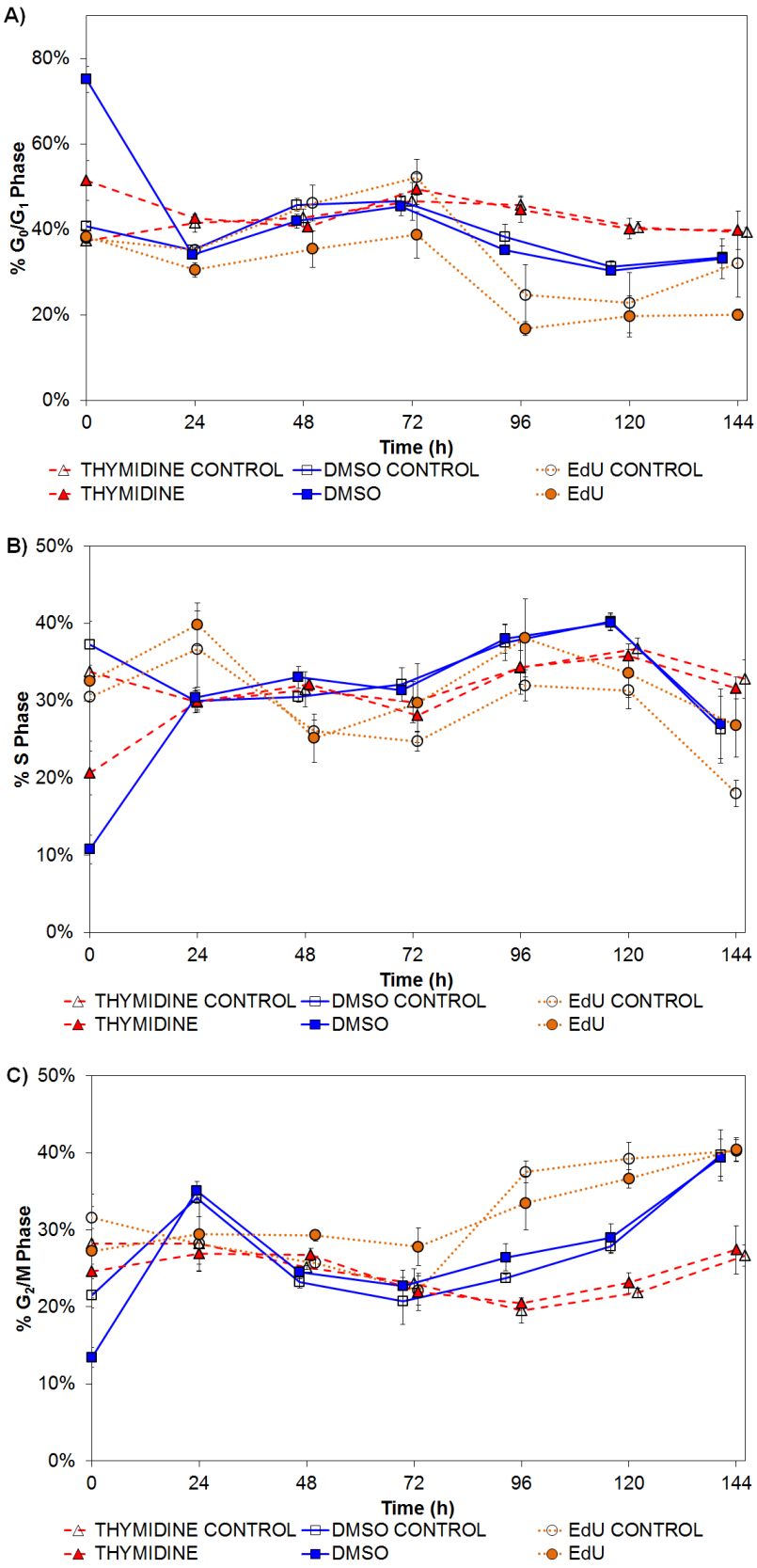


Figure 4.13. Batch cell culture profiles. A) G_0/G_1 phase distribution; B) S phase distribution; C) G_2//M phase distribution; (n=3, error bars=standard deviation).

4.5. Conclusions

In this chapter, the cell cycle blueprint for the GS-NS0 cell line was elucidated. The blueprint encompasses the cell cycle timings, the cyclin pattern and thresholds, as well as the proliferative state (non-G_0 phase cells).

Two distinctive approaches were used as an experimental tool. In first place, chemical cell arrest to synchronise the cell population was used. However, the effectiveness of chemical synchronisation, as well as some drawbacks of using DNA inhibitors for synchronisation have been reported (Cooper, 2003). Thus, it should be emphasised that by the synchronisation herein refers only to the DNA alignment of the cells. Even though the DNA alignment does not guarantee that the cells will share the same state, it does facilitate the reconstruction of the cyclin profiles and cell cycle progression times. In addition, cells that have restarted proliferation together and passed a cell control mechanism will most likely share a similar state. Moreover, the use of two chemical agents provides a useful tool to study the system under different arrest mechanisms, as well as increasing the confidence in the results. Nonetheless, control experiments are used throughout for validation purposes of normal cell behaviour. A second approach using a proliferation assay was carried out. This approach differentiates the cells into two populations and enables to further study the system. Similarly, a control serves for validation purposes. Overall, the results are consistent between the approaches (arrest and proliferation assay), complement each other, and confirmed the observed cyclin blueprint.

Clear timings and thresholds were obtained for cyclin E1 and B1, while cyclin D1 appeared to be linked to the proliferative state of the GS-NS0 cell line. The effect of nutrient exhaustion was identified on the cyclin expression, and provides a first link between the culture environment and the cell cycle machinery. The observed glutamate effect led us to explore further specific culture conditions (i.e. temperature variations, substrate availability). In particular, effects on the cyclin expression, cell cycle, and the link with apoptosis are presented in chapter 5. The elucidated blueprint is not only cell line-specific but is expected to be dependent on culture conditions (e.g. temperature, medium formulation, serum, growth factors, etc.).

Similarly, different cell lines and culture conditions may need different normalisation compared to the ones presented herein since cyclin expression patterns may vary.

The conserved profiles for cyclin E1 and B1 render them as excellent candidates to be distributed variables in cell cycle models given the clear observed timings and thresholds. Moreover, the blueprint provides a unique tool for describing the cell cycle using a relevant biological marker, avoiding weakly supported markers (e.g. mass, age) as presented in chapter 6.

CHAPTER 5

Effect of Culture Conditions on the Cell Cycle

Chapter 5 includes a set of experiments that aimed to identify the effect of culture conditions both on the cell cycle and apoptosis. Specifically, the effect of temperature shifts, as well as medium shifts (using spent medium) were screened in culture. The expressions of cyclins and apoptotic markers were studied by flow cytometry in batch cultures of GS-NS0. The results stress the close link and balance between the cell cycle machinery and programmed cell death.

5.1. Introduction

Process parameters can affect the growth of mammalian cells and their antibody production. These include dissolved oxygen concentration, nutrient concentrations, pH, osmolality, shear stress, toxic metabolite accumulation, and temperature, among others. However, the reported effects are variable between cell lines, expression systems, and expressed recombinant product (Kumar et al., 2007; Sunley and Butler, 2010). Therefore, the improvement of productivity is based on the proliferation control mainly by using optimised culture media (Wurm, 2004) or reduced temperature cultivation. Particularly, proliferation control aims to find a balance between the viable biomass, viability, and culture length, as all these impact directly the productivity (Kumar et al., 2007). However, the underlying mechanisms of these approaches are not fully understood and finding a balance has proved to be challenging.

The use of optimised culture media serves as a tool to regulate the positive signals (e.g. growth factors) that promote the cell cycle progression, while the withdrawal of growth factors correlates with cell arrest and induces apoptosis (Fussenegger and Bailey, 1998). Similarly, cell cycle control and improvement of productivity by temperature shifts have been reported to be variable, although reduced growth is usually observed under mild hypothermia. However, many of the reported effects lack the study on both the cell cycle and apoptosis.

The difficulties in optimising or improving the cultures are related to the intimate link between the cell cycle proliferation and programmed death. These two cell events overlap at multiple specific points, which make the control a difficult task. For instance the entrance to apoptosis seems to take place at late G_1 (entry to S phase), while arrest prior to that stage delays or blocks apoptosis (Fussenegger and Bailey, 1998). Moreover, cyclins, CDKs and cyclin-CDK complexes – particularly G_1-S and G_2-M regulators (Meikrantz and Schlegel, 1996) - have been also reported to be required for apoptosis in a number of differentiated cell types (Rubin et al., 1994). Therefore, the study of temperature and nutrient variations and its effects on the cell cycle and apoptosis are of interest to expand the elucidated blueprint presented in chapter 4.

5.2. Objectives

The aim of this chapter is to study the effect of temperature and medium composition on the cell cycle and apoptosis for the GS-NS0 cell line. The following scientific objectives were set:

- Design and perform GS-NS0 culture experiments that would allow evaluating the temperature effect on cyclin D1 expression and apoptosis.
- Design and perform GS-NS0 culture experiments that would allow evaluating the nutrient variations short-term effect on cyclins expression (D1, E1, and B1) and apoptosis.
- Identify relevant links between the cell cycle and apoptosis for future model development.

5.3. Methodology

A series of batch culture experiments varying the temperature of GS-NS0 cells in mid-exponential batch culture were carried out. Cyclin D1 expression and apoptosis induction were studied by flow cytometry. In addition, a short-duration (24h) study on the rapid effect of medium shift on the cell cycle and apoptosis was carried out. All the specifics of the materials and methods were reported in chapter 3.

5.3.1. Temperature shifts

Batch cultures of GS-NS0 carried out in triplicates covered hypothermia (35 °C), hyperthermia (39 °C), and baseline (37 °C) conditions in 1L Erlenmeyer flasks. The medium composition was reported in chapter 3 using dialyzed FBS and cells seeded at $2.5*10^5$ cells/mL. The cultures were started at 37 °C for 30h and then the incubator temperature was shifted to either 35 °C or 39 °C. The outputs investigated were the cell growth, metabolic profiles, cell cycle (distribution and cyclin D1), apoptosis markers, and antibody productivity. Cyclin D1 was selected based on the premise that it provides a link with the culture environment (Sherr, 1993). The experiments were carried out with the collaboration of Chonlatep Usaku (PhD candidate) and Anne Gauthier during her MSc project in our lab (Gauthier, 2013).

5.3.2. Medium shifts

The medium shift experiments consisted on the quick transfer of GS-NS0 cells in mid-exponential growth (prior to glutamate exhaustion) to three different medium compositions of fresh and conditioned medium (cell-free spent medium). The medium compositions consisted on a 100% fresh medium, 50/50% (v/v) fresh/conditioned medium and 0% fresh medium (i.e. 100% conditioned medium). The cells in mid-exponential growth were centrifuged for 5min at 800rpm. The medium was aspirated and the cells were re-suspended in 50mL working volume of one of the levels (carried in triplicates) at a cell density of $5*10^5$ cells/mL.

Samples were taken every 6h for 12h, and then at 24h. The aim was to monitor the response to the medium compositions changes in a short-period. The outputs investigated included the cell growth, metabolic profiles, cell cycle (distribution, Ki-67 proliferation marker, and cyclins), apoptosis markers (and genes), and antibody productivity. The experiments were carried out with the collaboration of Chonlatep Usaku (PhD candidate).

5.4. Results & Discussion

5.4.1. Temperature shifts

Cell growth, viability, and apoptosis

The temperature shift showed a direct effect on the achieved cell densities (Figure 5.1A). Whereas the 39 °C shift showed a similar growth to the baseline (37 °C), the 35 °C shift batch showed a significant lower peak cell density. Particularly after the temperature shift (30h), cell growth seemed slower and the cell density did not vary significantly at 35 °C. Similarly, the 39 °C batch did not show significant changes soon after the temperature shift. However, a faster cell density decline was observed at late stages (96h onwards) of the 39 °C culture when compared to the 37 °C culture. The cell viability of both temperature shifted cultures showed a sharper decrease in viability after 48h, which was significant when compared to the 37 °C batch. Despite the fact that the 35 °C shift batch culture started with a lower viability, it seemed to recover during the first 24h. A similar effect was also observed in the fraction of early stage apoptotic (ESA) cells (Figure 5.1B), as the ESA fraction of the 35 °C shifted culture significantly decreased during the first 24h. After the temperature shifts, there was no immediate (48h) significant change in the ESA fraction in both cases (35 °C and 39 °C). Whereas both the 37 °C and 39 °C cultures showed a significant increase in the ESA fraction (compared to 48h) after glutamate was exhausted (48h), the 35 °C culture showed no significant change until 96h in the ESA fraction (compared to 48h). This suggests that the 35 °C culture displayed a delay in the induction of apoptosis compared to the other cultures. After 96h, the ESA fraction of the 35 °C culture was comparable to the 37 °C culture. The 39 °C culture showed no further changes in the ESA fraction after the glutamate exhaustion despite the observed continuous drop in viability. Such effect can be due to either a fast transition from the ESA fraction to the LSA fraction or a high lysis rate due to the high temperature. An experimental error in the cell counts did not seem supported given the satisfactory correlation between the manually counted cell viability and the apoptosis analysis via flow cytometry (Figure 5.1C).

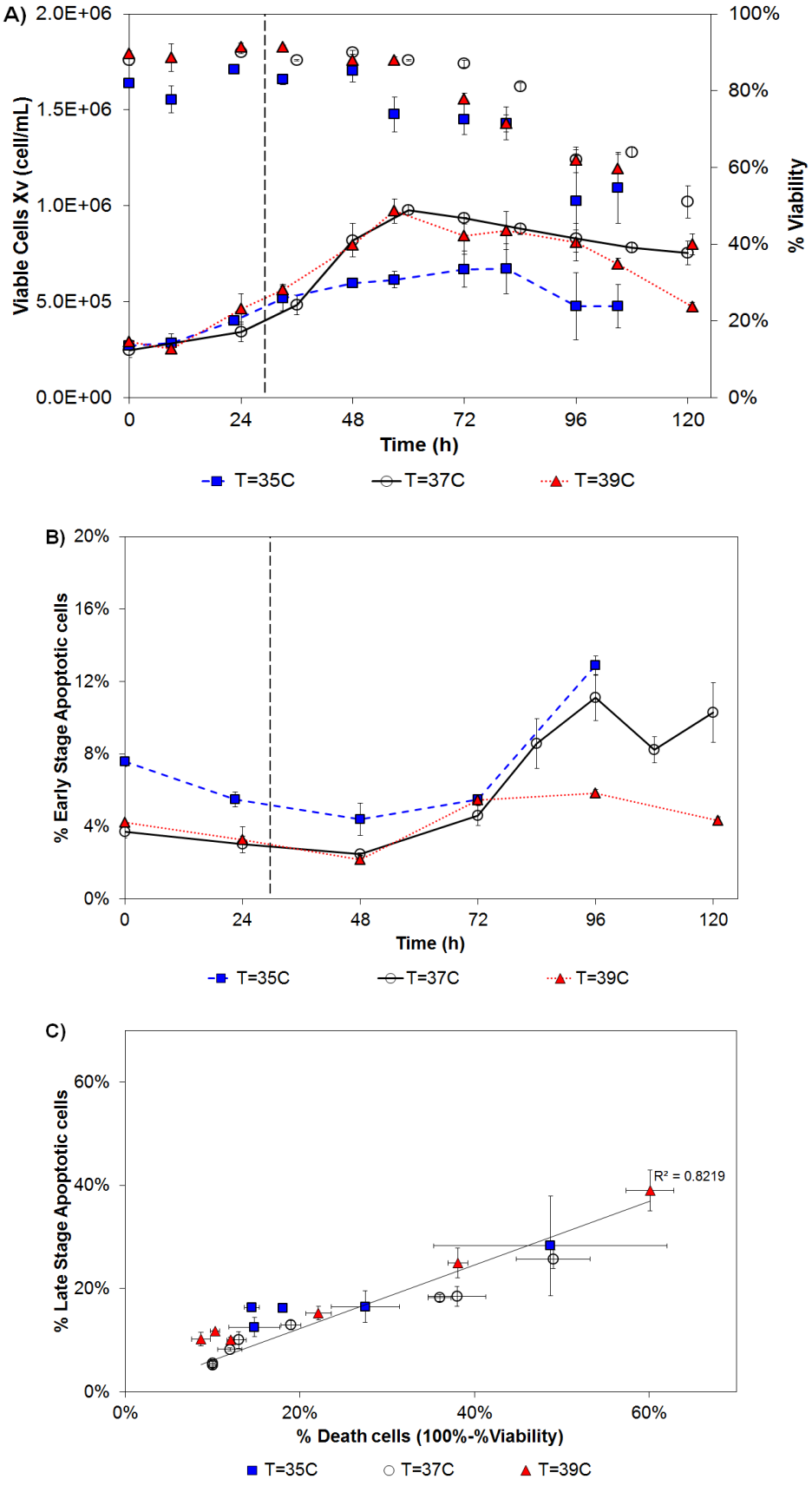


Figure 5.1. Batch temperature cell growth and apoptosis. A) Cell growth and viability; B) % Early Stage Apoptotic cells; C) % Late Stage Apoptotic cells versus % Death cells. Notation: vertical dotted line indicates time of the temperature shift, (n=3, error bars=standard deviation).

The observed results for the mild hypothermia are in agreement with previous reports. Both a lower cell density (Chong et al., 2008; Kaufmann et al., 1999; Moore et al., 1997) and an apparent delay on the onset of apoptosis have been reported (Furukawa and Ohsuye, 1998; Reuveny et al., 1987; Swiderek and Al-Rubeai, 2007). In contrast, for mild hyperthermia (39 °C) lower densities or no growth have been reported (Bloemkolk et al., 1992; Furukawa and Ohsuye, 1998). However, herein a sharper viability decrease at late stages of the 39 °C culture was observed, as previously reported (Barnabe and Butler, 1994; Furukawa and Ohsuye, 1998).

Metabolic profiles and mAb productivity

The glutamate consumption was comparable across all the temperature conditions. Glutamate was consumed at a similar rate during the first 30h, as the culture conditions are identical, and glutamate is exhausted (below detection) after 48h (Figure 5.2A). The glucose profile is similar for all runs and the lactate profile showed some differences (Appendix I.). However, in order to make a direct comparison due to the differences in cell density, the consumption and production rates were estimated based on the linear regression between the substrate/metabolite concentration and the integral viable cell (IVC). The glucose specific consumption rate (Figure 5.2B) showed an increasing trend in glucose consumption with the increase of temperature, as indicated by the slopes of the regression. Similarly, the lactate specific production rate (Figure 5.2C) showed an increasing trend as a function of the temperature. Thus, the yield of lactate on glucose seemed to be the lowest for the 35 °C culture (approx. 1.22 mol lactate/mol glucose) compared to the 37 °C and 39 °C cultures (approx. 1.63 and 1.59 mol lactate/mol glucose, respectively). These results are in agreement with previous studies reporting an enhanced metabolism at higher temperatures (Barnabe and Butler, 1994) and a reduced metabolism at lower temperature (Furukawa and Ohsuye, 1998; Reuveny et al., 1987).

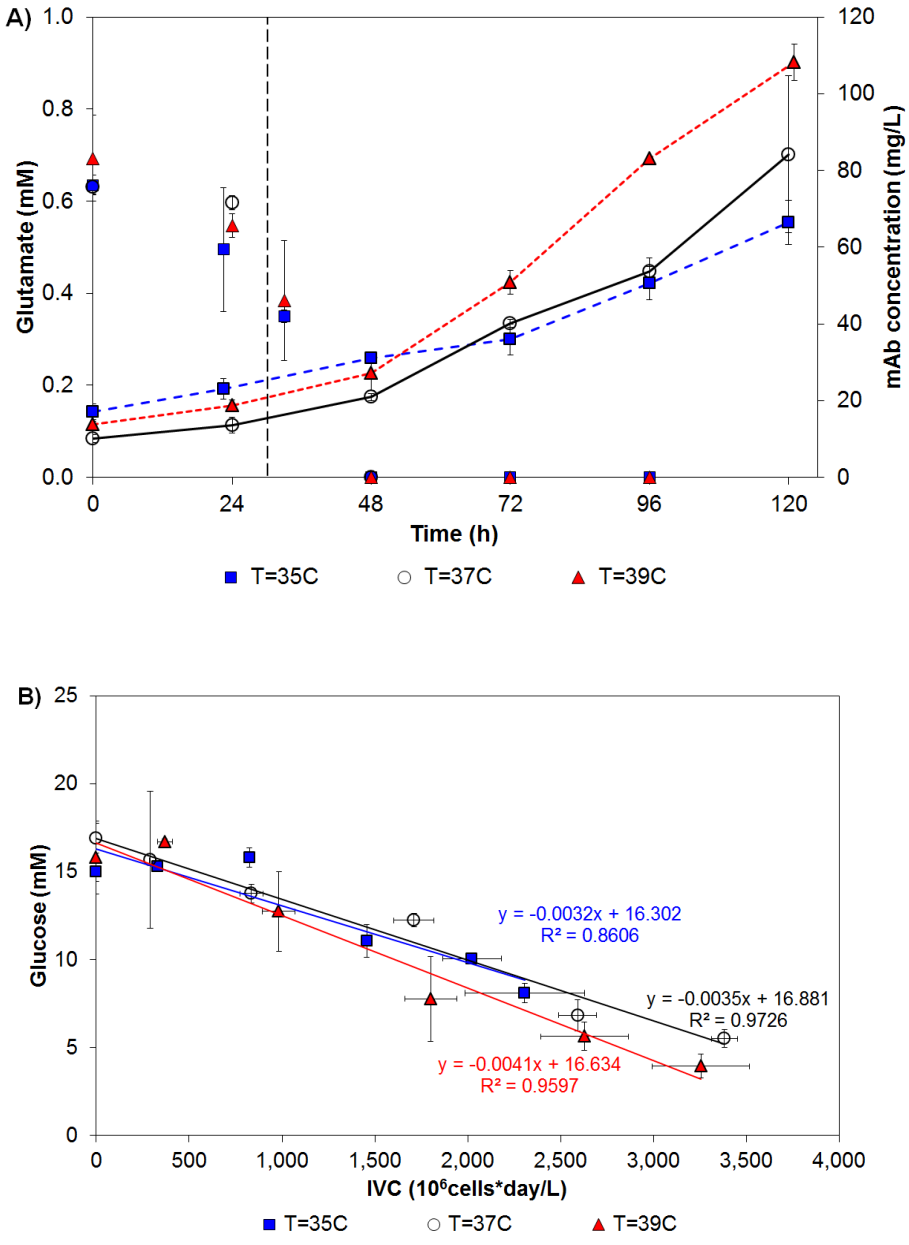
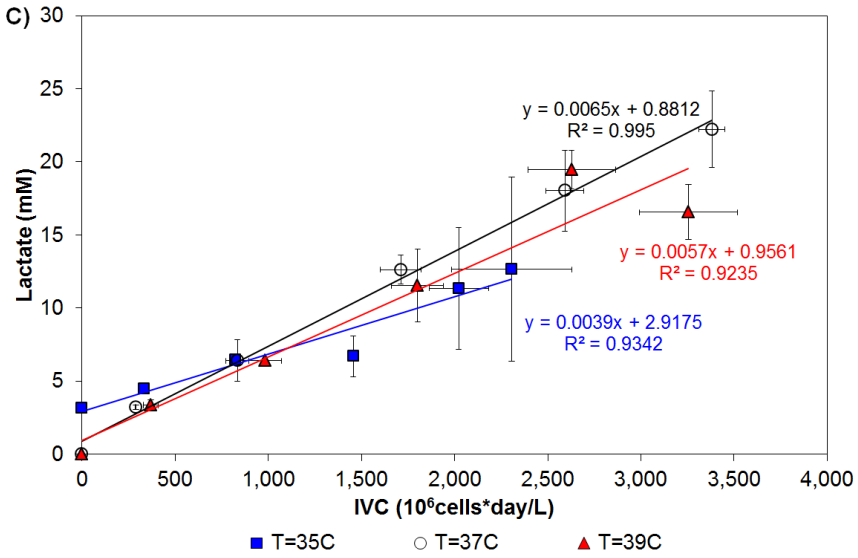


Figure 5.2. Batch temperature shift metabolic and antibody profiles. A) Glutamate concentration and mAb titre; B) Glucose specific consumption rate; C) Lactate specific production rate; D) Antibody specific production rate. Notation: vertical dotted line indicates time of the temperature shift, (n=3, error bars=standard deviation).



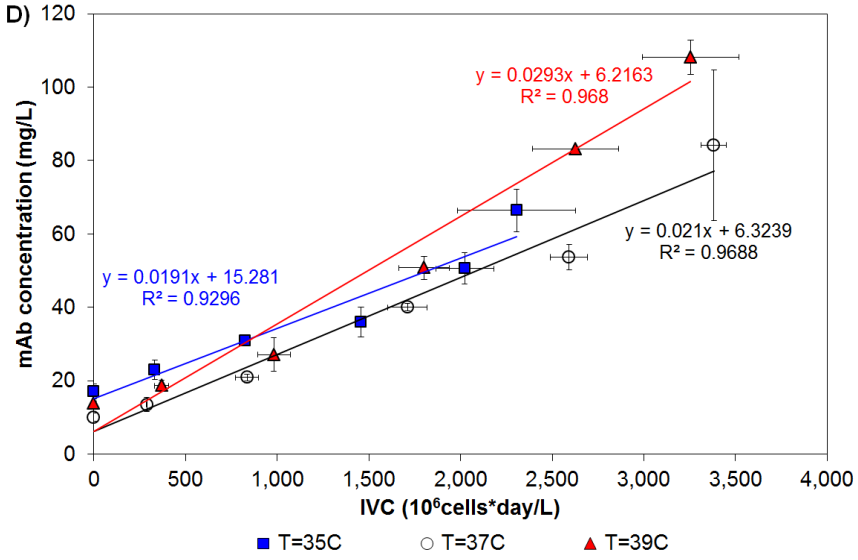


Figure 5.2. (Continued). Batch temperature shift metabolic and antibody profiles. A) Glutamate concentration and mAb titre; B) Glucose specific consumption rate; C) Lactate specific production rate; D) Antibody specific production rate. Notation: vertical dotted line indicates time of the temperature shift, (n=3, error bars=standard deviation).

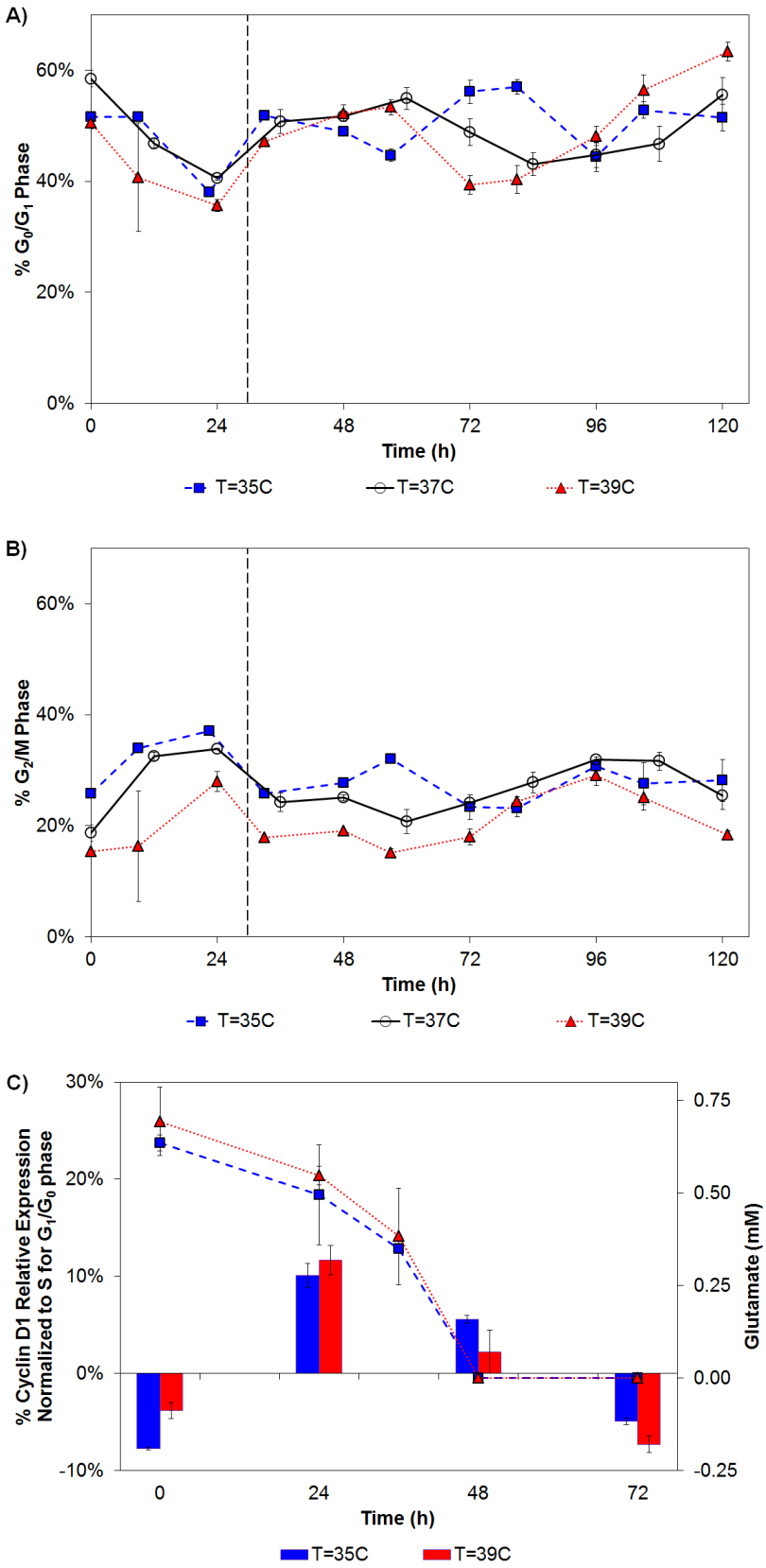


Figure 5.3. Batch temperature cell cycle and cyclin D1 profiles. A) %G_1/G_0 phase; B) %G_2/M phase; C) Cyclin D1 profile for G_1/G_0 phase. Notation: vertical dotted line indicates time of the temperature shift, (n=3, error bars=standard deviation).

The antibody titre showed a comparable trend for the first 48h, after that point a higher titre was observed for the 39 °C culture (Figure 5.2A). A significant higher mAb titre was observed for the 39 °C culture between 72-96h compared to the other cultures. However, at 120h due to the mAb titre variability on the 37 °C culture, the 39 °C culture mAb titre was only statistically significantly different compared to the 35 °C. The specific mAb productivity was calculated for all cultures (Figure 5.2D). The mAb rates between the 35 °C and 37 °C cultures are comparable, whereas the 39 °C culture did show a higher rate. However, some of the most significant increments in the mAb titre occurred during the death phase and it could be attributed to the lysis of cells. Thus, productivity was divided in culture phases (0-1 day, 1-3 day, 3-5 day) and a higher rate was observed in all cases during the 3-5 days (Appendix I.). Particularly, the temperature shifted cultures showed a higher mAb rate (between day 3-5) than the 37 °C, around 1.3 and 1.5-fold higher for the 35 °C and 39 °C cultures, respectively.

Cell cycle and cyclin D1 expression

The G_1/G_0 lumped phase was the highest cell cycle fraction across the experiments (Figure 5.3A). The profiles were similar and follow the same trend up to the temperature shift point. An immediately evident effect on the cell cycle distribution from the temperature shift was not observed. In contrast, a temporary G_2/M increase was observed between 48-72h (Figure 5.3B), prior to the increase in the G_1/G_0 cell fraction at 72h of the 35 °C culture. Shi et al. (2005) reported a temperature arrest at G_2/M when lowering the temperature, as well as previous reports have observed an accumulation in this phase at low temperature (Moore et al., 1997; Swiderek and Al-Rubeai, 2007; Trummer et al., 2006). However, there is no other evidence to support that this is part of a cell arrest either at the G_2/M or G_1/G_0 lumped phases. Nonetheless, the increase in the G_1/G_0 fraction was observed prior to the increment of the ESA fraction (at 96h) for the 35 °C culture. Similarly, prior to the increase in the ESA fraction (at 72h) for the 37 °C and 39 °C cultures, an accumulation in the G_1/G_0 phase was observed on both culture conditions. These trends seem to confirm the report that cells must progress to late G_1 for apoptosis to occur (Fussenegger and Bailey, 1998).

The cyclin D1 expression for the G_1/G_0 lumped phase showed a similar profile as reported in chapter 4, despite the temperature shifts (Figure 5.3C). Mild hyperthermia has been reported to induce cyclin D1 expression (Han et al., 2002), however herein it was not observed. In contrast, the previously observed correlation between substrate availability (i.e. glutamate) and the cyclin D1 expression was confirmed. The cyclin D1 expression started at a low level (due to subculture process every 3 days, which is in the limits of glutamate exhaustion) and it increased in the presence of fresh medium. Once again, soon after the glutamate was exhausted (after 48h), the cyclin D1 expression decreased. The significantly lower cyclin D1 expression at the start of the 35 °C temperature shift culture seemed to correlate with the lower starting viability and higher ESA fraction, as previously discussed. Although the cyclin D1 induction due to the hyperthermia conditions cannot be completely discarded, it seems that the substrate availability is the dominant event.

5.4.2. Medium shifts

Cell growth, viability, and apoptosis

The medium shift experiments showed differences on the cell growth. After 12h and 24h, a significant difference was observed between the medium compositions containing fresh medium (50% and 100%) compared to the conditioned medium (0% fresh medium, Figure 5.4A). Although a higher average cell density was observed for the 50% blend at 24h compared to the 100% fresh medium, the difference was not statistically significant ($p>0.05$). The cell viability also showed significant differences between the 0% fresh medium and the other two medium compositions, both after 12h and 24h (Figure 5.4A). Despite all the cultures starting with the same viability, after 24h an approximately 10% decrease in viability was observed in the 0% fresh medium.

In contrast, no significant differences were observed in the percentage of cells expressing the proliferation marker Ki-67 (Figure 5.4B). Although after 6h of culture the 0% fresh medium showed on average a lower fraction of cells expressing Ki-67, it was not found to be statistically significant due to the broad variance in the measurement. However, statistical differences in the percentage of ESA were observed. The 0% fresh medium showed a statistically higher percentage of ESA cells (at 0, 12, and 24h) compared to the other groups (Figure 5.4B). Further, the 0%

fresh medium showed a statistically significant increase in the percentage of ESA cells between 0h and 24h, whereas the other medium compositions did not.

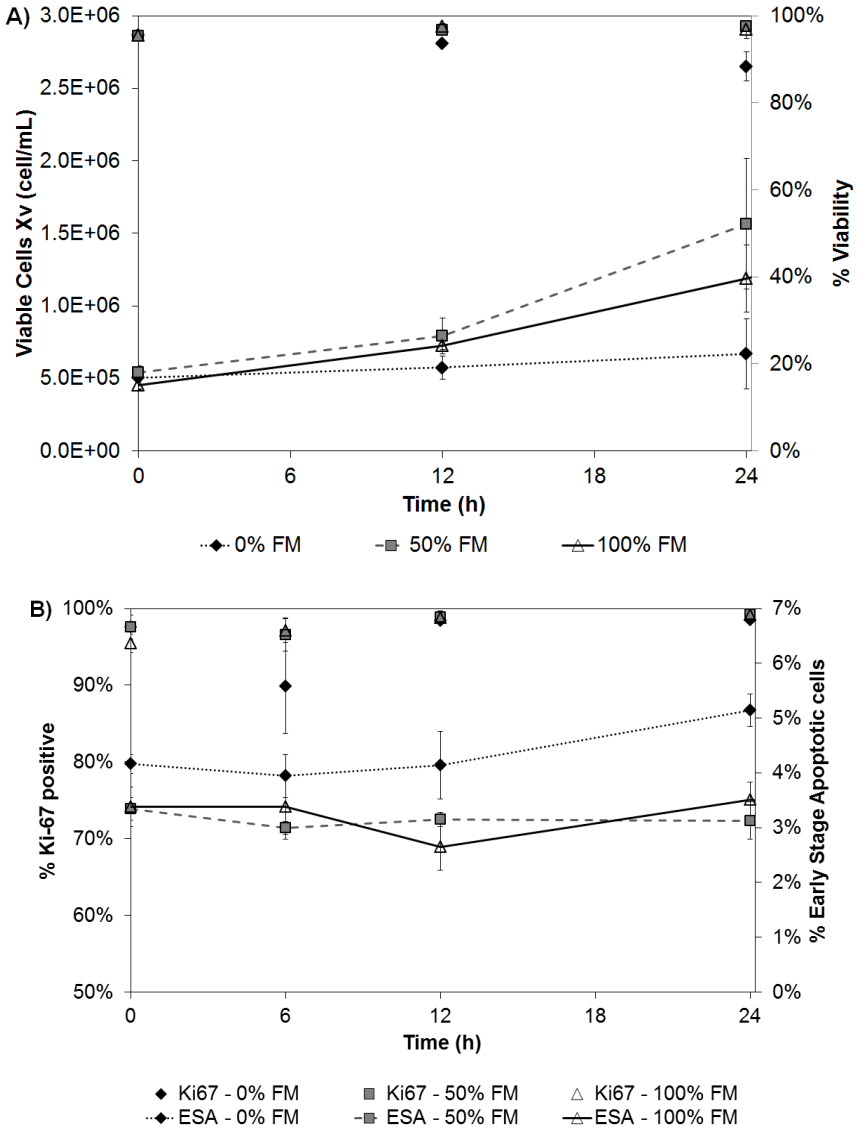


Figure 5.4. Medium shift experiment cell growth and apoptosis. A) Cell growth and viability; B) % Ki-67 positive cells and % Early Stage Apoptotic cells. Notation: Fresh medium (FM), % viability and % Ki-67 positive without connecting lines, viable cells (Xv) and % Early apoptotic with connecting lines, (n=3, error bars=standard deviation).

Metabolic profiles and mAb productivity

The glucose and lactate concentration profiles showed differences among the medium compositions (Figure 5.5A). The glucose profiles of the 100% fresh medium and 50% blend showed a significant glucose concentration decrease between 0h and 24h. Similarly, these two medium compositions showed a significant increase in

the lactate concentration between the same time points. The increase in the lactate concentration was steeper in the 100% fresh medium compared to the 50% blend. This could be attributed to the feedback inhibition of lactate on the lactate on glucose yield (Ozturk et al., 1992). In contrast, glucose consumption in the 0% fresh medium was not evident; whereas a significant lactate decrease was observed between 0h and 24h. Such profiles seemed to indicate a shift in the cell metabolism, going from lactate production (commonly observed) to lactate consumption. This effect has been previously reported in fed-batch cultures (deZengotita et al., 2000; Zhou et al., 1996).

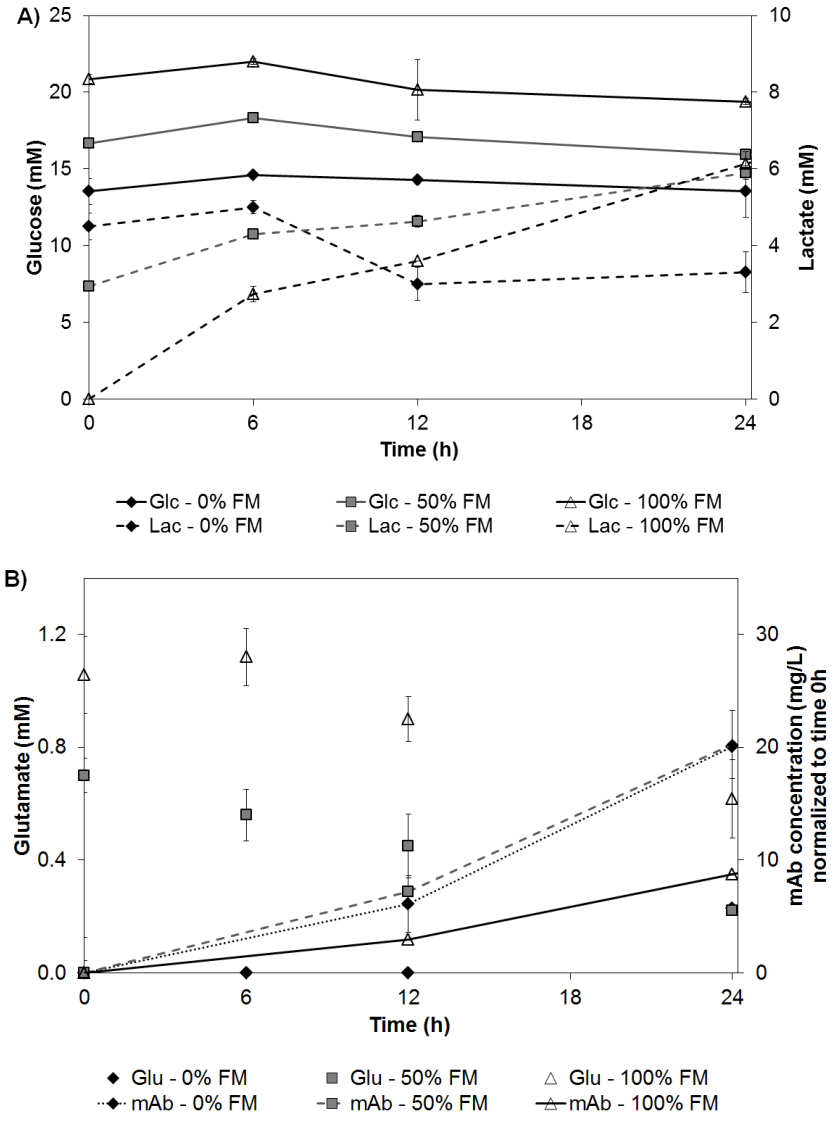


Figure 5.5. Medium shift experiment metabolic and antibody profiles. A) Glucose and lactate concentration; B) Glutamate concentration and mAb titre. Notation: Fresh medium (FM), substrate (glucose, glutamate) without connecting lines, lactate and mAb with connecting lines, (n=3, error bars=standard deviation).

Glutamate was consumed when present (i.e. 100% and 50% fresh medium) and it was at the limit of detection for the 50% blend after 24h (Figure 5.5B). The mAb titre (shown normalised to time 0h for comparison purposes) was comparable between the 0% fresh medium and 50% blend, despite the observed differences in cell growth. In contrast, the mAb titre in the 100% fresh medium was significantly lower when compared to the 50% blend at 24h, despite showing a similar cell growth. The higher mAb titre in the 50% blend and 0% fresh medium seems to be related to the use of conditioned medium. These two medium compositions (0% and 50%) have in common the conditioned medium, which contains lactate and most likely other factors released by the cells during growth. Although it has been reported that higher osmolality can increase the antibody titre (Wu et al., 2004), it is expected (not measured) that the osmolality differences between the three medium compositions are not enough to cause the high titre in 0% fresh medium and 50% blend. However, the contribution of cell lysis to the mAb titre on the 0% fresh medium needs to be also considered. Nonetheless, the mAb differences reflect that the cells experience an adaptation process even if the new conditions were favourable such as the 100% fresh medium.

Cell cycle and cyclins expression

The cyclin expression profiles were reported in relative terms to the expression at time 0h. This representation allowed a direct comparison between the cultures, as well as to quantify the differences in time within each culture. The 100% fresh medium showed a fast increase in the cyclin D1 levels and cyclin E1 levels soon after the medium shift (Figure 5.6A). However, the cyclin B1 did not show a statistically higher level until 12h. The expression of the three cyclins was in general above the initial expression level, which is in agreement with the shift to a 100% fresh medium (that provided favourable conditions for proliferation). The 50% medium blend showed a similar expression profile (Figure 5.6B). Both cyclin D1 and E1 were expressed above the initial levels after 6h of culture. However, at 24h a decrease in the cyclin D1 levels was observed. The decrease was in agreement with the previous observed trends of cyclin expression with the exhaustion of glutamate, which in the 50% blend was in the limits of detection at 24h. Cyclin B1 showed throughout a significantly higher expression compared to the initial level. However, cyclin B1 showed a decrease at 24h compared to the levels at 12h that correlates

with the lower glutamate levels. Finally, the 0% fresh medium showed a significant increase in the cyclin E1 and D1 levels from 0 to 12h (Figure 5.6C). Particularly at 12h, the levels of both cyclin D1 and E1 were the highest among all cultures. However, at 24h both cyclins' expression seemed to decrease and cyclin E1 is even at a significantly lower level than at 0h. Cyclin B1 expression decreased throughout and it was significantly lower at 24h when compared to 0h. The lower cyclin B1 expression correlates with the higher G_2/M fraction observed (Figure 5.6F). In addition, the G_1/G_0 and S (Figure 5.6D-E) cell fractions of the 0% fresh medium showed a different trend compared to the medium compositions containing fresh medium (50% and 100%). The 0% fresh medium cell cycle fractions seemed to show qualitatively a less oscillatory trend, in agreement with the apparent absence of cell growth reported at the cell density.

Cyclin D1 expression has been reported to depend on the quantity of growth factors available (Fussenegger and Bailey, 1998), which is in agreement with the observed trends in the 50% blend and 100% fresh medium. However, the increase of both cyclin D1 and E1 in the 0% fresh medium could be attributed either to the presence of not quantified factors (as the medium formulation contains serum) in the conditioned medium, or cyclin D1/E1 involvement in other cell events. Particularly, between 12h and 24h a decrease in the 0% fresh medium viability was observed, as well as an increase in the percentage of ESA cells. It has been previously reported (Rubin et al., 1994) that cyclins-CDKs complexes - such as cyclin D1 - can be required for apoptosis. In addition, the overexpression of cyclin D1 is sufficient to induce apoptosis in neuronally differentiated cells (Kranenburg et al., 1996).

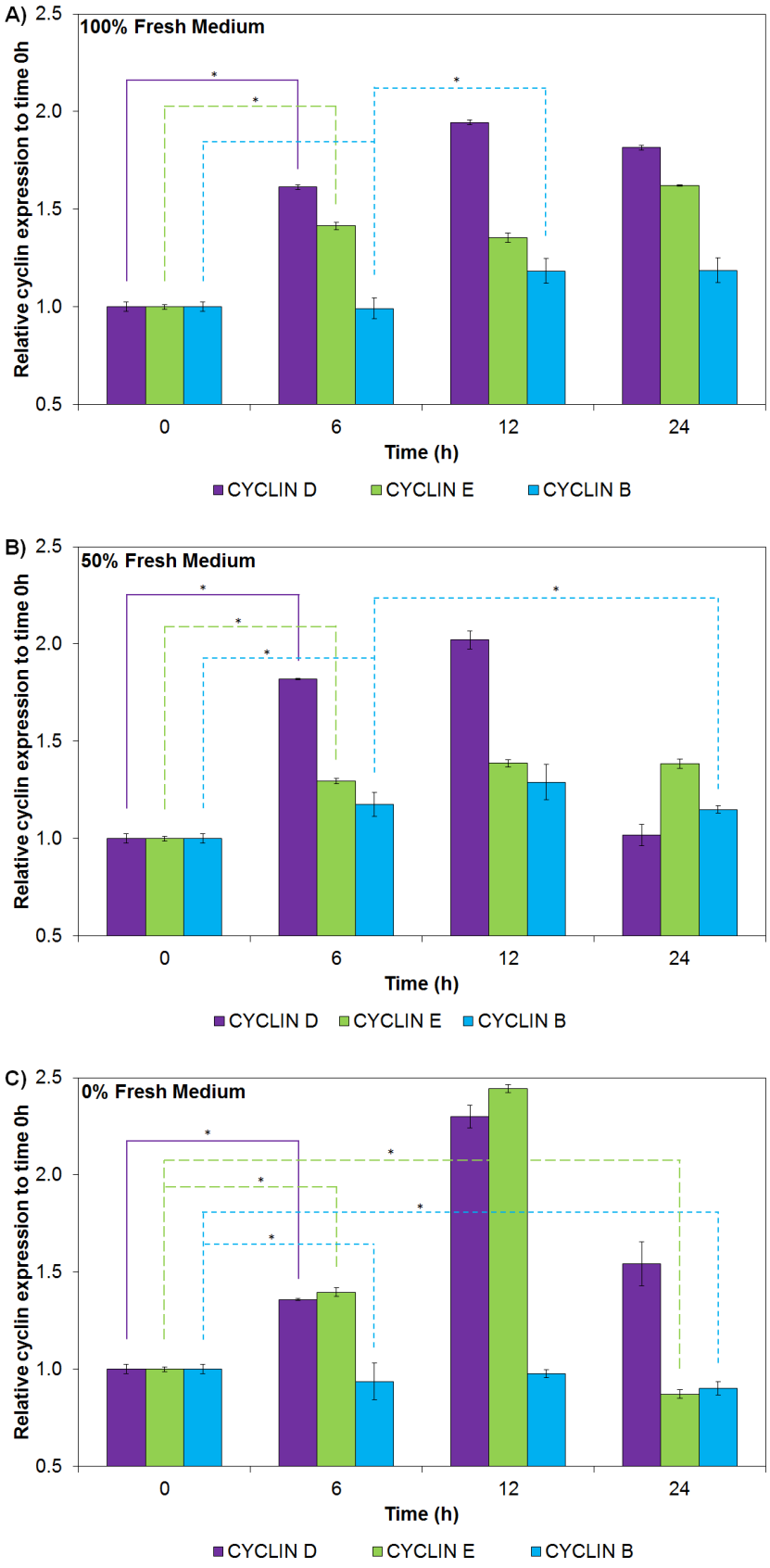


Figure 5.6. Medium shift experiment cyclin profiles. A) Cyclin profiles in the 100% fresh medium; B) Cyclin profiles in the 50% fresh medium; C) Cyclin profiles in the 0% fresh medium; D) $\%G_1/G_0$ phase; E) %S phase; F) $\%G_2$/M phase. Notation: Fresh medium (FM), (n=3, error bars=standard deviation).

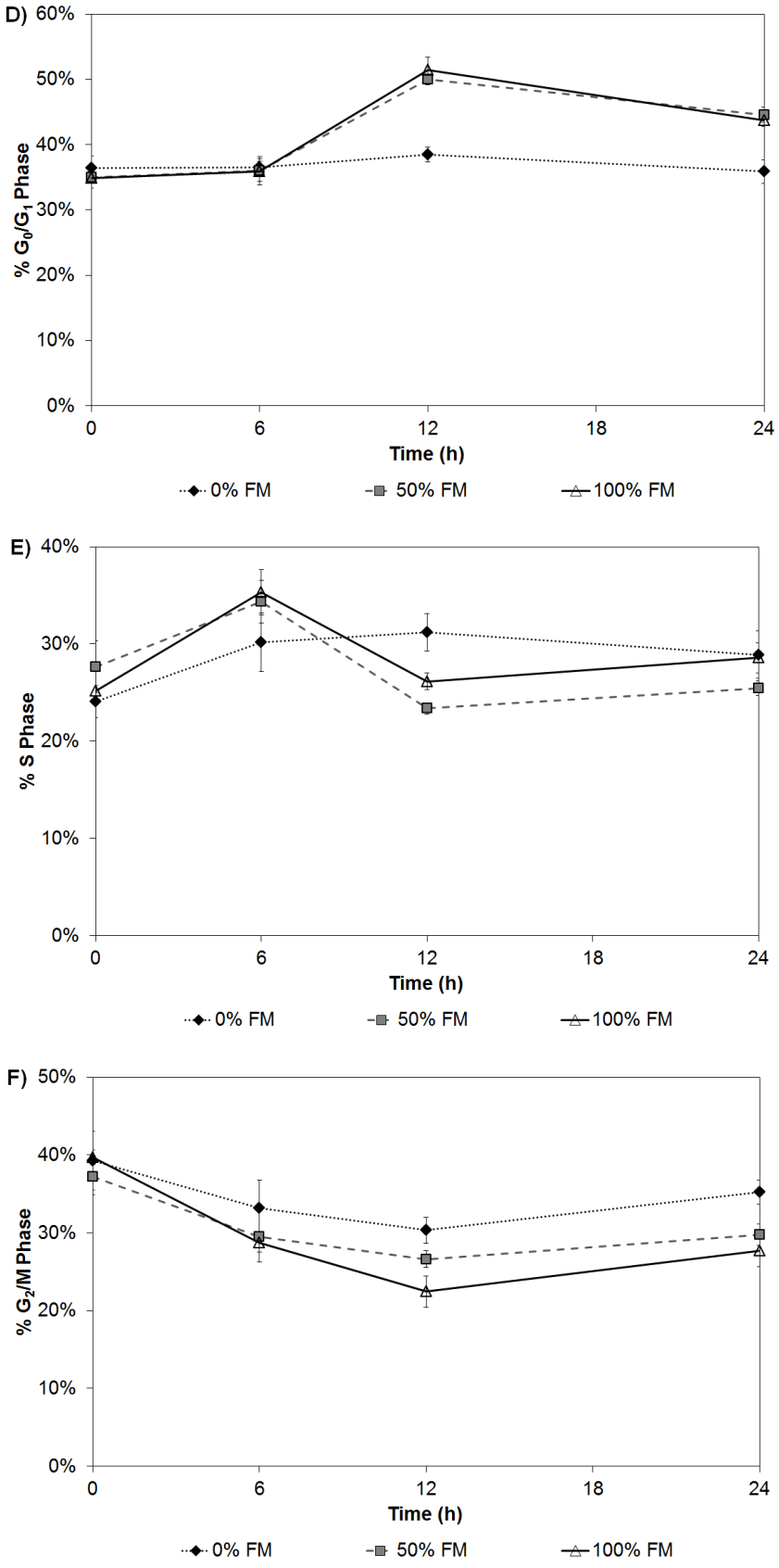


Figure 5.6. (Continued). Medium shift experiment cyclin profiles. A) Cyclin profiles in the 100% fresh medium; B) Cyclin profiles in the 50% fresh medium; C) Cyclin profiles in the 0% fresh medium; D) $\%G_1/G_0$ phase; E) %S phase; F) $\%G_2$/M phase. Notation: Fresh medium (FM), (n=3, error bars=standard deviation).

As mentioned, there is a close link between the cell cycle progression and the programmed cell death. A simplified schematic representation of the two cell events is presented (Figure 5.7). In particular, there is a fine balance between cyclins, CDKs (and their complexes), CDIs (e.g. *p21*), and *p53* (transcription factor that functions as a tumour suppressor inducing apoptosis) in the regulation of both processes.

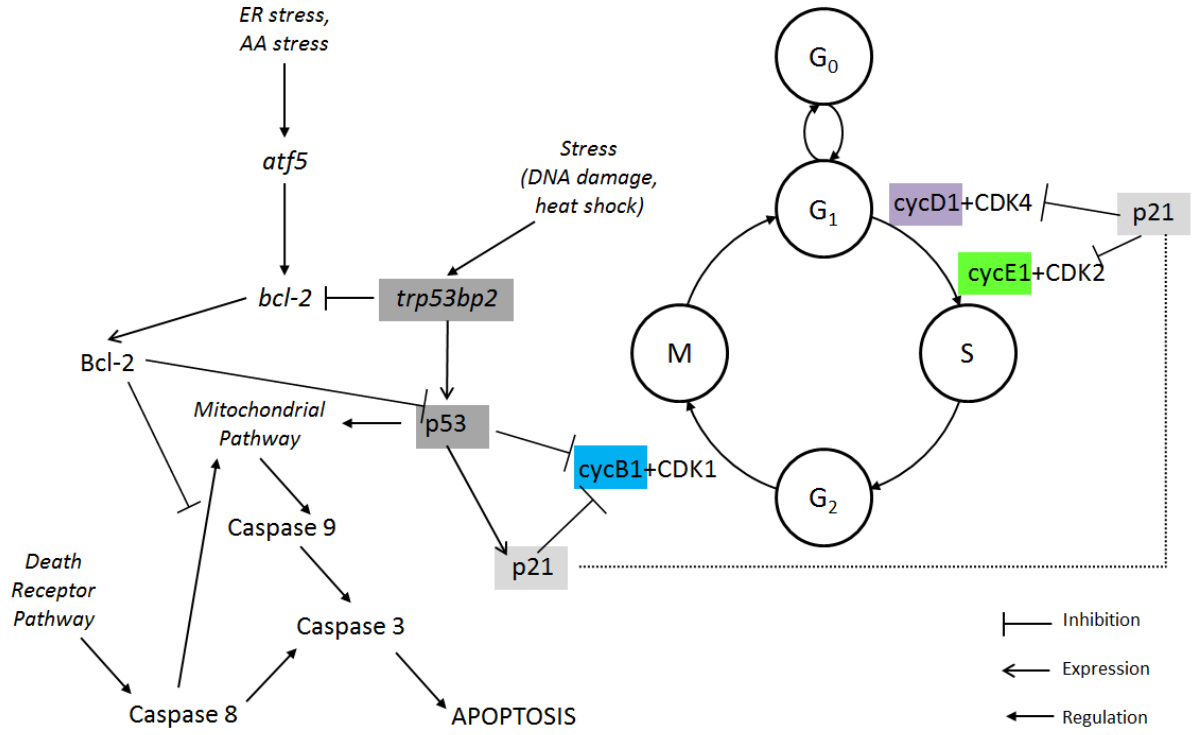


Figure 5.7. Schematic representation of the cell cycle and apoptosis.

Gene expression was measured as part of the collaboration work conducted with Chonlatep Usaku (PhD candidate). Among the quantified genes, two are of interest to the link between the cell cycle and apoptosis, *p21* and *trp53bp2*. The relevance of these two genes is due to their reported roles. First, p21 is a CDI that regulates the cell cycle (Gartel and Tyner, 2002; Niculescu et al., 1998). Specifically, p21 has been reported to inhibit CDKs for the G_1-S transition and its complexes, as well as other cyclin-CDK complexes (Fussenegger and Bailey, 1998; Meikrantz and Schlegel, 1995; Xiong et al., 1993). Second, *trp53bp2* encodes 53BP2, which interacts with p53 to mediate apoptosis via the mitochondrial pathway (Kobayashi et al., 2005; Samuels-Lev et al., 2001). Both p53 and p21 have been reported to inactivate cyclin B complexes (Dulic et al., 1998; Innocente et al., 1999). Therefore, plots of the

relative expression of cyclins versus the relative gene expression (*p21, trp53bp2*) were used to evaluate the existence of a relation or association.

Based on the presented results some links between the cyclin expression and *p21/trp53bp2* gene expression were identified. The cyclins (D1, E1, and B1) expression versus the *p21* gene expression did show correlation patterns. In particular, it was observed (Figure 5.8A-C) that if *p21* was expressed below the reference level (0h) then there was a positive cyclin expression above the reference (0h). However, if *p21* was expressed above the reference, the cyclin expression was decreased (Figure 5.8C). Two points in the cyclin D1 and E1 (Figure 5.8A-B) expression seemed not to follow the above mentioned pattern. These points corresponded to the 6h of the 0% fresh medium culture, where it was previously discussed a decrease in the Ki-67 positive cell fraction (although not statistically significant). Therefore, it can be inferred that *p21* expression is partially responsible for the cell arrest (Bi et al., 2004; Khoo and Al-Rubeai, 2009) and the observed cyclins (D1 and E1) imbalances.

The *trp53bp2* gene expression did not show a clear link with the expression of cyclin D1 and E1 (Figure 5.8D-E). Both cyclins seemed to be expressed above the reference, regardless of the *trp53bp2* gene expression. In the cyclin B1 case (Figure 5.8F) a weak association was identified. Whenever the *trp53bp2* gene was expressed above the reference (particularly above 1.5-fold), there was no cyclin B1 expression. The highest *trp53bp2* expression was observed for the 0% fresh medium at 6h and 24h. It could be inferred that the cells are driven at these points towards apoptosis given the existing links between *trp53bp2* and p53 (Yang et al., 1999). The herein identified links are subject to the experimental conditions and further experimentation is required to fully confirm these associations. The presence of serum in our medium formulation gives an undefined character to it, which complicates the analysis. However, the observed results stressed the importance and need to link the cell cycle and apoptosis.

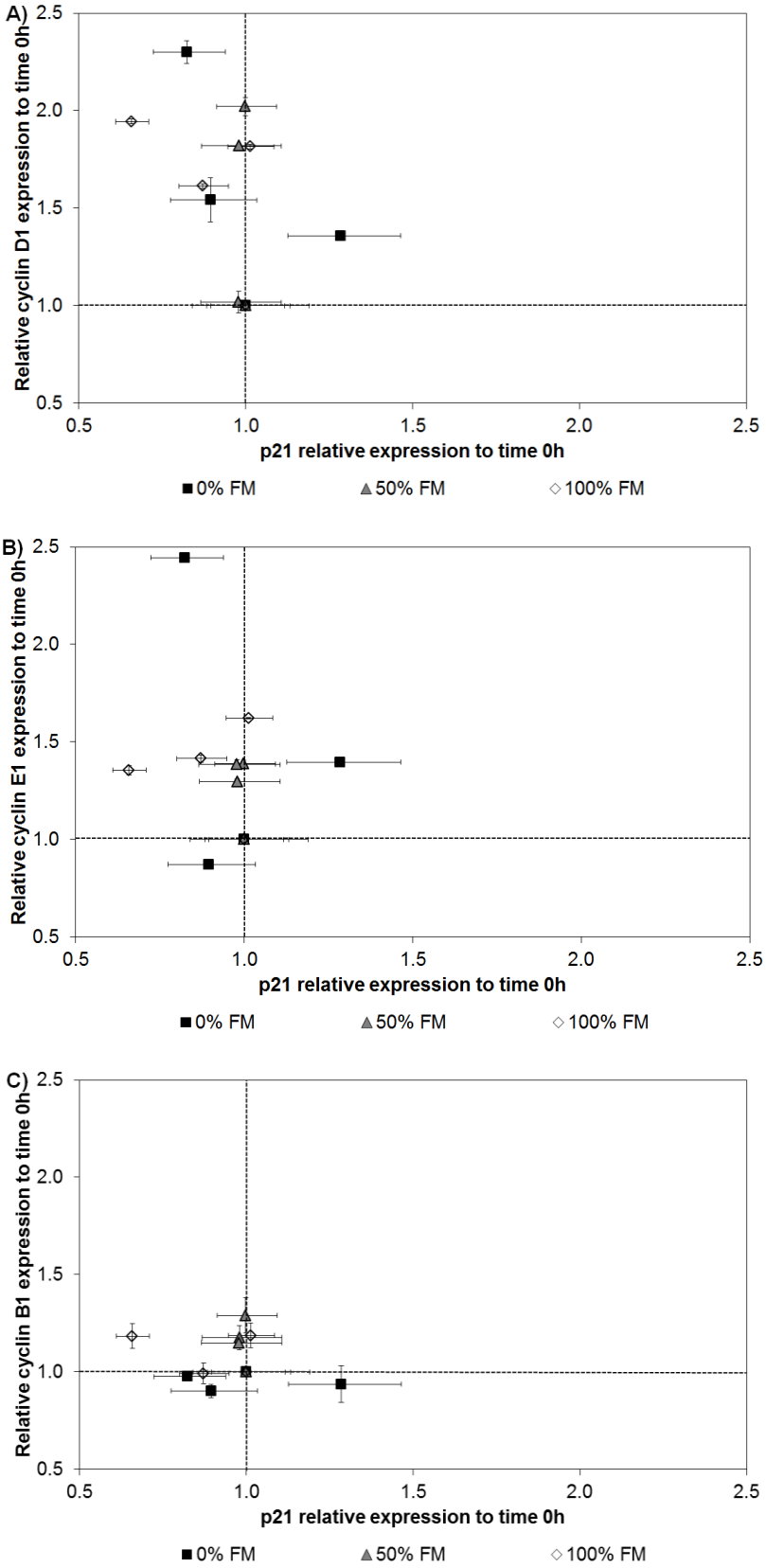


Figure 5.8. Medium shift experiment cyclin versus gene expression. A) Cyclin D1 vs p21 expression; B) Cyclin E1 vs p21 expression; C) Cyclin B1 vs p21 expression; D) Cyclin D1 vs trp53bp2 expression; E) Cyclin E1 vs trp53bp2 expression; F) Cyclin B1 vs trp53bp2 expression. Notation: Fresh medium (FM), (n=3, error bars=standard deviation).

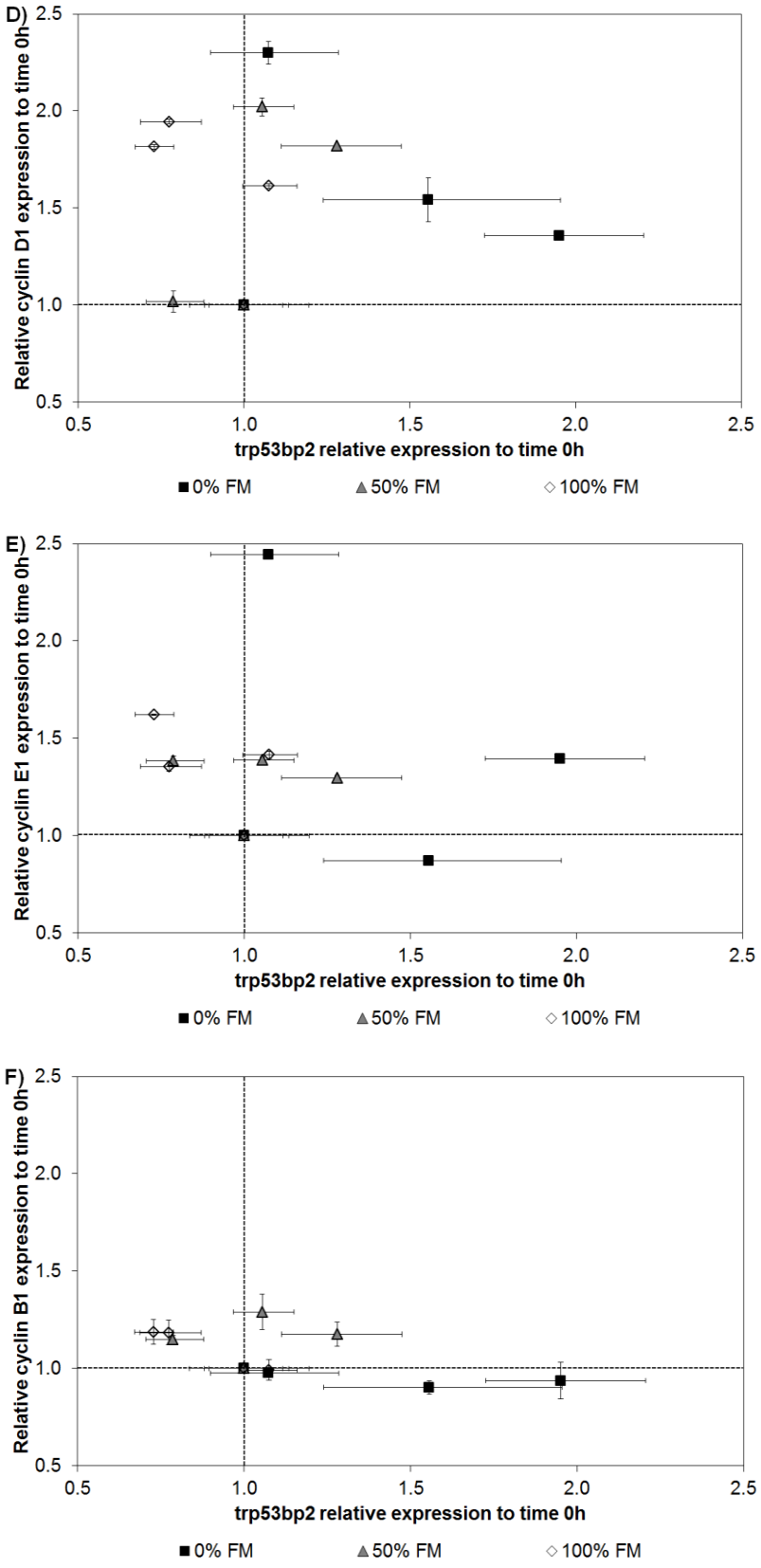


Figure 5.8. (Continued). Medium shift experiment cyclin versus gene expression. A) Cyclin D1 vs p21 expression; B) Cyclin E1 vs p21 expression; C) Cyclin B1 vs p21 expression; D) Cyclin D1 vs trp53bp2 expression; E) Cyclin E1 vs trp53bp2 expression; F) Cyclin B1 vs trp53bp2 expression. Notation: Fresh medium (FM), (n=3, error bars=standard deviation).

5.5. Conclusions

The aim of this chapter was to study the effect of temperature and medium composition on the cell cycle and apoptosis for the GS-NS0 cell line. The temperature shift experiments allowed screening the effect of this control variable on the cell culture. Particularly, at mild hypothermia (35 °C) a slower growth, a delay in the onset of apoptosis, a reduced metabolism, and similar mAb productivity compared to the 37 °C case were observed. Whereas at hyperthermia (39 °C) a similar cell growth, a faster cell death, an enhanced metabolism, and an apparent increased productivity compared to the 37 °C experiment were observed. Cyclin D1 induction due to hyperthermia conditions was not observed, although cyclin D1 expression was confirmed to be partially-associated to the substrate availability (glutamate). At the cell cycle distribution, a weak increase of the G_1/G_0 cell fraction was observed, prior to the onset of apoptosis under hypothermic conditions.

The medium shift experiment provided an overview of the effect of medium changes directly on a high viable growing mid-exponential population. In the absence of fresh medium (0%), growth suppression, low levels of cyclin B1 expression, and a decrease in viability was observed in a period of 24h. Apoptosis was confirmed to be induced after the shift to 0% fresh medium, both at the gene level and by morphological changes (%ESA). Moreover, the metabolic shift from lactate production to consumption was observed, and it correlates with the absence of glutamate. The experiments containing fresh medium (50% and 100%) showed a comparable cell growth, a high viability and the expression of all the cyclins (D1, E1, and B1). Cyclin D1 and E1 seemed to be temporarily overexpressed in the 0% fresh medium. The overexpression was correlated to the induction of apoptosis at the gene level. Similarly, the results showed the fine balance between the cell cycle and apoptosis. Some patterns between the gene expression (*p21* and *trp53bp2*) and the expression of the cyclins (D1, E1, and B1) were identified. These results confirmed the intricate and intimate link between the cell cycle machinery and the programmed cell death. Moreover, the observed patterns, although dependent to the culture conditions, render these entities (cyclins, *p21* and *trp53bp2*) as excellent candidates for the coupling between the cell cycle and apoptosis mathematical models.

CHAPTER 6

Development of a Cyclin Distributed Cell Cycle Model of GS-NS0 Cell Line

The cell cycle blueprint elucidated in chapter 4 & 5 provides a unique tool for describing the cell cycle using biologically relevant markers for each of the cell cycle phases. In chapter 4, key cell cycle metrics (cell cycle timings, cell cycle distribution, and cyclin expressions) were experimentally quantified by flow cytometry. These results are herein integrated in a novel experimental-modelling approach to formulate a cyclin and DNA distributed model for the industrially relevant cell line GS-NS0. In addition, the model structure was studied by global sensitivity analysis (GSA) following the model development framework. The parameters identified with a significant effect on the model outputs were further re-estimated from a set of batch experiments. After, the model accuracy and predictive power was tested and compared to experimental data. Most importantly, the presented approach can easily be extended to include further biological detail, as well as to other cell cycle relevant systems such as clinical problems (tumours, cancer treatments, etc.).

6.1. Introduction

A key underlying source of heterogeneity in mammalian cell culture systems is the cell cycle segregation (Karra et al., 2010; Pilbrough et al., 2009). The cell cycle is at the centre of cellular growth, death, and mAbs productivity that varies during the different cell cycle phases. Both productivity (Alrubeai et al., 1992) and glycosylation (Fussenegger and Bailey, 1998) have been reported to be influenced by the cell cycle state. Thus, the development of these industrially relevant systems can be improved through a better understanding of the cell cycle and its association with the productivity (Dutton et al., 2006).

As reviewed in chapter 2, the development of relevant segregated cell cycle models has proved to be challenging, particularly due to difficulties in providing quantitative experimental validation. PBMs represent the most accurate description

of the cell culture heterogeneity; alas the age/mass/volume formulations lack biological relevance (non-mechanistic and/or hardly quantifiable) for the cell cycle transition in mammalian cell cultures. Moreover, the absence of biological mechanism in the model descriptors limits its applicability and extension to include further biological detail. For example, the intimate link of the cell cycle and the cell programmed death would require relevant cell markers in order to meaningfully couple the two events (chapter 5). Furthermore, computationally intensive nature of PBM needs to be considered towards model-based applications. The development of biological mathematical models can aid the study of these complex systems and contribute to understand its features (Bailey, 1998). Thus, biologically relevant computational models can offer insight in the biological process and support a systematic process development.

6.2. Objectives

The aim of this chapter is to formulate a biologically-relevant distributed cell cycle model for the industrial cell line GS-NS0 that captures cell population heterogeneity, whilst being computationally fast to be used for model-based applications. The following scientific objectives were set:

- Formulate a biologically-relevant distributed cell cycle model for the industrial cell line GS-NS0 using first principles with fast computational solution times.
- Study the model structure using GSA (Section 3.3.11.) and identify the most significant model parameters.
- Re-estimate the subset of significant parameters.
- Compare the simulation results to experimental data to test the accuracy and predictive power of the model.

6.3. Methodology

The methodology adopted for the model development followed the framework for biological systems illustrated in Figure 2.7. Experimental and modelling aspects were integrated in the model development. Most of the experimental results presented in this chapter, were derived from chapter 4 (Section 4.4.4.). Specifically the control and arrest release experiments, which are compared to the model simulations.

The model implementation and all simulations were carried out in gPROMS®. The details of the employed GSA software tool and parameter estimation procedure can be found in Section 3.3.11. The control runs for the arrest release experiments presented in chapter 4 were used for the parameter re-estimation, whereas the after arrest release experiments (after thymidine and DMSO arrest release) were used to test the model against disturbed growth scenarios.

The undisturbed cell growth experiment with higher starting cell density used for model validation was conducted as described (Section 3.1.3.) and the employed analytical techniques can be found in Section 3.3.

6.4. Model Development & Experimental Validation

Based on the literature review and the experimental cell cycle blueprint (chapter 4), a multivariable and multistage PBM is proposed. The model is cyclin distributed for the lumped phases - G_1/G_0 in Equation (6.1) and G_2/M in Equation (6.3) - and it is DNA distributed for the S phase as presented in Equation (6.2). The lumped G_1/G_0 phase is justified due to the observed high percentage of cells positively expressing the Ki-67 proliferation marker (chapter 4 & 5). Although the fraction of proliferating cells decreased throughout the culture, it was identified to be correlated with the viability and plausibly with the onset of apoptosis. Thus, as an initial approximation, the lumped phases provide enough detail. Similarly, the G_2/M lumped phase is justified on the basis of the M phase short duration in mammalian cell cultures (i.e. usually less than 1h).

The truthful biological representation of the system should consider the bivariate distribution of the S phase with internal coordinates DNA and cyclin B1 (as experimentally observed). However, under specific conditions for the rate functions, a mathematical dimensionality reduction of the S equation can be achieved as detailed in Appendix II. The approximation is justified as cyclin B1 is not biologically relevant for the S to G_2 phase transition (Darzynkiewicz et al., 1996), and the modelled cells will enter the G_2/M phase with an approximated cyclin B1 content equal to the one observed experimentally between these two phases (S-G_2/M) in chapter 4.

G_1/G_0 phase: (6.1)

$$\frac{\partial N_{G1}(cycE,t)}{\partial t}+\frac{\partial r_{G1}(cycE,S)N_{G1}(cycE,t)}{\partial cycE}=-\Gamma_{G1}(cycE,S)N_{G1}(cycE,t)-k_d(S)N_{G1}(cycE,t)$$
$$+2\delta(cycE)\int_{cycB\min}^{cycB\max}\Gamma_{G2}(cycB,S)N_{G2}(cycB,t)dcycB$$

S phase: (6.2)

$$\frac{\partial N_S(DNA,t)}{\partial t}+\frac{\partial r_S(DNA,S)N_S(DNA,t)}{\partial DNA}=\delta(DNA-1)\int_{cycE\min}^{cycE\max}\Gamma_{G1}(cycE,S)N_{G1}(cycE,t)dcycE$$
$$-k_d(S)N_S(DNA,t)$$

G_2/M phase: (6.3)

$$\frac{\partial N_{G2}(cycB,t)}{\partial t}+\frac{\partial r_{G2}(cycB,S)N_{G2}(cycB,t)}{\partial cycB}=-\Gamma_{G2}(cycB,S)N_{G2}(cycB,t)-k_d(S)N_{G2}(cycB,t)$$
$$+\delta(cycB-cycB_{S-G2/M})r_S(DNA=2,S)N_S(DNA=2,t)$$

The number distribution ($N_{i=G1,S,G2}$) correspond to the number of cells distributed on a variable for each phase. The selected distributed variables for each phase are experimentally derived from the cell cycle blueprint presented in chapter 4. The model utilises cyclin E1 (*cycE*, key for the transition from G_0/G_1 to S phase), *DNA* (key for the transition between S phase and G_2/M) and cyclin B1 (*cycB*, key for the transition between G_2/M phases to G_0/G_1). Cyclin B1 regulates the G_2-M transition, although herein is used for the lumped G_2/M to lumped G_0/G_1 phase transition due to the G_2/M lumped approximation.

The growth functions (r_i) are responsible for the transition of the cells within each cell cycle phase. The cyclin growth functions ($r_{i=G1,G2}$) in Equation (6.4) denote cyclin (E1 or B1) build-up on the corresponding phase (G_0/G_1 or G_2/M). These functions are responsible for the transition of the cells within each cyclin domain. Similarly, the DNA growth function ($r_{i=S}$) in Equation (6.5) denotes the DNA build-up or synthesis in the S phase and is responsible for the transit of the cells within that phase. The growth functions (r_i) are coupled to the substrate/metabolite concentrations in the culture medium. Specifically, glutamate dependence was introduced for all the growth functions based on the energy-yielding importance of glutamine (Dorka et al., 2009; Naderi et al., 2011; Zhou et al., 2007), which is derived from glutamate in the GS system (Barnes et al., 2000). In the GS-NS0 cell line, over 90% of the glutamate has been identified to flow into the TCA cycle (Zhao et al., 2009) for further

metabolism (biomass synthesis and antibody production). Furthermore, the cyclin growth functions ($r_{i=G1,G2}$) were formulated as lactate-dependent based on the reports that lactate concentration inhibits cell growth (Mulukutla et al., 2012; Ozturk et al., 1992). The lactate dependence was not introduced in the S phase ($r_{i=S}$) given the common acceptance that the duration of this phase shows minor variability (Heath, 2001) and that the main control checkpoints are in the gap phases.

$$r_{i=G1,G2}\left(cyc,S\right)=Cycgrow\cdot f_{\lim Glu}\cdot f_{\lim Lac} \tag{6.4}$$

$$r_{S}\left(DNA,S\right)=DNAgrow\cdot f_{\lim Glu} \tag{6.5}$$

The glutamate (f_{limGlu}), glucose (f_{limGlc}) and lactate (f_{limLac}) dependences utilise Monod kinetics (Kiparissides et al., 2010b; Kontoravdi et al., 2005), Equation (6.6). The *Glu, Glc,* and *Lac* terms represent the extracellular glutamate, glucose, and lactate concentrations, respectively. The $K_{i=Glu,Glc,Lac}$ parameters represent the Monod constant, while the exponential factors (*n, m,* and *p*) capture the sensitivity towards the respective substrate/metabolite.

$$f_{\lim Glu}=\frac{Glu^{n}}{Glu^{n}+K_{Glu}{}^{n}}\quad;\quad f_{\lim Glc}=\frac{Glc^{m}}{Glc^{m}+K_{Glc}{}^{m}}\quad;\quad f_{\lim Lac}=\frac{K_{Lac}{}^{p}}{K_{Lac}{}^{p}+Lac^{p}} \tag{6.6}$$

The cyclin transition functions (Γ_i) are defined as the probability of transition between the phases. The transition functions between G_0/G_1 and S phases ($\Gamma_{i=G1}$), as well as between G_2/M and G_0/G_1 phases ($\Gamma_{i=G2}$) are formulated as a step function, Equation (6.7). The functions take a value of zero below the respective cyclin threshold for the phases G_1 (cyclin E1) and G_2 (cyclin B1), and become positive above the threshold while being glucose dependent (f_{limGlc}), Equation (6.6). Although glucose has not been identified as growth limiting, it does prolong the stationary phase and delay the decline phase (Sellick et al., 2011).

$$\Gamma_{i=G1,G2}\left(cyc,S\right)=\begin{cases}0 & ,\ below\ \ threshold\\ prob_{i}\cdot f_{\lim Glc} & ,\ above\ \ threshold\end{cases} \tag{6.7}$$

The cell cycle transition proceeds as follows. The cells transit from G_1/G_0 (Γ_{G1}) to the S phase - by means of the Dirac delta function *δ(DNA-1)* - with an initial DNA content. After the cells doubled their DNA content, transit occurs immediately from the S to the G_2/M phase, i.e. $\Gamma_S(DNA=2)=1$. Then, the cells enter G_2/M phase by

means of the Dirac delta function $\delta(cycB\text{-}cycB_{S\text{-}G2/M})$ - with a cyclin B1 content equal to the one observed experimentally between these two phases (as discussed). The cycle is completed by giving birth to two daughter cells (Γ_{G2}) and enter the G_1 phase - by means of the Dirac delta function $\delta(cycE)$ - with a minimum cyclin E1 content.

The phase populations are calculated over each domain as in Equation (6.8), whereas the total population is the sum over all the three distributed domains, see Equation (6.9).

$$phase_{i=G1,S,G2} = \int_{phase_\min}^{phase_\max} N_i(x_i)dx_i \quad \text{where } x_{G1}=cycE,\ x_S=DNA,\ x_{G2}=cycB \tag{6.8}$$

$$total = phase_{G1} + phase_S + phase_{G2} \tag{6.9}$$

The cell cycle distribution can be estimated as in Equation (6.10), while the viable cell density (X_V) is expressed by dividing over the reactor working volume (V), see Equation (6.11). The model is presented in batch operation mode and under the standard assumption of ideal mixing within the flasks.

$$f_{i=G1,S,G2} = \frac{phase_i}{total} \tag{6.10}$$

$$X_V = \frac{total}{V} \tag{6.11}$$

The dead cell population (X_D) accounts for the specific death rate (k_d) of the viable cells and the lysis specific rate (k_{lys}) of the dead cells, Equation (6.12). The specific death rate – Equation (6.13) - is linked to the extracellular glutamate concentrations due to glutamate's essential role in the GS system (Barnes et al., 2000) and exhaustion from the culture medium in batch mode. The sensitivity of the cell death to glutamate is given by the affinity death parameter (k_{dGlu}) and the exponential factor (q).

$$\frac{d\left(X_D V\right)}{dt} = k_d X_V V - k_{lys} X_D V \tag{6.12}$$

$$k_d = k_{d\max}\left(\frac{k_{dGlu}}{k_{dGlu} + Glu}\right)^q \tag{6.13}$$

The PBM is coupled to an unstructured metabolic model in order to fully represent the system. The unstructured metabolic model supports fast computational times, as well as a good description without introducing too many parameters (Ho et al., 2006). The dynamics of the substrate/metabolite changes are linked to the cell growth rate. The growth rate (μ) utilised in the metabolic model is calculated based on the cyclin and DNA growth functions, Equation (6.14).

$$t_{i=G1,G2} = \frac{cyclin_threshold}{r_{i=G1,G2}} \quad ; \quad t_S = \frac{1}{r_S} \quad ; \quad \mu = \frac{\ln(2)}{t_{G1} + t_S + t_{G2}} \tag{6.14}$$

The basic metabolism is accounted for through the reactor mass balances. The biomass yield ($Y_{i=Glu,Glc}$) on substrates (glutamate and glucose) defines the consumption rates ($Q_{i=Glu,Glc}$), Equation (6.15). The material mass balance for the substrates is presented in Equation (6.16).

$$Q_{i=Glu,Glc} = \frac{\mu}{Y_{i=Glu,Glc}} \tag{6.15}$$

$$\frac{dS}{dt} = -Q_{i=Glu,Glc} X_V V \tag{6.16}$$

Lactate is modelled to be produced on a yield basis (Y_{Lac}) from glucose and glutamate consumption as supported by previous reports (Dorka et al., 2009; Nolan and Lee, 2011), see Equation (6.17). In addition, lactate is considered to be consumed (Q_{Lac}) as experimentally observed (Mulukutla et al., 2012; Templeton et al., 2013), which herein is considered to be triggered by glutamate's exhaustion.

$$\frac{dLac}{dt} = Q_{Glc} Y_{Lac} f_{\lim Glu} + Q_{Glu} \frac{Y_{Lac}}{2} X_V V - Q_{Lac} \left(1 - f_{\lim Glu}\right) \tag{6.17}$$

Finally, the antibody production (mAb) is specific for each cell cycle phase ($Q_{i=G1,S,G2}$) as stated in Equation (6.18).

$$\frac{dmAb}{dt} = \left(Q_{G1} f_{G1} + Q_S f_S + Q_{G2} f_{G2}\right) X_V V \tag{6.18}$$

The presented PBM coupled with an unstructured metabolic model consists of a system of hyperbolic partial integrodifferential equations. The system is discretised in the cell content space using conservative first order finite differences (Kostoglou and

Karabelas, 1995), which transforms it into ordinary differential equations with respect to time. The model was implemented in gPROMS® modelling software and all simulations were performed using a desktop computer with an Intel® Core™ i7 CPU.

6.5. Model Analysis & Re-estimation of Significant Model Parameters

The next step in the model development was to evaluate the model structure using GSA (Section 3.3.11.). As outlined in chapter 2 and in the biological model development framework (Section 2.5), GSA systematically evaluates output variability. GSA is a key step in the model analysis due to the nonlinearity nature of the system. However, prior to GSA, where a substantial number of scenarios are evaluated, a cell conservation test was carried out.

The aim of the cell conservation test was to ensure that the selected discretisation space (i.e. maximum number of bins or intervals) would minimise the cell losses. Thus, the number of bins for the cyclin E1 and B1 domains was increased in order to ensure that over 99% of the cells remained in the system after 120h of simulation. The DNA space can be fixed (i.e. 20 bins) as the transition from S to G_2/M is deterministic and does not affect the cell conservation. For this purpose, the full range of 24 parameters is varied ±50% (Sidoli et al., 2006) from their nominal value and the cell conservation is evaluated. In addition, the birth term is fixed to 1 (to avoid generation), the death rate is fixed to zero (k_{dmax}=0, to neglect cell death) and the interaction with the nutrients is neglected ($f_{limGlu/Glc/Lac}$=1, to maintain maximum rates). A uniform distribution is applied for all domains (cyclin E1 between 0-95%, DNA between 1-2, and cyclin B1 between 0-95%). Such formulation evaluates the worst case scenario for cell conservation in the system. The number of bins was increased to 200, both for cyclin E1 and cyclin B1, which ensured 99% retention of cells in the system after 120h (Appendix III.).

GSA followed the cell conservation test, after restoring the birth term, death rate and limiting functions. In order to evaluate the relative influence of the uncertainty of the parameters in the outputs, a large number of sampling points is typically required. A total of five outputs were evaluated (X_v, f_{G1}, f_S, f_{G2}, and mAb) at three characteristic simulation time points. The simulation time points covered the early-

exponential stage (36h), entrance to stationary phase (72h), and the onset of death phase (120h). A total of 40,000 scenarios were evaluated varying the 24 parameters ±50% from their nominal value. The nominal values were taken from experimental data (e.g. chapter 4) and when data were not available an approximated order-of-magnitude values were assigned (Kiparissides, 2012; Sidoli et al., 2006). The output of the scenarios was used to estimate the SIs using the GUI-HDMR software as outlined in chapter 3. The computational solution time for a single run was fast (< 4s), and two fold faster compared to the mass structured PBM of Karra et al. (2010). Similarly, the GSA was completed in less than 30h, which is also fast compared to previous contributions (Karra et al., 2010; Pinto et al., 2007; Sidoli et al., 2006). From the initial 24 varied parameters, 9 were found significant (above the threshold, chapter 3), see Table 6.1. These parameters are reviewed next.

The viable cell population output (X_v) was found to be sensitive to the cyclin and DNA growth rates, as well as the exponential death factor *(q)* at early stage (i.e.36h). Also an increasing sensitivity (from mid stage 72h towards late stage 120h) to the biomass yield on glutamate (Y_{Glu}) and to the maximum death rate (k_{dmax}) was observed. The cell fractions ($f_{i=G1,S,G2}$) showed higher sensitivity towards the respective growth rates (i.e. *CycEgrow, DNAgrow*, *CycBgrow*) at all stages. Similarly, the cell fractions ($f_{i=G1,S,G2}$) showed mild sensitivity to the growth rates governing the preceding cell cycle phase. However, none of the transition probabilities or thresholds for the cyclins were identified as significant. This should not be interpreted as irrelevant, as it factually reflects the structure of the model. Hence, a few aspects should be considered on this result. First, the model uses the transition probabilities to determine the dispersion around the cyclin thresholds. Thus, if there is a positive transition probability, the cells will transit to the next stage and only the dispersion around the threshold is affected. Second, the transitions are not independent of the threshold. However, from a pure numerical value perspective, once a cell reaches the threshold (regardless of its value), the cell is a candidate to proceed to the next stage. Therefore, the cyclin thresholds alone are not relevant, as it should be considered in connection with the cyclin growth rates - together determine the transitions.

Table 6.1. GSA Indexes and parameters values for the cyclin distributed cell cycle model. Outputs: X_V=viable cell density, f_{G1}=G_1/G_0 cell fraction, f_S=S cell fraction, f_{G2}=G_2/M cell fraction, and mAb=antibody titre.

		Outputs																	
		Xv			f_{G1}			f_S			f_{G2}			mAb			Nominal Value	Units	Estimated Value	95% Conf. Interval	DMSO delay simulation
	time (h)	36	72	120	36	72	120	36	72	120	36	72	120	36	72	120					
Parameters	critE threshold																15	% cyc E			
	critB threshold																37	% cyc B			
	$prob_{G1}$																0.6	n/a			
	$prob_{G2}$																0.6	n/a			
	CycEgrow																3.33	% cyc E/h	3.49	1.46E-01	1.52
	DNAgrow																0.15	DNA/h	0.16	4.76E-03	
	CycBgrow																8.22	% cyc B/h	8.07	2.99E-01	
	k_{dmax}																3.0E-02	h^{-1}	2.31E-02	1.90E-03	
	k_{lys}																5.0E-03	h^{-1}			
	K_{Lac}																50	mM			
	Q_{Lac}																2.5E-11	mM/h			
	k_{dGlu}																0.05	mM			
	Y_{Glc}																2.1E+08	cell/mM			9.1E+07
	K_{Glc}																5	mM			
	Y_{Glu}																1.8E+09	cell/mM	1.70E+09	7.20E+07	7.4E+08
	K_{Glu}																0.20	mM			
	Y_{lac}																2.3	n/a			
	Q_{G1}																5.0E-10	mg/cell/h	9.57E-10	2.10E-09	
	Q_S																5.0E-10	mg/cell/h	1.00E-10	4.30E-09	
	Q_{G2}																5.0E-10	mg/cell/h	1.00E-11	2.00E-09	
	m = expglc																2	n/a			
	n = expglu																1	n/a			
	q = expdeath																2	n/a	2		
	p = explac																1	n/a			
	SI colour value	**below 0.1**			**0.1-0.3**			**0.3-0.5**			**0.5-0.7**										

An important aspect of the GSA is that the results are subject to the proposed model structure and outputs considered. Thus, other model structures or outputs might result in other identified significant parameters. Finally, the antibody titre output (*mAb*) was sensitive to all the specific productivities ($Q_{i=G1,S,G2}$) at early stage (36h), though Q_{G2} was not sensitive at the other times points and Q_S was not sensitive at 120h. These results suggest some association of the specific cell cycle production with the mAb titre. A better correlation seems to be observed towards the G_1 specific productivity (identified throughout significant). Such correlation could be attributed to the longer cell cycle time experimentally observed for the G_1 phase, which usually translates into higher G_1 cell fractions when compared to the other two phases (S, G_2/M).

Following the biological model development framework (Section 2.5), the identified significant parameters were re-estimated; whereas the non-significant parameters were fixed to their nominal value. The control runs for the arrest release experiments presented in chapter 4 were used for the parameter re-estimation.

6.6. Results & Discussion

In this section, the model simulation results are shown and compared to the experimental data. The simulation results are carried with the same set of parameters and only varying the initial culture conditions, unless otherwise stated.

6.6.1. Model results for the control runs

The model simulation results for the control runs (used for parameter estimation) of the arrest experiments showed a good agreement with the experimental data. The cell growth kinetics, peak and decline, as well as the timing in viability decline of the culture for both control runs were captured by the model simulations (Figure 6.1A). Similarly, the glucose/lactate (Figure 6.1B) and glutamate/mAb (Figure 6.1C) simulations captured the experimental trends. The model predicted cell cycle distributions showed a good agreement, particularly at early stages of the culture (Figure 6.1D). Overall, the model predictions showed a good fit to the experimental data.

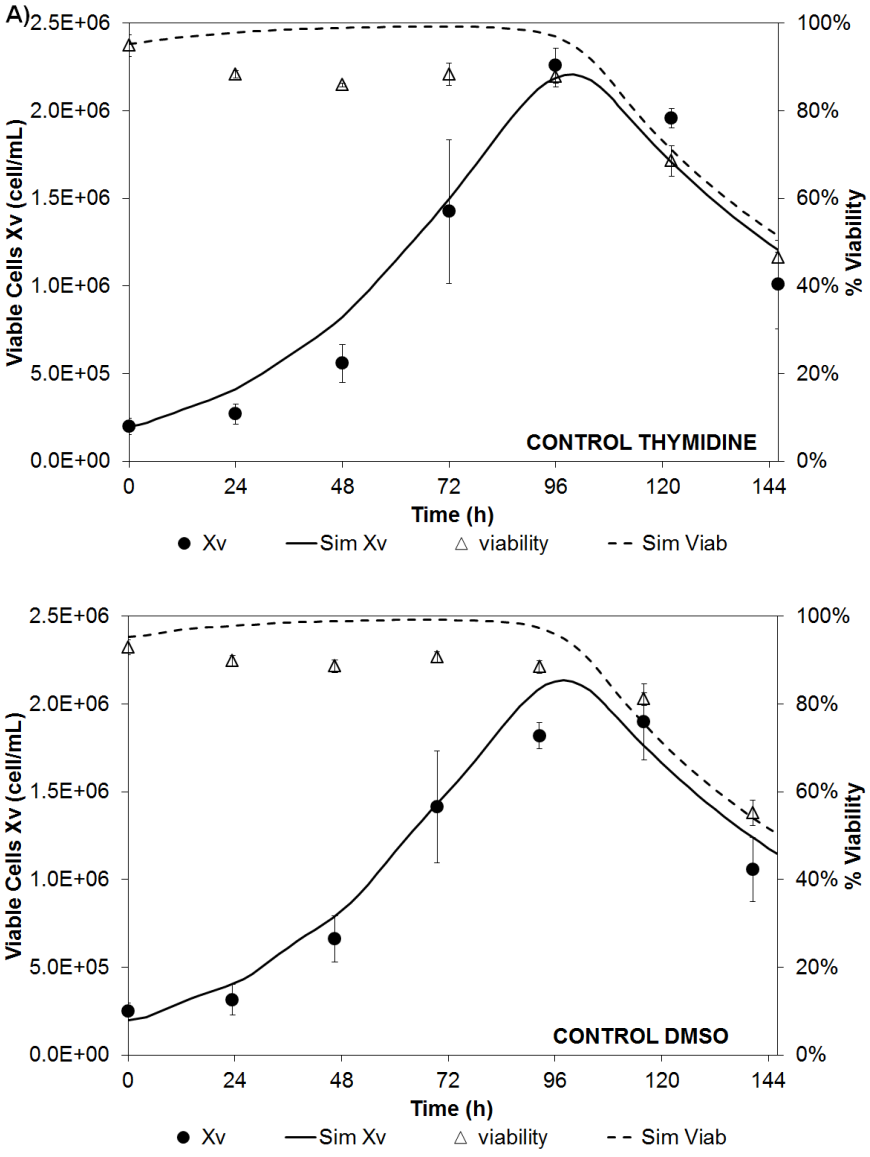


Figure 6.1. Model results for the control experiments. A) Cell growth and viability; B) Glucose and lactate concentration profiles; C) Glutamate and mAb concentration profiles; D) Cell cycle distribution. Notation: dots represent experimental data (n=3, error bars=standard deviation), lines represent the simulation results.

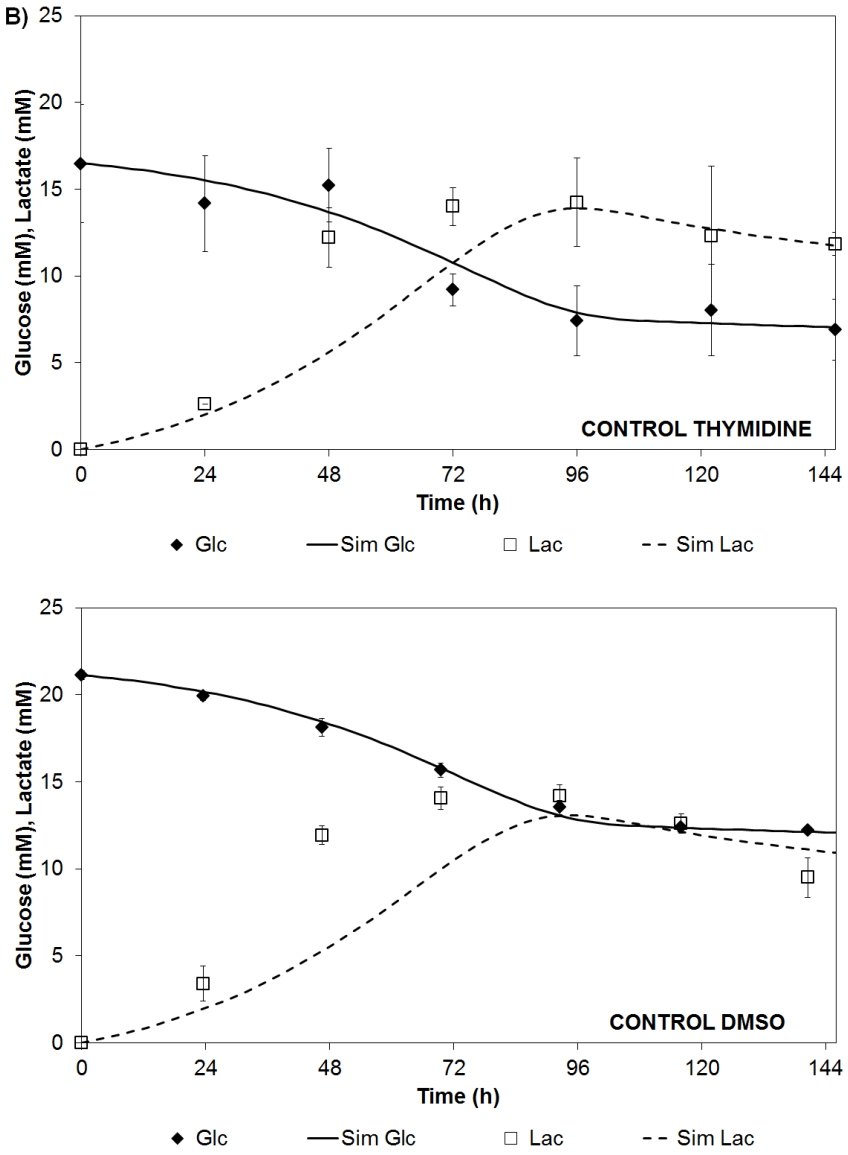


Figure 6.1. (Continued). Model results for the control experiments. A) Cell growth and viability; B) Glucose and lactate concentration profiles; C) Glutamate and mAb concentration profiles; D) Cell cycle distribution. Notation: dots represent experimental data (n=3, error bars=standard deviation), lines represent the simulation results.

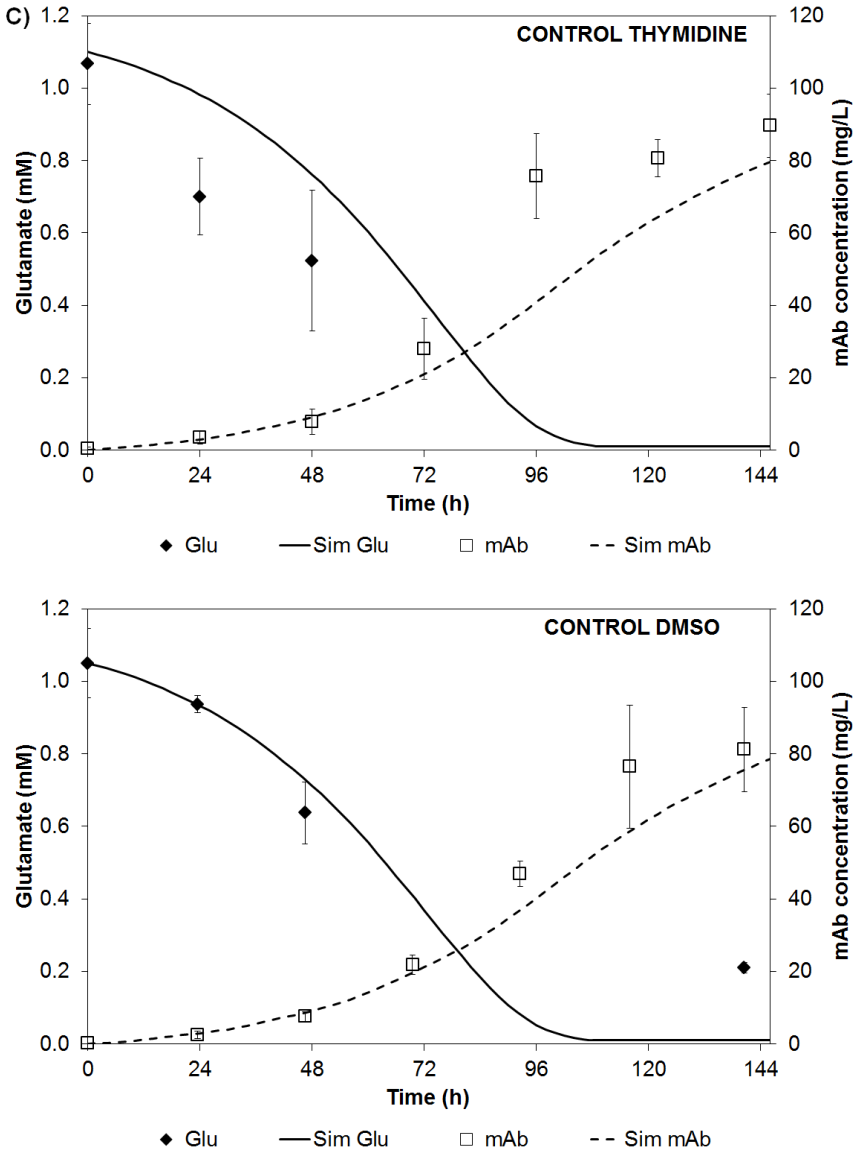


Figure 6.1. (Continued). Model results for the control experiments. A) Cell growth and viability; B) Glucose and lactate concentration profiles; C) Glutamate and mAb concentration profiles; D) Cell cycle distribution. Notation: dots represent experimental data (n=3, error bars=standard deviation), lines represent the simulation results.

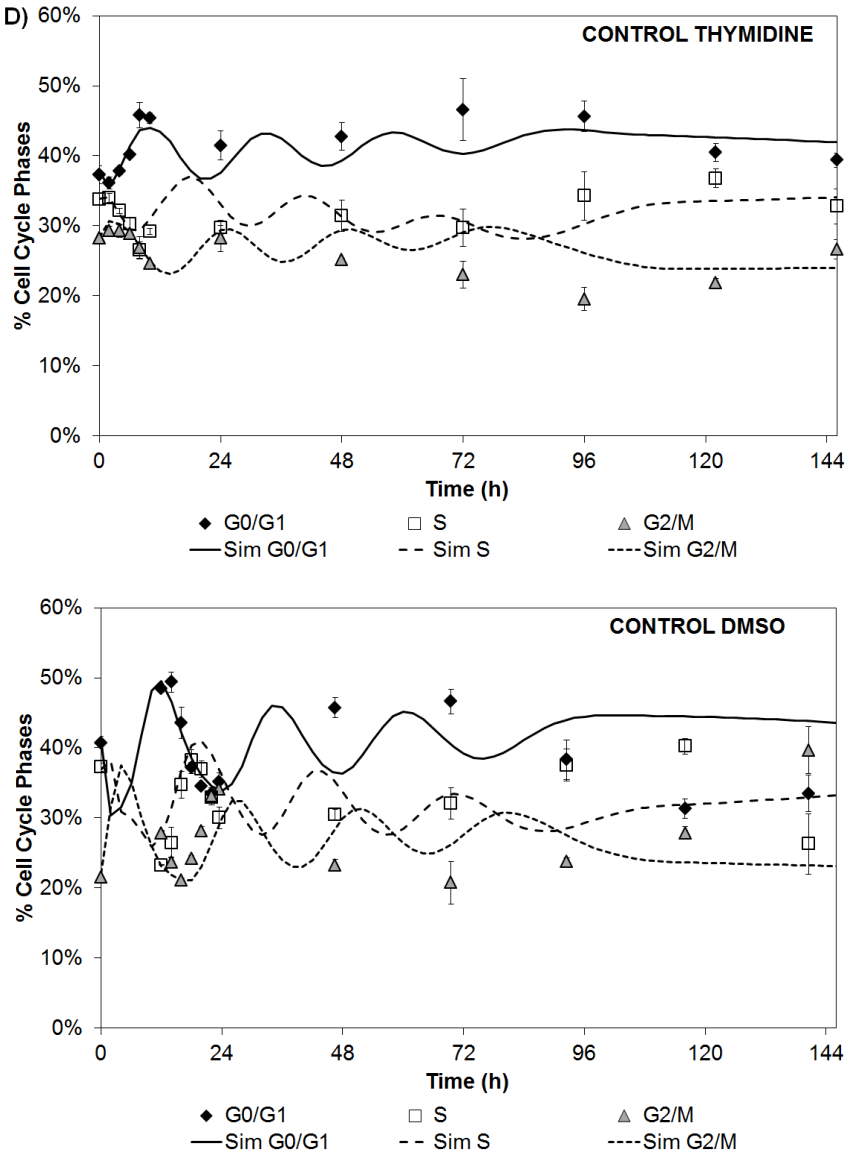


Figure 6.1. (Continued). Model results for the control experiments. A) Cell growth and viability; B) Glucose and lactate concentration profiles; C) Glutamate and mAb concentration profiles; D) Cell cycle distribution. Notation: dots represent experimental data (n=3, error bars=standard deviation), lines represent the simulation results.

6.6.2. Model results for the arrest release experiments

The model was tested against the disturbed growth scenarios (after thymidine and DMSO arrest release). These experiments provide significantly different starting cell cycle scenarios (chapter 4) when compared to the control runs. For the thymidine arrest release case, a good model prediction was observed for the cell growth (Figure 6.2A), substrate consumption (Figure 6.2B-C), and mAb titre (Figure 6.2C). The lactate predictions followed the trends (Figure 6.2B), particularly after 48h of culture. However, the high lactate levels at 24h were not captured by the model, which were attributed to an effect of the cell arrest (chapter 4). Despite this difference, the cell cycle distribution (Figure 6.2D) was satisfactorily predicted. The sharp oscillations soon after the arrest release were captured by the model prediction. The relevance of the model formulation using cyclins/DNA distribution is evident on the ability to predict the cell cycle variations.

The DMSO arrest release case proved to be more challenging due to the discussed effects on the cell cycle machinery (chapter 4). The model predictions using the re-estimated set of parameters showed overall a good agreement in terms of cell growth and viability (Figure 6.3A, grey lines) with an apparent systematic difference between the predictions and experimental data. The systematic difference seems to be due to the pronounced experimental lag phase. Nonetheless, the glucose/lactate (Figure 6.3B, grey lines) and glutamate (Figure 6.3C, grey lines) predictions showed a good experimental agreement. In contrast, the mAb titre prediction (Figure 6.3C, grey lines) showed a poor fit, overestimating the final titre. The mAb prediction deviation could be partially attributed to differences in cell density prediction, as well as to the discussed effects of the DMSO on the productivity (chapter 4). However, the cell cycle predicted distribution (Figure 6.3D) showed that the model was not accurately capturing the cell cycling behaviour. The cell cycle simulation trends are correct, but there seems to be a systematic difference.

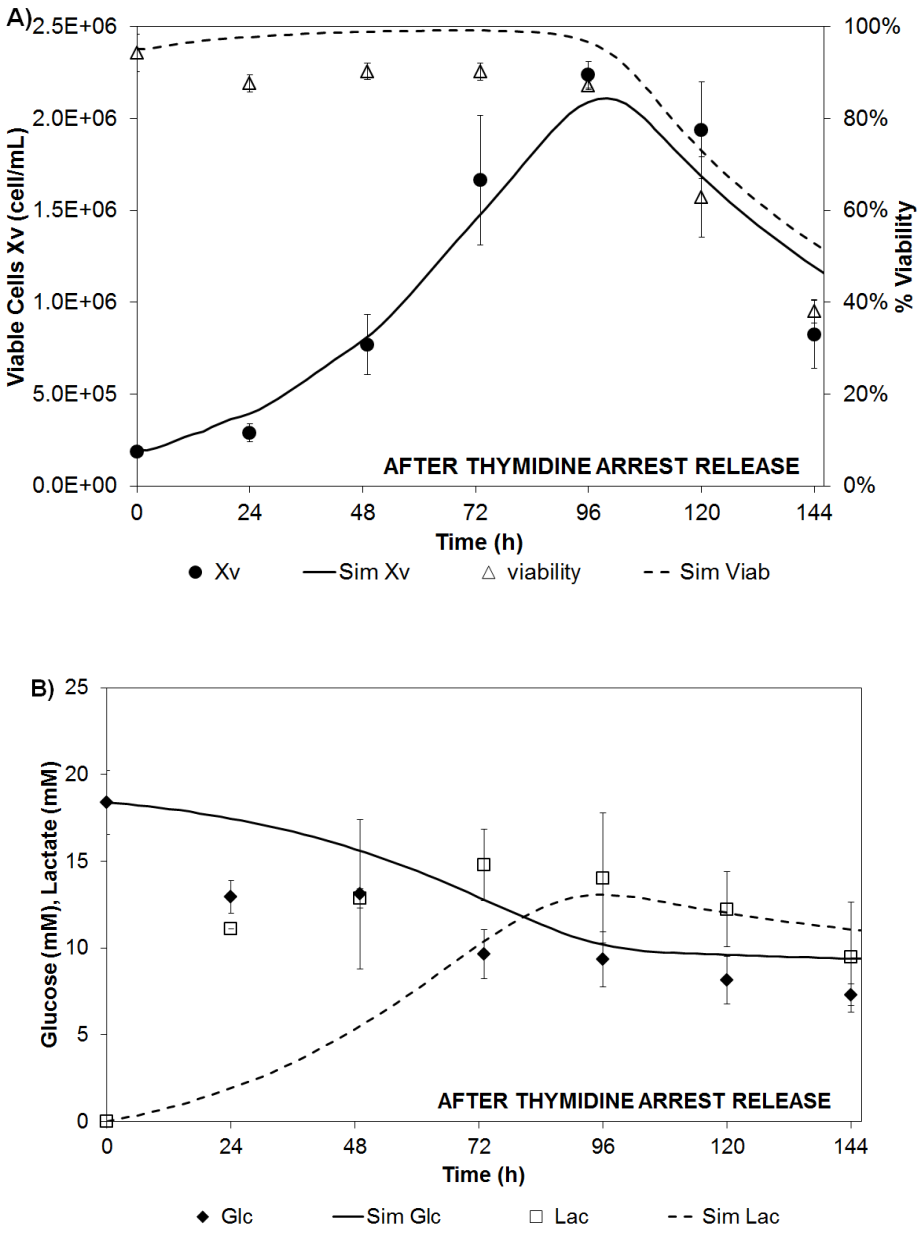
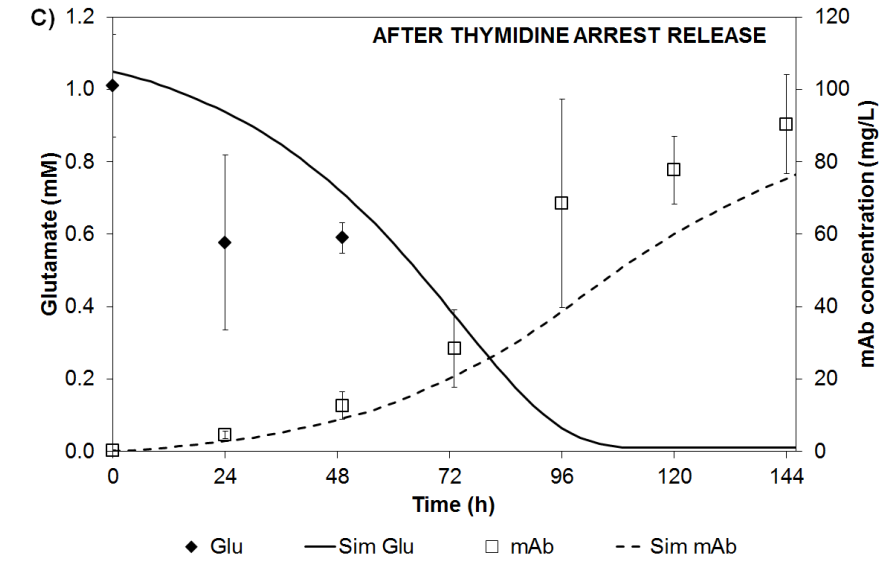


Figure 6.2. Model results for the thymidine arrest release experiment. A) Cell growth and viability; B) Glucose and lactate concentration profiles; C) Glutamate and mAb concentration profiles; D) Cell cycle distribution. Notation: dots represent experimental data (n=3, error bars=standard deviation), lines represent the simulation results.



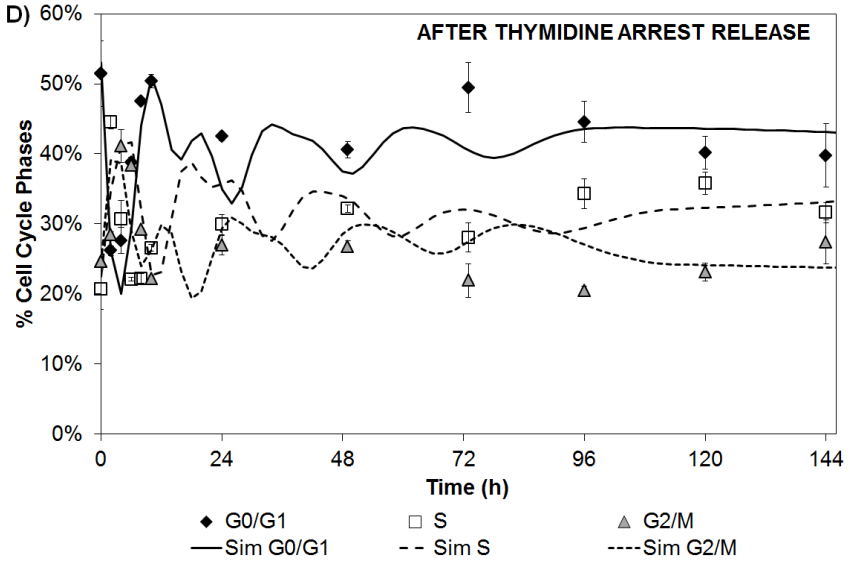


Figure 6.2. (Continued). Model results for the thymidine arrest release experiment. A) Cell growth and viability; B) Glucose and lactate concentration profiles; C) Glutamate and mAb concentration profiles; D) Cell cycle distribution. Notation: dots represent experimental data (n=3, error bars=standard deviation), lines represent the simulation results.

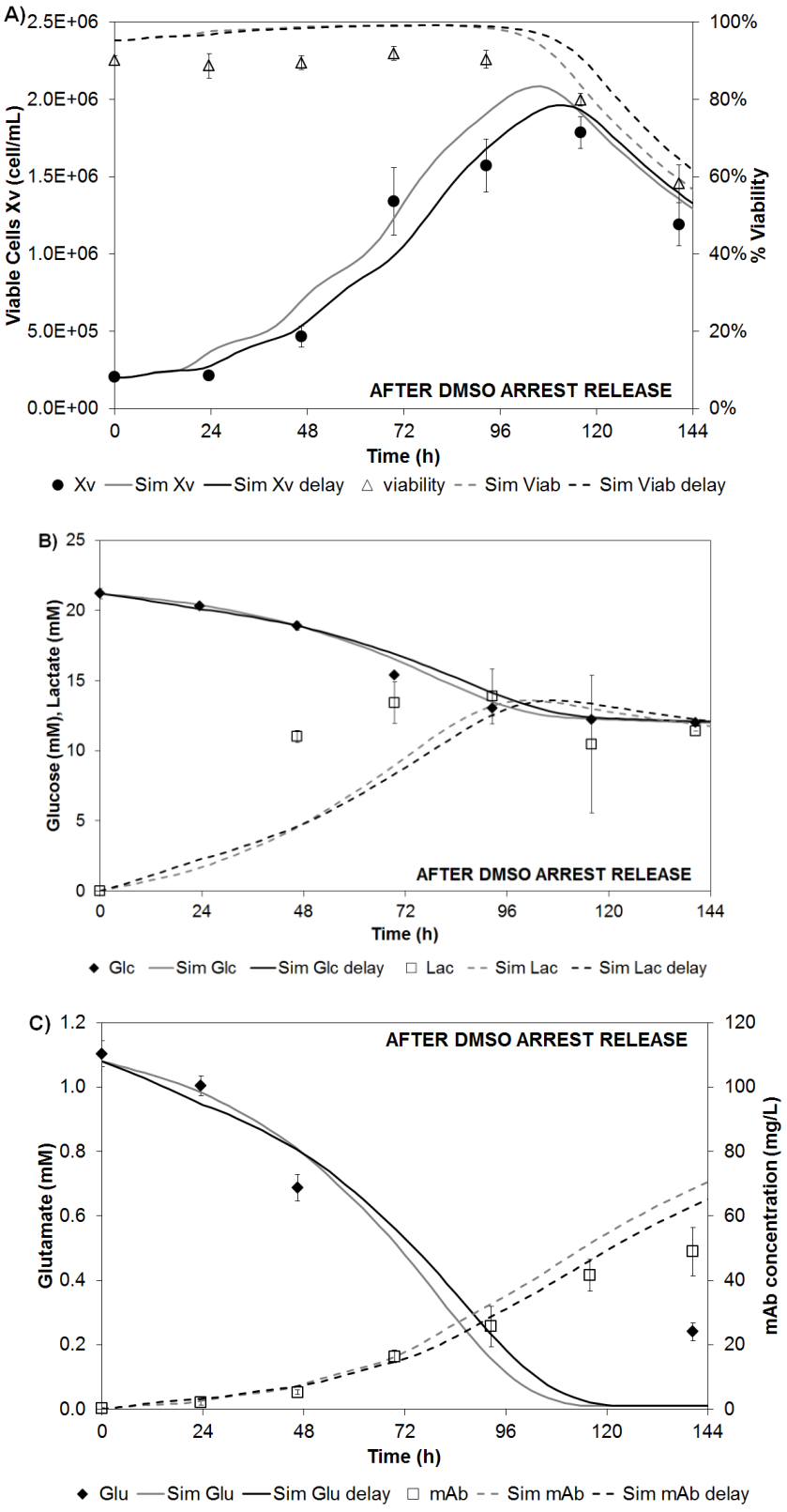
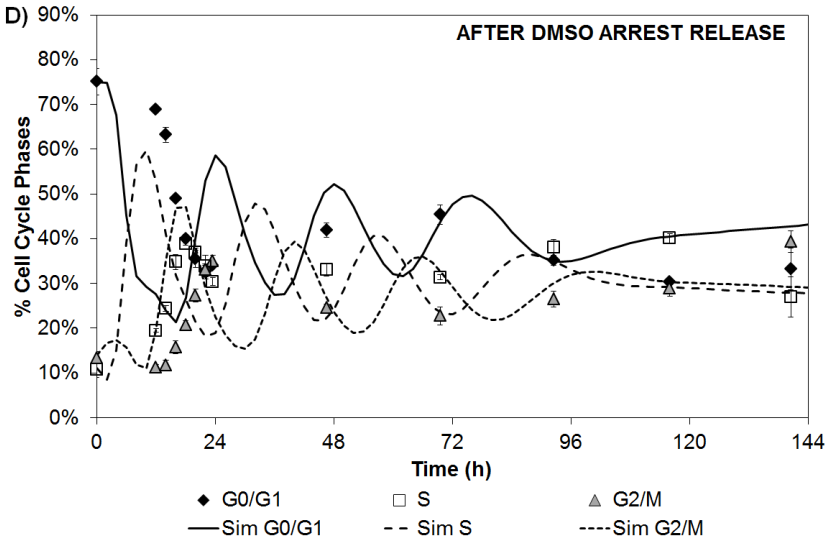


Figure 6.3. Model results for the DMSO arrest release experiment. A) Cell growth and viability; B) Glucose and lactate concentration profiles; C) Glutamate and mAb concentration profiles; D) Cell cycle distribution; E) Cell cycle distribution delay growth. Notation: dots represent experimental data (n=3, error bars=standard deviation), lines represent the simulation results. Grey lines: simulation with estimated parameters (Table 6.1). Black lines: simulation with DMSO delay parameters (Table 6.1).



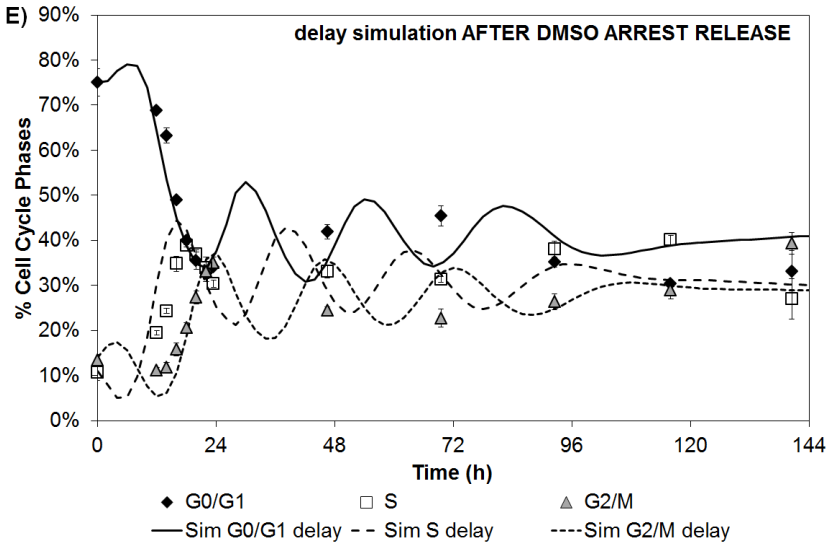


Figure 6.3. (Continued). Model results for the DMSO arrest release experiment. A) Cell growth and viability; B) Glucose and lactate concentration profiles; C) Glutamate and mAb concentration profiles; D) Cell cycle distribution; E) Cell cycle distribution delay growth. Notation: dots represent experimental data (n=3, error bars=standard deviation), lines represent the simulation results. Grey lines: simulation with estimated parameters (Table 6.1). Black lines: simulation with DMSO delay parameters (Table 6.1).

The observed differences are hypothesised to be due to the imbalances caused by the DMSO. DMSO action has been reported to indirectly inhibit the cyclin E1/CDK2 complex (Ponzio et al., 1998), and herein a cyclin E1 imbalance was observed experimentally (chapter 4). Thus, the hypothesis of a slower G_1 phase completion during the first 24h due to DMSO's effect was tested in the model. This was captured by slowing the Cyclin E1 growth rate (*cycEgrow*) during the first 24h of simulation. For comparison purposes to the initial simulated scenario, the yields on substrates ($Y_{i=Glu,Glc}$) were adjusted by the same factor. The decreased factor for the cyclin E1 growth rate was found to be approximately 2.3-fold slower.

The three parameters were modified for the first 24h of simulation (DMSO delay simulation values, Table 6.1) and set back to their initial values (nominal or estimated values, Table 6.1) after 24h. All other model parameters were kept at the reported values. The simulation results for the delay growth are shown in Figure 6.3A-C (black lines). The cell growth and viability predictions showed an improved fit to the experimental data and the lag phase was captured (Figure 6.3A). Similarly, the mAb titre prediction was improved (Figure 6.3C). Alas, the final titre is still overpredicted, suggesting that the lower experimental titre is due to a DMSO treatment effect. The metabolism predictions were comparable to the initial scenario as intended (Figure 6.3B-C). The sharp cell cycle predictions captured the experimentally observed oscillations (Figure 6.3E). The biological relevance of the model allowed to uniquely postulate an *in silico* plausible explanation to the experimental observations. Previous models based on mass/volume cannot account for a mechanistic delay in the cell cycle transition. Although, the imbalances caused by the DMSO are several and complex, the model provides a platform for more structured studies. Thus, the introduced temporary variation of three parameters (by the same factor) justified the experimentally observed cell growth delay, lower peak density and moderately explained the lower mAb productivity.

6.6.3. Model results for the undisturbed cell growth experiment with higher starting cell density

The predictive power of the model was tested against an undisturbed growth experiment with a two fold higher starting cell density. The model predictions for cell growth, viability (Figure 6.4A) and substrate consumption (Figure 6.4B-C) showed a good fit. Few deviations in the predictions when compared to the experimental data were observed. The cell density peak and decline timing were captured by the model, although the peak cell density was overpredicted. Similarly, around 96h, glutamate was observed experimentally in the culture (either produced or released by cell lysis), which the model does not account for. The lactate predicted profile showed the largest deviations, particularly after 48h of culture (Figure 6.4B). The overall lactate trends are correct, but the lactate consumption seemed to be pronounced after 48h, which the model moderately captured. Thus, the shift in the lactate metabolism needs further consideration and study. In contrast, the observed mAb titre was closely predicted (Figure 6.4C). The cell cycle distribution (Figure 6.4D) predictions showed a fair fit to the experimental data. The overall trends are accurate but some deviations were observed during the first 12h.

The observed model predictions discrepancies stressed the importance between the cell growth and the culture environment. Particularly, the lactate metabolism needs to be further considered. Although, the current formulation accounts for the lactate being produced from two sources (glucose, glutamate), other sources might be available in the used medium formulation such as pyruvate (Dean and Reddy, 2013). The glutamate exhaustion seemed to be a fair descriptor for the onset of the lactate consumption, although this needs further validation. However, the undefined character of the medium (serum containing) obscures such studies. In particular, the use of chemically defined medium would enable the refinement of the modelled cyclin-extracellular substrate/metabolite concentrations links. This is a key feature as it was experimentally observed how the metabolic shift (or use of other carbon sources) has an effect in the cell cycle progression and ultimately in the cell growth.

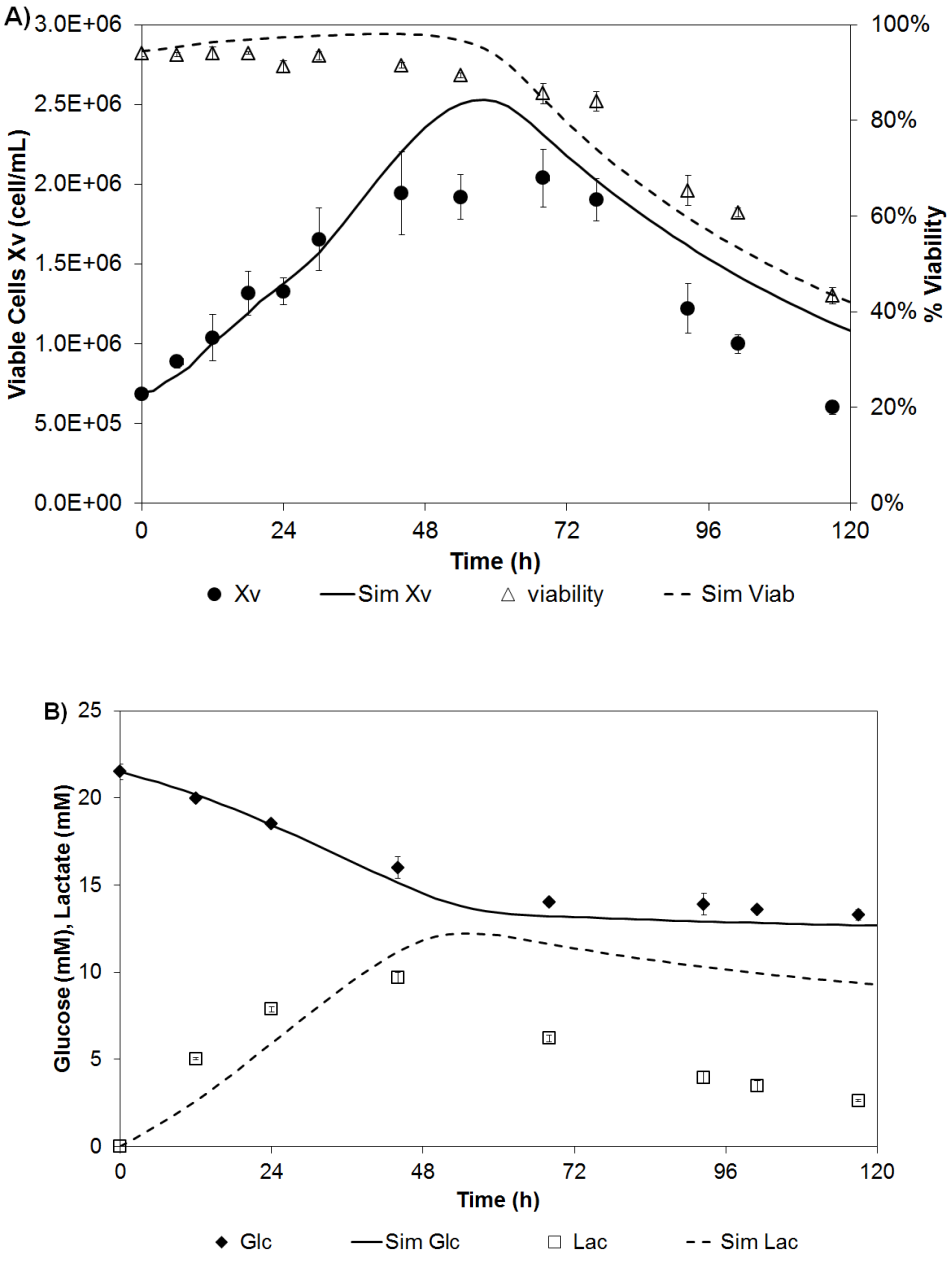
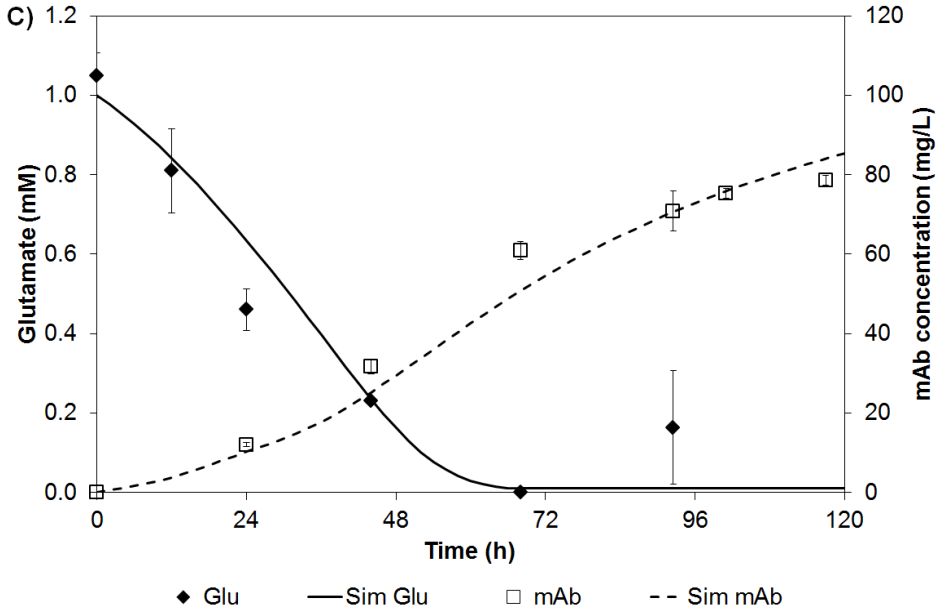


Figure 6.4. Model results for undisturbed higher cell density experiment. A) Cell growth and viability; B) Glucose and lactate concentration profiles; C) Glutamate and mAb concentration profiles; D) Cell cycle distribution. Notation: dots represent experimental data (n=3, error bars=standard deviation), lines represent the simulation results.



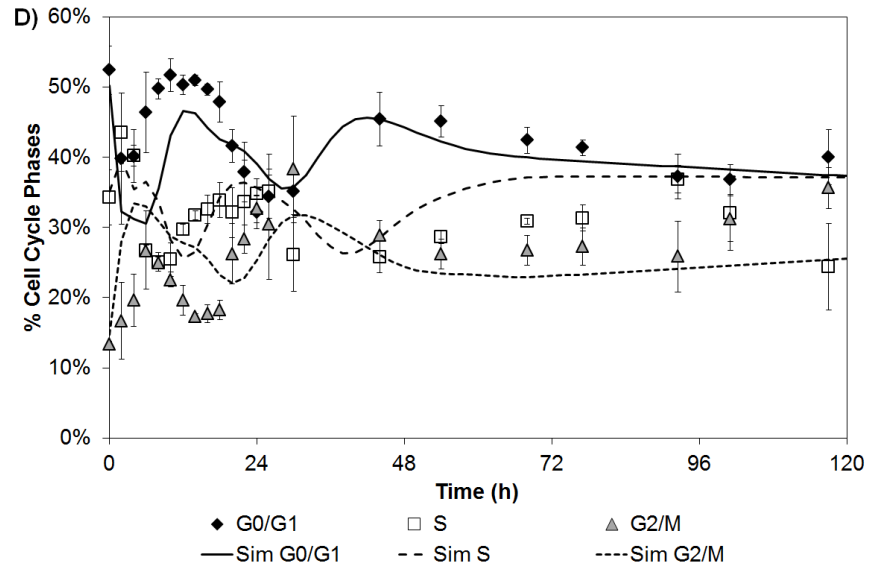


Figure 6.4. (Continued). Model results for undisturbed higher cell density experiment. A) Cell growth and viability; B) Glucose and lactate concentration profiles; C) Glutamate and mAb concentration profiles; D) Cell cycle distribution. Notation: dots represent experimental data (n=3, error bars=standard deviation), lines represent the simulation results.

6.7. Conclusions

A biologically and mechanistically relevant cell cycle distributed model for an industrial cell line was presented in this chapter. The model formulation captured the cyclins key role as a quantifiable marker determining the proliferating state of the culture. Moreover, the experimental approach presented in chapter 4 is integrated seamlessly into the model. As a result, the model is able to capture the complex heterogeneity and multi-scale nature of mammalian cell culture systems. The versatile model structure can easily accommodate further biological detail (e.g. apoptosis, energy requirements, proliferation cessation, among others), which is the next logical step.

As intended, the model formulation resulted in low computational requirements finding a balance between model detail and solution times. The fast solutions enabled the model analysis completion in a short period of time. The GSA allowed identifying the most significant parameters and by re-estimating such, the model output uncertainty is reduced. These results encourage the use of the model in model-based applications of industrial relevance such as control and optimisation. In particular, it can be used as a computer-aided tool to derive optimal operating policies to improve product titre and product quality while satisfying tight operating constraints and product specifications. Product quality (i.e. glycosylation) has been suggested to be cell cycle dependent (Fussenegger and Bailey, 1998). Moreover, post-translational modifications are dependent on the culture environment (Osman et al., 2001; Trummer et al., 2006), as well as dependent on the proliferation control strategy (Andersen et al., 2000; Gawlitzek et al., 2009; Kaufmann et al., 2001). Therefore, the model can accommodate for environmental factors as well as proliferation control strategies, which can include mechanistic effects in the presented model formulation. The significance of this approach is not limited to industrial scenarios (where the cell cycle productivity, cell growth or product quality can be optimised) but also to clinical environments (tumours growth models, design, and optimisation of cancer treatments, etc.).

The model predictions were compared to different experimental scenarios including both disturbed and undisturbed growth. Overall, the model showed a good

prediction throughout the different experiments. However, a few aspects that need further refinement were identified. In particular, studies on the link between the substrate/metabolite and the cell cycle machinery will help to further develop the model structure. The model development framework can be applied recursively for the formulation and refinement of relevant cell cycle models both at the industrial and clinical environments.

CHAPTER 7

Development of an Unstructured Metabolic and Temperature Dependent Cell Cycle Model in Hybridoma Cell Cultures

Mammalian cell fed-batch cultures are the preferred operation mode at an industrial scale for the production of monoclonal antibodies (mAbs). Improvements in the product yields have been fostered partially by the better understanding of fed-batch bioprocessing. A commonly used strategy in industrial fed-batch processes is based on the temperature shift of the bioreactor in order to obtain a good balance between temperature induced growth limitation and cell cycle specific enhanced productivity. Herein, the biological model development framework is used to formulate an unstructured cell cycle model considering the distribution of proliferating (G_1, S, G_2/M) and arrested cells (G_0) in batch and fed-batch cultures for a murine hybridoma cell line. The model is applied to predict temperature shifts from 37 °C to 33 °C, while capturing the cell growth, basic cell metabolism, and cell cycle distribution.

7.1. Introduction

Over the last three decades, improvements in product yields have been reported in mammalian cell cultures. Those improvements are due to the use of advanced production cell lines (Munro et al., 2011), optimised culture media, and process control (Wurm, 2004). Typical process controlled parameters are temperature, pH, and dissolved oxygen due to their influence on the cell proliferation and productivity (Trummer et al., 2006). In particular, reduced temperature control is a well established and preferred strategy to improve productivity due to its proven reliability and efficiency (Kumar et al., 2007). However, the reported temperature effects are variable between cell lines, expression systems, and expressed recombinant product (Al-Fageeh et al., 2006; Sunley and Butler, 2010).

The implementation of a reduced temperature control strategy commonly results in a reduced cell growth and cell arrest. Therefore, a balance between growth limitation, integral viable cell density (IVCD), and cell specific productivity must be achieved in order to increase the final antibody titre (Dutton et al., 1998; Sunley and Butler, 2010). Successful examples include the increase in total antibody production of GS-NS0 cells accumulated in G_1 and S phases at 34 °C (Swiderek and Al-Rubeai, 2007) and CHO cells arrested at G_2/M at 30 °C reporting an enhancement in the production (Shi et al., 2005). However other studies, despite reporting prolonged viability (Reuveny et al., 1987) or maximum viable cell concentration (Sureshkumar and Mutharasan, 1991) at low temperature, did not observe an improvement in productivity. Thus, the systematic study of temperature shifts in fed-batch cultures can aid the bioprocess development to improve product titre and product quality.

The development and selection of the culture temperature profiles seem to be empirical, lacking a systematic model-based approach. Early contributions used mathematical models to study the cell cycle and temperature effect (Slater et al., 1977; Watanabe and Okada, 1967). However, further developed cell cycle models excluded the temperature effects when considering productivity (Cazzador and Mariani, 1993; Kromenaker and Srienc, 1994; Linardos et al., 1992; Suzuki and Ollis, 1989), whereas Fox et al. (2004) aimed to optimise the temperature shift time without accounting for the cell cycle segregation. Recently, a mass based-PBM describing the cell cycle coupled to an unstructured model did account for the temperature effect (Karra et al., 2010). Alas, the model was validated only with batch cultures, limiting its industrial relevance. Thus, the opportunity to study the temperature shift effect on fed-batch cultures accounting for the cell cycle segregation remains open.

7.2. Objectives

The aim of this chapter is to formulate a (fed)-batch temperature dependent cell cycle model for a mAb producing hybridoma cell line. The overall methodology maps the path to systematically develop industrially relevant mathematical models to optimise temperature profiles. The following scientific objectives were set:

- Formulate a temperature dependent cell cycle model for the HFN 7.1 murine hybridoma cell line.
- Design and perform HFN 7.1 (fed)-batch cell culture experiments that would allow evaluating the temperature effect.
- Study the model structure using GSA (Section 3.3.11.) and identify the most significant model parameters.
- Re-estimate the subset of significant parameters from a set of (fed)-batch experiments.
- Predict temperature shift fed-batch cultures and compare to the experimental data.

7.3. Methodology

The model development followed overall the methodology proposed in the biological systems framework (Figure 2.7). Experimental and modelling aspects were integrated in the model development. Cell culture protocols and used experimental set-ups can be found in Section 3.2 and analytical techniques can be found in Section 3.3.

The model was implemented in gPROMS®. The employed model analysis tools, GSA software and parameter estimation procedure, can be found in Section 3.3.11. The identified significant parameters were re-estimated from representative batch and fed-batch cultures. Specifically, the batch and fed-batch covered the two temperatures (37 °C and 33 °C), which were set at the start of the cultures (t=0h) after seeding.

The model was validated against two independent fed-batch experiments with temperature shift (from 37 °C to 33 °C) at different culture times (i.e. 30 and 76h).

7.4. Model Development & Experimental Validation

Based on the literature review and experimental observations the cell cycle model was formulated using an unstructured-segregated approach. As addressed in chapter 2, the unstructured segregation provides fast computational times, is experimentally less intense and can be rapidly developed. The model was formulated using first principles and applying the existing model development framework (Kiparissides et al., 2011; Kontoravdi et al., 2007a; Sidoli et al., 2004).

Similarly, the model cell cycle structure was adapted and further developed from previous contributions (Basse et al., 2003; Lam et al., 2008; Uchiyama and Shioya, 1999). The cell cycle description includes the G_0, G_1, S, G_2/M phases (X_{G0}, X_{G1}, X_S, X_{G2M}) and it is stated as ordinary differential equations (7.1)-(7.4).

$$\frac{d(X_{G1}V)}{dt} = 2k_{G2M-G1}X_{G2M}V - k_{G1-S}X_{G1}V - k_{G1-G0}X_{G1}V - k_dX_{G1}V - F_{OUT}X_{G1} \quad (7.1)$$

$$\frac{d(X_SV)}{dt} = k_{G1-S}m_{stress}X_{G1}V - k_{S-G2M}X_SV - k_dX_SV - F_{OUT}X_S \quad (7.2)$$

$$\frac{d(X_{G2M}V)}{dt} = k_{S-G2M}X_SV - k_{G2M-G1}X_{G2M}V - k_dX_{G2M}V - F_{OUT}X_{G2M} \quad (7.3)$$

$$\frac{d(X_{G0}V)}{dt} = k_{G1-S}(1 - m_{stress})X_{G1}V + k_{G1-G0}X_{G1}V - k_dX_{G0}V - F_{OUT}X_{G0} \quad (7.4)$$

The viable cell population (X_V) and dead cell population (X_D) are calculated from the sum over all the cell cycle phases, Equations (7.5) and (7.6) respectively. The cell cycle fractions (f_i) are calculated dividing by the viable cell population, Equation (7.7).

$$\frac{d(X_VV)}{dt} = \frac{d(X_{G0}V)}{dt} + \frac{d(X_{G1}V)}{dt} + \frac{d(X_SV)}{dt} + \frac{d(X_{G2M}V)}{dt} \quad (7.5)$$

$$\frac{d(VX_D)}{dt} = X_Vk_dV - X_Dk_{lys}V \quad (7.6)$$

$$f_{i=G0,G1,S,G2M} = \frac{X_i}{X_V} \quad (7.7)$$

The transition between the proliferating subpopulations (X_{G1}, X_S, X_{G2M}) are declared ($k_{G1\text{-}S}$, $k_{S\text{-}G2M}$, and $k_{G2M\text{-}G1}$) in Equations (7.8)-(7.10) as previously derived (Uchiyama and Shioya, 1999); while the transition to G_0 from G_1 is triggered by two types of stresses: a temperature dependent stress ($k_{G1\text{-}G0}$) and/or a metabolic stress (m_{stress}). The temperature stress ($k_{G1\text{-}G0}$) is assumed to occur at a constant rate (r_T) when the temperature is lowered from 37 °C to 33 °C, Equation (7.11). The metabolic stress (m_{stress}) is defined as the product of the substrate limitation, toxic metabolite inhibition, and a resistance to such stresses (f_{res}), Equation (7.12). When the metabolic stress takes values below 1, it will divert a fraction of the typically proliferating cells transiting from G_1-S to the arrest phase G_0.

$$k_{G1-S} = \left(\mu + \frac{F_{OUT}}{V}\right)\left(\frac{2 - f_{G1}}{f_{G1}}\right) \tag{7.8}$$

$$k_{S-G2M} = \left(\mu + \frac{F_{OUT}}{V}\right)\left(\frac{1 + f_{G2M}}{f_S}\right) \tag{7.9}$$

$$k_{G2M-G1} = \left(\mu + \frac{F_{OUT}}{V}\right)\left(\frac{1}{f_{G2M}}\right) \tag{7.10}$$

$$k_{G1-G0} = \begin{cases} if & T = 33°C \quad = r_T \\ else & = 0 \end{cases} \tag{7.11}$$

$$m_{stress} = \begin{cases} if & f_{inh1}f_{inh2}f_{lim1}f_{res} > 1 \quad = 1 \\ else & = f_{inh1}f_{inh2}f_{lim1}f_{res} \end{cases} \tag{7.12}$$

The transitions between the proliferating subpopulations, Equations (7.8)-(7.10), are growth associated (μ). The growth rate (μ), Equation (7.13), is stated as a function of a characteristic time to complete every cell cycle phase (t_{G1}, t_S, t_{G2M}). Several biological contributions were considered to affect the characteristic cell cycle times, Equation (7.14): a temperature factor (k_T), the substrate availability (f_{lim1}), and the presence of toxic metabolites ($f_{inh1/inh2}$). The temperature factor (k_T), Equation (7.15), is supported by the consistently reported slower proliferation at lower temperatures (Kumar et al., 2007); while the substrate and toxic metabolite (lactate [*Lac*], ammonia [*Amm*]) effect for the employed hybridoma cell line are reported (Ozturk et al., 1992). These effects are included using Monod kinetics (Kontoravdi, 2006).

$$\mu = \frac{ln(2)}{t_{G1} + t_S + t_{G2M}} \tag{7.13}$$

$$t_{G1,G2M} = \frac{t_{G1,G2M\ initial}k_T}{f_{lim1}f_{inh2}f_{inh1}{}^n} \quad ; \quad t_S = \frac{t_{S\ initial} + k_T}{f_{lim1}f_{inh2}f_{inh1}{}^n} \tag{7.14}$$

$$k_T = \begin{cases} if & T = 33°C \quad = k_T \\ else & = 1 \end{cases} \tag{7.15}$$

$$f_{lim1} = \frac{[Gln]}{K_{Gln} + [Gln]} \tag{7.16}$$

$$f_{inh1} = \frac{K_{Lac}}{K_{Lac} + [Lac]} \quad ; \quad f_{inh2} = \frac{K_{Amm}}{K_{Amm} + [Amm]} \tag{7.17}$$

The death rate (k_d) was based on previous reports (Jang and Barford, 2000; Kontoravdi, 2006) and it was modified to consider the glutamine limitation (f_{lim1}), Equation (7.18).

$$k_d = \frac{k_{dMAX}}{\left(1 + f_{lim1}\frac{K_{dAmm}}{[Amm]}\right)} \tag{7.18}$$

The bioreactor works under the assumptions of perfect mixing and operates under both batch and fed-batch mode, Equation (7.19). Thus, volume (*V*) changes are considered due to substrate feeding (F_{Glc}, F_{Gln}) or sampling (F_{OUT}). Substrate and metabolites changes are calculated accounting for the cell metabolism and a mass balance around the bioreactor. Glutamine concentration ([*Gln*]) changes are due to glutamine uptake (Q_{Gln}), glutamine degradation into ammonia (K_{deg}) and presence of glutamine in the feed ([Gln_{feed}]), Equation (7.20). The glutamine uptake, (Q_{Gln}) in Equation (7.21), depends on the cell growth at a specific yield on glutamine (Y_{Gln}), an uptake limiting function with Monod kinetics (f_{upt}), and a maintenance term (m_{Gln}) (Tatiraju et al., 1999). The ammonia mass balance ([*Amm*]), Equation (7.22), is linked to the degration and consumption of glutamine producing ammonia on a constant yield basis (Y_{Amm}).

$$\frac{dV}{dt} = F_{Glc} + F_{Gln} - F_{OUT} \tag{7.19}$$

$$\frac{d([Gln]V)}{dt} = -Q_{Gln}X_V V - K_{deg}[Gln]V + F_{Gln}[Gln_{Feed}] - F_{OUT}[Gln] \tag{7.20}$$

$$Q_{Gln} = \left(\frac{\mu}{Y_{Gln}}\right) f_{upt} + m_{Gln} \quad ; \quad f_{upt} = \frac{[Gln]}{K_{Gln} + [Gln]} \quad ; \quad m_{Gln} = \frac{\alpha 1[Gln]}{\alpha 2 + [Gln]} \tag{7.21}$$

$$\frac{d([Amm]V)}{dt} = Q_{Gln}Y_{Amm}X_V V + K_{deg}[Gln]V - F_{OUT}[Amm] \tag{7.22}$$

Similar to glutamine, Glucose ([*Glc*]) concentration in Equation (7.23) varies due to the uptake rate (Q_{Glc}), the maintenance consumption (m_{Glc}), and the glucose concentration in the feed ([Glc_{feed}]). Glucose consumption has been shown to be temperature dependent (Reuveny et al., 1987), lactate inhibited (Nolan and Lee, 2011), and dependent on the presence of essential biosynthetic (glutamine) precursors (Zhao et al., 2009); these effects were combined in Equation (7.24). In addition, it was assumed that cells in the quiescent state G_0 consumed glucose at a maintenance rate due to the minimal cell growth observed in this phase (Jenkins and Hovey, 1993). The lactate mass balance ([*Lac*]), Equation (7.25), is linked to the consumption of glucose producing lactate on a variable yield basis (Y_{Lac}). The variable yield of lactate on glucose (Y_{Lac}) was reduced by a feedback inhibition as

previously reported (Ozturk et al., 1992), Equation (7.26). Finally, the monoclonal antibody balance ([*mAb*]) is stated as growth associated and cell cycle segregated with specific productivities (q_i), Equation (7.27).

$$\frac{d([Glc]V)}{dt} = -Q_{Glc}X_V(1-f_{G0})V - m_{Glc}X_V f_{G0}V + F_{Glc}[Glc_{Feed}] - F_{OUT}[Glc] \quad (7.23)$$

$$Q_{Glc} = \left(\frac{\mu}{Y_{Glc}}\right) f_{upt} {f_{inh1}}^{k_T} \quad (7.24)$$

$$\frac{d([Lac]V)}{dt} = Y_{Lac}Q_{Glc}X_V(1-f_{G0})V - Y_{Lac}m_{Glc}X_V f_{G0}V - F_{OUT}[Lac] \quad (7.25)$$

$$Y_{Lac} = Y_{Lac\,initial}{f_{inh1}}^{(m+k_T)} \quad (7.26)$$

$$\frac{d([mAb]V)}{dt} = \mu[q_{G1G0}(X_{G1}+X_{G0}) + q_S X_S + q_{G2M}X_{G2M}] - F_{OUT}[mAb] \quad (7.27)$$

An important aspect of the proposed model is the cell behaviour at the temperature transition. Particularly, the cell growth (μ) has been formulated as temperature dependent and a cell adaptation is expected to take place when the reactor temperature is switched (i.e. from normal conditions 37 °C to mild hypothermia 33 °C). However, the temperature shift is not expected nor experimentally observed to be instantaneously reflected in the cell growth. The dynamic and adaptive process of cell growth has been described. For example, previous reports describe a gradual decrease in the S phase after a temperature shift (Moore et al., 1997), a partial blockage in G_2/M (Shi et al., 2005), and an eventual increase in the G_1 phase (Swiderek and Al-Rubeai, 2007). In order to capture the dynamic and adaptive process, the model considers the state of the cells at the moment when the temperature shift takes place. Thus, herein it is assumed that after a temperature shift, the existing cell population will proliferate at a transitory rate. The existing population will proliferate at a fast rate in the G_1 and S phase (i.e. $t_{G1/S}$ calculated using T= 37 °C) and G_2/M will be affected immediately (i.e. t_{G2} calculated using T= 33 °C). However, every new born cell of the existing population will proliferate under the new reactor temperature (i.e. $t_{G1/S/G2}$ calculated using T= 33 °C), Figure 7.1.

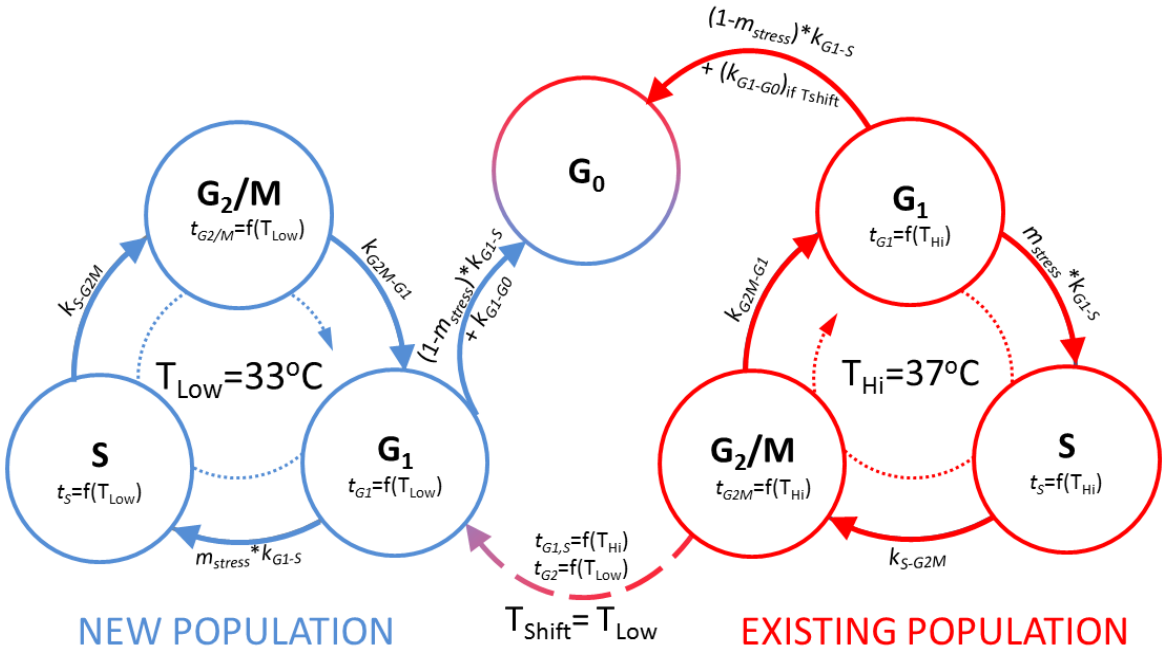


Figure 7.1. Cell cycle model schematic representation.

Thus, the existing population will remain metabolically active at the transition conditions until this population disappears (either because it completes the cell cycle, gets arrested at G_0 or dies). In addition, in the case of a temperature shift the cells at G_0 will consume glutamine at the transition conditions until the end of the culture. The assumed glutamine enhanced metabolism of G_0 cells is supported by the active biosynthetic state (but not growth) and due to glutamine's key role in cell metabolism (Becerra et al., 2012; Rossler et al., 1996; Sanfeliu and Stephanopoulos, 1999). Moreover, an enhanced metabolism is supported if G_0 cells are committing to apoptosis, which is energy intensive (Eguchi et al., 1997). On the other hand, the metabolism of all new born cells will be immediately affected and calculated at the new reactor temperature.

7.5. Model Analysis & Re-estimation of Significant Model Parameters

The next step in the model development was to evaluate the model structure and output variability using GSA (Section 3.3.11.). A total of six outputs were evaluated (X_v, f_{G1}, f_S, f_{G2M}, f_{G0}, and *mAb*) at six time points (12, 24, 36, 48, 96, and 144h) of a fed-batch culture. The time points were selected in order to evaluate different phases of the process including a temperature shift during exponential growth phase at 40

hours. Specifically the time points from the lag phase (12h), early exponential (24h), exponential phase (36h), exponential after the temperature shift (48h), stationary phase (96h), and decline phase (144h) were evaluated. A total of 40,000 scenarios were evaluated varying the 26 parameters ±50% from their nominal value. The majority of the initial nominal values were set to literature values as previously reported (Kontoravdi et al., 2005). As outlined in chapter 3, the output of the scenarios was used to estimate the SIs using the GUI-HDMR software. The significant parameters were determined using a 0.1 cut-off value attributed to 10% experimental errors (Sidoli et al., 2005). Thus, a total of 9 significant parameters were identified (Table 7.1).

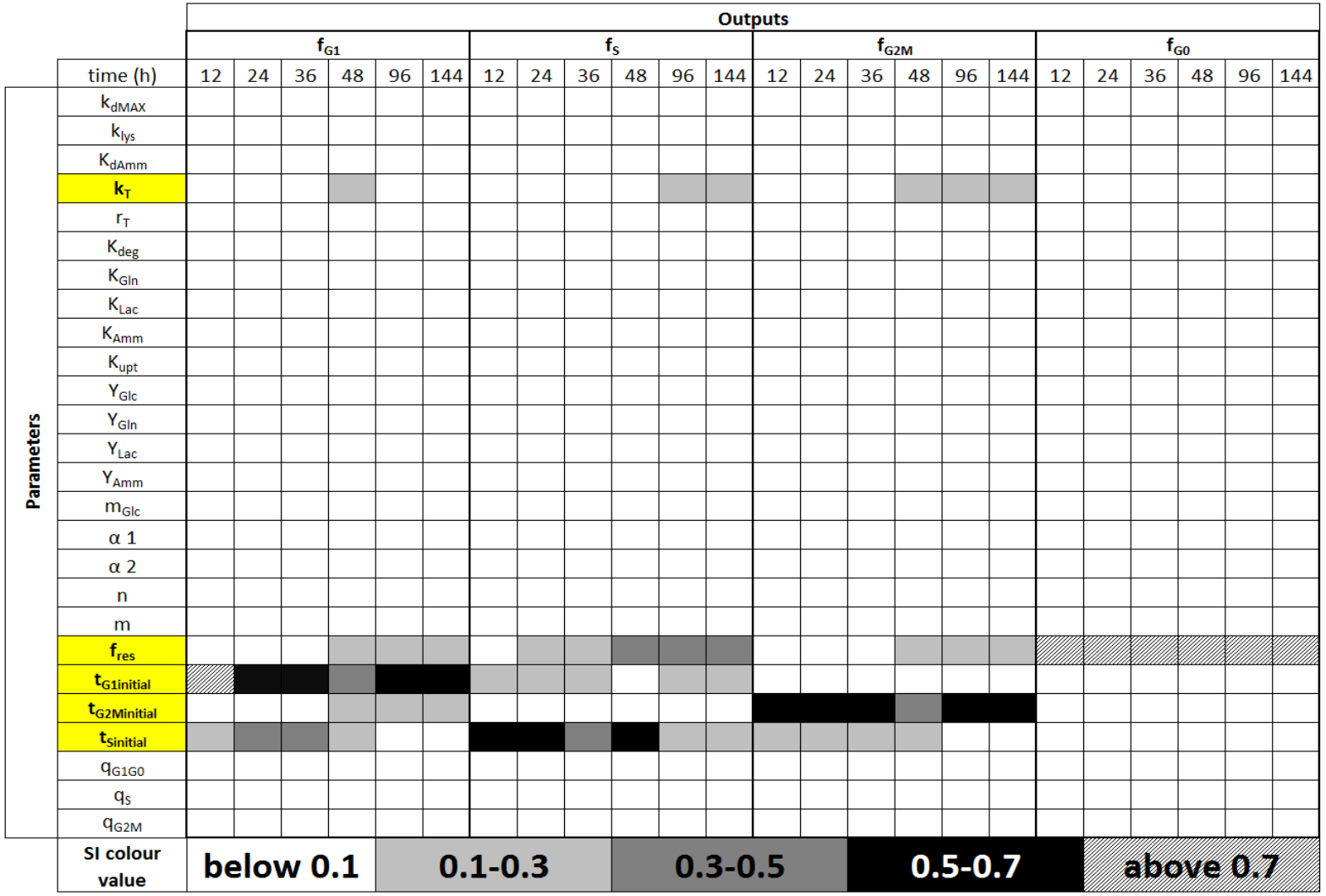
The viable cell density (X_V) showed a decreasing sensitivity (though remaining significant) throughout the evaluated time points to the variation of the cell cycle times ($t_{Sinitial}$, $t_{G2Minitial}$), whereas the resistance to the metabolic stresses (f_{res}) was significant at the stationary and decline phase. Differently, the sensitivity towards the yield of biomass on glutamine (Y_{Gln}) peaked at 36h, just before the glutamine feed was started. The *mAb* output was sensitive throughout to the same cell cycle times as X_V. In addition, the G_1/G_0 phases (q_{G1G0}) and S phase (q_S) specific productivities were found significant at early stages of the culture, while the cell cycle temperature factor (k_T) and the cell cycle times' sensitivity to lactate inhibition (n) were significant during both the stationary and the decline growth phase. Similarly, the proliferative cell cycle fractions (f_{G1}, f_S, f_{G2M}) showed also sensitivity to the cell cycle temperature factor (k_T) after the temperature shift. The recurrent identification of the cell cycle temperature factor as sensitive for several outputs supports the importance of finding a balance between growth and productivity when using temperature to optimise fed-batch processes. Moreover, the cell cycle fractions (f_{G1}, f_S, f_{G2M}) were sensitive to the resistance to the metabolic stresses (f_{res}) after 36h. In general, each proliferative cell cycle fraction was highly sensitive throughout to the corresponding initial time estimate to complete the phase ($t_{G1initial}$,$t_{Sinitial}$,$t_{G2Minitial}$). In addition, the cell fractions (f_{G1}, f_S, f_{G2M}) showed sensitivity to the preceding cell cycle phase time. The cell cycle time estimates were associated with most of the studied outputs, which stresses the importance of considering the cell cycle heterogeneity. The non-proliferative cell fraction (f_{G0}) was highly sensitive throughout the culture to the resistance to metabolic stresses (f_{res}).

The identified 9 significant parameters were re-estimated simultanuosly from the selected representative batch and fed-batch cultures. The batch and fed-batch covered the two temperatures (37 °C and 33 °C), which were set at the start of the cultures after seeding. In addition, the batch experiments covered nutrient exhaustion (Sellick et al., 2011), while the fed-batch allowed the study of the accumulation of toxic metabolites. The re-estimated parameters are reported with the 95% confidence intervals (Table 7.1). In general, the confidence intervals reflect a good estimation, except for the cycle specific productivities (q_{G1G0}, q_S). The large confidence intervals of the specific productivities reflect a weak estimation of these parameters, which can be attributed to the observed growth associated (to the proliferating cell cycle fractions) antibody production of HFN 7.1 cells. The model predictions for the batch and fed-batch cultures used for the parameter estimation are compared to the experimental data in the next section. Similarly, the model predictions are compared to two experiments with temperature shift at different culture times (i.e. 30 and 76h).

Table 7.1. GSA Indexes and parameters values for the temperature dependent cell cycle model. Outputs: X_V=viable cell density, [mAb]=antibody titre, f_{G1}=G_1 cell fraction, f_S=S cell fraction, f_{G2M}=G_2/M cell fraction, and f_{G0}=G_0 cell fraction.

		Outputs														
		Xv						[mAb]								
	time (h)	12	24	36	48	96	144	12	24	36	48	96	144	Nominal Value	Units	Estimated Value	95% Conf. Interval
Parameters	k_{dMAX}													0.06	h^{-1}		
	k_{lys}													0.04	h^{-1}		
	K_{dAmm}													60	mM		
	k_T													3	n/a	3.20723	2.70E-08
	r_T													0.013	h^{-1}		
	K_{deg}													4.80E-03	h^{-1}		
	K_{Gln}													0.075	mM		
	K_{Lac}													90	mM		
	K_{Amm}													15	mM		
	K_{upt}													0.4	mM		
	Y_{Glc}													1.241E+08	cell/mM		
	Y_{Gln}														cell/mM	6.09644E+08	11
	Y_{Lac}													5.564E+08	mmol/mmol		
	Y_{Amm}													0.6	mmol/mmol		
	m_{Glc}													2.778E-12	mmol/cell/h		
	α 1													3.40E-13	mM*L/cell/h		
	α 2													4	mM		
	n													2	n/a	2	
	m													2	n/a		
	f_{res}													2	n/a	1.5281	1.30E-08
	$t_{G1initial}$													3.3	h	2.72952	2.70E-08
	$t_{G2Minitial}$													2.5	h	2.7861	2.60E-08
	$t_{Sinitial}$													6	h	5.06568	4.30E-08
	q_{G1G0}													2.80E-11	mg/cell	2.00E-11	1.00E-12
	q_S													2.80E-11	mg/cell	3.00E-11	1.40E-12
	q_{G2M}													2.80E-11	mg/cell		
	SI colour value	**below 0.1**				**0.1-0.3**				**0.3-0.5**		**0.5-0.7**				**above 0.7**	

Table 7.1 (Continued). GSA Indexes and parameters values for the temperature dependent cell cycle model. Outputs: XV=viable cell density, [mAb]=antibody titre, f_{G1}=G_1 cell fraction, f_S=S cell fraction, f_{G2M}=G_2/M cell fraction, and f_{G0}=G_0 cell fraction.



7.6. Results & Discussion

The simulation results are performed with the same set of parameters (after parameter estimation from the representative batch and fed-batch cultures, Section 7.5, Table 7.1) and only varying the operation mode or the timing for the temperature shift.

7.6.1. Temperature shifted batch cultures

The 37 °C batch shake flask culture showed the typical batch operation profiles (Figure 7.2). Briefly, the viable cell concentration (X_v) increased exponentially after seeding and peaked around the time glutamine (*Gln*, key substrate) was exhausted (around 36h). After glutamine depletion a significant death rate was observed with the concurrent increase of the lumped G_1/G_0 cell cycle fraction (f_{G1G0}), while the other cell cycle fractions (f_S and f_{G2M}) showed a decrease. The consumption of substrates (i.e. *Glc, Gln*) was accompanied by the production of toxic metabolites (i.e. *Lac, Amm*) and the antibody concentration (*mAb*) correlated to the viable cell concentration.

The model predictions captured in general all the trends, although some deviations were observed (Figure 7.2). The cell density and antibody titre were well predicted (Figure 7.2A), whereas the viability prediction deviated from the experimental values towards to the end of the culture. Overall, the cell cycle trends were captured, including the shifts in the trends after the glutamine exhaustion (Figure 7.2B). At early stages of culture (12h), deviation from the model predictions for the S and G_2/M cell cycle fractions were observed. However, these early deviations could be partially attributed to the oscillatory behaviour (specific cell cycle transitions) between the cell cycle fractions. Alas, the model herein considers the cell cycle population as homogenous and represents the average cell behaviour within a cell cycle phase. Thus, sharp oscillations or specific transitions cannot be captured by the model. In order to capture such cell cycle changes, another internal coordinate needs to be employed in a segregated formulation (as in chapter 6). Nonetheless, the substrate profiles and lactate production were well predicted by the model (Figure 7.2C), while the ammonia profile was consistently over-estimated though following the correct trend (Figure 7.2D). This deviation can be explained due

to the constant yield of ammonia on glutamine (Y_{Amm}) used in the model. However, the constant yield of ammonia on glutamine has been reported to be dependent on temperature and pH (Ozturk and Palsson, 1991; Seo et al., 2013). Particularly, pH is not controlled in the shake-flask cultures.

The 33 °C batch shake flask culture included the effect of temperature reduction at the start (i.e. 0h) of the culture (Figure 7.3). Similar profile trends were observed when compared to the 37 °C culture, although the 33 °C batch culture time was 1.5-fold longer. The main differences included a lower cell peak density (1.8-fold lower compared to the 37 °C batch) and a corresponding lower final mAb titre (1.4-fold lower). As in previous cases the substrates and metabolites showed a correlation. However, the lactate production was further increased towards the end of the culture (with increasing dispersion) despite the apparent low glucose consumption. The cell cycle fractions did not show significant changes at early stages (12h), coinciding with the invariable cell density. However at 24h, a significant and sharp change in the cell cycle fraction was observed with the start of the exponential phase. After the sharp oscillations, the cell cycle fractions remained rather constant. Once glutamine was exhausted, the dispersion of the lumped G_1/G_0 and G_2/M cell cycle fractions increased. The increased dispersion indicated that the cells were gathering in one of these two phases, which could suggest a cell arrest.

The model predictions captured most of the observed experimental trends of the 33 °C batch culture. The viable cell density and mAb prediction profiles showed a good fit to the data (Figure 7.3A). However, the cell viability was overestimated, particularly towards the end of the culture. The model prediction of the cell cycle fractions included a sharp oscillation due to the temperature shift, which seemed to be partially in agreement with the experimentally observed (Figure 7.3B). Alas, the timing of the predicted oscillation appeared earlier than the observed experimentally. The experimentally observed oscillation could be as well attributed to a cohort or synchronised cell population initiating the cell cycle. Thus, as previously mentioned, the model is not able to capture such events due to its structure. Further differences were observed in the predictions of the G_1/G_0 and G_2/M cell cycle fractions.

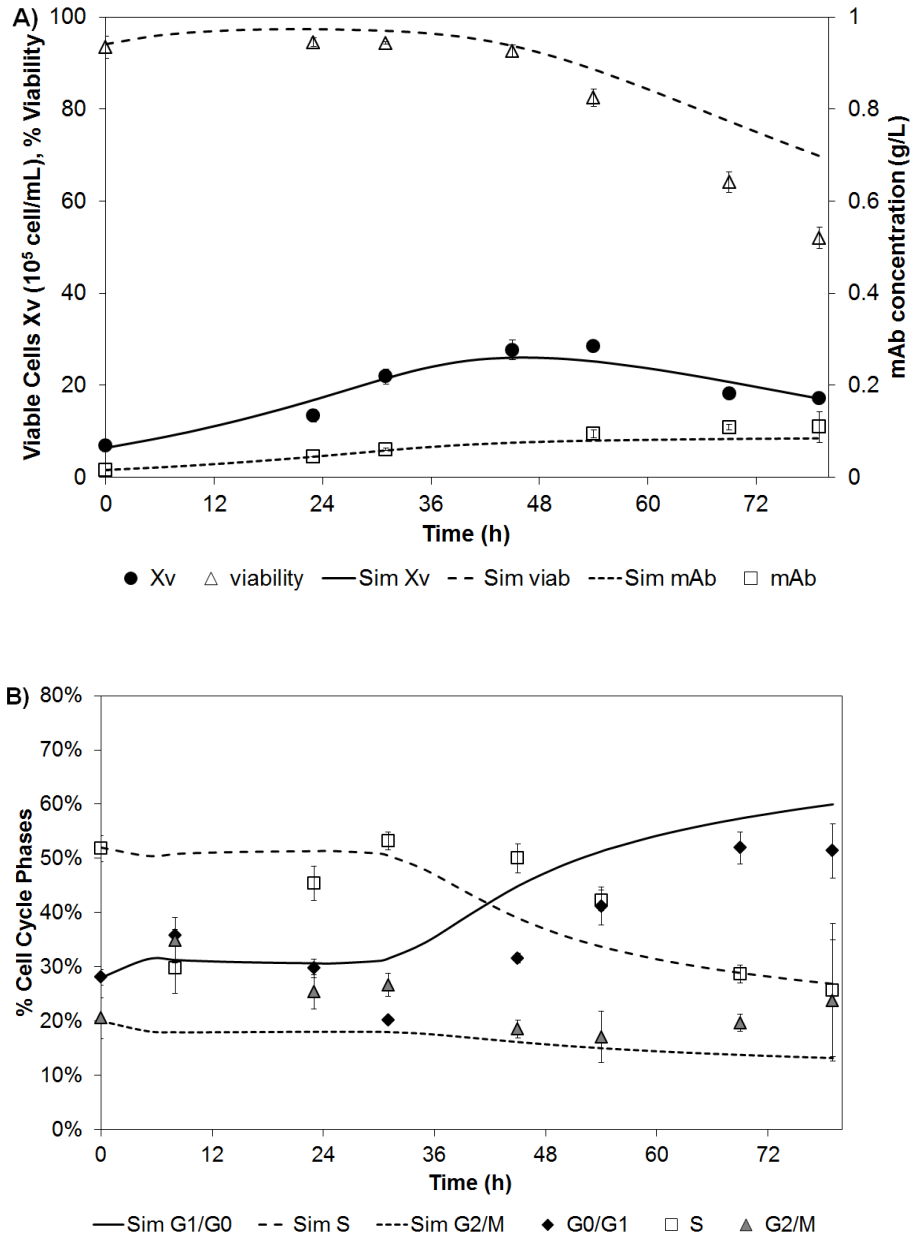


Figure 7.2. Batch shake flask cultures at 37 °C. A) Cell growth, viability and mAb profiles; B) Cell cycle distribution; C) Glucose and lactate profiles; D) Glutamine and Ammonia profiles. Notation: dots represent experimental data (n=3, error bars=standard deviation), lines represent the simulation results.

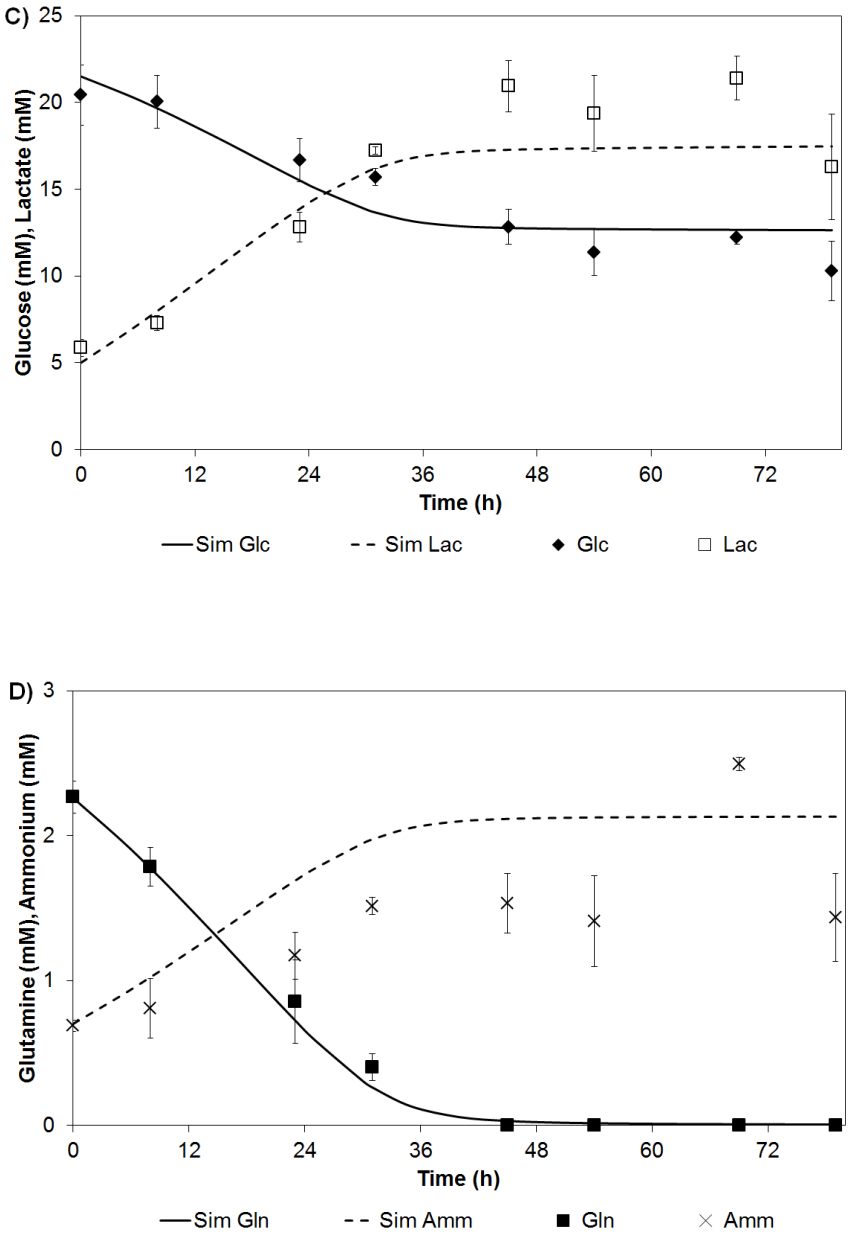


Figure 7.2. (Continued). Batch shake flask cultures at 37 °C. A) Cell growth, viability and mAb profiles; B) Cell cycle distribution; C) Glucose and lactate profiles; D) Glutamine and Ammonia profiles. Notation: dots represent experimental data (n=3, error bars=standard deviation), lines represent the simulation results.

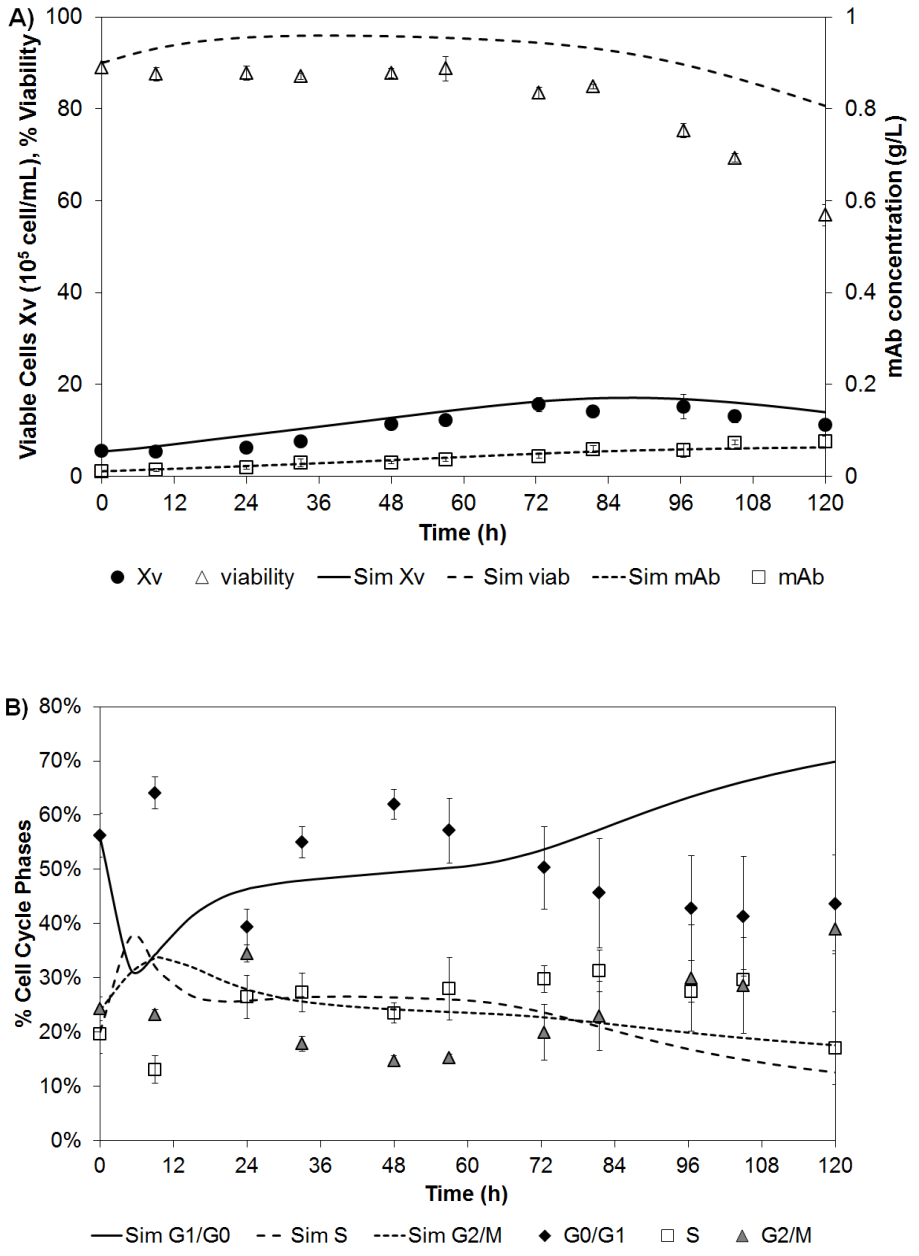


Figure 7.3. Batch shake flask cultures shifted to 33 °C at the start of cultivation. A) Cell growth, viability and mAb profiles; B) Cell cycle distribution; C) Glucose and lactate profiles; D) Glutamine and Ammonia profiles. Notation: dots represent experimental data (n=3, error bars=standard deviation), lines represent the simulation results.

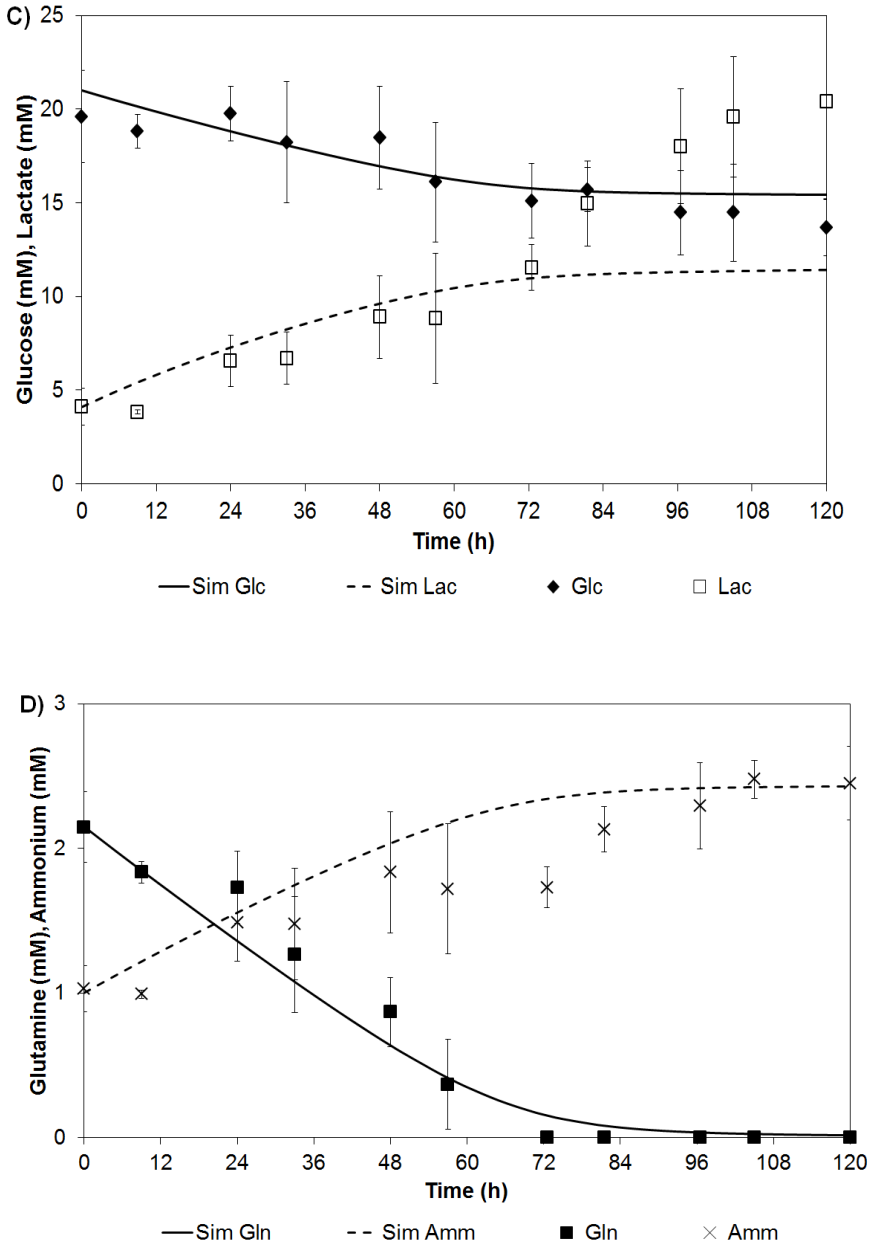


Figure 7.3. (Continued). Batch shake flask cultures shifted to 33 °C at the start of cultivation. A) Cell growth, viability and mAb profiles; B) Cell cycle distribution; C) Glucose and lactate profiles; D) Glutamine and Ammonia profiles. Notation: dots represent experimental data (n=3, error bars=standard deviation), lines represent the simulation results.

The substrate and metabolite prediction profiles captured the experimental results (Figure 7.3C-D). However, the lactate prediction could not account for the constant increase towards the end of the culture (Figure 7.3C). Similarly as for the cell cycle fractions (G_1/G_0, G_2/M), the lactate profile also showed an increasing dispersion towards the end of the culture. This increasing dispersion suggests some differences in the cells' behaviour reflected at both the metabolic and the cell cycle level. Such differences can be partially explained due to the rather uncontrolled pH operation of the batch flask cultures (Osman et al., 2001; Trummer et al., 2006).

7.6.2. Temperature shifted fed-batch cultures

The second set of experiments used for the parameter estimation included fed-batch cultures performed in controlled bioreactors. The 37 °C fed-batch culture was carried out in duplicate and provides the baseline of typical fed-batch operation profiles (Figure 7.4).

As expected the continuous feed of substrates (glucose, glutamine, vitamins, trace elements, and other amino acids) resulted in an increase of the viable cell concentration (2.1-fold compared to the 37 °C batch culture). Similarly, a prolonged stationary phase with a high viability was maintained due to the feeding. Glucose and glutamine (*Glc, Gln*) were consumed throughout the culture, which resulted in high toxic metabolite (*Lac, Amm*) concentration towards the end of the culture (Ozturk et al., 1992). Particularly, ammonia reached 5.5-fold higher concentrations compared to the 37 °C batch. After 72h, when ammonia reached toxic concentration, the lactate concentration seemed to plateau. These events showed a correlation with the start of the G_0 cell cycle phase arrest and increase of the G_0 fraction until the end of the cultivation. The lactate profile showed a large experimental variation, which was attributed to the pH control strategy using CO_2 sparging and varying amount of base (2M NaOH). Lactate production and base addition in pH controlled bioreactors accompanied by high osmolarity have been shown in industrial fed-batch processes to result in big differences in the final lactate profile, without affecting the growth profile (Le et al., 2012). As observed herein, the measured lactate differences did not affect significantly the other measured variables (Xv, viability, mAb titre, cell cycle distribution) as reflected in the good reproducibility.

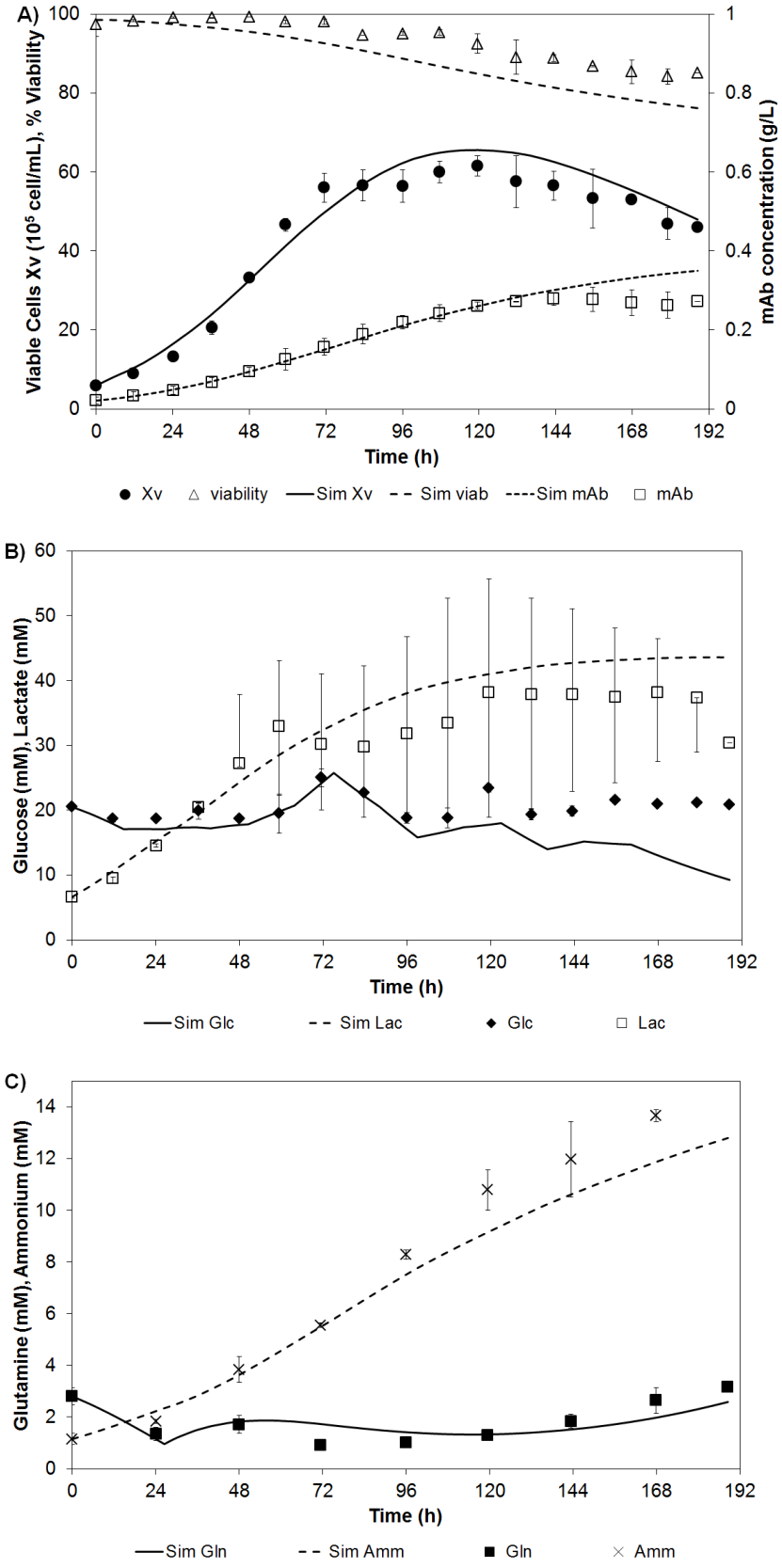


Figure 7.4. Fed-batch bioreactor cultures at 37 °C. A) Cell growth, viability and mAb profiles; B) Glucose and lactate profiles; C) Glutamine and Ammonia profiles; D) G1/G0 phase; E) S phase; F) G_2/M phase. Notation: dots represent experimental data (n=2, error bars=standard deviation), lines represent the simulation results.

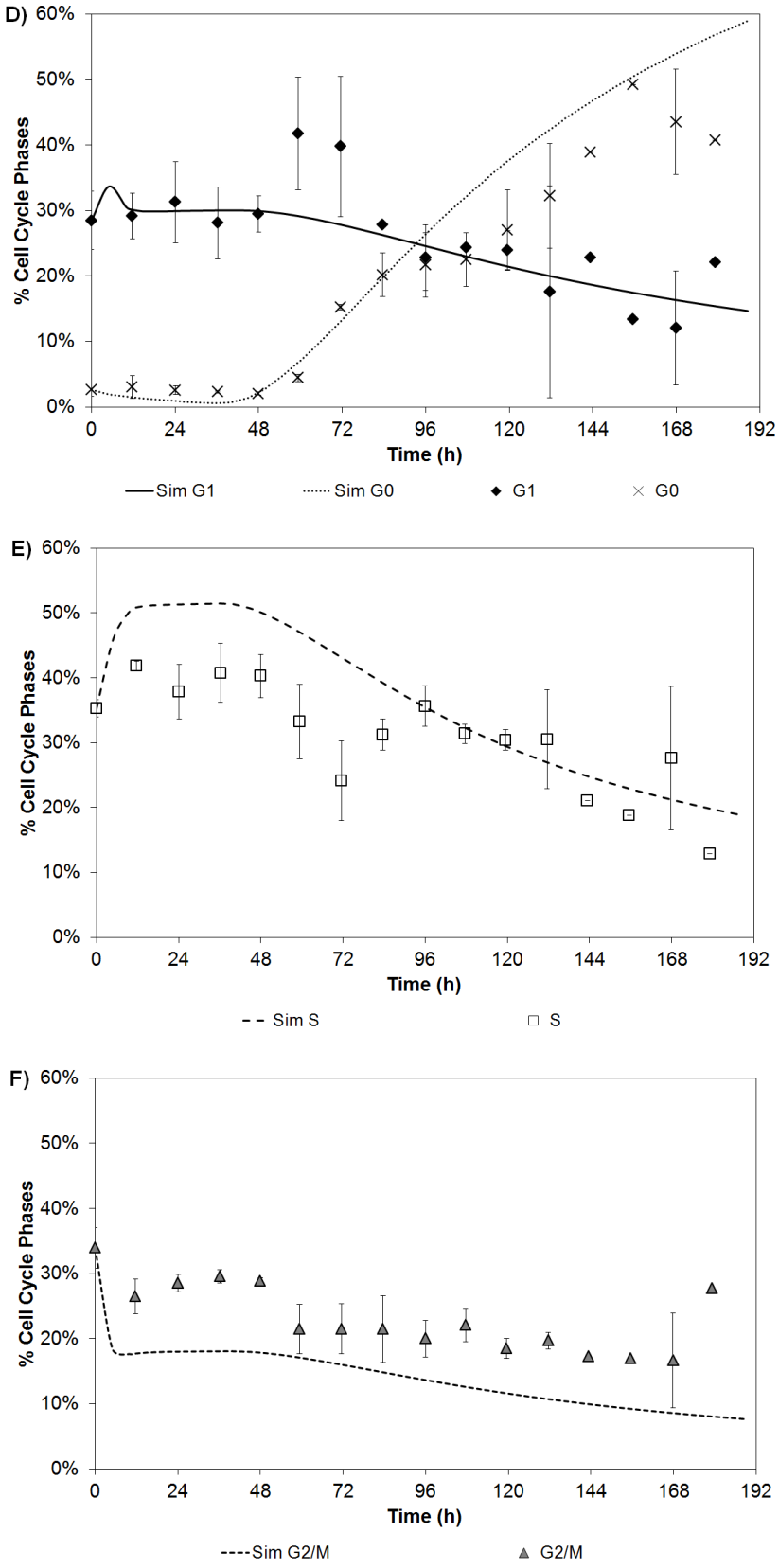


Figure 7.4. (Continued). Fed-batch bioreactor cultures at 37 °C. A) Cell growth, viability and mAb profiles; B) Glucose and lactate profiles; C) Glutamine and Ammonia profiles; D) G1/G0 phase; E) S phase; F) G_2/M phase. Notation: dots represent experimental data (n=2, error bars=standard deviation), lines represent the simulation results.

The model simulation for the fed-batch at 37 °C showed a satisfactory prediction. The increase, peak, and decline of the viable cells were well described (Figure 7.4A). The viability showed a better fit than in batch cases, although at late stages was underestimated. Part of the difficulties to predict the viability correctly between the two operation modes (batch vs fed-batch) was attributed to the methods used to estimate this process variable. In batch culture, viable cells were counted manually (at Imperial College), whereas in fed-batch cells were determined automatically with a lower cell cut-off size set of 9 μm (at ETH Zurich). Initial 37 °C batch cultures performed in both flask (Imperial) and bioreactor (ETH) showed good agreement, except for cell viability profiles (which remained higher in the controlled bioreactor). A second source that could account for the viability differences are the hydromechanical stress rates, which are considerably smaller in shake flask (Peter et al., 2006). Thus, the cell lysis rate is expected to be different in the two systems, which is not considered in the model.

The antibody titre prediction showed a good agreement to the experimental data, though minor differences were observed towards the end of the culture. The mAb differences can be attributed to protein degradation due to increased proteolytic activity during prolonged culture times (Sandberg et al., 2006). Overall, the substrate consumption showed a fair prediction (Figure 7.4B-C). The glutamine profile showed a good description, whereas glucose consumption seemed to be largely decreased at the end of the culture. Although the model did account for a decrease in the consumption rates, glucose consumption decrease seemed to be more severe experimentally. The metabolite profiles (*Lac, Amm*) showed a good prediction. Finally, the trend of cell cycle fractions (f_{G0}, f_{G1}, f_S, f_{G2M}) including the timing of G_0 increase triggered by metabolite accumulation was well described (Figure 7.4D-F).

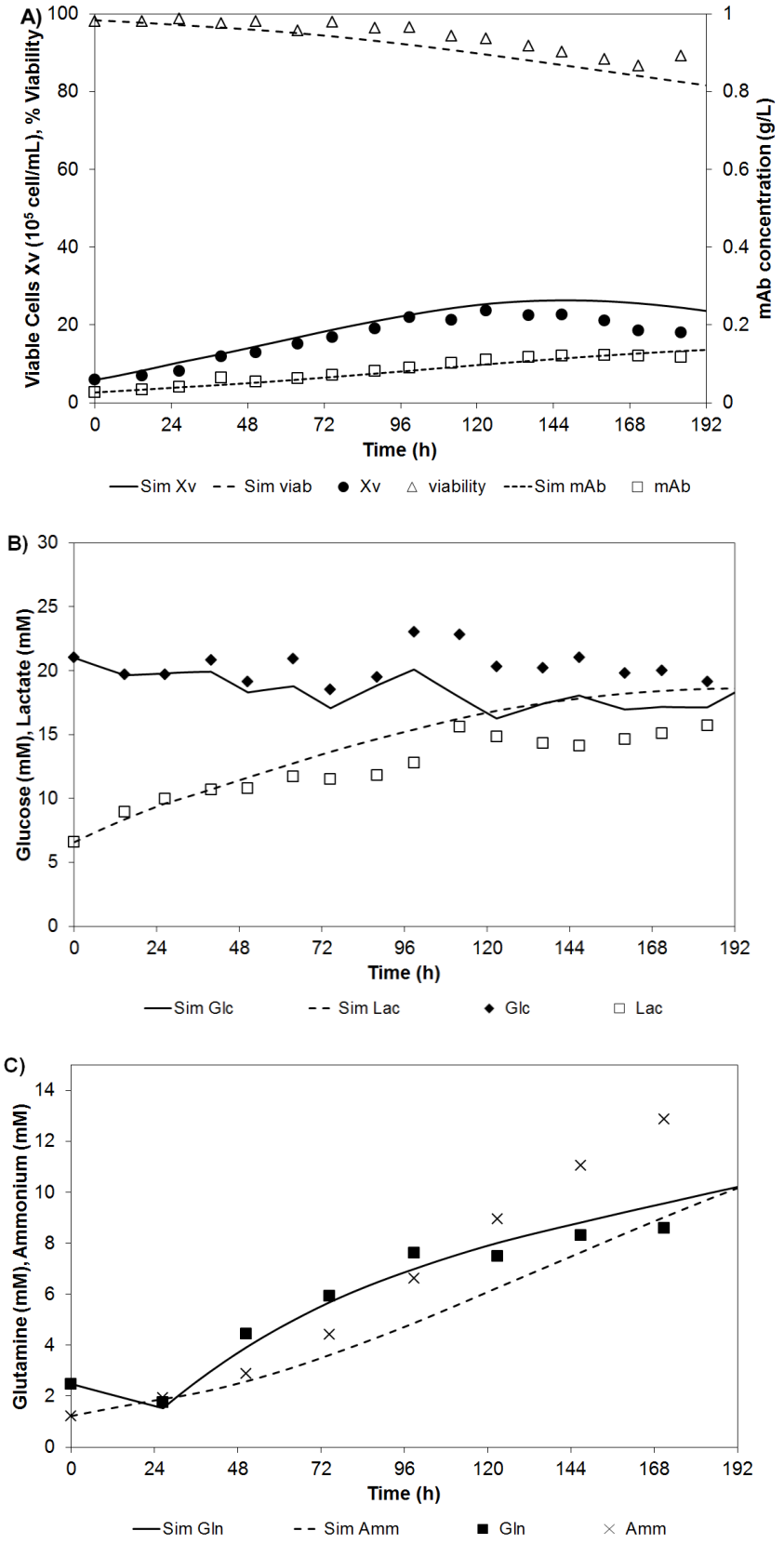


Figure 7.5. Fed-batch bioreactor culture shifted to 33 °C at the start of cultivation. A) Cell growth, viability and mAb profiles; B) Glucose and lactate profiles; C) Glutamine and Ammonia profiles; D) G1/G0 phase; E) S phase; F) G_2/M phase. Notation: dots represent experimental data (n=1), lines represent the simulation results.

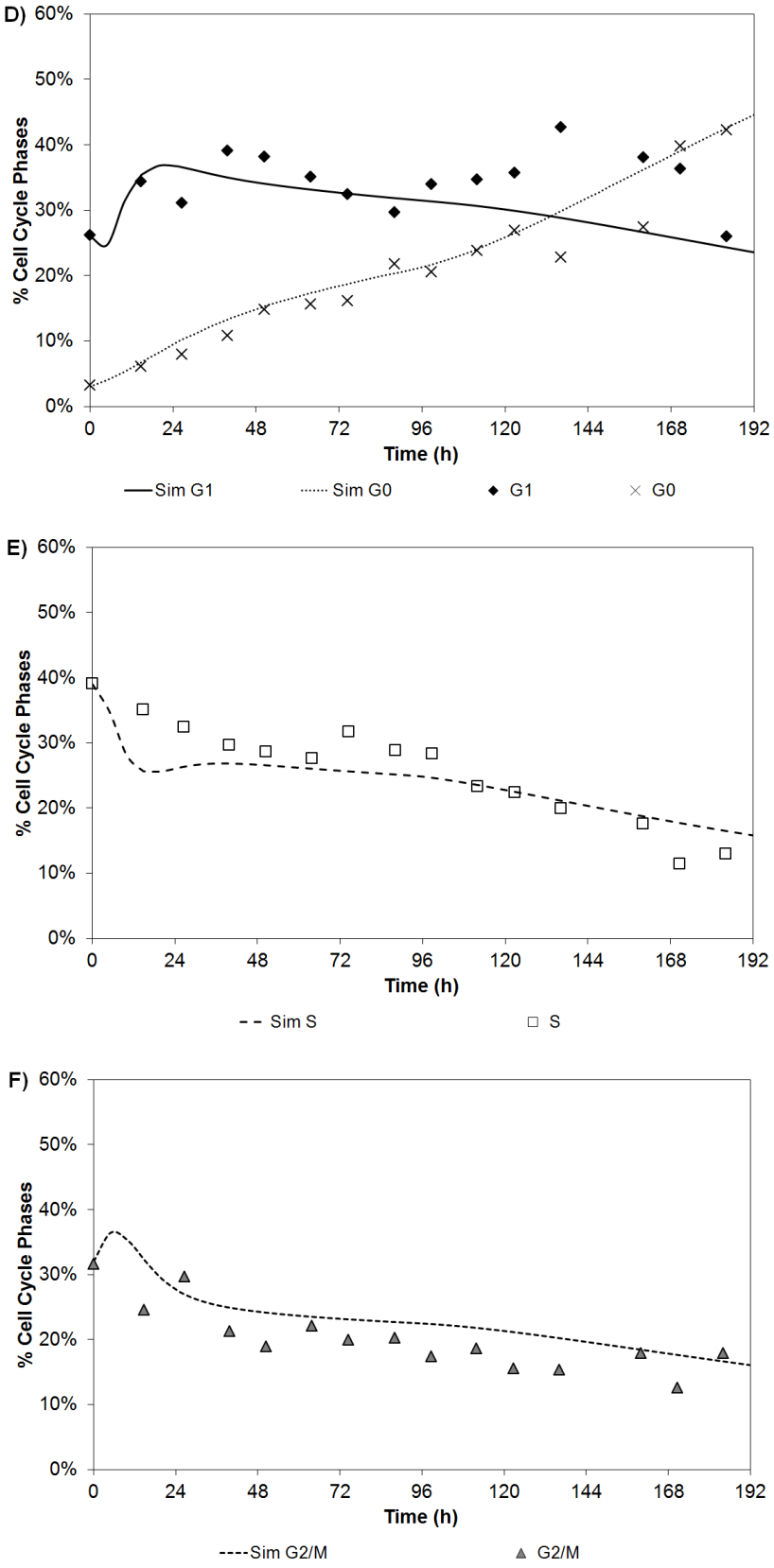


Figure 7.5. (Continued). Fed-batch bioreactor culture shifted to 33 °C at the start of cultivation. A) Cell growth, viability and mAb profiles; B) Glucose and lactate profiles; C) Glutamine and Ammonia profiles; D) G1/G0 phase; E) S phase; F) G_2/M phase. Notation: dots represent experimental data (n=1), lines represent the simulation results.

A 33 °C fed-batch culture with initial temperature shift (at time point 0h) completed the experiments used for the parameter estimation. Similar to the 33 °C batch, this experiment set the baseline for this temperature and operation mode (Figure 7.5). Briefly, a significant lower cell concentration was reached (2.6-fold lower than the 37 °C fed-batch culture) with a comparable viability to the 37 °C fed-batch. Glucose consumption resulted in lower lactate concentration; whereas ammonia concentration reached comparable levels to 37 °C fed-batch, despite the lower glutamine consumption. Most importantly, a cell arrest in the G_0 cell cycle fraction was evident from the beginning of the culture, which increased steadily throughout the cultivation time. Thus, cell cycle arrest was identified herein to be triggered by hypothermia.

The 33 °C fed-batch simulation predictions showed a good agreement to the experimental data. The viable cell density was satisfactorily predicted, although it was slightly over-estimated during the decline phase (Figure 7.5A). Cell viability and antibody concentration were well described by the model. Similarly, the substrates (*Glc, Gln*) showed a fair fit to the data, as well as the lactate profile (Figure 7.5B-C). Although the ammonia prediction captured the trend, it underestimated the ammonia production after 72h (Figure 7.5C). Such discrepancy can be due to the fact that the model considers ammonia to be produced only by glutamine consumption and degradation. However, ammonia can be produced from other sources such as from asparagine consumption (McCracken et al., 2014). In addition, amino acid consumption has been reported to be affected by temperature (Furukawa and Ohsuye, 1998), which is something considered indirectly by the model through the growth rate but it might require further revision. All the cell cycle fraction predictions (Figure 7.5D-F) captured the trends.

7.6.3. Prediction of temperature shift time fed-batch cultures

The model prediction power was tested against two fed-batch experiments with temperature shifts from 37 °C to 33 °C during the exponential growth phase (30h, Figure 7.6) and the early stationary phase (76h, Figure 7.7).

Overall, the model prediction for the temperature reduction after 30 hours was well in agreement with the experimental data. The viable cell profile captured the experimental trend with minor discrepancies (Figure 7.6A). Before the temperature shift, the viable cell density was slightly over-estimated, whereas after the shift it was under-estimated (though within the experimental error). The viable cell profile was comparable to the 37 °C fed-batch culture, though with a lower maximum cell peak density (85% of the 37 °C fed-batch). The antibody concentration was slightly underestimated during the stationary phase (in agreement with the under-estimated cell density), though predicting the final mAb titre. In contrast, the cell viability was closely predicted throughout the culture. The obtained mAb titre was 90% of the reported for the 37 °C fed-batch.

After the temperature shift, the glucose consumption was decreased with a corresponding lower lactate production. The model captured to satisfaction both profiles (Figure 7.6B). Similarly, the ammonia production was high and well predicted, despite the systematic difference between the glutamine model prediction (after 48h) and the experimental data (Figure 7.6C). The observed difference in the glutamine profile suggests that glutamine was consumed at a higher rate than predicted. The dual effect of the toxic metabolite accumulation and temperature shift was reflected in the increase of the G_0 fraction (after the temperature shift time) and further rise throughout the culture (Figure 7.6D). Furthermore, the temperature shift was followed by changes in the proliferating cell cycle fractions. Overall, all the cell cycle trends were satisfactorily captured, while early differences in the S and G_2/M fraction predictions (similarly as observed in the 37 °C fed-batch culture) were observed (Figure 7.6E-F).

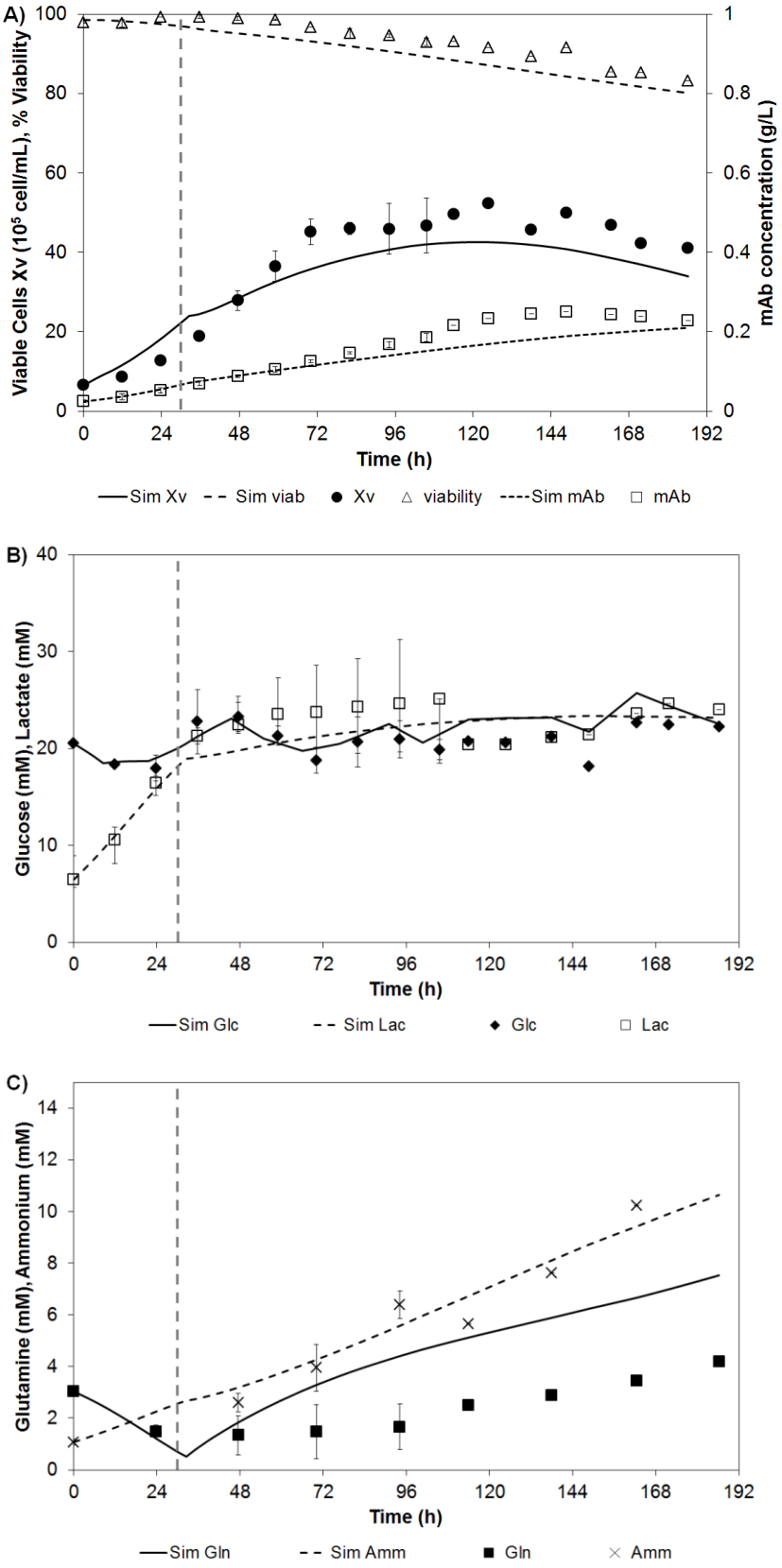


Figure 7.6. Temperature shifted fed-batch cultures to 33 °C at 30h. A) Cell growth, viability and mAb profiles; B) Glucose and lactate profiles; C) Glutamine and Ammonia profiles; D) G1/G0 phase; E) S phase; F) G_2/M phase. Notation: vertical grey dotted line indicates time of the temperature shift, dots represent experimental data (n=2, error bars=standard deviation), black lines represent the simulation results.

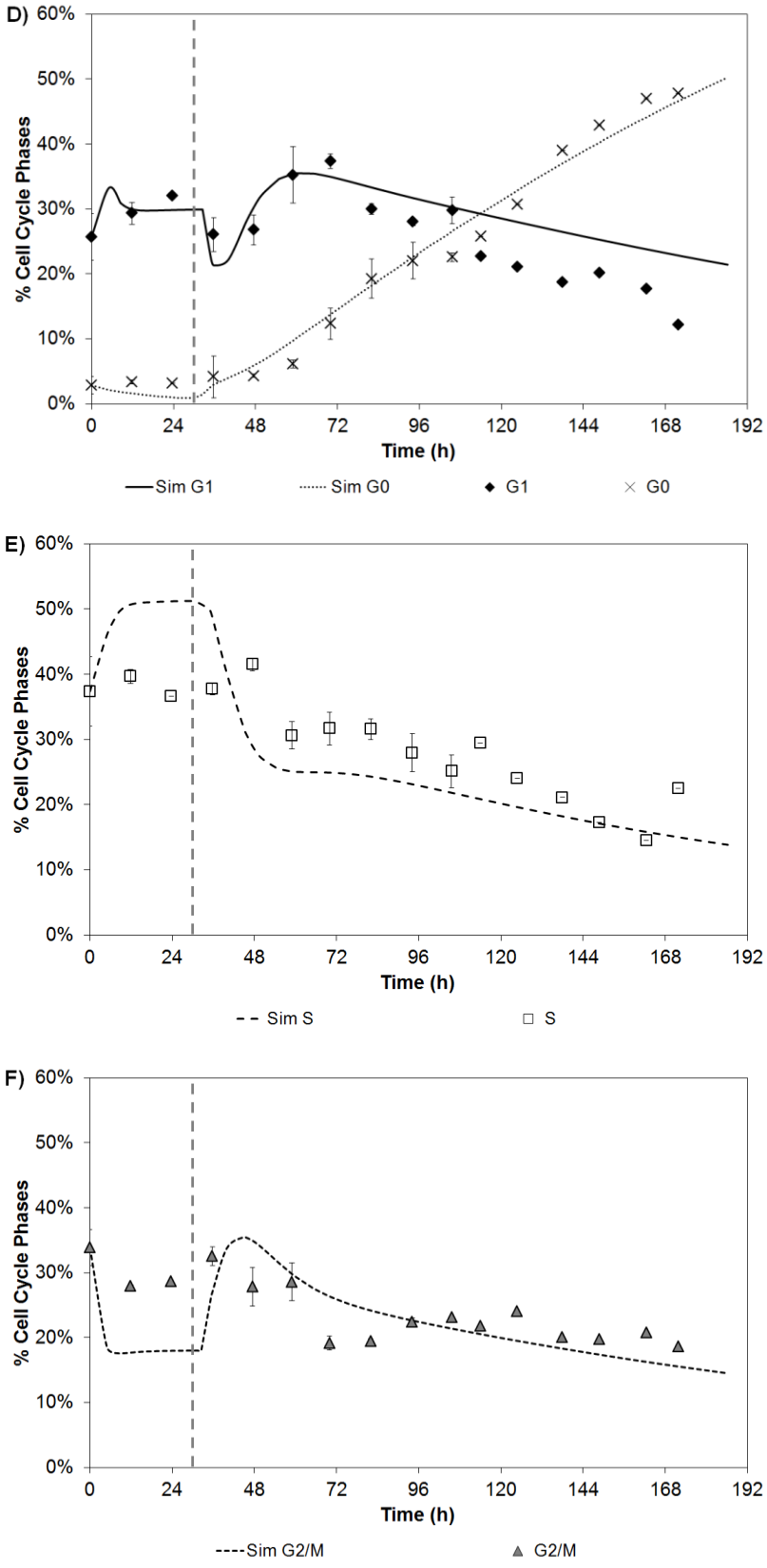


Figure 7.6. (Continued). Temperature shifted fed-batch cultures to 33 °C at 30h. A) Cell growth, viability and mAb profiles; B) Glucose and lactate profiles; C) Glutamine and Ammonia profiles; D) G1/G0 phase; E) S phase; F) G_2/M phase. Notation: vertical grey dotted line indicates time of the temperature shift, dots represent experimental data (n=2, error bars=standard deviation), black lines represent the simulation results.

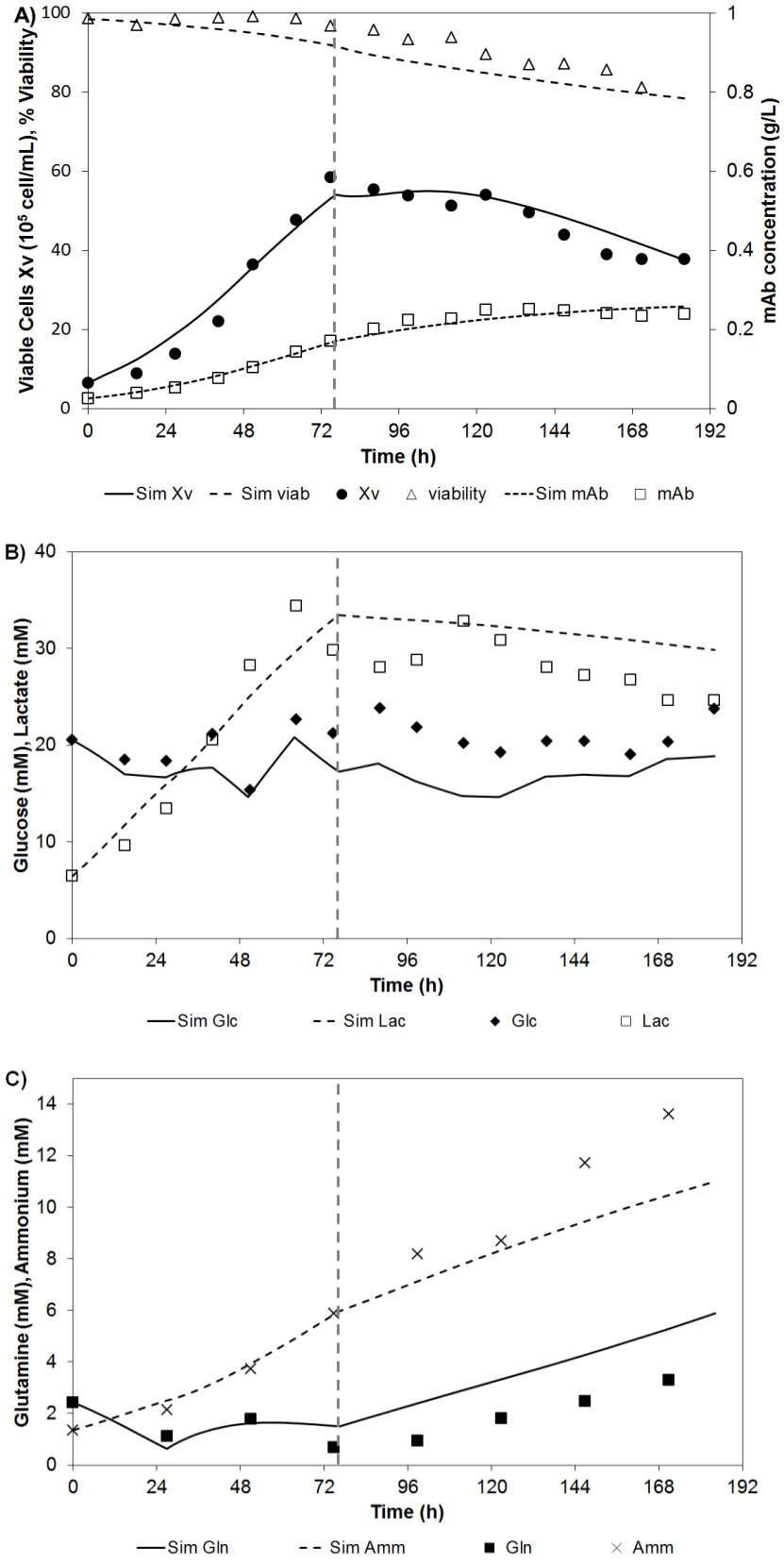


Figure 7.7. Temperature shifted fed-batch culture to 33 °C at 76h. A) Cell growth, viability and mAb profiles; B) Glucose and lactate profiles; C) Glutamine and Ammonia profiles; D) G1/G0 phase; E) S phase; F) G_2/M phase. Notation: vertical grey dotted line indicates time of the temperature shift, dots represent experimental data (n=1), black lines represent the simulation results.

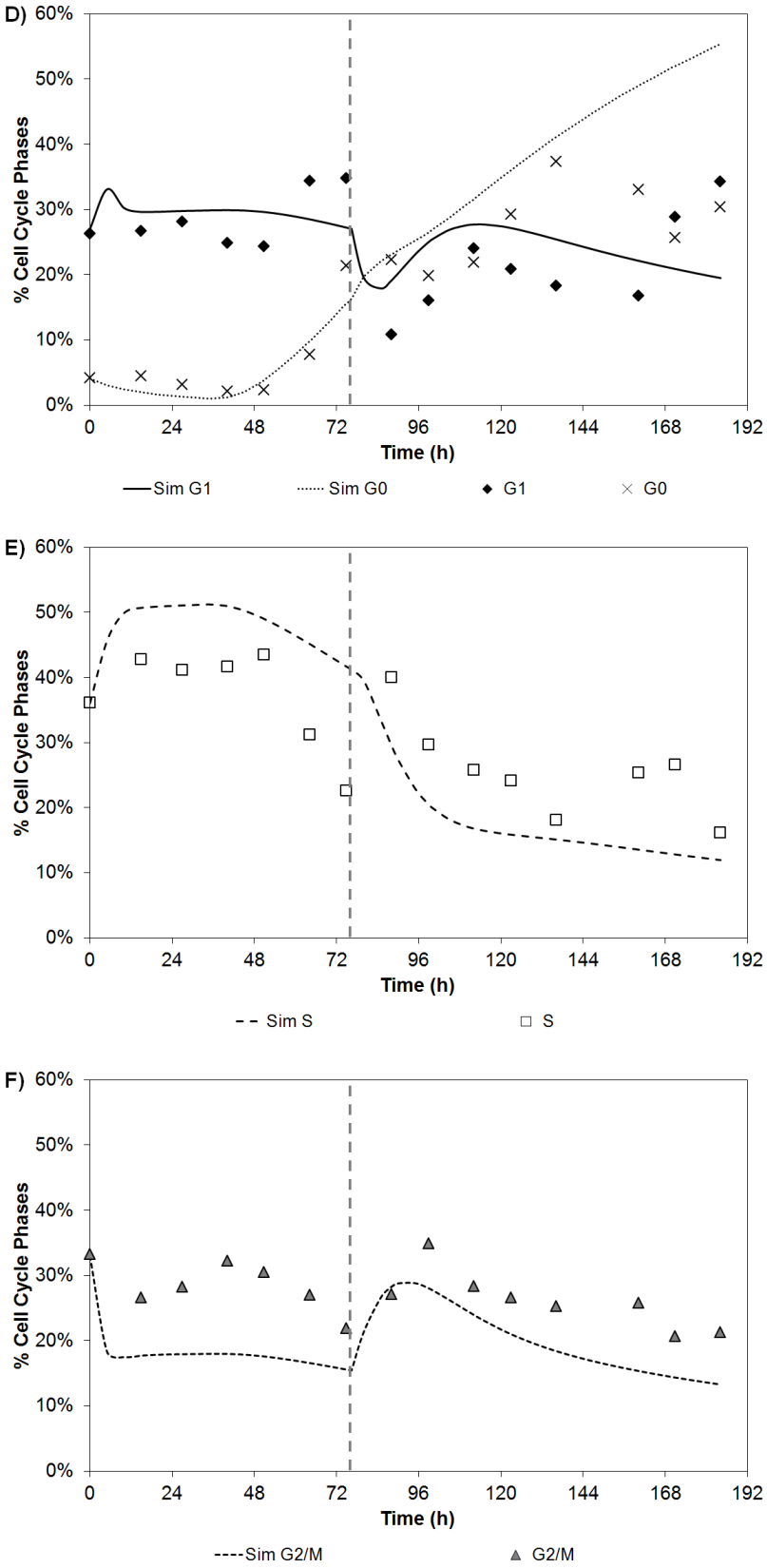


Figure 7.7. (Continued). Temperature shifted fed-batch culture to 33 °C at 76h. A) Cell growth, viability and mAb profiles; B) Glucose and lactate profiles; C) Glutamine and Ammonia profiles; D) G1/G0 phase; E) S phase; F) G_2/M phase. Notation: vertical grey dotted line indicates time of the temperature shift, dots represent experimental data (n=1), black lines represent the simulation results.

The second model prediction considered a fed-batch culture with temperature shift from 37 °C to 33 °C at 76 hours (Figure 7.7). The delayed temperature shift time was expected to result in higher cell concentrations compared to the previous shift times. The viable cell density reached 95% of the peak cell density when compared to the 37 °C fed-batch. The model prediction captured the viable cell density throughout, as well as the viability and mAb titre (Figure 7.7A). Despite achieving a higher cell density than in the 30h temperature shift fed-batch, the mAb titre remained at 90% of the achieved in the 37 °C fed-batch culture. The glucose and lactate profiles were well predicted with a systematic under-estimation of the glucose profile after the temperature shift (Figure 7.7B). Similarly, the glutamine profile showed a systematic difference, though in this case the glutamine profile was overestimated (Figure 7.7C). Such differences suggest a preference to consume glutamine over glucose under the culture conditions, which the model cannot fully capture. Nonetheless, the glutamine predicted trend was correct and it was accompanied with a fair prediction of the ammonia profile. The G_0 fraction was triggered before the temperature shift due to metabolic effectors (Figure 7.7D) and was further enhanced by the temperature shift. The overall trend of the G_0 fraction is correct with some differences at late stages of culture. Towards the end of the culture, the G_0 fraction decreased with a simultaneous increase in the G_1 fraction, which the model did not account for. As in the previous cases, the other cell cycle fraction prediction showed a good agreement to the experimental data, particularly after the temperature shift sharp changes (Figure 7.7E-F).

The proposed model was able to capture overall the experimental trends of both batch and fed-batch cultures. In particular, the model considered the relationship between temperature and the cell cycle (growth), which impacted the productivity and basic metabolism. Some discrepancies were observed mostly related to the metabolism. In general, the glucose consumption seemed to be decreased along the culture further than the model predictions. Similarly, ammonia production was modelled to depend only on glutamine (consumption and degradation), which resulted in an underestimation in some cases. Thus, the metabolic relations need to be further redefined in order to improve the predictions. Despite those differences, the model was able to successfully predict two temperature shift scenarios. The model prediction captured the overall trends at the cell cycle level, growth, and

metabolism. Most importantly, the cell cycle predictions included the non-proliferating phase G_0. The G_0 cell cycle phase has received considerable attention in a number of studies (Alrubeai et al., 1992; Hendrick et al., 2001; Kaufmann et al., 1999; Moore et al., 1997; Trummer et al., 2006) due to the possibility to increase productivity in commercially relevant cell lines. Moreover, the cell cycle regulation via temperature control is of industrial interest as this is the method of choice for improving productivity (Kumar et al., 2007). Although the HFN 7.1 cells showed a growth associated antibody production (reflected in a weak estimation of cell cycle specific productivities - q_{G1G0}, q_S), other cell lines productivities has been associated to specific cell cycle phases (Alrubeai and Emery, 1990; Alrubeai et al., 1992; Dutton et al., 2006). Thus, the developed model is readily applicable and provides a mean to systematically optimise the cell cycle-to-productivity-relationship.

7.7. Conclusions

The development of an unstructured model of metabolic and temperature dependent cell cycle arrest in hybridoma batch and fed-batch cultures was presented this chapter.

The model formulation used first principles, experimental observations, and the existing model development framework. Commonly used experimental measurements (metabolic profiles and process variable information) and fast cell cycle analytical techniques (such as DNA staining and proliferation marker) allowed capturing the basic heterogeneity of the system. In addition to temperature effects, metabolic stresses such as substrate depletion or toxic metabolite accumulation are considered on the cell cycle level to account for different process modes (batch and fed-batch).

A set of batch and fed-batch experiments were designed at two culture conditions to baseline the performance under both culture operation modes and temperatures. The integrated modelling and experimental approach allowed re-estimating the significant parameters from the baseline experimental data. Moreover, the model predictive power was successfully tested in two temperature shifted cultures using a fed-batch operation mode. However, few metabolic relations were identified for further refinement in order to improve the predictions. Nonetheless, the presented

modelling approach can capture the complex dynamic relations of the mammalian culture systems, thus advantages the commonly industry-adopted design of experiment (DoE) approach. Furthermore, the model-based temperature profile optimisation to improve productivity can account not only for the cell cycle regulation but also for other factors such as the mAb proteolytic degradation and downstream impurities (e.g. lysed cells). The importance of the results presented herein lies on the development of relevant modelling-experimental approaches to assist the mammalian cell culture process development with focus on temperature control.

CHAPTER 8

Conclusions & Future Directions

The development of integrated modelling and experimental approaches that facilitate the study of cell cultures including the cell cycle heterogeneity was presented in this thesis. The presented experimental approach combined analytical techniques and assays that allowed capturing the heterogeneity of different cell culture systems. Specifically, the cell cycle blueprint (cell cycle distribution, cyclin expression and transition profiles) for an industrial cell line was elucidated using flow cytometry (chapter 4). In addition, the study of the effect of culture conditions (chapter 5) resulted in the identification of significant links between the cell cycle and apoptosis. The experimental blueprint was used to formulate a first of its kind cyclin and DNA distributed cell cycle model (chapter 6). Following the model development framework (Kiparissides et al., 2011; Kontoravdi et al., 2010; Sidoli et al., 2005), the model was systematically studied and refined through the model analysis tools. The methodology was similarly applied to the industrial relevant subject of temperature profile selection in cell culture systems, while considering an unstructured-segregated cell cycle model (chapter 7). A number of key conclusions can be drawn from the above findings:

- The cell cycle blueprint as herein defined and elucidated serves as an experimentally quantifiable tool to develop biologically accurate cell cycle models.
- Cyclins are key regulatory molecules that can act as model distributed variables to capture the cell cycle biology with adequate detail and enable a mechanistic link with the cell programmed death.
- As previous contributions, the effect of culture conditions (such as substrate and metabolite concentrations and cultivation temperature) was confirmed on both the cell cycle machinery and the induction or repression of programmed cell death. Despite the difficulties due to the complex and multiple connections of the cell cycle and apoptosis, the simultaneous

study of both events can help to refine (and include further biological detail) the presented cell cycle models.

- Different types of cell cycle models were formulated applying the model development framework. The framework provides a systematic tool to assist the parallel model and experimental development allowing the cross-check and flow of information, which facilitates the process.
- A computational fast and biologically accurate cyclin and DNA distributed cell cycle model was presented herein for the first time. The model can be further refined and used in model-based applications of industrial relevance. Most importantly, the proposed modelling approach is not limited to industrial scenarios but it is transferable to clinical environments, as evidence of the generalisation of this result.
- The development of a temperature-dependent cell cycle unstructured model exemplified the modelling-experimental approach in an industrial relevant problem. The temperature profile can be optimise using the model to improve productivity while accounting for the systems dynamics.
- Overall, the presented contributions of this thesis are in the area of systematically developing meaningful mathematical models with predictive capabilities accounting for the cell cycle segregation in bioprocesses. This experimental and modelling approach avoids repetitive trial and error, while efficiently closing the gaps between experimentation and model formulation.

In addition, this final chapter aims to provide a broader look to the thesis contributions, as well as suggest future research directions.

8.1. How to Capture the Heterogeneity

The study of the cell culture heterogeneity has been enabled by the development of analytical techniques. In particular, flow cytometry is a powerful technique that unveils single cell attributes. Alas, the full potential of flow cytometry has still not been exploited in the bio-industry (Kuystermans et al., 2012). In this thesis, a modest fraction of flow cytometry's potential is used to develop relevant cell cycle models. In chapter 4 & 5, flow cytometry was used to elucidate the GS-NS0 cell cycle blueprint. The blueprint was later (chapter 6) used for the development of the cyclin and DNA

distributed cell cycle model. However, the relevance of the cell cycle blueprint goes beyond the model formulation as it acts as an accurate indicator of the culture's state. Thus, the development of automated flow cytometry (Kuystermans et al., 2012; Sitton and Srienc, 2008) will assist the establishment of this technique as a routine analysis. Alas, the adoption of flow cytometry will also result in a considerable increase in the data to analyse. Despite the availability of flow cytometry software packages, an area that needs further development is the flow cytometry data quantification. Currently, flow cytometric data are used for semi-quantitative studies by sequentially gating and selecting subpopulations, thus resulting mainly in the identification of positive/negatively expressing fractions of a given attribute. However the quantitative differences in the expression, as reflected in the fluorescence intensity, are not fully utilised. As presented in this thesis, the quantification of the flow cytometric data can provide additional information, which can be later used in systematic approaches/studies.

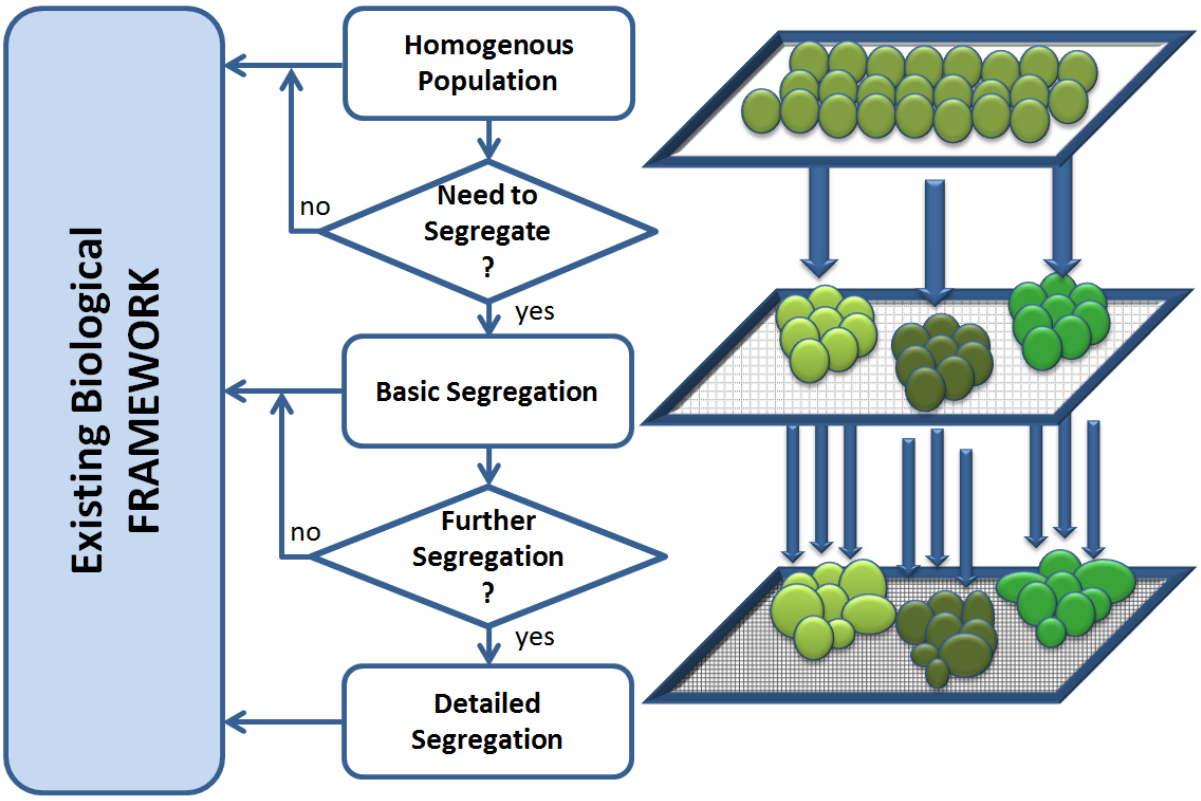


Figure 8.1. Cell cycle model development.

In general, the heterogeneity of the cell culture systems can be captured nowadays, though the question of how and to what extent still remains. In order to answer these questions, a multi-disciplinary (modellers and experimentalists)

expertise is usually required, while considering the end application. Herein, two different cell cycle models were presented. First, a segregated approach (chapter 6) proved to capture the biology of the system while remaining computationally tractable. However, in order to support this model formulation, intense experimentation is required. The second model formulation (chapter 7) due to its unsegregated nature requires a less intense experimentation. Overall, a top-down design approach is advised in order to capture the system heterogeneity, unless the need for a detailed segregation is known beforehand. Regardless of the selected level of segregation, the biological model framework can be applied to assist the development (Figure 8.1) in all the cases. The basic segregation, defined as which cell cycle fractions to consider, should be addressed early in the model development. Though this seems to be driven both by the cell line behaviour (e.g. the cell is prompted to enter – or not – the quiescent state G_0, or if there is a significant variability in the G_2/M phase), as well as the availability for cell markers. Similarly, the detailed cyclin segregation depends on both the availability of bio-markers and the patterns of expression; as in some cases, the cyclin expression pattern might not render the cyclin suitable for modelling purposes (e.g. the herein reported cyclin D expression).

8.2. Linking Cell Cycle & Apoptosis

The cell cycle relevance lays at growth, proliferation, cell death and product quality levels. Particularly, the intimate link between the cell cycle and apoptosis has been reported (Meikrantz and Schlegel, 1995). The herein reported cell cycle blueprint and gene expression profiles are expected to be cell line and culture condition dependent (e.g. temperature, medium formulation, serum, growth factors, etc.). Nonetheless in chapter 5, the link between the cell cycle and apoptosis was suggested at different points. Moreover, the consideration of apoptotic related gene expression, cell cycle regulators, and cyclin expression mapped an important relationship that requires further study. The bivariate graphs of relative gene expression versus relative cyclin expression proved to provide insight on the link between the two cell events (cell cycle progression and apoptosis). An apparent bi-stable (Lavrik et al., 2009; Pomerening, 2008) pattern was identified between *p21* and all the studied cyclins (D, E and B), as well as between *trp53bp2* and cyclin B. Although these are preliminary results (and other associations need to be

considered), the observed links render some of these biomarkers as promising coupling points between a mechanistic accurate cell cycle and apoptosis model.

The simultaneous study of cyclin expression and apoptosis related gene expression can aid the understanding of these intimately related processes. However, the experimental conditions to study the relation should be carefully considered, as well as the timing of events. The experimental conditions to study jointly these two events are narrow (e.g. exhaustion of substrate, toxic metabolite concentrations, among other) and within a short spam. Thus, the experimental set-up requires careful consideration to avoid the recurrent disruption of the cell culture environment while performing a frequent sampling (as occurs in shake flask cultures), as it may affect the reliability and reproducibility of the results.

8.3. Metabolism & Segregation

A last aspect that was identified through the developed models is the link between the cell metabolism and the cell cycle. A classical modelling approach utilises Monod kinetics to model the growth rate, which is stated substrate and/or metabolite dependent. In this thesis, a similar approach was adopted by declaring the cyclins and DNA growth rates as substrate dependent. Such relation was supported by the experimentally observed differences in the expression levels in the presence or absence of glutamate for the GS-NS0 cell line. However, the undefined nature of the used medium (serum containing) limits the generalisation of the observed results. As observed in the medium shift study, the results of the 50% (v/v) medium blend were comparable to the 100% fresh medium, despite the significant differences in glucose and glutamate concentrations. This was attributed to the non-quantified growth factors present due to the use of serum in the medium formulation. Thus, the use of chemically defined media can enable a more comprehensive study of industrial relevance.

On the contrary, the use of a chemically defined medium does not guarantee or imply a simpler analysis. As presented in the unstructured-segregated cell cycle model for the HFN 7.1 cell line, the cell metabolism was one of the most challenging aspects to capture (despite the use of a chemically defined medium). The use of a chemically defined medium needs to be accompanied with a complete metabolic

profiling, at least until the key substrates and metabolites are fully identified. This also poses a challenge as the amount of data increases (amino acids, metabolites, vitamins, trace elements) and the need to develop systematic techniques to identify early significant relationships for modelling purposes are therefore required. However, even the extreme case of considering all the possible entities in the metabolic profile does not guarantee to be able to model the cell metabolism accurately. Although metabolic flux analysis (MFA) has become a key tool for the study of mammalian cell cultures, the cell metabolism is still an open research area. The applicability of MFA to mammalian cells is limited due to their complexity, adaptation to changing environments (Gòdia and Cairó, 2002; Niklas and Heinzle, 2012), as well as neglecting the intrinsic heterogeneity (Wang and Bodovitz, 2010) of the systems. Thus, cell metabolic studies need to start incorporating the real drive behind the metabolic and adaptation processes. Such change and drive in the metabolism goes back to the energy metabolism (and metabolite availability), which includes the anabolic and catabolic pathways. Thus, considering both the available metabolites and the energy requirements (and energy favourable pathways) could provide answer to the frequently unresolved changes in cell metabolism. Finally, the energy based model can be linked both to the expression of cell cycle regulatory molecules (cyclin) and/or to the up/down-regulation of apoptosis related gene expression. Overall, the simultaneous advancement of analytical techniques and computational power (as well as data mining and solution algorithms) will pave the way for the development of biologically accurate models moving away from the heuristic approaches.

Bibliography

Aggarwal, S., (2014) What's fueling the biotech engine - 2012 to 2013. Nature biotechnology 32, 32-39.

Al-Fageeh, M.B., Marchant, R.J., Carden, M.J., Smales, C.M., (2006) The cold-shock response in cultured mammalian cells: Harnessing the response for the improvement of recombinant protein production. Biotechnology and Bioengineering 93, 829-835.

Alberts, B., Johnson, A., Lewis, J., Raff, M., Roberts, K., Walter, P., (2008) Molecular Biology of The Cell, 5th Edition ed. Garland Science, Taylor & Francis Group.

Allen, M.J., Boyce, J.P., Trentalange, M.T., Treiber, D.L., Rasmussen, B., Tillotson, B., Davis, R., Reddy, P., (2008) Identification of novel small molecule enhancers of protein production by cultured mammalian cells. Biotechnology and Bioengineering 100, 1193-1204.

Alrubeai, M., Emery, A.N., (1990) Mechanisms and kinetics of monoclonal-antibody synthesis and secretion in synchronous and asynchronous hybridoma cell-cultures. Journal of Biotechnology 16, 67-86.

Alrubeai, M., Emery, A.N., Chalder, S., Jan, D.C., (1992) Specific monoclonal-antibody productivity and the cell cycle-comparisons of batch, continuous and perfusion cultures. Cytotechnology 9, 85-97.

Andersen, D.C., Bridges, T., Gawlitzek, M., Hoy, C., (2000) Multiple cell culture factors can affect the glycosylation of Asn-184 in CHO-produced tissue-type plasminogen activator. Biotechnology and Bioengineering 70, 25-31.

Bailey, J.E., (1998) Mathematical modeling and analysis in biochemical engineering: Past accomplishments and future opportunities. Biotechnology Progress 14, 8-20.

Barnabe, N., Butler, M., (1994) Effect of temperature on nucleotide pools and monoclonal antibody production in a mouse hybridoma. Biotechnology and Bioengineering 44, 1235-1245.

Barnes, L.M., Bentley, C.M., Dickson, A.J., (2000) Advances in animal cell recombinant protein production: GS-NS0 expression system. Cytotechnology 32, 109-123.

Basse, B., Baguley, B.C., Marshall, E.S., Joseph, W.R., van Brunt, B., Wake, G., Wall, D.J.N., (2003) A mathematical model for analysis of the cell cycle in cell lines derived from human tumors. J. Math. Biol. 47, 295-312.

Batt, B.C., Kompala, D.S., (1989) A structured kinetic modeling framework for the dynamics of hybridoma growth and monoclonal-antibody production in continuous suspension-cultures. Biotechnology and Bioengineering 34, 515-531.

Bebbington, C.R., Renner, G., Thomson, S., King, D., Abrams, D., Yarranton, G.T., (1992) High-level expression of a recombinant antibody from myeloma cells using a glutamine synthetase gene as an amplifiable selectable marker. Bio/technology (Nature Publishing Company) 10, 169-175.

Becerra, S., Berrios, J., Osses, N., Altamirano, C., (2012) Exploring the effect of mild hypothermia on CHO cell productivity. Biochemical Engineering Journal 60, 1-8.

Bi, J.X., Shuttleworth, J., Al-Rubeai, M., (2004) Uncoupling of cell growth and proliferation results in enhancement of productivity in p21(C1P1)-arrested CHO cells. Biotechnology and Bioengineering 85, 741-749.

Bibila, T.A., Flickinger, M.C., (1991) A model of interorganelle monoclonal-antibody transport and secretion in mouse hybridoma cells. Biotechnology and Bioengineering 38, 767-780.

Bibila, T.A., Flickinger, M.C., (1992a) Use of a Structured Kinetic-Model of Antibody-Synthesis and Secretion for Optimization of Antibody-Production Systems .1. Steady-State Analysis. Biotechnology and Bioengineering 39, 251-261.

Bibila, T.A., Flickinger, M.C., (1992b) Use of a structured kinetic-model of antibody-synthesis and secretion for optimization of antibody-production systems .2. Transient analysis. Biotechnology and Bioengineering 39, 262-272.

Bloemkolk, J.W., Gray, M.R., Merchant, F., Mosmann, T.R., (1992) Effect of temperature on hybridoma cell-cycle and mab production. Biotechnology and Bioengineering 40, 427-431.

Browne, S.M., Al-Rubeai, M., (2011) Analysis of an artificially selected GS-NS0 variant with increased resistance to apoptosis. Biotechnology and Bioengineering 108, 880-892.

Butler, M., Jenkins, H., (1989) Nutritional aspects of the growth of animal cells in culture. Journal of Biotechnology 12, 97-110.

Cain, S.J., Chau, P.C., (1998) Transition probability cell cycle model with product formation. Biotechnology and Bioengineering 58, 387-399.

Cappella, P., Gasparri, F., Pulici, M., Moll, J., (2008) A novel method based on click chemistry, which overcomes limitations of cell cycle analysis by classical determination of BrdU incorporation, allowing multiplex antibody staining. Cytom. Part A 73A, 626-636.

Carvalhal, A.V., Marcelino, I., Carrondo, M.J.T., (2003) Metabolic changes during cell growth inhibition by p27 overexpression. Applied Microbiology and Biotechnology 63, 164-173.

Cazzador, L., Mariani, L., (1993) Growth and production modeling in hybridoma continuous cultures. Biotechnology and Bioengineering 42, 1322-1330.

Chong, S.L., Mou, D.G., Ali, A.M., Lim, S.H., Tey, B.T., (2008) Cell growth, cell-cycle progress, and antibody production in hybridoma cells cultivated under mild hypothermic conditions. Hybridoma 27, 107-111.

Cooper, S., (2003) Rethinking synchronization of mammalian cells for cell cycle analysis. Cellular and Molecular Life Sciences 60, 1099-1106.

Darzynkiewicz, Z., Bedner, E., Smolewski, P., (2001) Flow cytometry in analysis of cell cycle and apoptosis. Seminars in Hematology 38, 179-193.

Darzynkiewicz, Z., Gong, J.P., Juan, G., Ardelt, B., Traganos, F., (1996) Cytometry of cyclin proteins. Cytometry 25, 1-13.

Davies, S.L., Lovelady, C.S., Grainger, R.K., Racher, A.J., Young, R.J., James, D.C., (2013) Functional heterogeneity and heritability in CHO cell populations. Biotechnology and Bioengineering 110, 260-274.

Dean, J., Reddy, P., (2013) Metabolic analysis of antibody producing CHO cells in fed-batch production. Biotechnology and Bioengineering 110, 1735-1747.

deZengotita, V.M., Miller, W.M., Aunins, J.G., Zhou, W.C., (2000) Phosphate feeding improves high-cell-concentration NS0 myeloma culture performance for monoclonal antibody production. Biotechnology and Bioengineering 69, 566-576.

Domach, M.M., Shuler, M.L., (1984) A finite representation model for an asynchronous culture of Escherichia-coli. Biotechnology and Bioengineering 26, 877-884.

Dorka, P., Fischer, C., Budman, H., Scharer, J., (2009) Metabolic flux-based modeling of mAb production during batch and fed-batch operations. Bioprocess. Biosyst. Eng. 32, 183-196.

Du, Z.M., Mujacic, M., Le, K., Caspary, G., Nunn, H., Heath, C., Reddy, P., (2013) Analysis of heterogeneity and instability of stable mAb-expressing CHO cells. Biotechnology and Bioprocess Engineering 18, 419-429.

Dulic, V., Stein, G.H., Far, D.F., Reed, S.I., (1998) Nuclear accumulation of p21Cip1 at the onset of mitosis: a role at the G2/M-phase transition. Molecular and cellular biology 18, 546-557.

Dutton, R.L., Scharer, J., Moo-Young, M., (2006) Cell cycle phase dependent productivity of a recombinant Chinese hamster ovary cell line. Cytotechnology 52, 55-69.

Dutton, R.L., Scharer, J.M., Moo-Young, M., (1998) Descriptive parameter evaluation in mammalian cell culture. Cytotechnology 26, 139-152.

Eguchi, Y., Shimizu, S., Tsujimoto, Y., (1997) Intracellular ATP levels determine cell death fate by apoptosis or necrosis. Cancer research 57, 1835-1840.

Fadda, S., Cincotti, A., Cao, G., (2012a) A novel population balance model to investigate the kinetics of in vitro cell proliferation: Part I. model development. Biotechnology and Bioengineering 109, 772-781.

Fadda, S., Cincotti, A., Cao, G., (2012b) A novel population balance model to investigate the kinetics of in vitro cell proliferation: Part II. numerical solution, parameters' determination, and model outcomes. Biotechnology and Bioengineering 109, 782-796.

Fiore, M., Degrassi, F., (1999) Dimethyl sulfoxide restores contact inhibition-induced growth arrest and inhibits cell density-dependent apoptosis in hamster cells. Exp. Cell Res. 251, 102-110.

Fiore, M., Zanier, R., Degrassi, F., (2002) Reversible G(1) arrest by dimethyl sulfoxide as a new method to synchronize Chinese hamster cells. Mutagenesis 17, 419-424.

Fox, S.R., Patel, U.A., Yap, M.G.S., Wang, D.I.C., (2004) Maximizing interferon-gamma production by Chinese hamster ovary cells through temperature shift optimization: Experimental and modeling. Biotechnology and Bioengineering 85, 177-184.

Fredrickson, A.G., McGee, R.D., III, Tsuchiya, H.M., (1970) Mathematical models in fermentation processes. Advanced Applied Microbiology 23.

Fredrickson, A.G., Ramkrishna, D., Tsuchiya, H.M., (1967) Statistics and dynamics of procaryotic cell populations. Mathematical Biosciences 1, 48.

Frisa, P.S., Jacobberger, J.W., (2009) Cell cycle-related cyclin B1 quantification. PLoS One 4.

Furukawa, K., Ohsuye, K., (1998) Effect of culture temperature on a recombinant CHO cell line producing a C-terminal alpha-amidating enzyme. Cytotechnology 26, 153-164.

Fussenegger, M., Bailey, J.E., (1998) Molecular regulation of cell-cycle progression and apoptosis in mammalian cells: Implications for biotechnology. Biotechnology Progress 14, 807-833.

Gartel, A.L., Tyner, A.L., (2002) The Role of the Cyclin-dependent Kinase Inhibitor p21 in Apoptosis 1 Supported in part by NIH Grant R01 DK56283 (to A. L. T.) for the p21 research and Campus Research Board and Illinois Department of Public Health Penny Severns Breast and Cervical Cancer grants (to A. L. G.).1. Molecular Cancer Therapeutics 1, 639-649.

Gauthier, A., (2013) An in vitro study of the effects of temperature on apoptosis and cell cycle in the GS-NS0 cell line.

Gawlitzek, M., Estacio, M., Fürch, T., Kiss, R., (2009) Identification of cell culture conditions to control N-glycosylation site-occupancy of recombinant glycoproteins expressed in CHO cells. Biotechnology and Bioengineering 103, 1164-1175.

Ghiani, C.A., Yuan, X.Q., Eisen, A.M., Knutson, P.L., DePinho, R.A., McBain, C.J., Gallo, V., (1999) Voltage-activated K+ channels and membrane depolarization regulate accumulation of the cyclin-dependent kinase inhibitors p277(Kip1) and p21(CIP1) in glial progenitor cells. Journal of Neuroscience 19, 5380-5392.

Gòdia, F., Cairó, J., (2002) Metabolic engineering of animal cells. Bioprocess. Biosyst. Eng. 24, 289-298.

Gong, J., Li, X., Traganos, F., Darzynkiewicz, Z., (1994) Expression of G(1) and G(2) cyclins measured in individual cells by multiparameter flow-cytometry - A new tool in the analysis of the cell-cycle. Cell Proliferation 27, 357-371.

Gong, J., Traganos, F., Darzynkiewicz, Z., (1995) Threshold expression of cyclin-E-type but not cyclin-D-type characterizes normal and tumor-cells entering S-phase. Cell Proliferation 28, 337-346.

Gong, J.P., Traganos, F., Darzynkiewicz, Z., (1993) Simultaneous analysis of cell-cycle kinetics at 2 different DNA-ploidy levels based on DNA content and cyclin-B measurements. Cancer Research 53, 5096-5099.

Han, S.I., Oh, S.Y., Jeon, W.J., Kim, J.M., Lee, J.H., Chung, H.Y., Choi, Y.H., Yoo, M.A., Kim, H.D., Kang, H.S., (2002) Mild heat shock induces cyclin D1 synthesis through multiple Ras signal pathways. FEBS letters 515, 141-145.

Harper, J.V., (2005) Synchronization of cell populations in G1/S and G2/M phases of the cell cycle. Methods in Molecular Biology 296, 10.

Hatzis, C., Srienc, F., Fredrickson, A.G., (1995) Multistaged corpuscular models of microbial-growth - Monte-Carlo Simulations. Biosystems 36, 19-35.

Heath, J.K., (2001) Principles of cell proliferation. Blackwell Science, Oxford.

Hendrick, V., Winnepenninckx, P., Abdelkafi, C., Vandeputte, O., Cherlet, M., Marique, T., Renemann, G., Loa, A., Kretzmer, G., Werenne, J., (2001) Increased productivity of recombinant tissular plasminogen activator (t-PA) by butyrate and shift of temperature: a cell cycle phases analysis. Cytotechnology 36, 71-83.

Henson, M.A., (2005) Cell ensemble modeling of metabolic oscillations in continuous yeast cultures. Computers & Chemical Engineering 29, 645-661.

Hill, A.V., (1910) The possible effects of the aggregation of the molecules of haemoglobin on its dissociation curves. Journal of Physiology 40, iv-vii.

Ho, Y., Varley, J., Mantalaris, A., (2006) Development and analysis of a mathematical model for antibody-producing GS-NS0 cells under normal and hyperosmotic culture conditions. Biotechnology Progress 22, 1560-1569.

Innocente, S.A., Abrahamson, J.L., Cogswell, J.P., Lee, J.M., (1999) p53 regulates a G2 checkpoint through cyclin B1. Proc. Natl. Acad. Sci. U. S. A. 96, 2147-2152.

Jang, D.J., Barford, J.P., (2000) An unstructured kinetic model of macromolecular metabolism in batch and fed-batch cultures of hybridoma cells producing monoclonal antibody. Biochemical Engineering Journal 4, 153-168.

Jenkins, N., Hovey, A., (1993) Temperature control of growth and productivity in mutant chinese-hamster ovary cells synthesizing a recombinant protein. Biotechnology and Bioengineering 42, 1029-1036.

Jimenez del Val, I., Nagy, J.M., Kontoravdi, C., (2011) A dynamic mathematical model for monoclonal antibody N-linked glycosylation and nucleotide sugar donor transport within a maturing Golgi apparatus. Biotechnology Progress 27, 1730-1743.

Karra, S., Sager, B., Karim, M.N., (2010) Multi-scale modeling of heterogeneities in mammalian cell culture processes. Industrial & Engineering Chemistry Research 49, 7990-8006.

Kaufmann, H., Mazur, X., Fussenegger, M., Bailey, J.E., (1999) Influence of low temperature on productivity, proteome and protein phosphorylation of CHO cells. Biotechnology and Bioengineering 63, 573-582.

Kaufmann, H., Mazur, X., Marone, R., Bailey, J.E., Fussenegger, M., (2001) Comparative analysis of two controlled proliferation strategies regarding product quality, influence on tetracycline-regulated gene expression, and productivity. Biotechnology and Bioengineering 72, 592-602.

Khoo, S.H.G., Al-Rubeai, M., (2009) Detailed understanding of enhanced specific antibody productivity in NS0 myeloma cells. Biotechnology and Bioengineering 102, 188-199.

Kiparissides, A., (2012) Development of a combined mathematical and experimental framework for the control and optimisation of mammalian cell culture systems. Chemical Engineering Department. Imperial College London, London, p. 247.

Kiparissides, A., Koutinas, M., Kontoravdi, C., Mantalaris, A., Pistikopoulos, E.N., (2011) 'Closing the loop' in biological systems modeling - From the in silico to the in vitro. Automatica 47, 1147-1155.

Kiparissides, A., Koutinas, M., Pistikopoulos, E.N., Mantalaris, A., (2010a) Model development and analysis of mammalian cell culture systems. Process Systems Engineering. Wiley-VCH Verlag GmbH & Co. KGaA, pp. 403-439.

Kiparissides, A., Kucherenko, S.S., Mantalaris, A., Pistikopoulos, E.N., (2009) Global sensitivity analysis challenges in biological systems modeling. Industrial & Engineering Chemistry Research 48, 7168-7180.

Kiparissides, A., Pistikopoulos, E.N., Mantalaris, A., (2010b) Towards energy-based dynamic optimization of monoclonal antibody producing GS-NS0 cultures. In: Pierucci, S., Ferraris, G.B. (Eds.), Computer Aided Chemical Engineering. Elsevier, pp. 589-594.

Kobayashi, S., Kajino, S., Takahashi, N., Kanazawa, S., Imai, K., Hibi, Y., Ohara, H., Itoh, M., Okamoto, T., (2005) 53BP2 induces apoptosis through the mitochondrial death pathway. Genes to cells : devoted to molecular & cellular mechanisms 10, 253-260.

Kontoravdi, C., (2006) Development of a combined mathematical and experimental framework model for modeling mammalian cell cultures. Department of Chemical Engineering and Chemical Technology. Imperial College London, London.

Kontoravdi, C., Asprey, S.P., Pistikopoulos, E.N., Mantalaris, A., (2005) Application of global sensitivity analysis to determine goals for design of experiments: An example study on antibody-producing cell cultures. Biotechnology Progress 21, 1128-1135.

Kontoravdi, C., Asprey, S.P., Pistikopoulos, E.N., Mantalaris, A., (2007a) Development of a dynamic model of monoclonal antibody production and glycosylation for product quality monitoring. Computers & Chemical Engineering 31, 392-400.

Kontoravdi, C., Pistikopoulos, E.N., Mantalaris, A., (2010) Systematic development of predictive mathematical models for animal cell cultures. Computers & Chemical Engineering 34, 1192-1198.

Kontoravdi, C., Wong, D., Lam, C., Lee, Y.Y., Yap, M.G.S., Pistikopoulos, E.N., Mantalaris, A., (2007b) Modeling amino acid metabolism in mammalian cells-toward the development of a model library. Biotechnology Progress 23, 1261-1269.

Kostoglou, A., Karabelas, A.J., (1995) Evaluation of numerical methods for simulating an evolving particle size distribution in growth processes. Chem. Eng. Commun. 136, 177-199.

Kranenburg, O., vanderEb, A., Zantema, A., (1996) Cyclin D1 is an essential mediator of apoptotic neuronal cell death. Embo Journal 15, 46-54.

Kromenaker, S.J., Srienc, F., (1994) Effect of lactic-acid on the kinetics of growth and antibody-production in a murine hybridoma - secretion patterns during the cell-cycle. Journal of Biotechnology 34, 13-34.

Kucherenko, S., Rodriguez-Fernandez, M., Pantelides, C., Shah, N., (2009) Monte Carlo evaluation of derivative-based global sensitivity measures. Reliability Engineering & System Safety 94, 1135-1148.

Kumar, N., Gammell, P., Clynes, M., (2007) Proliferation control strategies to improve productivity and survival during CHO based production culture - A summary of recent methods employed and the effects of proliferation control in product secreting CHO cell lines. Cytotechnology 53, 33-46.

Kuystermans, D., Mohd, A., Al-Rubeai, M., (2012) Automated flow cytometry for monitoring CHO cell cultures. Methods 56, 358-365.

Lam, C.M., Sriyudthsak, K., Kontoravdi, C., Kothari, K., Park, H.-H., Pistikopoulos, E.N., Mantalaris, A., (2008) Cell cycle modelling for off-line dynamic optimisation of mammalian cultures. In: Joulia, B.B.a.X. (Ed.), 18th European Symposium on Computer Aided Process Engineering – ESCAPE 18.

Lavrik, I.N., Eils, R., Fricker, N., Pforr, C., Krammer, P.H., (2009) Understanding apoptosis by systems biology approaches. Mol. Biosyst. 5, 1105-1111.

Le, H., Kabbur, S., Pollastrini, L., Sun, Z., Mills, K., Johnson, K., Karypis, G., Hu, W.S., (2012) Multivariate analysis of cell culture bioprocess data--lactate consumption as process indicator. Journal of Biotechnology 162, 210-223.

Linardos, T.I., Kalogerakis, N., Behie, L.A., (1992) Cell-cycle model for growth-rate and death rate in continuous suspension hybridoma cultures. Biotechnology and Bioengineering 40, 359-368.

Ling, W.L.W., Deng, L., Lepore, J., Cutler, C., Connon-Carlson, S., Wang, Y., Voloch, M., (2003) Improvement of monoclonal antibody production in hybridoma cells by dimethyl sulfoxide. Biotechnology Progress 19, 158-162.

Liu, C.H., Chu, I.M., Hwang, S.M., (2001) Enhanced expression of various exogenous genes in recombinant Chinese hamster ovary cells in presence of dimethyl sulfoxide. Biotechnol. Lett. 23, 1641-1645.

Liu, Y.H., Bi, J.X., Zeng, A.P., Yuan, J.Q., (2007) A population balance model describing the cell cycle dynamics of myeloma cell cultivation. Biotechnology Progress 23, 1198-1209.

Mantzaris, N.V., Daoutidis, P., Srienc, F., (2001a) Numerical solution of multi-variable cell population balance models: I. Finite difference methods. Computers & Chemical Engineering 25, 1411-1440.

Mantzaris, N.V., Srienc, F., Daoutidis, P., (2002) Nonlinear productivity control using a multi-staged cell population balance model. Chemical Engineering Science 57, 1-14.

Martens, D.E., Sipkema, E.M., Degooijer, C.D., Beuvery, E.C., Tramper, J., (1995) A combined cell-cycle and metabolic model for the growth of hybridoma cells in steady-state continuous-culture. Biotechnology and Bioengineering 48, 49-65.

McCracken, N.A., Kowle, R., Ouyang, A., (2014) Control of galactosylated glycoforms distribution in cell culture system. Biotechnology Progress 30, 547-553.

Meikrantz, W., Schlegel, R., (1995) Apoptosis and the cell cycle. Journal of Cellular Biochemistry 58, 160-174.

Meikrantz, W., Schlegel, R., (1996) Suppression of apoptosis by dominant negative mutants of cyclin-dependent protein kinases. Journal of Biological Chemistry 271, 10205-10209.

Meister, A., (1985) Glutamine synthetase from mammalian tissues. Methods in enzymology 113, 185-199.

Michaelis, L., Menten, M.L., (1913) Die kinetik der invertinwirkung. Biochem Z. 49, 333–369.

Monod, J., (1949) The growth of bacterial cultures. Annual Review of Microbiology 3, 371-394.

Moore, A., Mercer, J., Dutina, G., Donahue, C.J., Bauer, K.D., Mather, J.P., Etcheverry, T., Ryll, T., (1997) Effects of temperature shift on cell cycle, apoptosis and nucleotide pools in CHO cell batch cultures. Cytotechnology 23, 47-54.

Morgan, D.O., (1995) Principles of CDK regulation. Nature 374, 131-134.

Mulukutla, B.C., Gramer, M., Hu, W.-S., (2012) On metabolic shift to lactate consumption in fed-batch culture of mammalian cells. Metab. Eng. 14, 138-149.

Munro, T.P., Mahler, S.M., Huang, E.P., Chin, D.Y., Gray, P.P., (2011) Bridging the gap: Facilities and technologies for development of early stage therapeutic mAb candidates. mAbs 3, 440-452.

Munzer, D.G.G., Kostoglou, M., Georgiadis, M.C., Pistikopoulos, E.N., Mantalaris, A., (2013) Developing a cyclin blueprint as a tool for mapping the cell cycle in GS-NSO. Biochemical Engineering Journal 81, 97-107.

Murray, A., (1994) Cell cycle checkpoints. Current Opinion in Cell Biology 6, 872-876.

Naderi, S., Meshram, M., Wei, C., McConkey, B., Ingalls, B., Budman, H., Scharer, J., (2011) Development of a mathematical model for evaluating the dynamics of normal and apoptotic Chinese hamster ovary cells. Biotechnology Progress 27, 1197-1205.

Niculescu, A.B., 3rd, Chen, X., Smeets, M., Hengst, L., Prives, C., Reed, S.I., (1998) Effects of p21(Cip1/Waf1) at both the G1/S and the G2/M cell cycle transitions: pRb is a critical determinant in blocking DNA replication and in preventing endoreduplication. Molecular and cellular biology 18, 629-643.

Niklas, J., Heinzle, E., (2012) Metabolic flux analysis in systems biology of mammalian cells. In: Hu, W.S., Zeng, A.-P. (Eds.), Genomics and Systems Biology of Mammalian Cell Culture. Springer Berlin Heidelberg, pp. 109-132.

Nolan, R.P., Lee, K., (2011) Dynamic model of CHO cell metabolism. Metab. Eng. 13, 108-124.

Osman, J.J., Birch, J., Varley, J., (2001) The response of GS-NS0 myeloma cells to pH shifts and pH perturbations. Biotechnology and Bioengineering 75, 63-73.

Ouadid-Ahidouch, H., Ahidouch, A., (2008) K+ channel expression in human breast cancer cells: Involvement in cell cycle regulation and carcinogenesis. J. Membr. Biol. 221, 1-6.

Ozturk, S.S., Palsson, B.O., (1991) Growth, metabolic, and antibody production kinetics of hybridoma cell culture: 2. Effects of serum concentration, dissolved oxygen concentration, and medium pH in a batch reactor. Biotechnology Progress 7, 481-494.

Ozturk, S.S., Riley, M.R., Palsson, B.O., (1992) Effects of ammonia and lactate on hybridoma growth, metabolism, and antibody production. Biotechnology and Bioengineering 39, 418-431.

Pardee, A.B., (1989) G1 events and regulation of cell-proliferation. Science 246, 603-608.

Peter, C.P., Suzuki, Y., Buchs, J., (2006) Hydromechanical stress in shake flasks: correlation for the maximum local energy dissipation rate. Biotechnology and Bioengineering 93, 1164-1176.

Pichler, J., Galosy, S., Mott, J., Borth, N., (2011) Selection of CHO host cell subclones with increased specific antibody production rates by repeated cycles of transient transfection and cell sorting. Biotechnology and Bioengineering 108, 386-394.

Pilbrough, W., Munro, T.P., Gray, P., (2009) Intraclonal protein expression heterogeneity in recombinant CHO cells. PLoS One 4.

Pinto, M.A., Immanuel, C.D., Doyle, F.J., (2007) A feasible solution technique for higher-dimensional population balance models. Computers & Chemical Engineering 31, 1242-1256.

Pomerening, J.R., (2008) Uncovering mechanisms of bistability in biological systems. Curr. Opin. Biotechnol. 19, 381-388.

Ponzio, G., Loubat, A., Rochet, N., Turchi, L., Rezzonico, R., Far, D.F., Dulic, V., Rossi, B., (1998) Early G(1) growth arrest of hybridoma B cells by DMSO involves cyclin D2 inhibition and p21(CIP1) induction. Oncogene 17, 1159-1166.

Pozarowski, P., Darzynkiewicz, Z., (2004) Analysis of cell cycle by flow cytometry. Methods in molecular biology (Clifton, N.J.) 281, 301-311.

Process_Systems_Enterprise, (1997-2012) gPROMS v3.5.3, Model Validation Guide. London, UK.

Rabitz, H., Alis, O.F., (1999) General foundations of high-dimensional model representations. Journal of Mathematical Chemistry 25, 197-233.

Reitzer, L.J., Wice, B.M., Kennell, D., (1979) Evidence that glutamine, not sugar, is the major energy source for cultured HeLa cells. The Journal of biological chemistry 254, 2669-2676.

Reuveny, S., Velez, D., Macmillan, J.D., Miller, L., (1987) Factors affecting monoclonal antibody production in culture. Developments in biological standardization 66, 169-175.

Rossler, B., Lubben, H., Kretzmer, G., (1996) Temperature: A simple parameter for process optimization in fed-batch cultures of recombinant Chinese hamster ovary cells. Enzyme and Microbial Technology 18, 423-427.

Rounseville, K.J., Chau, P.C., (2005) Three-dimensional cell cycle model with distributed transcription and translation. Med. Biol. Eng. Comput. 43, 155-161.

Rubin, L.L., Gatchalian, C.L., Rimon, G., Brooks, S.F., (1994) The molecular mechanisms of neuronal apoptosis. Current Opinion in Neurobiology 4, 696-702.

Saltelli, A., Chan, K., Scott, E.M., (2000) Sensitivity Analysis. Wiley Press.

Samuels-Lev, Y., O'Connor, D.J., Bergamaschi, D., Trigiante, G., Hsieh, J.K., Zhong, S., Campargue, I., Naumovski, L., Crook, T., Lu, X., (2001) ASPP proteins specifically stimulate the apoptotic function of p53. Molecular cell 8, 781-794.

Sandberg, H., Lutkemeyer, D., Kuprin, S., Wrangel, M., Almstedt, A., Persson, P., Ek, V., Mikaelsson, M., (2006) Mapping and partial characterization of proteases expressed by a CHO production cell line. Biotechnology and Bioengineering 95, 961-971.

Sanderson, C.S., Barford, J.P., Barton, G.W., (1999) A structured, dynamic model for animal cell culture systems. Biochemical Engineering Journal 3, 203-211.

Sanfeliu, A., Stephanopoulos, G., (1999) Effect of glutamine limitation on the death of attached Chinese hamster ovary cells. Biotechnology and Bioengineering 64, 46-53.

Schoen, R.C., Bentley, K.L., Klebe, R.J., (1982) Monoclonal antibody against human fibronectin which inhibits cell attachment. Hybridoma 1, 99-108.

Sellick, C.A., Croxford, A.S., Maqsood, A.R., Stephens, G., Westerhoff, H.V., Goodacre, R., Dickson, A.J., (2011) Metabolite profiling of recombinant CHO cells: designing tailored feeding regimes that enhance recombinant antibody production. Biotechnology and Bioengineering 108, 3025-3031.

Seo, J.S., Kim, Y.J., Cho, J.M., Baek, E., Lee, G.M., (2013) Effect of culture pH on recombinant antibody production by a new human cell line, F2N78, grown in suspension at 33.0 degrees C and 37.0 degrees C. Applied microbiology and biotechnology 97, 5283-5291.

Seth, G., Hossler, P., Yee, J.C., Hu, W.S., (2006) Engineering cells for cell culture bioprocessing - Physiological fundamentals. Cell Culture Engineering, pp. 119-164.

Sherr, C.J., (1993) Mammalian G(1)-cyclins. Cell 73, 1059-1065.

Shi, M., Xie, Z.G., Yu, M., Shen, B.F., Guo, N., (2005) Controlled growth of Chinese hamster ovary cells and high expression of antibody-IL-2 fusion proteins by temperature manipulation. Biotechnol. Lett. 27, 1879-1884.

Sidoli, F.R., Asprey, S.P., Mantalaris, A., (2006) A coupled single cell-population-balance model for mammalian cell cultures. Industrial & Engineering Chemistry Research 45, 5801-5811.

Sidoli, F.R., Mantalaris, A., Asprey, S.P., (2004) Modelling of mammalian cells and cell culture processes. Cytotechnology 44, 27-46.

Sidoli, F.R., Mantalaris, A., Asprey, S.P., (2005) Toward global parametric estimability of a large-scale kinetic single-cell model for mammalian cell cultures. Industrial & Engineering Chemistry Research 44, 868-878.

Singhania, R., Sramkoski, R.M., Jacobberger, J.W., Tyson, J.J., (2011) A hybrid model of mammalian cell cycle regulation. PLoS Comput. Biol. 7.

Sitton, G., Srienc, F., (2008) Growth dynamics of mammalian cells monitored with automated cell cycle staining and flow cytometry. Cytom. Part A 73A, 538-545.

Slater, M.L., Sharrow, S.O., Gart, J.J., (1977) Cell-cycle of saccharomyces-cerevisiae in populations growing at different rates - (flow microfluorometry-yeast-mithramycin-dna replication). Proc. Natl. Acad. Sci. U. S. A. 74, 3850-3854.

Sobol, I.M., (2001) Global sensitivity indices for nonlinear mathematical models and their Monte Carlo estimates. Mathematics and Computers in Simulation 55, 271-280.

Stacey, D.W., Hitomi, M., (2008) Cell cycle studies based upon quantitative image analysis. Cytom. Part A 73A, 270-278.

Stamatakis, M., (2013) Cell population balance and hybrid modeling of population dynamics for a single gene with feedback. Computers & Chemical Engineering 53, 25-34.

Sunley, K., Butler, M., (2010) Strategies for the enhancement of recombinant protein production from mammalian cells by growth arrest. Biotechnology Advances 28, 385-394.

Sureshkumar, G.K., Mutharasan, R., (1991) The influence of temperature on a mouse mouse hybridoma growth and monoclonal-antibody production. Biotechnology and Bioengineering 37, 292-295.

Suzuki, E., Ollis, D.F., (1989) Cell-cycle model for antibody-production kinetics. Biotechnology and Bioengineering 34, 1398-1402.

Swiderek, H., Al-Rubeai, M., (2007) Functional genome-wide analysis of antibody producing NS0 cell line cultivated at different temperatures. Biotechnology and Bioengineering 98, 616-630.

Tatiraju, S., Soroush, M., Mutharasan, R., (1999) Multi-rate nonlinear state and parameter estimation in a bioreactor. Biotechnology and Bioengineering 63, 22-32.

Templeton, N., Dean, J., Reddy, P., Young, J.D., (2013) Peak antibody production is associated with increased oxidative metabolism in an industrially relevant fed-batch CHO cell culture. Biotechnology and Bioengineering 110, 2013-+.

Trummer, E., Fauland, K., Seidinger, S., Schriebl, K., Lattenmayer, C., Kunert, R., Vorauer-Uhl, K., Weik, R., Borth, N., Katinger, H., Mueller, D., (2006) Process parameter shifting: Part I. Effect of DOT, pH, and temperature on the performance of Epo-Fc expressing CHO cells cultivated in controlled batch bioreactors. Biotechnology and Bioengineering 94, 1033-1044.

Turchi, L., Loubat, A., Rochet, N., Rossi, B., Ponzio, G., (2000) Evidence for a direct correlation between c-Jun NH2 terminal kinase 1 activation, cyclin D2 expression, and G(1)/S phase transition in the murine hybridoma 7TD1 cells. Exp. Cell Res. 261, 220-228.

Uchiyama, K., Shioya, S., (1999) Modeling and optimization of alpha-amylase production in a recombinant yeast fed-batch culture taking account of the cell cycle population distribution. Journal of Biotechnology 71, 133-141.

Villadsen, J., (1999) On the use of population balances. Journal of Biotechnology 71, 251-253.

Wang, D., Bodovitz, S., (2010) Single cell analysis: the new frontier in ‘omics’. Trends in Biotechnology 28, 281-290.

Wang, X.-H., He, S.-Y., Zhang, Y., Xu, J., Feng, Q., Li, L., Mi, L., Chen, Z.-N., (2004) DMSO arrested hybridoma cells for enhanced antibody production. Sheng Wu Gong Cheng Xue Bao 20, 568-571.

Watanabe, I., Okada, S., (1967) Effects of temperature on growth rate of cultured mammalian cells (L5178Y). Journal of cell biology 32, 309-323.

Wu, M.H., Dirnopoulos, G., Mantalaris, A., Varley, J., (2004) The effect of hyperosmotic pressure on antibody production and gene expression in the GS-NS0 cell line. Biotechnology and Applied Biochemistry 40, 41-46.

Wurm, F.M., (2004) Production of recombinant protein therapeutics in cultivated mammalian cells. Nature biotechnology 22, 1393-1398.

Xiong, Y., Hannon, G.J., Zhang, H., Casso, D., Kobayashi, R., Beach, D., (1993) p21 is a universal inhibitor of cyclin kinases. Nature 366, 701-704.

Yang, J.P., Hori, M., Takahashi, N., Kawabe, T., Kato, H., Okamoto, T., (1999) NF-kappaB subunit p65 binds to 53BP2 and inhibits cell death induced by 53BP2. Oncogene 18, 5177-5186.

Zhao, L., Fan, L., Wang, J.Q., Niu, H.X., Tan, W.S., (2009) Responses of GS-NS0 myeloma cells to osmolality: cell growth, intracellular mass metabolism, energy metabolism, and antibody production. Biotechnology and Bioprocess Engineering 14, 625-632.

Zhou, F., Bi, J.X., Zeng, A.P., Yuan, J.Q., (2007) A macrokinetic model for myeloma cell culture based on stoichiometric balance. Biotechnology and Applied Biochemistry 46, 85-95.

Zhou, W.C., Bibila, T., Glazomitsky, K., Montalvo, J., Chan, C., DiStefano, D., Munshi, S., Robinson, D., Buckland, B., Aunins, J., (1996) Large scale production of recombinant mouse and rat growth hormone by fed-batch GS-NS0 cell cultures. Cytotechnology 22, 239-250.

Ziehn, T., Tomlin, A.S., (2009) GUI–HDMR – A software tool for global sensitivity analysis of complex models. Environmental Modelling & Software 24, 775-785.

Appendix I.

Glucose and lactate profiles for the batch temperature shift experiments.

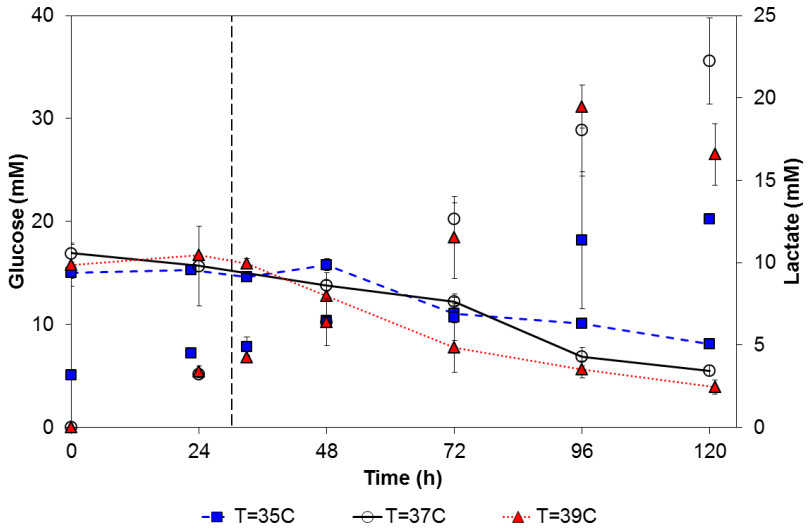


Figure AI.1. Batch temperature shift glucose and lactate profiles.

Productivity profiles divided in three culture phases: 0-1 day, 1-3 day, 3-5 day.

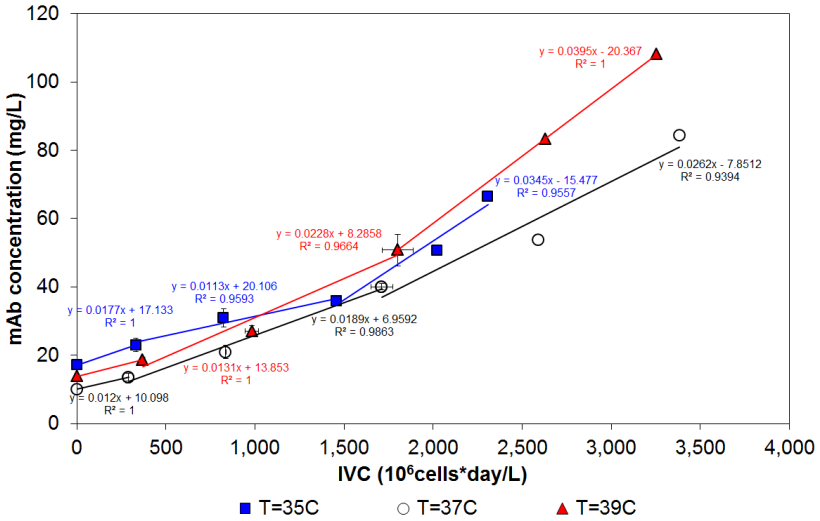


Figure AI.2. Batch temperature shift productivity profiles divided in culture phases.

Appendix II.

The S phase general representation depends on both DNA and cyclin B. Then the governing equations are stated below following the symbol and functions of chapter 6.

G_1/G_0 phase: (AII.1)

$$\frac{\partial N_{G1}(cycE,t)}{\partial t}+\frac{\partial r_{G1}(cycE,S)N_{G1}(cycE,t)}{\partial cycE}=-\Gamma_{G1}(cycE)N_{G1}(cycE,t)-k_d(S)N_{G1}(cycE,t)$$

$$+2\delta(cycE)\int_{cycB\min}^{cycB\max}\Gamma_{G2}(cycB,S)N_{G2}(cycB,t)dcycB$$

S phase: (AII.2)

$$\frac{\partial N_S(cycB,DNA,t)}{\partial t}+\frac{\partial r_{ScycB}(cycB,S)N_S(cycB,DNA,t)}{\partial cycB}+\frac{\partial r_{SDNA}(DNA,S)N_S(cycB,DNA,t)}{\partial DNA}=$$

$$\delta(cycB)\delta(DNA-1)\int_0^{\infty}\Gamma_{G1}(cycE)N_{G1}(cycE,t)dcycE-k_d(S)N_S(cycB,DNA,t)$$

G_2/M phase: (AII.3)

$$\frac{\partial N_{G2}(cycB,t)}{\partial t}+\frac{\partial r_{G2}(cycB,S)N_{G2}(cycB,t)}{\partial cycB}=-\Gamma_{G2}(cycB)N_{G2}(cycB,t)-k_d(S)N_{G2}(cycB,t)$$

$$+r_{SDNA}(DNA=2,S)N_S(cycB,DNA=2,t)$$

The model approximation is based on: (i) the fact that all cells enter stage S in the same conditions (DNA=1, cycB=0) and (ii) the form of functions rSDNA(DNA), rScycB(cycB) with the same explicit time dependence function flimGlu. The S stage equation is hyperbolic in both internal coordinates so the characteristics along each coordinate can be described by the following ordinary differential equations:

$$\frac{dcycB}{d\tau}=r_{ScycB}(cycB,S)=CycBgrow\cdot f_{\lim Glu} \quad \text{(AII.4)}$$

$$\frac{dDNA}{d\tau}=r_{SDNA}(DNA,S)=DNAgrow\cdot f_{\lim Glu} \quad \text{(AII.5)}$$

where τ is the age of the cell in the S stage. Combining the above equations:

$$\frac{dcycB}{dDNA}=\frac{r_{ScycB}(cycB,S)}{r_{SDNA}(DNA,S)}=\frac{CycBgrow}{DNAgrow} \quad \text{(AII.6)}$$

which can be integrated to give

$$cycB^*=FF(DNA) \quad \text{(AII.7)}$$

The bivariate function N_S(cycB,DNA) can be replaced by the univariate N_S(DNA) using the following relation:

$$N_S\left(cycB, DNA, t\right) = N_S\left(DNA, t\right)\delta\left(cycB - FF(DNA)\right) \tag{AII.8}$$

The error of the above approximation is only restricted to the cycB-distribution in S stage and it is related to the initial condition. However, it should be noted that the approximation is exact when all initial S cells abandon S stage i.e. for almost the entire time of practical simulations. Even at the initial time period the error can be very small depending on the initial condition. Therefore the modified problem takes the form of Equation (6.1)-(6.3) with $cycB_{S-G2/M} = FF(1)$.

Appendix III.

The herein formulated PBM is multivariable (cyclin E, DNA, cyclin B) and multistage (G_1/G_0, S, G_2/M). A schematic representation of the cell cycle model is presented (Figure AIII.1).

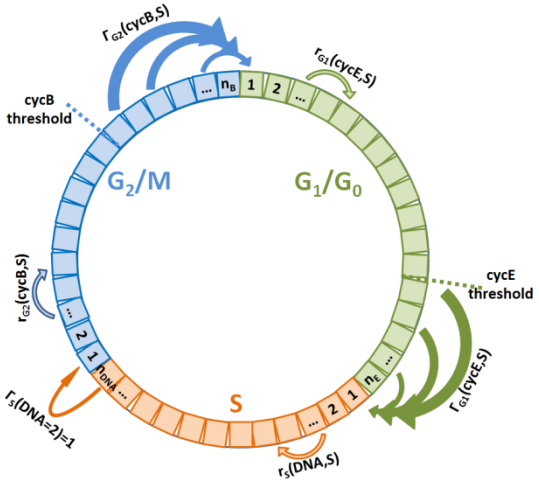


Figure AIII.1. Cell cycle model schematic representation.

As observed, it is possible to define/select a maximum content on each distributed domain (i.e. cycE, DNA, cycB), as well as the discretisation interval (i.e. number of intervals or bins within each domain). The discretisation intervals will mainly affect the resolution of the results (the higher number of bins within each domain, the higher the resolution). However, for each bin an ordinary differential equation is introduced, which will increase the computational effort. Although a high resolution is in general desired, it should account for your experimental resolution. Therefore, for each domain the following resolution was selected: G_1/G_0=0.5 %cycE, S= 0.05 DNA, and G_2/M=1 %cycB.

The cell conservation test guide the selection of a suitable maximum content on each domain that would minimise the numerical cell losses (i.e. cells that reach the maximum content of a given domain and are numerically lost). However, since the transition from S to G_2/M is deterministic $\Gamma_S(DNA=2)=1$, it does not affect the cell conservation. Thus, only the maximum content of the cyclin E1 and B1 domains was varied. The DNA domain was fixed to 20 bins, keeping a resolution of 0.05 DNA (i.e. DNA duplication from 1 to 2, over 20 bins). The maximum content of the cyclin domains were increased in order to ensure that over 99% of the cells remained in the system (were conserved) after 120h of simulation. To evaluate the conservation, the birth term was fixed to 1 to avoid generation, therefore the cells that transit from

G_2/M to G_1/G_0 would not duplicate and the number of cells (or cell density) in the system should remain constant. In addition, the death rate was fixed to zero (k_{dmax}=0) in order to neglect cell death, as it would normally be a source for cell losses. The interaction with the nutrients was also neglected ($f_{limGlu/Glc/Lac}$=1), which allows to maintain the rates ($r_{i=G1,S,G2}$, $\Gamma_{j=G1,G2}$) at maximum levels. Finally, a uniform distribution is applied for all domains (cyclin E1 between 0-95 %cycE, DNA between 1-2, and cyclin B1 between 0-95 %cycB). Both by applying a uniform distribution and maintaining maximum rates, the system is evaluated against a worst case scenario.

The cell conservation was evaluated under the above mentioned conditions and while varying the full range of 24 parameters ±50% (Sidoli et al., 2006) from their nominal values. The maximum content was increased, both for cyclin E1 and cyclin B1 keeping the resolutions constant, until the desired conservation was achieved (Table AIII.1).

Table AIII.1. Conservation test.

	Case 1		**Case 2**		**Case 3**		**Case 4**	
Phase (distributed variable)	G_1/G_0 (cycE)	G_2/M (cycB)	G_1/G_0 (cycE)	G_2/M (cycB)	G_1/G_0 (cycE)	G_2/M (cycB)	G_1/G_0 (cycE)	G_2/M (cycB)
# bins	100	100	150	150	200	200	250	250
Maximum content	50	100	75	150	100	200	125	250
Conservation (120h)	**73%**		**95.6%**		**99.1%**		**99.8%**	

The cell conservation for each of the cases was evaluated at three time points (36, 72, 120h) as presented in Figure AIII.2. Based on the results, cyclin E1 and cyclin B1 were distributed over 200 bins (Case 3, Table AIII.1) and DNA over 20 bins, to ensure above 99% cell conservation.

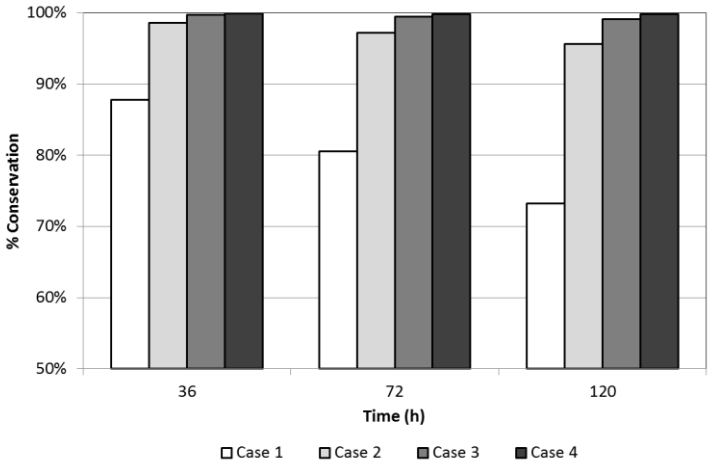


Figure AIII.2. Conservation test study.